The role of *Tcfap2a* in cardiovascular development

Amy-Leigh Johnson

Submitted in accordance with the requirements for the degree of Doctor of Philosophy

Institute of Genetic Medicine

Newcastle University

September 2013

Abstract

Congenital cardiovascular malformations (CCVM) are the most common human birth defects, occurring in up to 1% of newborn infants. Many cell populations are required for correct cardiovascular development, including the neural crest cells (NCC). NCCs migrate from the dorsal neural tube into the pharyngeal arches and contribute to the asymmetric remodelling of the pharyngeal arch arteries (PAA). A subset of NCCs continue to migrate into the outflow tract (OFT) of the heart, and aid in the septation of the OFT into the aorta and pulmonary trunk. *Tcfap2a*, which encodes the murine transcription factor AP-2α, is highly expressed within NCCs and the pharyngeal surface ectoderm (PSE), and mutations in this gene causes CCVM affecting the OFT, PAAs and the formation of the interventricular septum.

This thesis investigates the tissue-specific requirements of *Tcfap2a* in cardiovascular development and the mechanisms of PAA malformation. Conditional deletion of *Tcfap2a* from NCCs resulted in a limited prevalence of CCVM, which was not increased by altering the genetic background or simultaneous deletion from the PSE. However, *Tcfap2a* expression within both the NCCs and PSE is required in craniofacial and thymus development. Immunohistochemical analysis in *Tcfap2a*-null embryos suggests that *Tcfap2a* is required in the formation of the PAAs, in addition to a possible role in their remodelling. Quantitative PCR analysis was used to investigate potential transcriptional targets of AP-2α within the pharyngeal arch region and we propose that *Dlx5* is regulated by AP-2α in a pathway independent of endothelin signalling. A study investigating the potential interaction between these genes is presented here.

This thesis presents further insights into the genetic networks regulating the formation of the PAAs, OFT and interventricular septum of the heart. We also highlight issues associated with the use of transgenic mouse models and the effect of genetic background in the study of cardiovascular development.

Acknowledgements

Firstly I would like to thank my supervisor Dr. Simon Bamforth for his constant support, encouragement and enthusiasm throughout my PhD. Additionally I would like to thank Prof. Deborah Henderson for all her guidance in the project.

I would like to thank Divya Venkatesh for support and advice during the initial stages of my PhD and for teaching me many of the protocols used throughout the project. In addition, I would also like to thank Rebecca Dodds, Alberto Briones-Leon, Kathleen Allinson and Kate Bailey for practical tips, discussion and entertainment in the lab. I would like to extend this thanks to all members, past and present, of the hanger lab. In particular, thanks to Dr. Lorraine Eley for advice and patience in teaching me her *in situ* hybridisation protocol and sharing reagents.

I am grateful to all my friends within the Institute of Genetic Medicine for their friendship and support throughout my PhD. In particular I would like to thank Ann Marie Hynes, Vipul Sharma and David Burns for always making me laugh (either with or at them).

Thank you to my family for always encouraging me and for their enthusiasm (real or otherwise) when hearing about my PhD project. Particularly to my Mam for always providing a welcome distraction from science and PhD life and to my brother for inspiring me to work on heart development.

Finally, thank you to Dr. Alan Merritt, for his continuous support and infinite patience throughout my PhD; for listening to me waffle on about pharyngeal arch arteries for years and still being willing to read my entire thesis (twice!); and for providing an endless supply of hot drinks, sweets and biscuits during the writing process. I really couldn't have done it without him.

Abbreviations

22q11DS	22q11 deletion syndrome
AB complex	Avidin-biotin complex
α-SMA	α-smooth muscle actin
ANR	Anterior neural ridge
Ao	Aorta
AoA	Aortic arch
AP-2α	Activator protein 2α
A-RSA	Anomalous right subclavian artery
ASD	Atrial septal defect
AV	Atrioventricular
AVSD	Atrioventricular septal defect
BAV	Bicuspid aortic valve
BC	Brachiocephalic trunk
bHSH	Basic helix-span-helix
BLAST	Basic local alignment search tool
BMP	Bone morphogenetic protein
BOFS	Branchio-ocular facial syndrome
bp	Base pairs
BSA	Bovine serum albumin
cAoA	Cervical aortic arch
ccne2	Cyclin E2
CCVM	Congenital cardiovascular malformation
CD	Carotid duct
cDNA	Complementary deoxyribose nucleic acid
cf	Craniofacial
CITED	CBP/p300 interacting transactivators with glutamic acid/aspartic acid-rich carboxy-terminal domain

cL	Cleft lip
cM	CentiMorgan
co-IP	Co-immunoprecipitation
CORSA	Cervical origin of the right subclavian artery
cP	Cleft palate
cRAA	Cervical right aortic arch
Ct	Threshold cycle
D	Aspartic acid
DA	Ductus arteriosus
DAB	3,3’-diaminobenzidine
dAo	Dorsal aorta
DAPI	4',6-diamidino-2-phenylindole
DART-PCR	Data analysis for real-time polymerase chain reaction
DEPC	Diethyl pyrocarbonate
dH_2O	Distilled water
DIG	Digoxygenin
DN	Dominant negative
DNA	Deoxyribose nucleic acid
dNTP	Deoxyribonucleotide triphosphate
DORV	Double outlet right ventricle
DPA	Dextraposed aorta
DTA	Diphtheria toxin fragment A
e	Embryonic day
E	Glutamic acid
E. coli	*Escherichia coli*
ec	Ectoderm
ECE-1	Endothelin converting enzyme
ECM	Extracellular matrix

Ed	Oedema
Edn1	Endothelin 1 (gene)
Ednra	Endothelin receptor A (gene)
EDTA	Ethylenediaminetetraacetic acid
EGFR	Epidermal growth factor receptor
EMSA	Electrophoretic mobility shift assay
EMT	Epithelial-to-mesenchymal transformation
en	Endoderm
EPDC	Epicardial-derived cell
ET-1	Endothelin 1 (protein)
ET_A	Endothelin receptor A (protein)
EtBr	Ethidium bromide
Ex	Exencephaly
EYFP	Enhanced yellow fluorescent protein
FACS	Fluorescence-activated cell sorting
FBS	Foetal bovine serum
floxed	Flanked with loxP sites
FN	Frontonasal
G	Gauge
GAPDH	Glyceraldehyde 3-phosphate dehydrogenase
GCV	Ganciclovir
Gd-DTPA	Gadopentetate dimeglumine
gDNA	Genomic deoxyribose nucleic acid
GDP	Guanine diphosphate
GFP	Green fluorescent protein
GTP	Guanine triphosphate
h	Heart
H_2O_2	Hydrogen peroxide

Hand1	Heart and neural crest-derived 1
Hand2	Heart and neural crest-derived 2
HAT	Histone acetyl transferase
HCl	Hydrochloric acid
Hdac3	Histone deacetylase 3 gene
hpf	Hours post fertilisation
hypoAoA	Hypoplastic aortic arch
IAA	Interrupted aortic arch
IAA-B	Interrupted aortic arch type B
I-LSA	Isolated left subclavian artery
IRES	Internal ribosome entry site
I-RSA	Isolated right subclavian artery
Isl1	Islet 1
IVS	Interventricular septum
KCl	Potassium chloride
kDa	Kilo Dalton
kPa	Kilo Pascals
LB	Luria Bertani
LCC	Left common carotid
LiCl	Lithium chloride
low	Lockjaw
LSA	Left subclavian artery
LV	Left ventricle
m	Mesoderm
mc	Mesenchyme
md	Mandible
MES	Midline epithelial seam
$MgCl_2$	Magnesium chloride

MLC2a	Atrial myosin light chain 2
MMP	Matrix metalloproteinase
mob	Mont blanc
MORE	Mox2cre
MRI	Magnetic resonance imaging
mx	Maxilla
Na_2HPO_4	Sodium phosphate dibasic
NaCl	Sodium chloride
NaH_2PO_4	Sodium phosphate monobasic
NaOH	Sodium hydroxide
NB	Neural border
NC	Neural crest
NCC	Neural crest cells
OA	Overriding aorta
ob	Olfactory bulb
OFT	Outflow tract
ot	Otocyst
P	Postnatal day
PA	Pharyngeal arch
PAA	Pharyngeal arch artery
PARP-1	Poly-(ADP-ribose) polymerase-1
PBS	Phosphate-buffered saline
PBT	Phosphate-buffered saline with Tween-20
PCR	Polymerase chain reaction
PDA	Patent ductus arteriosus
PE	Proepicardium
PECAM-1	Platelet endothelial cell adhesion molecule-1
PFA	Paraformaldehyde

PGK	3-phosphoglycerate kinase
PS	Pulmonary stenosis
ps	Palatal shelves
PSE	Pharyngeal surface ectoderm
PT	Pulmonary trunk
PTA	Persistent truncus arteriosus
PVDF	Polyvinyl difluoride
qPCR	Quantitative polymerase chain reaction
RAA	Right aortic arch
rara	Retinoic acid receptor α
rarb	Retinoic acid receptor β
RCC	Right common carotid
RNA	Ribose nucleic acid
RSA	Right subclavian artery
RT-PCR	Real time PCR
RV	Right ventricle
s	Somites
S.E.M	Standard error of the mean
SDS	Sodium dodecyl sulphate
Sema3C	Semaphorin 3C
SHF	Second heart field
SHFM	Split hand-foot malformation
Shh	Sonic hedgehog
SMC	Smooth muscle cells
SRJ	Serine-glycine-rich junction
SSC	Saline-sodium citrate
T	Tongue
TAE	Tris-acetic acid-EDTA

TBST	Tris-buffered saline with Tween-20
TBS-TX	Tris-buffered saline with Triton-X 100
Tcfap2a	Transcription factor activator protein 2 α (gene, mouse)
TE	Tris-EDTA
TFAP2A	Transcription factor activator protein 2 α (gene, human)
tfap2a	Transcription factor activator protein 2 α (gene, zebrafish)
TGA	Transposition of the great arteries
TGF	Transforming growth factor
Th	Thymus
.tiff	Tagged image file format
TK	Thymidine kinase
T_m	Melting temperature
TOF	Tetralogy of Fallot
Tr	Trachea
Tris	Trizma base
tRNA	Transfer RNA
V	Volts
v/v	Volume per volume
VEGF	Vascular endothelial growth factor
VEGFR2	Vascular endothelial growth factor receptor 2
VR	Vascular ring
VSD	Ventricular septal defect
w/v	Weight per volume
WISH	Whole mount *in situ* hybridisation
X-gal	5-Bromo-4-chloro-3-indolyl β-D-galactopyranoside
ΔRn	Raw fluorescence data

Table of Contents

List of Figures

List of Tables

Chapter 1. Introduction

1.1. Heart development

The heart is one of the first organs to develop within vertebrates, and begins functioning during the fourth week of human development. The organ develops from two populations of cells in the splanchnic mesoderm, which migrate anteriorly and fuse at the midline to form a linear heart tube. The heart tube then undergoes a complex remodelling process to form the mature mammalian heart. Disruptions to this process can result in congenital defects which affect the ability of the heart to function correctly. It is estimated that between 0.5 and 39.5% of spontaneous terminations during pregnancy may be due to heart developmental deficiencies. In addition, approximately 1% of infants are born with a congenital cardiovascular malformation (CCVM) (Hoffman, 1995).

1.1.1. Basic heart development in mice

The heart is the first organ to form during murine development. It begins at embryonic day (e) 7.0 with the formation of the primary heart fields from the splanchnic mesoderm, and is completed at approximately e15.5 with the remodelling of the aortic arch arteries and the outflow tract (OFT).

The cardiac precursor cells are specified from the splanchnic mesoderm shortly after gastrulation in response to bone morphogenetic protein (BMP) signals from the endoderm. These mesodermal cells form two primary heart fields (Figure 1.1a), which migrate anteriorly and fuse at the ventral midline forming the cardiac crescent (e7.5) (Figure 1.1b). By e8.0 a beating linear heart tube has formed (Figure 1.1c), composed of an endocardial tube surrounded by a layer of myocardial cells, with an intervening layer of extracellular matrix termed ‘cardiac jelly’. The segments which will form the major structures of the mature heart are already visible at this stage. At the anterior end, the aortic sac connects the conotruncus (primitive OFT) to the pharyngeal arch arteries (PAAs). These arteries join the OFT to the dorsal aortae, and later remodel into the vessels of the mature aortic arch. At the posterior end, the vitelline veins drain blood from the yolk sac into the sinus venosus. The ventricular and atrial chambers fall in the intermediate region, and join the inflow region (vitelline veins and

sinus venosus) to the outflow region (conotruncus and aortic sac) (reviewed in Bruneau, 2008; High and Epstein, 2008; Srivastava and Olson, 2000).

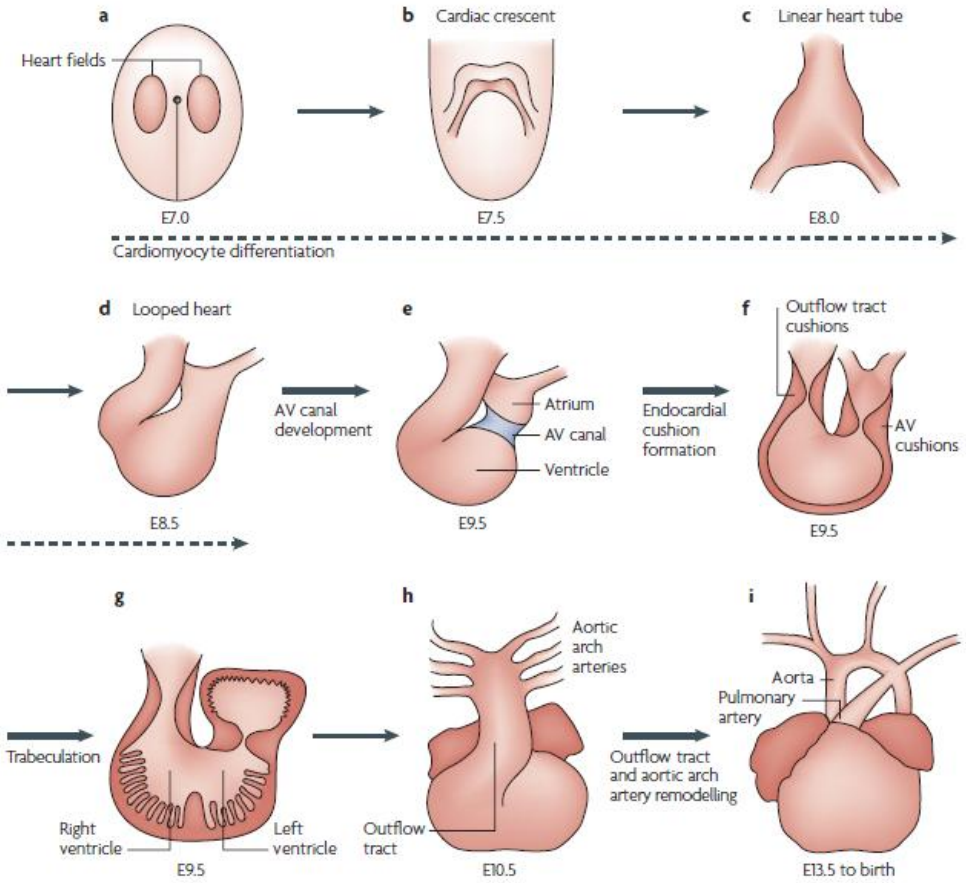

Figure 1.1: Normal heart development in the mouse.
The heart begins as two primary heart fields (a) which merge at the ventral midline to form the cardiac crescent (b). By e8.0 the linear heart tube has formed and the segments which will form the structures of the mature heart are visible (c). The linear tube loops (d) and the atrioventricular (AV) canal forms, separating the atria from the ventricles (e). The endocardial cushions, which will develop into the major valves of the heart form within the OFT and AV canal (f). At e9.5 ventricular trabeculation occurs by the invasion of cardiomyocytes (g). The OFT undergoes septation and the PAAs are remodelled (h) to form the final aortic arch arteries of the mature heart (i). (Figure taken from High and Epstein, 2008).

The heart tube undergoes a rightward cardiac looping event, initiated by the ballooning of the cardiac chamber segments (e8.5) (Figure 1.1d). Further cardiac progenitor cells, derived from the pharyngeal mesoderm are added to the linear heart tube at the conotruncus (Mjaatvedt *et al.*, 2001). This population, termed the second heart field (SHF), is multipotent and contributes to the OFT, right ventricle and both atria. The atrioventricular (AV) canal, which separates the atrial and ventricular segments, forms in response to *TBX2* repression of chamber-specific genes (Figure 1.1e). The endocardial layer, separated from the myocardium by the cardiac jelly, receives signals from the myocardial cells, which induces an epithelial-to-mesenchymal transition (EMT) of a number of endocardial cells. This process activates pathways

within the endocardium, which allows cells to dissociate from the epithelium and invade the cardiac jelly. These cells form the endocardial cushions within the AV canal and OFT (Figure 1.1f), which will later form the mitral, tricuspid, pulmonary and aortic valves.

Ventricular trabeculation begins at around e9.5 (Figure 1.1g). This requires the cardiomyocytes to proliferate inwards, producing the 'finger-like' projections which invade the ventricular lumen. It is thought that the trabeculae provide a surface for rapid oxygen diffusion to occur, before the coronary arteries form (Breckenridge *et al.*, 2007). This process is not well understood, but is likely to involve signalling of paracrine factors, originating in the epicardium. Molecules such as retinoic acid and erythropoietin are implicated in initiating mitosis in the myocytes, and are therefore candidates for inducing the inward proliferation required for ventricular trabeculation (Stuckmann *et al.*, 2003). BMP10 is also expected to play a role in this process, as mutations in this gene result in abnormal ventricular trabeculation, likely caused by a decrease in proliferation at e9.0-9.5 (Chen *et al.*, 2004).

At e11.5-12.0, the caudal PAAs begin remodelling to form the asymmetrical aortic arch arteries of the mature heart (Figure 1.1h-i). The OFT becomes septated to form the pulmonary trunk and the aorta. These processes will be described in detail later (see sections 1.2.3 and 1.3.2).

1.1.2. Addition of cells to the linear heart tube

Following the formation of the linear heart tube, the heart receives further cellular contributions from other sources: the SHF, the neural crest cells (NCCs) and the proepicardium.

The SHF originates from a region of pharyngeal mesoderm anterior to the primary heart-forming fields that produce the linear heart tube. The cells of the SHF begin migrating into the linear heart tube at e8.0 of murine development, through two regions which remain connected to the splanchnic mesenchyme of the dorsal body wall. At the anterior end, these cells enter through the aortic sac and at the posterior end they enter at the dorsal mesocardium (Cai *et al.*, 2003).

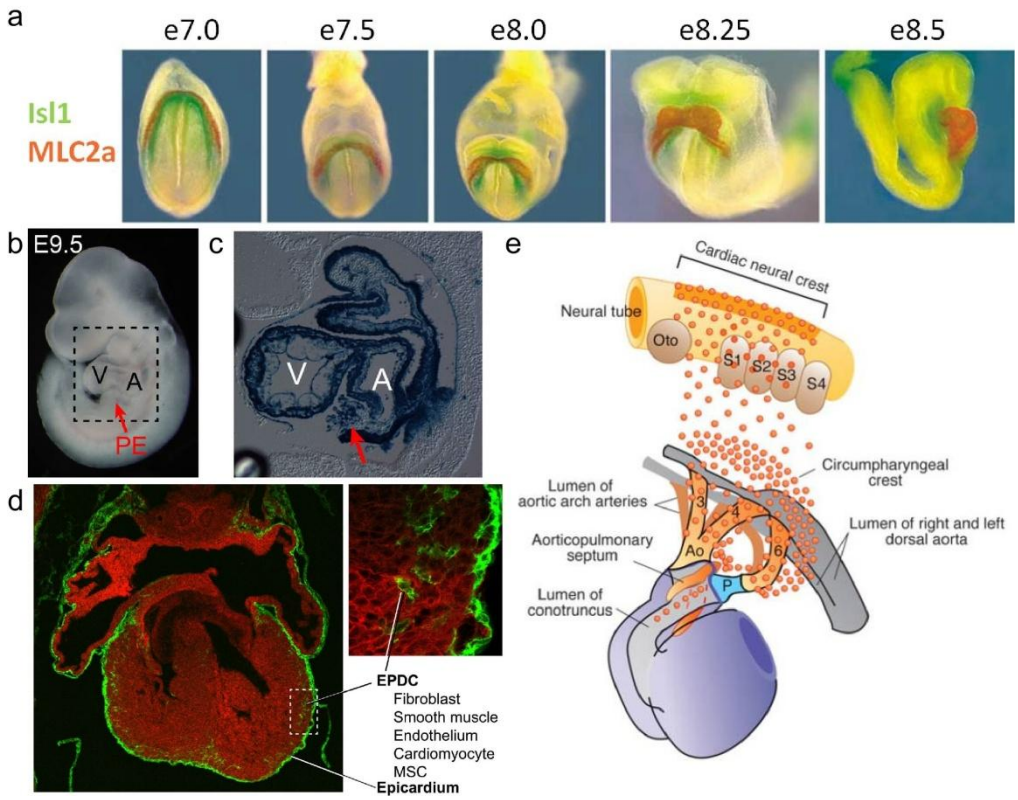

Figure 1.2: Addition of cells to the linear heart tube.
(a) Double whole mount *in* situ hybridisation demonstrates two distinct populations contributing to the primitive heart. *MLC2a* expression (orange) marks the primary heart field, while *Isl1* expression (green) marks the SHF (Image adapted from Cai *et al.*, 2003). (b-d) Addition of cells from the proepicardium (Images adapted from von Gise and Pu, 2012). (b) Whole mount photograph of an e9.5 embryo. The proepicardium (PE, red arrow) is situated by the sinus venosus. (c) Sagittal section through an e9.5 embryo demonstrating the position of the proepicardium (red arrow). Blue staining represents lineage tracing of *Nkx2.5*-positive cells. (d) Left panel: Transverse section through an e15.5 heart demonstrates a monolayer of epicardial cells (green) over the heart. Right panel: Magnified view of the dashed box in the left panel. Epicardial cells undergo EMT to become EPDCs which migrate into the myocardium and give rise to a number of cells types. (e) NCC contribution to the developing PAAs and outflow tract. NCCs migrate from the dorsal neural tube, between the otocyst and the third somite. These cells surround the PAAs, forming the smooth muscle lining of these vessels, and then continue to migrate to the outflow tract where they initiate the septation of the aorticopulmonary region (Image taken from Hutson and Kirby, 2007). A, atrium; V, ventricle; PE, proepicardium.

Islet1 (*Isl1*) is expressed from e7.0 in a population of cells anterior to the primary heart field, and was therefore proposed as a marker of the SHF. Indeed, double *in situ* hybridisation of *Isl1* with an early marker of differentiated cardiomyocytes, atrial myosin light chain 2 (*MLC2a*), demonstrates the mutually exclusive expression of these markers (Figure 1.2a). As these cells enter the linear heart tube, they differentiate into cardiac precursors and downregulate *Isl1* expression, likely indicating that *Isl1* expression is required to maintain the undifferentiated state of these cells. *Isl1*-expressing cells give rise to the OFT, most of the cells of the right ventricle and the atria, and a small number of cells of the left ventricle, while the primary heart field contributes the majority of cells of the right ventricle. Loss of *Isl1* expression in these

cells affects proliferation, migration and survival of these cells, and a loss of those portions of the heart derived from *Isl1*-expressing cells (Cai *et al.*, 2003).

The proepicardium, situated near the sinus venosus (Figure 1.2b-c), is a source of extracardiac mesenchyme, which produces the majority of the epicardium of the heart. The cells migrate from the proepicardium as multicellular aggregates, which adhere to the myocardium and flatten. The flattened aggregates fuse together to form the primitive epicardium. The epicardium then extends by migration from the periphery (Komiyama *et al.*, 1987). EMT of a subset of epicardial cells results in the formation of epicardial-derived cells (EPDCs) which migrate into the underlying myocardium and form connective tissue and the endothelium and smooth muscle cells (SMCs) of the coronary arteries (Figure 1.2d) (Reviewed in von Gise and Pu, 2012).

A further extracardiac population required in the development of the heart is the NCCs. This multipotent population of cells delaminates from the neural tube, undergoes EMT and migrates towards the heart. The NCCs populate the caudal pharyngeal arches (PAs) (see section 1.2.1 below) and differentiate into SMCs which line the PAAs. A sub-population of these cells continue to migrate into the OFT where they form part of the aorticopulmonary septation complex required in the septation of the OFT into the aorta and the pulmonary trunk (Figure 1.2e) (Reviewed in Hutson and Kirby, 2007). The NCCs will form a major focus of this thesis and therefore will be discussed in greater detail later (see section 1.3).

1.1.3. Congenital cardiovascular malformations

A CCVM is defined as a structural defect of the heart or associated vessels, which severely affects cardiac function (Mitchell *et al.*, 1971). Figure 1.3 summarises the types of defects that can occur during cardiovascular development and the prevalence per 1000 live births (shown in brackets). The most common form of CCVM is bicuspid aortic valve (BAV), which is caused by the fusion of two leaflets of the tricuspid valve of the aorta and results in regurgitation of blood from the aorta back into the ventricle. This mild phenotype is often asymptomatic at birth and in childhood, but is thought to predispose an affected individual to more severe heart disease in later life (Tadros *et al.*, 2009; Siu and Silversides, 2010).

The next most common CCVM is a ventricular septal defect (VSD), which occurs to varying degrees in around 3.5 per one thousand live births. A VSD is the failure in the formation of the interventricular septum which separates the two ventricles. Small VSDs, along with atrial septal defects (ASDs) and small patent ductus arteriosus (PDA) are considered the least severe CCVMs, and usually close naturally or do not cause problems to the patient (Hoffman *et al.*, 2004).

The most severe forms of CCVM include double outlet right ventricle (DORV), persistent truncus arteriosus (PTA), transposition of the great arteries (TGA), tetralogy of Fallot (TOF), atrioventricular septal defects (AVSDs) and large VSDs. These occur collectively at a rate of around 2.5-3 per thousand live births and cause infants to become seriously ill within the immediate postnatal period, or soon after (Hoffman *et al.*, 2004). Each of these defects put additional strain on the heart of the patient by allowing the mixing of oxygenated and deoxygenated blood. DORV is a condition in which both the aorta and pulmonary trunk arise from the right ventricle. In live born infants this defect is often accompanied by a VSD in order to allow oxygenated blood from the left side of the heart to reach the aorta and be pumped out into systemic flow. PTA is a continuation of a more primitive state of OFT development, in which the early OFT, then termed the truncus arteriosus, has not yet septated into the aorta and the pulmonary trunk. TGA is another defect of OFT formation in which the major arteries become aligned incorrectly, so that the aorta arises from the right ventricle and the pulmonary trunk arises from the left ventricle. TOF is a collection of four cardiovascular defects: a large VSD, an overriding aorta (OA) which arises from a central position directly above the VSD, right ventricular hypertrophy and pulmonary stenosis. An AVSD is the failure of the formation of both the atrial and ventricular septum.

In addition to the defects of the OFT and interventricular septum many defects affecting the aortic arch arteries can also occur. The most severe of which is interruption of the aortic arch (IAA) which prevents the blood from passing from the aorta into systemic flow. Other malformations may be mostly asymptomatic such as anomalous right subclavian artery (A-RSA). This results in the right subclavian artery (RSA) passing behind the oesophagus, putting pressure on the oesophagus. This

presents in patients as a difficulty in swallowing (dysphagia), but is often asymptomatic (Erami *et al.*, 2013).

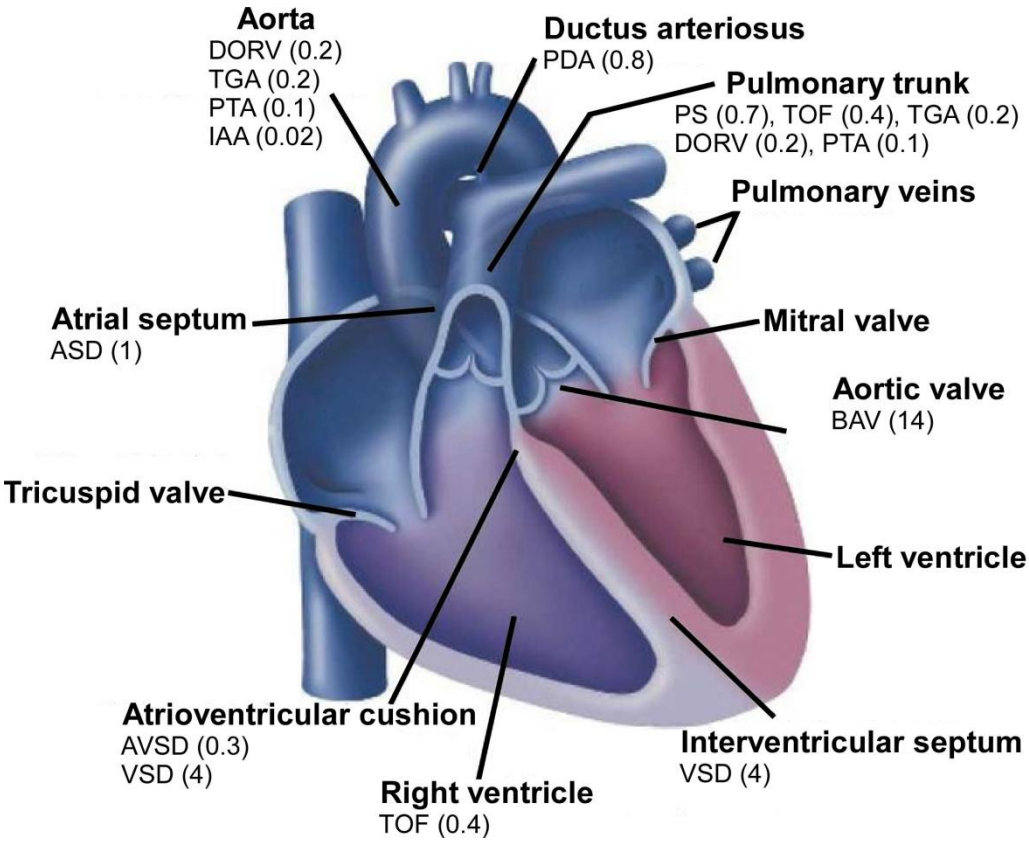

Figure 1.3: Congenital cardiovascular malformations and incidence.
Diagram of the heart, showing a number of regions affected by CCVM. The incidence of each defect in newborn infants per thousand live births is shown in brackets. DORV, double-outlet right ventricle; TGA, transposition of the great arteries; PTA, persistent truncus arteriosus; IAA, interrupted aortic arch; PDA, patent ductus arteriosus; PS, pulmonary stenosis; TOF, tetralogy of Fallot; BAV, bicuspid aortic valve; VSD, ventricular septal defect; AVSD, atrioventricular septal defect; ASD, atrial septal defect. (Modified from Bruneau, 2008).

1.2. Pharyngeal arch artery development

1.2.1. The pharyngeal arches

The PAs are transient structures which contribute to the skeleton, musculature, ligaments and glands of the body. There are five PAs which form during embryonic development numbered 1-4 and 6. The fifth PA never fully forms and does not carry a vessel in mammals and is therefore generally excluded. Each PA is composed of four tissue types: ectoderm, endoderm, mesoderm and NCC-derived mesenchyme (Figure 1.4). The mesoderm and NCC-derived mesenchyme form the bulk of the PA tissue and are required to support the PAAs which develop within. The NCCs also contribute SMCs to the tunica media layer of the vessels. The pharyngeal ectoderm covers the PAs externally, and forms invaginations between the PAs named pharyngeal clefts. The endoderm forms the inner lining of the PAs and also forms invaginations which

meet with the pharyngeal clefts, termed pharyngeal pouches (reviewed in Graham and Smith, 2001; Lindsay, 2001; Grevellec and Tucker, 2010).

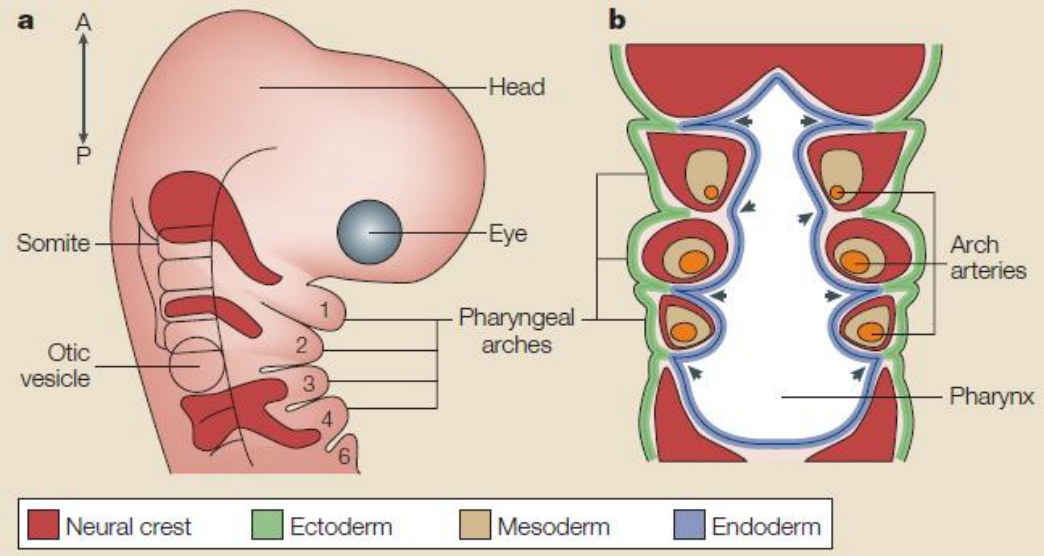

Figure 1.4: The structure of the embryonic pharyngeal arch system.
(a) Cartoon of the pharyngeal arches. Five pharyngeal arches form during embryonic development (1-4 and 6). (b) Coronal section through the PAs. Each arch consists of mesoderm (beige) and NC-derived mesenchyme (red), surrounded by ectoderm (green) and endoderm (blue). The pharyngeal pouches are formed from the endoderm between each PA (arrows). Each PA contains a single vessel. (Image taken from Lindsay, 2001).

1.2.2. The pharyngeal pouches

The pharyngeal pouches, as described above, form at the point where the pharyngeal endoderm meets the ectoderm, between the arches (arrows, Figure 1.4b). The third pharyngeal pouch gives rise to the developing thymus and inferior parathyroid gland, the fourth pharyngeal pouch gives rise to the superior parathyroid gland and the ultimobranchial body (required in calcium homeostasis) (reviewed in Grevellec and Tucker, 2010).

Although the development of these structures does not directly affect the developing cardiovascular system, many syndromes which have abnormalities of the PAAs also show abnormal development of these structures, presumably due to an overall disruption in the development of the PA system. Therefore, it is also useful to understand the formation of these tissues.

The formation of the thymus and parathyroid glands begins at e11.5 with the migration of endodermal cells of the third pharyngeal pouch into the underlying NCC-derived mesenchyme on either side of the pharynx. These cells then begin to express *Foxn1*, a marker of differentiated thymic tissue. It is likely that signals of the Wnt, BMP

and sonic hedgehog pathways are involved in the initiation and maintenance of *Foxn1* expression, and in the regulation of the size of the thymic rudiments (reviewed in Boehm, 2008). As the thymus/parathyroid primordia develop they begin to detach from the ectoderm. By e12 the remaining connections to the ectoderm are lost through apoptosis and the primordia are able to begin migration to their final location above the heart. By e13.0 the thymus and parathyroids are beginning to separate (reviewed in Manley and Blackburn, 2003).

There is much controversy over which pharyngeal lineages are responsible for each layer of tissue in the final thymus. Although it is well established that the endoderm plays a key role in the thymic epithelia, with the surrounding capsule being contributed by the NCC-derived mesenchyme, many others propose a 'dual-origin' of the thymic epithelia. The dual-origin model suggests that the internal medullary epithelium is derived from the endoderm, while the surrounding cortex epithelial cells originate within the ectoderm of the pharyngeal cleft (Reviewed in Manley and Blackburn, 2003).

1.2.3. Pharyngeal arch arteries

The PAAs form within the PAs, as bilaterally paired vessels connecting the aortic sac to the paired dorsal aortae at mid-embryogenesis (Figure 1.5a). Each artery arises from a single PA and is surrounded by an endothelial wall, formed from pharyngeal mesoderm, and SMCs and connective tissue, derived from NCC-derived mesenchyme (Graham and Smith, 2001; Kirby, 1987).

These vessels later undergo a complex remodelling process to develop into the aortic arch and associated vessels of the mature mammalian heart (Figure 1.5b). The processes by which the vessels both form and remodel are not fully understood; however, what is currently known will be discussed here.

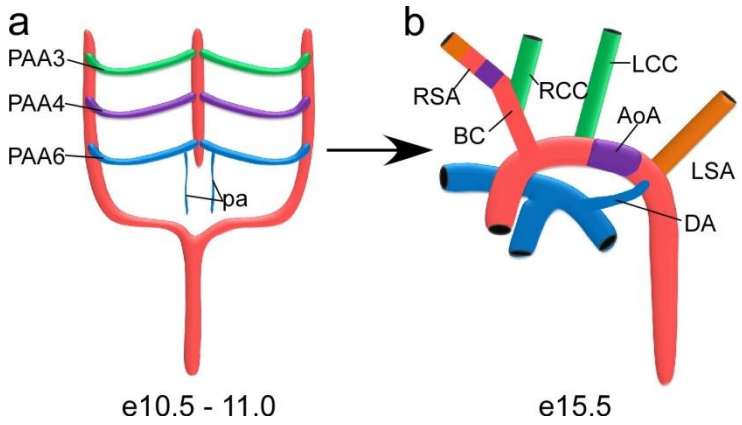

Figure 1.5: Pharyngeal arch artery development.
The PAAs begin as a symmetrical structure (a) consisting of 5 pairs of arteries, which are remodelled into the mature aortic arch (b). pa, pulmonary artery; RSA, right subclavian artery; RCC, right common carotid artery; BC, brachiocephalic trunk; LCC, left common carotid artery; AoA, aortic arch; LSA, left subclavian artery; DA, ductus arteriosus.

1.2.3.1. Formation

In 2002, Hiruma *et al*. characterised the development of the PAAs using a vascular casting technique, at various stages throughout murine development. Formation of the PAAs begins at e8.5-9.0 (12 somite stage) of murine development with the formation of the first PAAs. The first PAAs develop as a loop between the bilaterally paired dorsal and ventral aortae (Figure 1.6a). By the 15 somite stage (early e9.0-9.5), the second PAAs have begun to sprout from the dorsal and ventral aortae, with the vessel becoming fully lumenised by the 16 somite stage (Figure 1.6b). The third PAAs appear as a thin network within the caudal part of the second pharyngeal pouch, connecting the dorsal and ventral aortae, by early e9.5-10.0 (22 somite stage). By mid e9.5-10.0 (24-26 somites) the first, second and third PAAs are clearly visible. The first PAAs begin to reduce in diameter, while the second PAA is at its greatest diameter (Figure 1.6c).

From the 27-29 somite stage (late e9.5-10.0) the fourth PAAs appear, although thin, and the first PAAs begin to regress (Figure 1.6d). The second PAAs regress from e10.0 (31-34 somites) (Figure 1.6e). At this stage the sixth PAAs are becoming apparent. The sixth PAA increases to a size similar to the third and fourth PAAs and by e10.5-11.0 the bilaterally symmetrical PAA system is fully-formed and well-developed (Figure 1.6f) (Hiruma *et al.*, 2002). At this time the paired dorsal aortae can be divided into three segments – α, β and γ. The α-segment forms the region from the bifurcation of the paired vessels to the base of the sixth PAAs. The β-segment forms the region between

the fourth and sixth PAAs and the γ-segment (also known as the carotid duct) form the region between the third and fourth PAAs (Figure 1.6f).

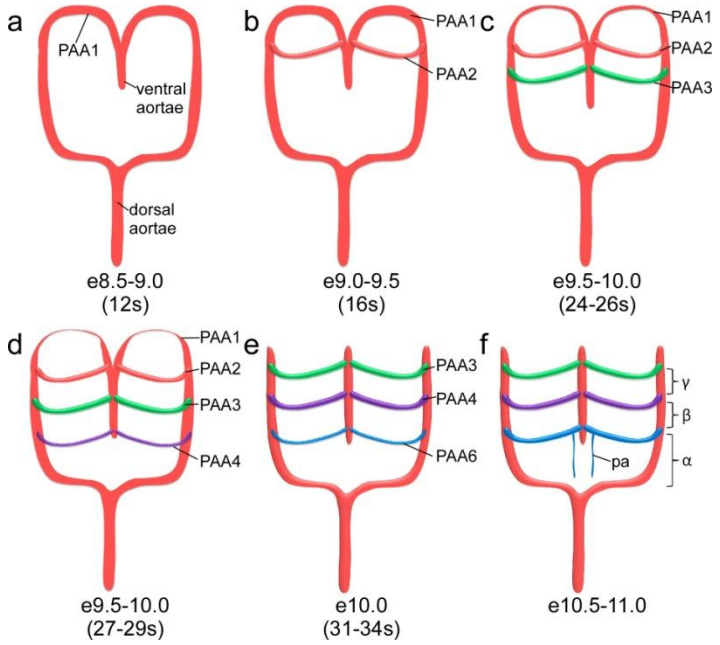

Figure 1.6: Development of the bilaterally symmetrical pharyngeal arch artery system.
(a) The first PAA (PAA1) forms as a loop between the dorsal and ventral aortae by the 12 somite (s) stage. (b) The second PAA (PAA2) is lumenised by the 16 somite stage. (c) By the 24-26 somite stage the first, second and third (PAA3) are fully formed. (d) The fourth PAA (PAA4) begins to form at the 27-29 somite stage and the first PAA begins to regress. (e) By 31-34 somites the first and second PAAs have fully regressed and the sixth PAA (PAA6) is beginning to form. (f) PAA formation is completed between e10.5 – e11.0. The third, fourth and sixth PAAs appear to be of equal size and three segments of the dorsal aortae (α, β and γ) can be distinguished. s, somite; pa, pulmonary artery.

There are two schools of thought on the mechanisms by which the PAAs form: angiogenesis and vasculogenesis. Angiogenesis is the process by which new vessels form from previously established vessels. Whereas, in a vasculogenesis model new vessels arise by the aggregation of nascent angioblast to form a string of endothelial cells, independently of other vessels. This endothelial string then joins to a pre-existing vessel before becoming lumenised to form the vessel. This mechanism is responsible for the formation of the primitive vasculature of the early embryo. Vessel formation then tends towards an angiogenic process, once the major vascular network has been established. The development of the PAAs lies in a somewhat grey area between these two processes, leading to much debate over how the vessels are produced (Anderson *et al.*, 2008; Li *et al.*, 2012).

Although the method of vascular casting has proven invaluable in demonstrating the timings of PAA formation, this technique is unable to identify the mechanisms of their

development. Vascular filling methods, such as the resin casting used by Hiruma *et al*. (2002), often suggest that the PAAs develop by an angiogenic mechanism, as they rely on the vessel being patent in order to take up the resin. Therefore, authors often describe the PAAs as forming from the dorsal aorta via angiogenesis, when in reality they are observing the luminisation of the vessels from each end. Studies of the formation of the pulmonary vasculature has demonstrated that the use of polymer casting is only able to detect patent vessels (Anderson-Berry *et al.*, 2005). This study used three techniques to investigate the development of the pulmonary vasculature in chicken embryos: vascular filling, histology and immunohistochemistry. Their results clearly demonstrate that neither histology, nor vascular filling methods were sensitive enough to identify vessels forming by vasculogenesis. However, the use of immunohistochemistry to detect the vascular endothelial growth factor (VEGF) and its receptor Flk-1 were able to identify coalescing angioblasts as expected during vasculogenesis.

Furthermore, recent work using immunohistochemistry of endothelial markers indicates that PAA formation occurs via vasculogenesis (Li *et al.*, 2012). This work demonstrates the aggregation of endothelial cells into a string, which later lumenises to form a patent PAA. In addition, confocal imaging of transgenic zebrafish embryos has yielded similar results. A fluorescent reporter driven by the zebrafish *flk1* promoter was used to visualise aortic arch development. The vessels were found to form from a cluster of endothelial cells between the dorsal and ventral aortae, which then grew out to join these vessels, followed by luminisation (Anderson *et al.*, 2008).

1.2.3.2. Remodelling

Once the PAAs have completed their formation at e11.0 they almost immediately begin remodelling to form the aortic arch of the mature heart (Figure 1.5b). The first and second PAAs regress into capillary beds and do not contribute to the final structure of the aortic arch. The third PAAs form the left and right common carotid arteries (LCC, RCC). The left fourth PAA forms part of the arch of the aorta between the LCC and left subclavian artery (LSA), and the right fourth arch artery forms the proximal region of the RSA. The sixth right PAA regresses and the sixth left forms the ductus arteriosus. The remodelling of the PAAs requires a complex array of cellular

processes, such as apoptosis, proliferation and differentiation, as well as other factors such as the rate of blood flow through the arteries (haemodynamics).

By e11.5-12.0 the proximal part of the aortic sac has septated into the aorta and pulmonary trunk and the pulmonary arteries begin to shift along the sixth PAAs to the site where the pulmonary trunk joins (Hiruma *et al.*, 2002) (Figure 1.7a). The OFT undergoes a 90° clockwise rotation, causing the sixth right PAA to lengthen and decrease in diameter. The reduced diameter of this vessel is thought to restrict the blood flow through the artery, which then leads to the regression of the vessel. This, in turn, reduces the blood flow through the α-segment of the right dorsal aorta, and this vessel often regresses immediately after the right sixth PAA (Yashiro *et al.*, 2007). Hiruma *et al*. (2002) report that the regression of the sixth right PAA begins at e11.5, closely followed by the loss of the right dorsal aorta by e12.5. At this time, the left and right carotid ducts, the γ-segments of the dorsal aortae, also begin to reduce in size and have fully regressed by e12.5 (Figure 1.7b) (Hiruma *et al.*, 2002). By e13.0 the α-segment of the right dorsal aorta has completely regressed (Figure 1.7c). The left fourth PAA now forms the aortic arch and the right horn of the aortic sac has become the brachiocephalic trunk. By e15.0 the remodelling process is complete (Figure 1.7d). The fourth right PAA forms the proximal portion of the RSA, which arises from the brachiocephalic trunk, and the right seventh intersegmental artery forms the distal portion. The sixth left PAA forms the ductus arteriosus and the left intersegmental artery has become the LSA.

Apoptosis is an important process in forming the asymmetric structure of the aortic arch. Molin *et al*. (2002) demonstrated that apoptosis begins in the mesenchyme surrounding the right dorsal aorta and right sixth PAAs immediately before the vessels regress. Apoptosis within the media of the vessel becomes more prominent as the vessel thins into a strand of SMCs before completely regressing. In addition, work in a rat model has also indicated an increased level of apoptosis surrounding the carotid ducts before they begin to regress (Molin *et al.*, 2004).

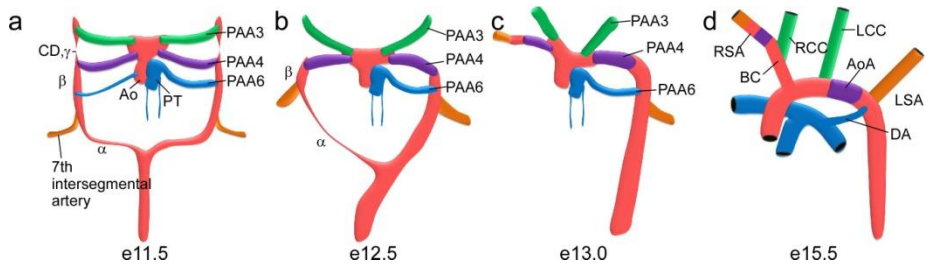

Figure 1.7: Pharyngeal arch artery remodelling.
(a) PAA remodelling begins at e11.5. The distal portion of the aortic sac becomes septated into the aorta (Ao) and pulmonary trunk (PT). The right sixth PAA and the γ-segment (carotid duct, CD) of the dorsal aorta on both sides begin to regress. The seventh intersegmental arteries, which will form the subclavian arteries, are now visible. (b) By e12.5 the carotid ducts and right sixth PAAs have completely regressed and the right α-segment of the dorsal aorta becomes very thin. (c) By e13.5 the α-segment of the right dorsal aorta has completely regressed. The right horn of the aortic sac forms the brachiocephalic trunk. (d) By e15.5 PAA remodelling is complete. Ao, aorta; PT, pulmonary trunk; CD, carotid duct; BC, brachiocephalic trunk; RSA, right subclavian artery; LSA, left subclavian artery; RCC, right common carotid artery; LCC, left common carotid artery; AoA, aortic arch; DA, ductus arteriosus.

1.2.3.3. Pharyngeal arch artery defects

The development of the PAAs is a very complex procedure, requiring the orchestration of many genes and processes in order to achieve the correct final aortic arch configuration. Therefore, it is unsurprising that perturbing these processes in any way can result in serious PAA malformations. Defects of the PAAs can develop either during the formation of the vessels (primary defect) or during the remodelling of the vessels into the mature aortic arch (secondary).

The most commonly identified defects appear to affect the fourth PAAs. Defects of the fourth left PAA are much more severe than defects affecting the development of the right fourth PAA. In the normal condition, the left fourth PAA provides the segment of the aortic arch, which lies between the LSA and the LCC. Absence of the left fourth PAA results in IAA type B (IAA-B), which prevents the blood from the ascending aorta entering the dorsal aorta and therefore, systemic flow (Figure 1.8a). Embryos carrying this malformation are often able to survive until birth and for a number of hours afterwards, as the ductus arteriosus provides blood to the dorsal aorta. However, shortly after birth the ductus arteriosus closes, preventing blood entering the systemic flow and resulting in death.

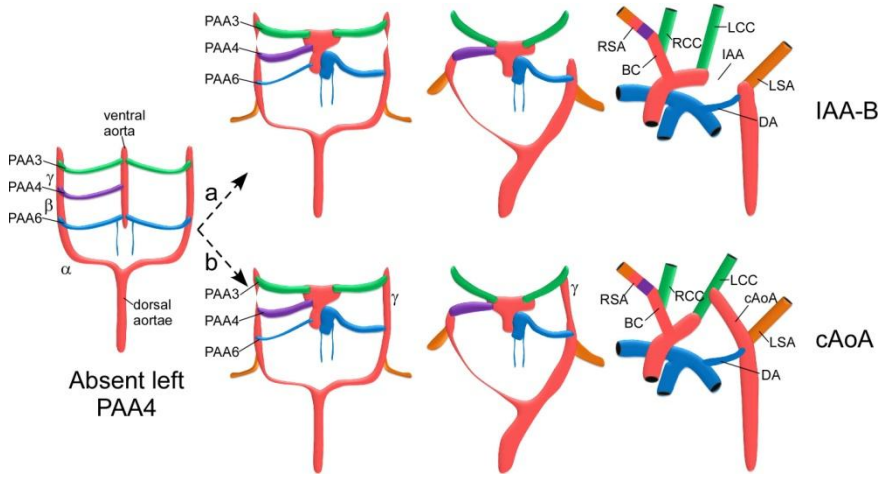

Figure 1.8: Defects of the left fourth PAAs.
Loss of the left fourth PAA results in two possible defects. (a) Loss of the left fourth PAA, with all remaining structures developing normally, results in an interruption between the LCC and LSA (IAA-B). (b) Loss of the left fourth PAA, accompanied by the persistence of the left carotid duct, results a cAoA in which the persistent carotid duct forms the connection between the ventral and dorsal aortae.

Another defect which can result from the absence of the fourth left PAA is a cervical aortic arch (cAoA). The left carotid duct persists in the absence of the fourth left PAA to produce an aortic arch which arises from the LCC at a more distal position (Figure 1.8b).

Defects of the right fourth PAA are often asymptomatic. In the normal condition the RSA is formed by the fourth right PAA and the seventh intersegmental artery, connected by the β-segment of the right dorsal aorta. The loss of the fourth right PAA can result in three altered routes for the formation of the RSA, as first described by Kutsche and van Mierop in 1984. This work investigated the anomalous origin of the RSA in infants with IAA-B, under the assumption that RSA defects primarily occur when the fourth PAAs are bilaterally absent. This study found that the most common route is an A-RSA, in which the RSA forms in a retroesophageal position. In this case the α-segment of the right dorsal aorta aberrantly persists, and passes behind the oesophagus to form the connection between the aortic arch and the seventh intersegmental artery (Kutsche and Van Mierop, 1984) (Figure 1.9a).

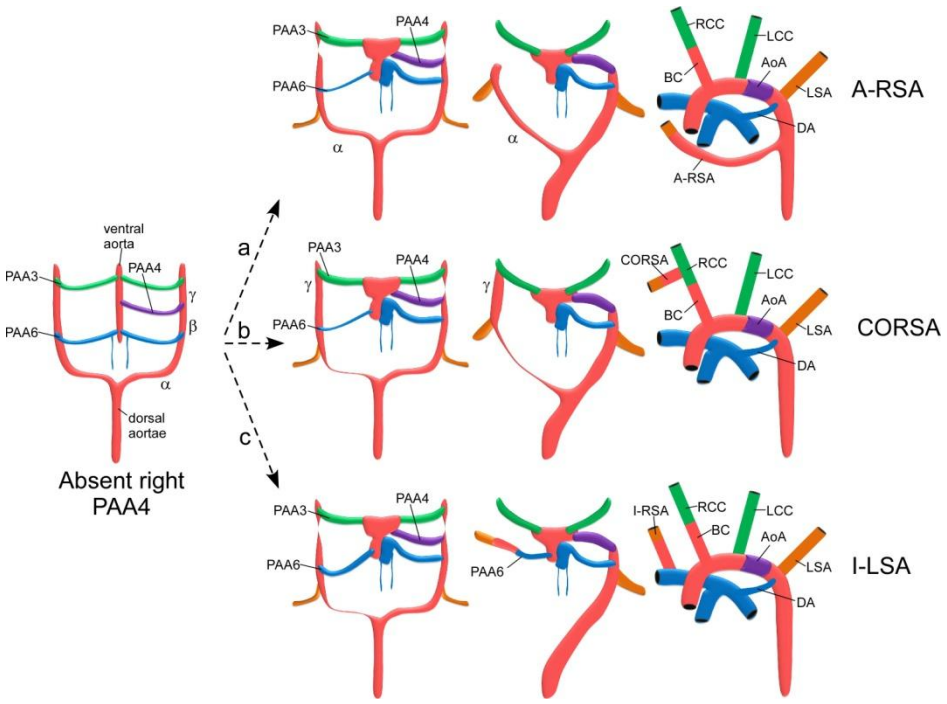

Figure 1.9: Defects of the right fourth PAAs.
Loss of the right fourth PAA results in three possible routes for RSA development. (a) Loss of the right fourth PAA accompanied by the persistence of the right α-segment of the dorsal aorta results in an A-RSA. (b) Loss of the right fourth right PAA accompanied by persistence of the right carotid duct results in CORSA in which the RSA arise from the RCC at a cervical position. (c) Loss of the right fourth PAA accompanied by the persistence of the right sixth PAA results in an I-LSA, in which the RSA arises from the pulmonary artery.

The next most common route for the RSA was arising from a more cervical position along the brachiocephalic trunk, at the point where the RCC bifurcates into the internal and external common carotid arteries. From here the vessel descends into the right arm. This defect occurs when the right carotid duct persists and joins the seventh intersegmental artery to the brachiocephalic trunk. This defect is known as cervical origin of the RSA (CORSA) due to the position in which the RSA arises (Figure 1.9b). The final and least common route for the RSA is arising from the pulmonary artery. In this system the right sixth PAA fails to regress and joins the seventh intersegmental artery to the blood flow from the aortic sac (Kutsche and Van Mierop, 1984) (Figure 1.9c). This study demonstrated that in the presence of IAA that two thirds (66%) of infants also carried RSA defects.

The PAAs pass through two main phases of development before reaching the final aortic arch configuration. These two phases, as described above, are formation and remodelling; and perturbation of the normal developmental pathways at either of these stages can cause severe disruptions to the correct formation of the aortic arch. During the formation stages, reduced aggregation of endothelial cells to form the

initial endothelial tube of the vessel, reduced NCC migration to the PAs or NCC differentiation into SMCs may all contribute to PAA defects. Later, in the remodelling stages, apoptosis and haemodynamic changes are the key to correct development, and aberrant patterns of apoptosis within the vessel walls may lead to abnormal regression or persistence of specific segments of the aortic arch.

1.3. Neural crest cells

A major event in the development of the heart involves the migration of the NCCs into the PAs and OFT. The neural crest (NC) is a transient structure, which assembles between the surface ectoderm and the neural tube of the embryo as these two structures contact each other. The concentrations of BMPs in the interacting tissues are crucial to the initiation of NC formation: the neural plate contains much lower levels of this paracrine factor than the ectoderm and the NC forms at intermediate concentrations. NCCs are a pluripotent population, which migrate from the neural tube to multiple areas of the body, where they differentiate and contribute to various structures. The fate of each cell is defined by the position of the cell along the anterior/posterior axis of the developing embryo and the region to which it migrates (reviewed in Hutson and Kirby, 2003; Snider *et al.*, 2007).

The NC is vital for cardiovascular development, and disruptions of this cell type are thought to be responsible for a number of congenital cardiac abnormalities. Following the formation of the NC, the cells undergo EMT before migrating to their required locations. Epithelium is composed of polarised cells, joined at adherens junctions consisting of E-cadherin, catenins and actin rings, and tight junctions. During EMT, EMT-inducing genes, such as Sox9, Foxd3 and Snail, are activated and E-cadherin is targeted for degradation, resulting in a loss of polarisation. The basement membrane is broken down and the cytoskeleton of the cell is rearranged to allow the NCCs to delaminate from the neural tube (Acloque *et al*., 2009).

The cardiac NCCs migrate from the dorsal neural tube to the PAs, where they differentiate into SMCs investing the tunica media of the PAAs. A sub-population continues to migrate into the OFT. Once in the OFT the condensed mesenchyme migrates inwards initiating the formation of the aorticopulmonary septum, separating

the aorta from the pulmonary trunk (reviewed in Hutson and Kirby, 2003; Snider *et al.*, 2007).

1.3.1. Pharyngeal arch arteries

Lineage tracing experiments in mice have been used to identify the route of the NCCs to the heart (Jiang *et al.*, 2000). NCCs infiltrate the PAs, and by e9.5 were found within the PA mesenchyme, but not in the endoderm, ectoderm or vascular endothelium. The presence of the NCCs in the walls of the ductus arteriosus, ascending aorta, LCC and RCC arteries was also demonstrated at e15.5. However, the dorsal aortae and pulmonary trunk are devoid of NCCs at this time. In the adult mouse, NCC-derivatives remain in the vessel wall of the PAA-derivatives: the aortic arch, LCC, RCC, the brachiocephalic trunk and the proximal portions of the LSA and RSA. The distal regions of the subclavian arteries, which are derived from the seventh intersegmental vessels do not carry any NCCs (Jiang *et al.*, 2000).

This work is in-keeping with two previous studies, which propose a NCC-origin of the SMCs surrounding these vessels in the chicken embryo (Topouzis and Majesky, 1996; Bergwerff *et al.*, 1998). These studies demonstrate that the ascending aorta, LCC, RCC, ductus arteriosus and the proximal LSA and RSA are surrounded by NCC-derived SMCs after the remodelling process. The authors also demonstrate a sharp boundary between the NCC-derived SMC of the fourth and sixth PAA, with the mesodermally-derived SMCs of the dorsal aorta. However, the carotid ducts show some NCC contribution to their SMCs (Bergwerff *et al.*, 1998).

The NCCs are important in the stabilisation of the vessels, required for remodelling. This is due to their differentiation into SMCs, which then secrete extracellular matrix (ECM) proteins, which are also required in the stabilisation of the arteries (Waldo *et al.*, 1996).

The processes by which NCCs differentiate into SMCs are not well understood, however, many genes have been implicated as playing a cell-autonomous role within the NCCs for correct migration, survival and differentiation to SMCs. For sexample, NCC-specific deletion of the histone deacetylase 3 gene (*Hdac3*) reduces the amount of SMCs and the expression of the Notch receptor Jagged-1, surrounding the fourth

PAAs, resulting in hypoplasia or interruption of the aortic arch at later stages (Singh *et al.*, 2011). Additionally, defective SMC differentiation is seen in the *Df1* heterozygotes, a mouse model of the 22q11 deletion syndrome (22q11DS) in humans (Lindsay and Baldini, 2001). The authors demonstrated normal migration of the NCCs and comparable levels of apoptosis to control mice in these mutants.

1.3.2. Outflow tract development

The majority of work on understanding the role of NCCs in OFT septation has been carried out in quail-chicken chimeras. The OFT is separated by the aorticopulmonary septal complex into the aorta and pulmonary trunk. The aorticopulmonary septal complex consists of condensed NC-derived mesenchyme (mostly derived from the fourth PA (Phillips *et al.*, 1987)), which forms an inverted 'U' shape within the aortic sac, separating the aorta and pulmonary trunk. Septation proceeds caudally towards the ventricles in a spiral pattern, separating the great vessels and causing their lumens to rotate around each other. OFT septation is completed by the fusion of the septum with the endocardial cushions of the AV canal and the interventricular septum (Waldo *et al.*, 1998).

OFT septation in the mouse is thought to occur in much the same way, as demonstrated by NC lineage tracing experiments. At e9.5, the NCCs begin to infiltrate the OFT of the heart, and by e11.5 are involved in the formation of the aorticopulmonary septum complex (Jiang *et al.*, 2000).

1.3.3. Cardiac neural crest ablation phenotype

Much of our understanding of the role of the NCCs in cardiovascular development comes from studies in which the NCCs have been ablated, and the effects of losing the NCCs examined. The majority of this work has been carried out in the chicken embryo due to the easy access to the neural tube; however, more recently new strategies for NCC-ablation in mouse have come into practise.

1.3.3.1. Chicken

Although the formation of the heart in the chicken is very similar to that of the mouse, the development of the aortic arch arteries varies somewhat. The chicken develops a right-sided aortic arch, with two brachiocephalic arteries and a ductus arteriosus on each side. The third PAAs of the chicken produce a brachiocephalic artery on either

side, which gives rise to a subclavian artery and a common carotid artery. The right fourth PAA gives rise to the arch of the aorta, while the left fourth PAA regresses. The distal portion of each sixth vessel forms the bilateral ductus arteriosi (Bergwerff *et al.*, 1998).

Initial studies using quail-chicken chimeras indicated that the NCCs between the otocyst and the caudal boundary of somite 3 are required to migrate through the PAs, and into the OFT of the heart. This population of NCCs became known as the 'cardiac' NCCs for this reason (Kirby *et al.*, 1985). Therefore, early studies investigated the ablation of this region, either bilaterally or unilaterally, and identified high proportions of embryos with VSD and PTA. In addition, smaller deletions – ablating only a single somite region unilaterally – also uncovered further, less severe OFT defects such as DORV and OA, which were grouped together in many of the subsequent studies as dextroposed aorta (DPA). It was also found that bilateral deletion of a region encompassing two somites (somites 1-2 or 2-3) resulted in 100% penetrance of PTA and VSD, while unilateral deletion of the same regions also gives rise to DORV in 40% cases. Additionally, bilateral deletion of the NCCs associated with somite 1 results in 100% DORV, while the penetrance of VSD was reduced to 80% (Besson *et al.*, 1986). Although this study was very small (n=5) in comparison to many other NCC-ablation experiments, it lead to the suggestion that DORV was caused by a small unilateral lesion of a single somite within the cardiac NC region, or a larger ablation in the pre-otic, or 'non-cardiac' NC. PTA, on the other-hand, was proposed to result from larger deletions of the cardiac NCCs – either encompassing a single somite bilaterally, or multiple somites unilaterally or bilaterally (Kirby, 1987).

As discussed above the septation of the OFT involves the cardiac NCCs and it is, therefore, quite clear that the removal of this important population of cells, or even a large proportion of these cells results in the aorticopulmonary septation complex being unable to septate the OFT. However, in the DPA phenotype, OFT septation occurs normally, but the vessels do not align properly with the correct ventricles. Insight into the role of the NCCs in this process came from the identification that the OFT of NCC-ablated embryos was shortened (Yelbuz *et al.*, 2002). This group examined the incorporation of the cells of the SHF into the OFT myocardium and found a significant

reduction within those embryos that underwent NCC-ablation. This suggests that the SHF cells are important in the elongation of the OFT in order for correct looping and alignment with the ventricles to occur. It is likely that the NCCs are required in this region to secrete signalling molecules which attract the SHF cells into the OFT (Yelbuz *et al.*, 2002). It has also been suggested that DPA and VSDs are the result of a haemodynamic effect, as these also occur with ablations of the non-cardiac NCCs (Kirby, 1987).

In addition to the high prevalence of intracardiac and OFT anomalies found in NCC-ablated embryos, there is also a high incidence of PAA defects including persistent left fourth PAA and absence or anomalous origin of the subclavian arteries. The highest rate of CCVM occurs when the NCC-ablation covers the region of NCCs destined for the fourth PA (somites 1-2), with 95.2% embryos having some form of cardiac anomaly. Ablation of the somite 1-3 region, which also encompasses the NCCs which will migrate to the sixth PAs, resulted in 100% penetrance of CCVM. Hypoplasia or aplasia of the third, fourth and sixth PAAs also occur most frequently in these embryos. Interestingly, defects of the sixth PAA were not present when NCCs destined for this arch alone were ablated. In most cases, where a defect of the fourth right PAA was observed, the vessel was absent and an OFT defect was also observed. In a number of cases the fourth left PAA persisted to act as a substitute aortic arch. In other cases only remnants of this vessel were observed (Nishibatake *et al.*, 1987).

It was later demonstrated using quail embryos that the NCCs are not required in the formation of these vessels, but in their stabilisation. Waldo *et al.* (1996) demonstrated that the NCCs are required to separate the developing vessel from the endoderm of the PA, but that this process occurs once the vessel has already begun to lumenise. The ablation of the NCCs causes a reduction in the size of the developing PA and also results in a misshapen vessel, which remains in contact with the endoderm, and in some cases the ectoderm, throughout the entire length of the PA. The loss of the NCC-derived ectomesenchymal sheath surrounding the third PAA resulted in asymmetry of these vessels, with a hypoplastic or collapsed third vessel occurring on one side while the other side was unusually large. These defects occur prior to the formation of the tunica media by the NCCs, which suggests that the NCCs are also required to stabilise

the vessels before differentiating into SMCs, in order to support the vessel as blood flow increases. This supporting role may involve the deposition of an elastic ECM by these cells (Waldo *et al.*, 1996).

Additionally, a number of NCC-ablated embryos also presented with extracardiac malformations including thoracic wall defects, hyoid and mandibular defects, exencephaly and microphthalmia. However, some of these defects are observed in sham-operated embryos at lower frequencies, and may therefore be partially attributed to the experimental procedure (Kirby *et al.*, 1985; Besson *et al.*, 1986; Nishibatake *et al.*, 1987).

Although NCC-ablation in chicken embryos has proved invaluable to our understanding of the role of NCCs in development, and in particular cardiovascular morphogenesis, the development of the heart in the chicken and in mammals varies, particularly in the formation of the aortic arch arteries. Therefore, the work already carried out in the chicken embryos should also be validated in the mouse. However, this is more difficult due to the *in utero* development of the mammalian embryo.

1.3.3.2. Mouse

The first study investigating NC ablation was carried out by inducing toxicity in those cells of the NC lineage (Porras and Brown, 2008). This study utilised NC-specific expression of the herpes simplex virus type 1 thymidine kinase (TK) suicide gene, which relies on the administration of the prodrug ganciclovir (GCV) in order to induce toxicity. TK expression causes susceptibility to GCV, which prevents the incorporation of guanosine residues into elongating DNA. Cells which are incapable of DNA synthesis undergo apoptosis. This therefore results in cell death, only in those cells having expressed TK and also receiving GCV.

GCV was administered to 3 groups, each with a different regimen. One group received a single injection at e7.5, which resulted in ablation of the cranial NCCs, but not the cardiac NCCs, as TK is not activated within that population at this time. The second group received two doses, at e7.5 and e8.5. The final group received an additional dose at e9.5. Of those in the single dose group, 52% developed normally, while the remaining 48% had VSDs. In addition, 10% also had DORV, and 19% had an OA.

Administration of a second dose at e8.5 resulted in only 32% embryos with normal cardiovascular development. Of those embryos with abnormal heart development 20% had DORV, 20% OA, 8% PTA and a further 20% had a VSD only. In addition, approximately 35% of embryos also had a PAA abnormality, including IAA, A-RSA and right aortic arch (RAA). In the final group, which received three injections of GCV, no embryos had normal cardiovascular development. 75% of these embryos had PTA, 10% OA and 15% DORV. In addition, all embryos of this group also had a PAA defect (Porras and Brown, 2008).

Another study of NCC-ablation in mouse used the diphtheria toxin fragment A (DTA) to induce toxicity in NCCs by interfering with RNA translation machinery and causing the cell to apoptose. Mouse mutants had 100% penetrance of PTA, although there was variability in the number of leaflets within the valve. Additionally, a number of PAA malformations were identified in e10.5 mutant embryos. The authors failed to describe these defects in detail, but indicate that a number of embryos display aberrant regression of vessels required in the final aortic arch structure, while other vessels that would normally regress were persistent (Olaopa *et al.*, 2011).

1.3.4. Signalling between NCCs and other cell types

The survival and the migration of the NCCs into the PAs is affected by signalling molecules originating from the surrounding tissues. The first step in the migration of the NCCs is their delamination from the neural tube, caused by repulsive semaphorin signalling from the neural tube. Signalling from the pharyngeal ectoderm then attracts the NCCs into the PAs. From here they are drawn to the developing OFT by signals originating in the SHF-derived myocardium, where they participate in the formation of the aorticopulmonary septum. Any disruptions to the signalling pathways required in the migration and survival of the NCCs can cause severe cardiovascular defects.

1.3.4.1. Second Heart Field

The NCCs require signalling cues to migrate into the cardiac OFT. These signals originate from the SHF-derived myocardium of the OFT and are received by the NCCs within the PAs, causing them to migrate into the OFT and initiate the formation of the aorticopulmonary septum.

Semaphorin3C (Sema3C) signals have been shown to attract NCCs and aid in their migration, as demonstrated by *in vitro* migration assays (Toyofuku *et al.*, 2008). In addition, *Sema3C* is expressed within the myocardium of the proximal OFT and the PA mesenchyme at e10.5, with expression also becoming evident in the aorticopulmonary septation complex by e12.5 (Feiner *et al.*, 2001). During this time the NCCs express the semaphorin co-receptor PlexinA2 (Brown *et al.*, 2001), suggesting an involvement of semaphorin signalling in NCC migration to the OFT.

Further evidence for the role of semaphorins in NCC migration comes from *Sema3C* mutant mice. 75% of *Sema3C* null mice exhibit PTA, accompanied by a single semilunar valve with 4 cusps and a VSD (Feiner *et al.*, 2001). This phenotype is characteristic of NCC-ablation in chicken and mouse embryos (see section 1.3.3), strengthening the link between *Sema3C* expression in the OFT and infiltration of NCCs into this region.

Work in chicken embryos suggests that the semaphorin receptor PlexinA2, expressed by NCCs, is responsible for receiving repulsive signals. *Sema6A* and *Sema6B* secreted from the neural tube are thought to cause the NCCs to delaminate from the neural tube and migrate away from this area. Additionally, these authors demonstrate that PlexinD2, in a heterodimeric complex with neuropilin-1, receive the SHF-derived *Sema3C* signals, which attract the NCCs to the OFT (Toyofuku *et al.*, 2008). This work demonstrates the multitude of heterodimer receptors that are used in semaphorin signalling and that the outcome of this signalling can differ depending on both the signalling molecule and the combination of co-receptors involved. As the NC-derived dorsal root ganglia remain unaffected in the *Sema3C* mutant mice, it has also been suggested that an as yet unidentified cardiac NCC-specific *Sema3C* co-receptor may exist within these cells (Brown *et al.*, 2001).

1.3.4.2. Pharyngeal Surface Ectoderm

The pharyngeal surface ectoderm (PSE) produces signals which affect the NCCs as they migrate through the PAs. The signalling pathways so far identified include FGFs, endothelins and sonic hedgehog. *Fgf8* has been identified as the main component of the FGF family that is involved in signalling from the pharyngeal ectoderm to the NCCs. *Fgf8* is expressed in the pharyngeal ectoderm and endoderm, and hypomorphic

mutations in the gene results in 100% penetrance of ASD and VSD. OFT defects, such as DORV and PTA, and PAA defects such as IAA and abnormalities of the RSA are also observed with lower penetrance (Abu-Issa *et al.*, 2002). The PAA defects are attributed to the loss or hypoplasia of the fourth PAAs as a result of disruptions to the NCCs. The authors demonstrate apoptosis of the NCCs within the PAs (Abu-Issa *et al.*, 2002), which could reduce the stability of the PAAs, causing aberrant regression of these vessels.

The *Fgf8* receptors, *FGFR1* and *FGFR3*, are expressed within the NCCs and are thought to be required in NCC migration. Plating NCCs onto *Fgf8 in vitro,* increased their migratory capacity, while inhibition of FGFR1 both *in vitro* and *in vivo* reduced migration (Sato *et al.*, 2011), indicating that this pathway may be required in NCC migration and survival within the PAs.

The *Fgf8* signal required in NCC migration to the PAs originates from the pharyngeal ectoderm. Tissue-specific removal of *Fgf8* from the ectoderm, phenocopies the fourth PAA defects seen in hypomorphs, suggesting that the pharyngeal ectoderm-derived *Fgf8* is required in fourth PAA formation and development (Macatee *et al.*, 2003).

A further signalling pathway, thought to mediate interactions between the pharyngeal ectoderm and the NCCs, is the endothelin pathway. The *Edn-1* gene which encodes endothelin-1 (ET-1) is expressed within the surface ectoderm and paraxial mesoderm of the PAs, while the endothelin receptor (ET_A) is expressed within the NCCs (Yanagisawa *et al.*, 1998a; Clouthier *et al.*, 1998). Mutations disrupting these genes result in PAA defects, such as IAA and absent RSA. In addition, many mutants have VSDs and OFT defects, such as OA, DORV, PTA and TGA (Kurihara *et al.*, 1995; Clouthier *et al.*, 1998; Yanagisawa *et al.*, 1998a). As these mutations do not affect the formation of the vessels, it is likely that the observed defects are due to reduced proliferation or differentiation of the NCCs or increased apoptosis, although the exact mechanism has not yet been described. This would reduce the number of NCCs within the PAs which results in reduced mesenchymal support for the vessels, and therefore aberrant regression of the vessel.

This work therefore demonstrates the importance of signalling between the surface ectoderm and other surrounding tissues to the NCCs. Loss of any element of these signalling pathways inhibits correct NCC development.

1.4. AP-2α

Activator protein 2α (AP-2α) was the first characterised member of the AP-2 family of transcription factors, which also consists of AP-2β, -γ,-δ and – ε (see Table 1-1 for a summary of AP-2 family genes in mice, humans and zebrafish). These proteins are localised to the nucleus where they activate specific genes, resulting in the increased proliferation and decreased differentiation of the cells (Pfisterer *et al.*, 2002). In the mouse, AP-2α, -β and –γ are co-expressed during embryonic development in the limb and facial mesenchyme, the trophectoderm, the peripheral nervous system and the NCCs (Mitchell *et al.*, 1991; Moser *et al.*, 1995; Chazaud *et al.*, 1996).

Table 1-1: Summary of AP-2 family members in mice, humans and zebrafish.

Gene name	Species	No. of exons	Chromosome
AP-2α			
Tcfap2a	Mouse	7	13
TFAP2A	Human	7	6
tfap2a	Zebrafish	7	24
AP-2β			
Tcfap2b	Mouse	7	1
TFAP2B	Human	7	6
tfap2b	Zebrafish	7	20
AP-2γ			
Tcfap2c	Mouse	7	2
TFAP2C	Human	7	20
tfap2c	Zebrafish	7	6
AP-2δ			
Tcfap2d	Mouse	8	1
TFAP2D	Human	8	6
tfap2d	Zebrafish	8	20
AP-2ε			
Tcfap2e	Mouse	7	4
TFAP2E	Human	7	1
tfap2e	Zebrafish	6	19

AP-2α was discovered in 1987 (Mitchell *et al.*, 1987), and was later found to be associated with the development of multiple organs such as the kidneys, heart and eyes, in addition to limb and skeletal development. A homozygous deletion of the murine AP-2α gene (*Tcfap2a*) results in severe craniofacial defects, thoracic wall defects and neural tube closure defects. In addition, defects in the development of the kidneys, cranial ganglia and skeleton were also observed (Schorle *et al.*, 1996; Zhang *et al.*, 1996). A wide range of cardiovascular defects have also been identified (Brewer *et al.*, 2002). These include OFT defects, such as DORV, PTA and occasionally cases of TOF. In addition, PAA defects such as A-RSA, IAA-B, right dorsal aorta, pulmonary stenosis and pulmonary atresia, were also observed.

1.4.1. AP-2α structure

AP-2α is a 48 kilo Dalton (kDa) transcription factor, which was first identified due to its association with viral and cellular enhancer elements (Mitchell *et al.*, 1987). The gene consists of seven exons, spanning 18 kb of genomic DNA. The protein consists of three major motifs: a transactivation domain, a basic region and a helix-span-helix motif (Williams and Tjian, 1991a; Williams and Tjian, 1991b) (Figure 1.10). The basic region and helix-span-helix domains are responsible for the DNA binding and dimerisation abilities of the transcription factor.

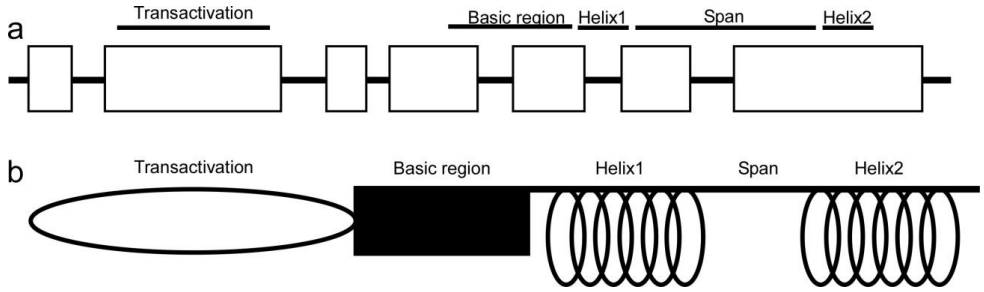

Figure 1.10: The structure of the *Tcfap2a* gene and AP-2α protein.
(a) The *Tcfap2a* gene consists of seven exons. The structural domains of the protein contributed by each exon are indicated above. (b) The AP-2α protein is composed of three main domains. The transactivation domain is involved in the binding of coactivator molecules. The basic region forms the DNA-binding domain of the protein. The dimerisation domain is composed by two α-helices separated by a short span of amino acids.

1.4.1.1. Transactivation domain

The transactivation domain of AP-2α consists of a proline and glutamine rich region within the N-terminal half of the protein, encoded entirely by exon 2 of the genomic sequence (Williams and Tjian, 1991a; Wankhade *et al.*, 2000). This region is responsible for recruiting coactivators to the protein in order to induce transcriptional activation.

1.4.1.2. DNA binding and dimerisation domains

The DNA binding and dimerisation domains consist of a basic helix-span-helix (bHSH) motif, formed by a 200 amino acid region at the C-terminus of the protein. The basic region is rich in positively charged amino acids and is responsible for the DNA binding activity of the transcription factor. The following HSH motif is composed of two amphipathic α-helices, separated by a span of around 80 amino acids, which is required for both dimerisation and DNA binding of the protein. The amphipathic nature of the helices causes the hydrophobic and hydrophilic residues to be orientated on opposing sides of the structure, therefore aiding in dimer formation. The HSH motif is unique to members of the AP-2 family of transcription factors. It differs from other motifs such as the helix-turn-helix and helix-loop-helix motifs in the number of residues separating the two α-helices (Williams and Tjian, 1991b). This structure is similar to the design of other DNA-binding and dimerisation motifs known as leucine zippers, which are found within many transcription factors. The leucine zipper motif is comprised of a helix with leucine residues spanning out from one face of the helix. Proteins containing this motif interact with each other through these leucine residues by forming a coiled-coil structure around each other. In these transcription factors, a string of basic amino acids is found directly adjacent to this helix and both regions are required for the DNA-binding activity of the dimer (Abel and Maniatis, 1989; Jones, 1990). It is suggested that the bHSH motif in AP-2α function in much the same way. Deletions within the basic region of AP-2α result in a protein which was able to dimerise with wild type AP-2α, but unable to bind DNA to stimulate transcription or form a homodimer, while mutations within the HSH domain result in a protein which is unable to dimerise or bind DNA (Williams and Tjian, 1991b).

1.4.2. AP-2α function

The transcription factor AP-2α has been linked with multiple cellular processes such as apoptosis and proliferation and has been found to be important in the development of many structures throughout the embryo. The role of this protein in cell death and proliferation has made it a target in many studies of cancer and it has found to be both repressive and inductive in different types of cancer.

The AP-2α recognition site, found within many viral and cellular enhancer elements, is a dyad repeat with the consensus sequence 5’ – GN_4GGG – 3’ (Williams and Tjian,

1991a). AP-2α is also capable of binding to various G/C rich regions with differing affinities (Eckert *et al.*, 2005). The repetition of this binding sequence on the complementary strand is consistent with AP-2α binding DNA as a dimer (Williams and Tjian, 1991a). This binding sequence is also found in the promoter region of the *TFAP2A* gene (at position -622 with respect to the ATG), suggesting this gene is positively regulated by its own product, or other AP-2 family members. It has also been suggested that the first exon of the gene is capable of negative regulation in the protein, as deletion of the first 51 amino acids resulted in transcriptional upregulation of the gene (Bauer *et al.*, 1994).

1.4.2.1. AP-2α in neural crest cells

The role of the transcription factor AP-2α in the NCCs of mammals has not been fully elucidated. In mice, the loss of *Tcfap2a* impacts on many derivatives of the NCCs, such as pigmentation, neurofilament development, the formation of multiple craniofacial bones and the fusion of the neural tube (Zhang *et al.*, 1996). This is also true of zebrafish mutations in the AP-2α gene (*tfap2a*), which causes reduced pigmentation at the 24 hours post fertilisation (hpf) stage and reduction in the size and organisation of the craniofacial bones and cartilaginous elements (Knight *et al.*, 2003; Knight *et al.*, 2004).

Work on the role of AP-2α in *Xenopus laevis* has identified a potential role in the induction of the NC from the surrounding ectoderm and epidermis (Luo *et al.*, 2002; Luo *et al.*, 2003; de Croze *et al.*, 2011). Morpholino-mediated knockdown of AP-2α followed by *in situ* hybridisation has demonstrated the reduced expression of both neural plate border (NB) specifying genes (e.g., *Msx1*, *Pax3*, *Zic1* and *Hairy2*) and NC specifying genes (e.g., *FoxD3*, *Sox10*, *Sox9* and *Snail2*/*Slug*). Furthermore, these embryos show an expansion of the neural plate marker *Sox2* expression domain, demonstrating that the failure of NB specification results in the tissue being specified as neural plate instead. Treatment of neuralised ectoderm (treated with either noggin or chordin) with AP-2α RNA, was sufficient to induce the full complement of NB specifying genes and rescue NC formation. It was also shown that the neuralisation of these tissues causes the repression of neural plate markers *Sox2* and *Otx2*. AP-2α gain of function at mid-neurula (stages 12-14 in *Xenopus*) demonstrated activation of NC-specifying genes, without further expansion of the neural border, therefore suggesting

a second role of AP-2α in NC-specification, independent of its role in NB-specification (Luo *et al.*, 2003; de Croze *et al.*, 2011).

As AP-2α plays such an important role in the formation of the neural crest in *Xenopus*, it has been proposed that the phenotype in AP-2α mutant mice may be the result of loss of NC-specification, rather than reduced migration or differentiation of the specified NC (Luo *et al.*, 2003). However, both Zhang *et al*. (1996) and Schorle *et al.* (1996), have demonstrated the normal migration of NCCs in *Tcfap2a*$^{-/-}$ mouse embryos, therefore, indicating the role of AP-2α in the mammalian NC differs from that of *Xenopus*. Furthermore, work on a zebrafish mutant of *tfap2a* (*lockjaw*, *low*) demonstrates that many of the NB and NC-specifier genes (*Pax3*, *Sox9b*, *Snail2/slug* and *Foxd3*) showing reduced expression in the *Xenopus* knockdown model are only marginally affected, if at all, in zebrafish (Knight *et al.*, 2003). At later, mid-migratory, stages (14-18 hpf, 12 somites) the expression of *Sox9b* becomes severely reduced, while other NC-markers remain unaffected. By 26 hpf, genes associated with melanocyte precursors, *dopachome tautomerase* (*dct*) and *kit*, are severely reduced in the post-otic NCCs. Additionally, the cranial ganglia, sympathetic neurons and NC-derived enteric neurons are all disrupted in *low* mutants at 72 hpf. The authors demonstrate, through fluorescent dye fate-mapping, that the NCCs are able to migrate to the PAs, but show a 3-9-fold increase in apoptosis in mutant embryos, suggesting that *tfap2a* is required in the survival, rather than specification of a subset of NCCs (Knight *et al.*, 2003).

Additionally, the specification and migration of NCCs appears unaffected in *Tcfap2a* mutant mice, where the path of the migrating NC has been followed using HNK-1 staining and a *Wnt1* promoter driving expression of LacZ. However, increased apoptosis again appears to be a clear consequence of the loss of *Tcfap2a*, with elevations in cell death being seen in the trigeminal ganglia and first PA at e9.0-9.5, and in the facial region at e12.5 (Schorle *et al.*, 1996; Zhang *et al.*, 1996).

1.4.2.2. AP-2α in cancer and disease

AP-2α is an important transcription factor associated with activation and repression of many genes. Disruption of the human *TFAP2A* gene has been implicated in many cancers, including melanomas (Huang *et al.*, 1998) and breast carcinomas (Bosher *et*

al., 1995). AP-2α was elevated in a number of mammary cell lines overexpressing the oncogene *ErbB2*, and was found to bind directly to the *ErbB2* promoter by DNA fingerprinting (Bosher *et al.*, 1995). AP-2α upregulation was also found to synchronise with *c-KIT* activation in a number of human melanoma lines. In addition, loss of AP-2α expression correlated with a loss of c-KIT activation (Huang *et al.*, 1998). c-KIT is known to activate downstream signalling pathways such as the PI3 kinase and MAP kinase pathways, which result in an increase in proliferation (Joensuu and Dimitrijevic, 2001). Luciferase assays demonstrated the specific and dose-dependent upregulation of c-KIT by AP-2α, with a loss of this regulation in the presence of a dominant negative AP-2 protein (Huang *et al.*, 1998).

A further link between AP-2α and cancer comes from its role in the regulation of p21, a cell-cycle exit protein involved in terminal differentiation. AP-2α was found to directly bind to the p21 promoter and is capable of activating the gene through this site. Furthermore, mutagenesis of the AP-2α binding site inhibited transcription of p21 (Zeng *et al.*, 1997), implicating AP-2α in the regulation of cell growth and in the activation of terminal differentiation.

In addition, AP-2α is capable of negatively regulating the oncogene c-myc, which is involved in various types of cancers. Wild type AP-2α can competitively inhibit c-myc function by binding to AP-2 binding sequences which overlap with the myc response element on many target genes. It is also capable of directly interacting with the DNA binding and dimerisation domains of the myc proteins via its own bHSH motif, impairing the DNA binding of the myc/max heterodimer to target genes (Gaubatz *et al.*, 1995). Furthermore, AP-2α and another AP-2 family member, AP-2β have been shown to inhibit c-myc-induced apoptosis in culture (Moser *et al.*, 1997a).

Angiogenesis is an important process in tumourigenesis as it generates a blood supply to support the tumour which allows it to survive and grow. An important gene in this process is VEGF (Leung *et al.*, 1989). AP-2α has been implicated in transforming growth factor (TGF)-α-mediated regulation of VEGF, through luciferase and gel-shift assays (Gille *et al.*, 1997).

In the later stages of cancer, as a tumour proceeds from benign to malignant, a number of protease genes become reactivated and are secreted from the cancer cells in order to break down the ECM. This breakdown of the ECM, including the basement membrane, allows the metastatic cells to migrate to other areas of the body. These proteases are also secreted to allow the metastatic cells access to new tissues of the body. Studies have implicated AP-2α in the regulation of this process through activation of matrix metalloproteinase (MMP)-2 (Frisch and Morisaki, 1990) and inhibition of the ECM protein Aggrecan (Tuli *et al.*, 2002).

Overall, the work described above implicates AP-2α in the activation of proliferation and both positive and negative regulation of apoptotic pathways in addition to the inhibition of ECM deposition and activation of ECM degradation. This infers that AP-2α may play a role as both a tumour suppressor and an oncogene, dependent on the type of cancer under investigation.

1.4.2.3. The role of transcriptional targets in cardiovascular development

Although the majority of studies investigating the transcriptional targets of AP-2α have intended to understand its role in cancer progression and development, many of the processes involved can be transferred to cardiovascular development. This work has identified significant involvement of AP-2α in basic cellular processes such as proliferation, apoptosis and differentiation, which play major roles in cardiovascular development. Additionally, many of the target genes discussed above have additional roles in cardiovascular development.

For example, *VEGF* and *ErbB2*, both of which are regulated by AP-2α (Bosher *et al.*, 1995; Gille *et al.*, 1997), are involved in ventricular trabeculation. *ErbB2* is also required in the development of the endocardial cushions of the OFT and AV canal (Camenisch *et al.*, 2002). VEGF is pivotal in both angiogenesis and vasculogenesis, and is therefore integral to the formation of the vasculature of the developing embryo. Deletion of 2 of 3 VEGF isoforms in mice results in severe malformations of the PAAs, including IAA, double aortic arch and persistence of the carotid duct segments of the dorsal aorta, which ordinarily regress during development. In addition, TOF was also observed in mutants only expressing the $VEGF^{120}$ isoform. Those mutants expressing

only $VEGF^{164}$ developed normally, suggesting this is the dominant isoform in cardiovascular development (Stalmans *et al.*, 2003).

It is therefore likely, as with many other cases in cancer, that mutations within *TFAP2A* in cancer cause a reactivation of early developmental pathways, many of which may be actively involved in cardiovascular development.

1.4.3. Coactivation

The transcriptional activation of target genes by AP-2α requires coactivator proteins. A number of coactivators have been implicated in the activation of AP-2 family members including two members of the CBP/p300 interacting transactivators with glutamic acid(E)/aspartic acid (D)-rich carboxy-terminal domain (CITED) family, Cited-2 and Cited-4 (Bamforth *et al.*, 2001) and Poly-(ADP-ribose) polymerase-1 (PARP-1) (Kannan *et al.*, 1999).

1.4.3.1. Cited2

Although there are multiple coactivator proteins capable of regulating AP-2α function most work has been carried out on the interaction of Cited2 with AP-2α. Cited2 is a ubiquitously-expressed, non-DNA binding transcription factor. Deficiencies in the mouse *Cited2* gene result in multiple cardiovascular defects, in addition to exencephaly, adrenal agenesis and abnormalities of the cranial ganglia. These embryos die during development, or soon after birth (Bamforth *et al.*, 2001).

Cardiac defects in *Cited2*$^{-/-}$ embryos included ASD, VSD, OA, DORV, PTA and RAA (Bamforth *et al.*, 2001). *Cited2* deficiency has also been shown to cause left-right patterning defects, such as cardiac looping defects and right isomerism on a C57BL/6J background. This phenotype was rescued on a mixed background, indicating the importance of genetic background on the penetrance of the phenotype (Bamforth *et al.*, 2004) . Further investigation of these laterality defects indicated a mechanism in which Cited2 acts upstream of *Pitx2*, an important gene in the determination of the left-right axis in mammals, to activate correct cardiovascular development (Bamforth *et al.*, 2004; Ryan *et al.*, 1998; Kitamura *et al.*, 1999).

CITED2 mutations have also been implicated in human CCVM. Seven mutations were identified only in patients with CCVM, three of which clustered within the serine-glycine-rich junction (SRJ) of the protein, suggesting a possible hotspot for *CITED2* mutations. Cardiovascular defects observed in patients with *CITED2* mutations were TOF, VSD, ASD, *situs inversus*, TGA and abnormal pulmonary venous return. These defects are somewhat similar to that seen in the *Cited2*$^{-/-}$ mouse model. Also, the role of *Cited2* in left-right patterning may explain the *situs inversus* observed in patients (Sperling *et al.*, 2005).

1.4.3.2. CBP/p300

Cited2 recruits the coactivators CBP/p300 to AP-2α in order to activate transcription. CBP and p300 are ubiquitously expressed and exhibit histone acetyl transferase (HAT) activity, which is involved in histone modification and also capable of acetylating transcription factors in order to modulate their functions (Kouzarides, 2000). Deletions of these proteins can result in cardiac, skeletal and neural tube closure defects (Yao *et al.*, 1998; Oike *et al.*, 1999). Functional studies have demonstrated that the Cited2 and p300/CBP complex bind to the transactivation domain of AP-2α, activating the transcriptional activity of the protein in a dose-dependent manner (Braganca *et al.*, 2003; Bamforth *et al.*, 2001). It has also been shown that p300 is capable of interacting with AP-2α independent of Cited2; however, this interaction alone is not sufficient to activate transcription, suggesting that this may be a secondary interaction required to stabilise the co-activation complex. Removal of the HAT domain from p300 inhibits this interaction, without affecting the DNA binding ability of AP-2α, indicating that the HAT domain of p300 is not required to modulate transcription factor function in this instance (Braganca *et al.*, 2003). *Cited2* deficiency prevents activation of AP-2α, however, this can be rescued by ectopic expression of *Cited2* (Bamforth *et al.*, 2001) further indicating the requirement for this protein in AP-2α activation.

1.4.4. AP-2α in development

Tcfap2a is frequently used as a marker of NCCs during their migration. It is also expressed in the developing kidney, the retina, the progress zone of the limb bud and the surface ectoderm (Brewer *et al.*, 2002). AP-2α is also required in the melanocytes in mice and zebrafish (Knight *et al.*, 2003; Brewer *et al.*, 2004).

In the mouse expression of *Tcfap2a* begins at e8.5 in the surface ectoderm and presumptive cranial NCCs, from the midbrain to the start of the hindbrain. By e9.5, expression was observed in the post-migratory NCCs that form the mesenchyme of PAs 1-3 and the pharyngeal ectoderm of these arches, but not the endoderm or vascular epithelium. Expression was also seen in the presumptive NCCs invading between the pharynx and distal OFT (Brewer *et al.*, 2002). At e10.5, expression was reduced in the first and second arch mesenchyme, however strong expression was seen in the surface ectoderm of these and more caudal arches. Expression was also observed in the distal OFT. By e11.5 expression becomes reduced throughout the embryo.

Tcfap2a$^{-/-}$ mice display a number of defects, affecting craniofacial morphogenesis, limb development, neural tube closure and cardiac development (Figure 1.11) (Schorle *et al.*, 1996; Zhang *et al.*, 1996; Brewer *et al.*, 2002). These defects affect the viability of the mouse post-parturition, and mutant embryos generally die at or before birth, as a result of these congenital defects. The most notable external characteristics of the phenotype are the severe craniofacial defects: absence of the eyes and mouth, and defects affecting the frontonasal process. In addition, these embryos also present with anencephaly, in which the forebrain region of the neural tube is open, the forebrain is absent, and the remaining brain regions are exposed; and thoraco-abdominoschisis, in which the ventral body wall is absent, causing the thoracic and abdominal organs to be exposed. Defects were also seen in limb development, resulting in the absence of the radius in the mature forelimb. This is consistent with *Tcfap2a* expression in the developing limb bud. Closer examination of these embryos indicated that the heart and kidneys were hypoplastic (Schorle *et al.*, 1996; Zhang *et al.*, 1996).

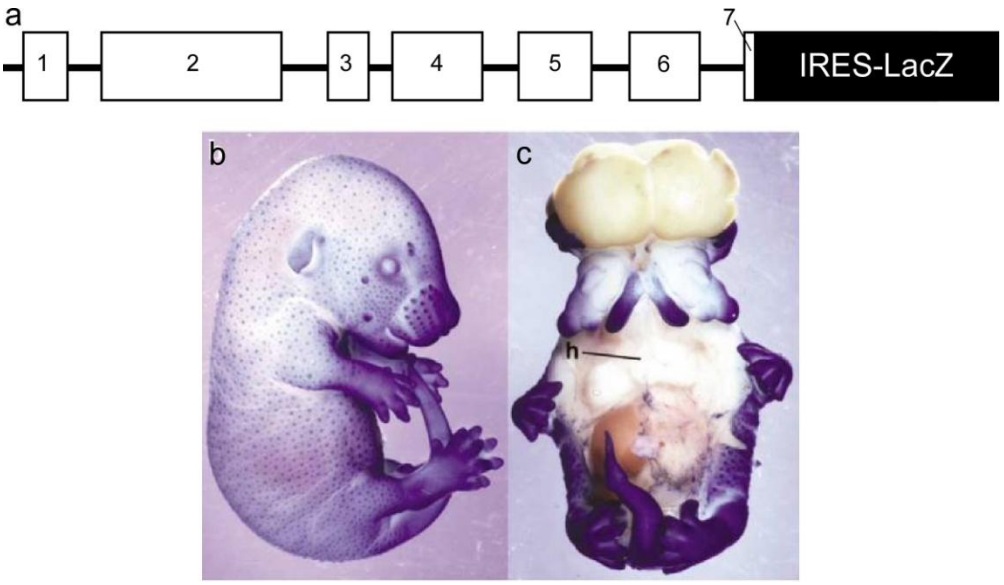

Figure 1.11: External phenotype of *Tcfap2a*$^{-/-}$ mutant embryo at e15.5.
(a) *Tcfap2a* mutant allele used to generate *Tcfap2a*$^{-/-}$ mutant embryos. An IRES-LacZ cassette was inserted into exon 7, generating a null allele. (b) Control (*Tcfap2a*$^{+/-}$) and (c) mutant (*Tcfap2a*$^{-/-}$) embryos, stained with X-gal. *Tcfap2a*$^{-/-}$ mutant embryos have an open neural tube, craniofacial malformations and failed closure of the ventral body wall, resulting in the organs being exposed. h, heart. (Figure a based on information from Brewer *et al.*, 2002; figures b and c taken from Brewer *et al.*, 2002).

1.4.4.1. AP-2α in cardiovascular development

The cardiovascular abnormalities observed include a VSD in all embryos examined and OFT defects, such as DORV in a large proportion of embryos, and PTA in a minority. In two embryos with DORV the VSD was sub-aortic and the embryos also showed signs of pulmonary atresia/stenosis and therefore were proposed by the authors to more accurately fit the criteria for TOF. In addition, a small number of embryos (5/15) also showed defects of the PAAs, including A-RSA, IAA-B and right dorsal aorta (Brewer *et al.*, 2002). Many of these cardiovascular defects are reminiscent of the malformations seen in studies of NCC ablation in both mouse and chicken models (see section 1.3.3). In addition, ventral body wall defects and exencephaly were also observed in a small proportion of NCC-ablation embryos.

1.4.4.2. NCC-specific deletion of Tcfap2a

Despite the similarities between NCC-ablation embryos and the phenotypes described for *Tcfap2a*$^{-/-}$ mouse embryos, the migration of the NCCs in the global knock-out occurs normally (Schorle *et al.*, 1996; Zhang *et al.*, 1996). A conditional deletion of *Tcfap2a* from the NCCs resulted in a severe reduction of the *Tcfap2a*$^{-/-}$ phenotype. The defects of neural tube closure were seen at much lower frequencies (6/39, ~15%) in these mutants, and no CCVM was described. Most embryos with a NCC-specific deletion failed to thrive post-parturition, however, some were able to survive to

adulthood. Perinatal death was attributed to cleft palate, causing respiratory problems and an inability to feed (Brewer *et al.*, 2004).

1.4.5. Other AP-2α mutations

In addition to the multitude of defects observed in the mouse model as described above, a number of mutations have also been identified in other organisms and suggest a conserved function of the transcription factor AP-2α during development in these organisms.

1.4.5.1. Humans

Mutations in the human *TFAP2A* gene have been found to cause branchio-oculo facial syndrome (BOFS). This disease is characterised by a branchial (or cutaneous) defect, abnormalities of the eyes and a distinct facial phenotype, and exhibits autosomal dominant inheritance (Milunsky *et al.*, 2011).

Many individuals with BOFS also present with cleft lip (cL), with or without cleft palate (cP), prematurely grey hair, kidney anomalies and mild mental retardation (reviewed in Milunsky *et al.*, 2011). In addition, an ectopically placed 'dermal' thymus has been described in a number of patients. This is a phenotype caused by the ectopic placement of the thymic rudiments, which results in tumour-like skin lesions on the neck of the patients. Upon excision of this tissue, it was identified that it was functional thymus tissue (Barr *et al.*, 1989; Bennaceur *et al.*, 1998; Drut and Galliani, 2003). It has been estimated that the incidence of this defect in BOFS is approximately 30%, although in many case studies the presence or absence of the defect was not addressed (Lin *et al.*, 2009; Milunsky *et al.*, 2011).

One study, analysing 37 BOFS patients at various ages, revealed a range of intellectual developmental anomalies, multiple incidences of partial syndactyly and a single case of congenital heart malformation in the form of an anomalous pulmonary venous return and an ASD (Gestri *et al.*, 2009). Two further patients have also been described with CCVM: another ASD (Milunsky *et al.*, 2011) and one with signs of TOF (Reiber *et al.*, 2010). Although the incidence of CCVM observed in BOFS patients is low, it is also of note that echocardiography is only performed in those patients suspected of

cardiovascular problems (approximately half). Therefore, the actual prevalence of CCVM in these patients may be higher (Milunsky *et al.*, 2011).

BOFS is caused by mutations in the *TFAP2A* gene, many of which cluster in exons 4 and 5, which encode parts of the DNA binding and dimerisation domains (Milunsky *et al.*, 2008; Milunsky *et al.*, 2011). It has therefore been suggested that the observed phenotypes may be due to the production of a dominant negative (DN) protein, capable of binding other isoforms of the AP-2 family and inhibiting their function. However, three cases (a father and his 2 children) were described with a heterozygous whole gene deletion (Gestri *et al.*, 2009), suggesting that the molecular mechanisms of the disease are more complex than first thought.

Additionally *TFAP2A* has been associated with the negative regulation of the T-box gene, *TBX20*, expression of which is increased in atrial and ventricular biopsies of patients with TOF. The *TBX20* promoter was found to contain AP-2 binding sites and its transcription was reduced in a luciferase assay when constructs encoding *TFAP2A* or *TFAP2C* were co-transfected (Hammer *et al.*, 2008). The TOF phenotype has also been observed in *Tcfap2a*-null mice (Brewer *et al.*, 2002), suggesting conservation of function between species.

1.4.5.2. Zebrafish

Expression of *tfap2a* is first seen at 8 hpf in the non-neural ectoderm. By 12 hpf expression has extended into the cardiac NC progenitors. From 18 hpf expression is found in the pronephric duct, and by 24 hpf expression has spread to the NC-derived mesenchyme and ectoderm of PAs. At 36 hpf *tfap2a* expression has extended to the optic tectum, the mid brain and hindbrain. By 52 hpf expression is also observed in the retina, the lateral line of the organs, and the pectoral fins (Knight *et al.*, 2003; Knight *et al.*, 2005).

A number of mutations in zebrafish, generated by a forward genetic screening approach, have been found to cause craniofacial defects and absent or aberrant PA cartilage formation. Two of these lines, *lockjaw* (*low*) and *mont blanc* (*mob*) are the result of mutations in *tfap2a* (Neuhauss *et al.*, 1996; Schilling *et al.*, 1996; Knight *et al.*, 2003; Barrallo-Gimeno *et al.*, 2004). Craniofacial defects in these lines include a ventral

protrusion of the jaw and the failure of the mesodermal and NC-derived trabeculae to fuse correctly to form the ethmoid plate. This phenotype is analogous to a cleft palate in mammals, which is observed in NC-specific inactivation of murine AP-2α (Brewer *et al.*, 2004) and in patients with BOFS (Lin *et al.*, 2009; Milunsky *et al.*, 2011). Other elements of the phenotype include defects in the positioning of the cartilage derived from the first arch. The derivatives of the second arch are also affected by mutation in *tfap2a*. Both the hyosymplectic and ceratohyal cartilages, which derive from this arch are reduced and fuse to the cartilage of the first arch. The more posterior ceratobranchial cartilages, which arise from the caudal arches (3-6) are severely reduced and disorganised (Neuhauss *et al.*, 1996; Schilling *et al.*, 1996; Barrallo-Gimeno *et al.*, 2004; Knight *et al.*, 2003; Knight *et al.*, 2005).

Studies of *tfap2a* mutant zebrafish have also shown the presence of pericardial oedema, indicative of cardiovascular defects (O'Brien *et al.*, 2004). Some deficiencies in the development of the aortic arch has been observed in *tfap2a* mutants, however, the phenotype has not been studied further, and therefore revealed nothing regarding the impact of this upon normal cardiovascular development (Knight *et al.*, 2003).

1.5. Preliminary data

Brewer *et al*. (2002) have demonstrated the fully penetrant cardiovascular defects observed in *Tcfap2a*$^{-/-}$ mutant embryos on a black swiss background. In addition, this group also investigated a conditional deletion of *Tcfap2a* from the NCCs, but failed to identify any cardiovascular defects in these mutant embryos (Brewer *et al.*, 2004).

Work in our group, examining *Tcfap2a*$^{-/-}$ mutant embryos on a congenic C57BL/6J background has also revealed a fully penetrant cardiovascular phenotype affecting the formation of the interventricular septum, OFT and the PAAs. In addition, a conditional deletion of *Tcfap2a* from the NCCs, on this genetic background, also indicated a number of defects affecting these regions. As this work forms the basis for much of the work within this thesis, this preliminary data will be presented here.

1.5.1. *Tcfap2a*$^{-/-}$ embryos

Preliminary work in our group (Dr Simon Bamforth) utilised the *Tcfap2a*-null allele created by Brewer *et al.* (2002). Mice were crossed onto a C57BL/6J background, to

limit the effect of genetic modifiers which would confound results, and the phenotypes of homozygous mutants were examined.

A number of cardiovascular defects were observed in these mutant embryos including VSDs, OFT defects (DORV, TGA and OA) and PAA defects (IAA-B, A-RSA, CORSA and cAoA), which were not seen in control embryos (Figure 1.12). Overall, each embryo had an OFT defect and VSD, as described previously (Brewer *et al.*, 2002). In addition, each embryo also presented with a PAA malformation. This is a dramatic increase in prevalence compared to the PAA malformation observed previously (33% PAA defects). The increase in the penetrance of PAA defects in this dataset is likely due to the change in genetic background. These results indicate a 100% penetrance of CCVM in the *Tcfap2a*$^{-/-}$ embryos examined here, on a ~95% C57BL/6J background.

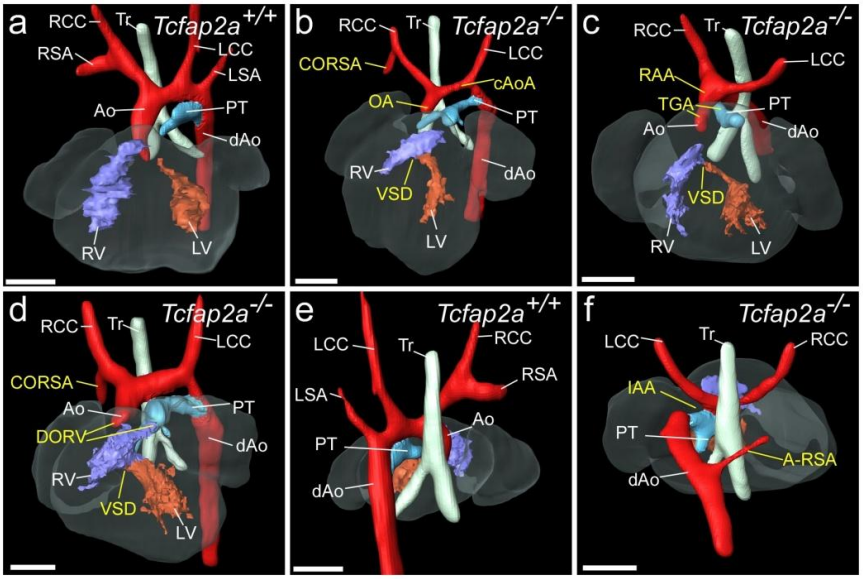

Figure 1.12: 3D reconstructions of cardiovascular phenotypes in *Tcfap2a*$^{-/-}$ mutant embryos.
Cardiovascular phenotypes of control (*Tcfap2a*$^{+/+}$) and mutant (*Tcfap2a*$^{-/-}$) embryos. (a) Ventral view of control embryo heart showing normal development of the cardiovascular system. (b) Ventral view of a mutant embryo with VSD, OA, CORSA and cAoA. (c) Mutant embryo with RAA, TGA and VSD. (d) Mutant embryo with VSD, DORV and CORSA. (e) Dorsal view of a control embryo showing normal cardiovascular development. (e) Dorsal view of a mutant embryo with A-RSA and IAA. Scale bar = 500 µm. Images provided by Dr Simon Bamforth. RCC, right common carotid artery; RSA, right subclavian artery; Ao, aorta; Tr, trachea; LCC, left common carotid artery; LSA, left subclavian artery; PT, pulmonary trunk; dAo, dorsal aorta; RV, right ventricle; LV, left ventricle.

1.5.2. NCC-specific deletion of *Tcfap2a*

As the work above demonstrates, changing the genetic background in the *Tcfap2a*$^{-/-}$ mutant embryos resulted in an increase in the penetrance of CCVM. Therefore, our group chose to investigate how the change in genetic background could affect the prevalence of CCVM in the conditional deletion from the NCCs.

Examination of mutant embryos on a 72.55% C57BL/6J background identified neural tube defects and a number of cardiovascular defects. Exencephaly was observed in 45% (4/9) of mutant embryos (Figure 1.13e). Cardiovascular defects in the form of VSD (Figure 1.13f-g), TGA (Figure 1.13g) and A-RSA (Figure 1.13h) were observed in 55% (5/9) of mutant embryos.

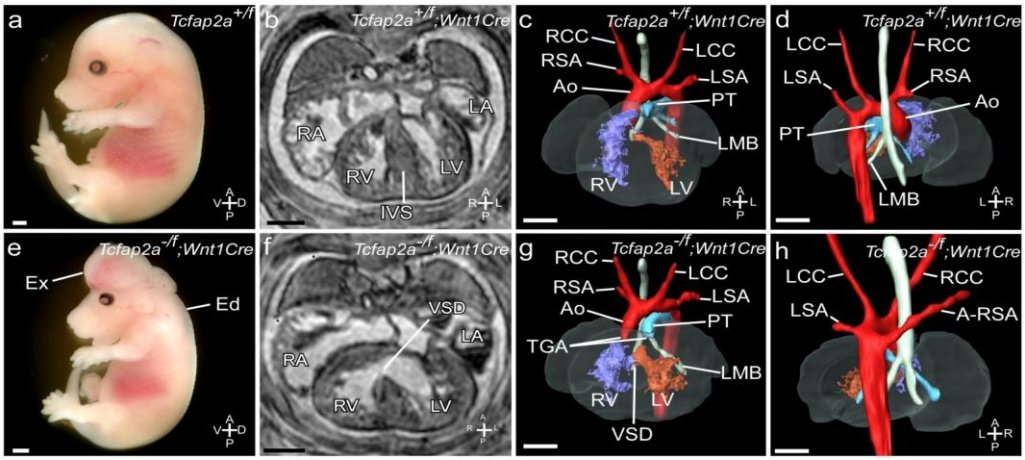

Figure 1.13: Preliminary data suggests a *Wnt1cre*-mediated deletion of *Tcfap2a* results in severe CCVM. Control (*Tcfap2a*$^{+/f}$ or *Tcfap2a*$^{+/f}$*;Wnt1cre*) (a-d) and mutant (*Tcfap2a*$^{f/-}$*;Wnt1cre*) (e-h) embryos on a 72.55% C57BL/6J background were collected at e15.5. Externally control embryos were phenotypically normal (a), whereas mutant embryos often had exencephaly (Ex) and oedema (Ed) along the spine (e). Examination by MRI revealed VSD in a number of mutants (f) that were not observed in controls (b). 3D reconstructions were created from the MRI datasets for controls (c, d) and mutants (g, h) and further defects such as TGA (g) and A-RSA (h) were identified. Scale bar = 500 µm. Figure provided by Dr Simon Bamforth.

1.6. Aims and objectives

AP-2α is required in the mouse for correct development of many structures, and for perinatal life. Deletions of this gene have been found to cause severe craniofacial malformations and cardiovascular defects, which result in death at, or before, birth (Zhang *et al.*, 1996; Brewer *et al.*, 2002). However, the precise role of AP-2α in the pathways required for development is yet to be defined. *Tcfap2a*$^{-/-}$ mutant embryos exhibit a cardiovascular phenotype similar to that seen in NCC ablation experiments (Brewer *et al.*, 2002) (see section 1.5.1), while a NCC-specific conditional deletion of *Tcfap2a* showed no cardiovascular phenotype (Brewer *et al.*, 2004).

However, further work in our group has indicated that *Tcfap2a* is important in PAA formation on a C57BL/6J background. In addition, it appears that upon breeding to a C57BL/6J background a proportion of the CCVM can be recapitulated through conditional deletion from the NCCs.

The aims of this thesis are as follows:

1) To investigate the role of *Tcfap2a* within the NCCs on a congenic C57BL/6J background.
2) To investigate the role of genetic background in the variation of CCVM observed.
3) To investigate the role of *Tcfap2a* in PAA formation and remodelling
4) To investigate potential transcriptional targets of *Tcfap2a* in cardiovascular and PAA development.

1.6.1. The role of *Tcfap2a* in NCCs on a congenic C57BL/6J background

Our preliminary work indicates that genetic background is an important factor in the penetrance of CCVM in *Tcfap2a* mutant embryos. We have demonstrated a number of PAA malformations in mutant embryos with a NCC-specific deletion of *Tcfap2a* on a 72% C57BL/6J background. In addition, a fully penetrant cardiovascular phenotype, including PAA malformations, was also identified in *Tcfap2a*$^{-/-}$ mutant embryos on a congenic C57BL/6J background.

This chapter, therefore, aims to investigate the NCC-specific deletion of *Tcfap2a* on a congenic C57BL/6J background, to determine the level of CCVM observed in these mutant (*Tcfap2a*$^{f/-}$*;Wnt1cre*) embryos. In addition, we also aim to investigate any changes in NCC behaviour that may occur in the *Tcfap2a*-null embryos, using lineage tracing techniques.

1.6.2. The role of genetic background in CCVM observed in *Tcfap2a* mutants

The genetic background appears to be important in the penetrance of PAA malformation in *Tcfap2a*$^{-/-}$ embryos, and in CCVM in general in the NCC-specific deletion of *Tcfap2a*. We aim to further investigate how changes in genetic background can affect the penetrance of cardiovascular and PAA malformation in *Tcfap2a* mutants.

1.6.3. *Tcfap2a* in PAA formation and remodelling

The preliminary data presented above indicates an increase in the prevalence of PAA malformation on a congenic C57BL/6J background compared to that previously observed by Brewer *et al*. (2002). Therefore, I aim to exploit this fully penetrant phenotype in order to investigate the role that *Tcfap2a* plays in PAA development and the molecular processes that are disrupted when *Tcfap2a* is removed.

1.6.4. *Tcfap2a* transcriptional targets in PAA development

Although a number of genes have been suggested to be regulated by *Tcfap2a*, the majority of these targets have been suggested based on the role of *Tcfap2a* in cancer progression. However, a number of these target genes have roles in basic cellular processes, such as proliferation and apoptosis. Therefore, I aim to investigate the differential expression of these target genes in the *Tcfap2a* wild type and null PA region. In addition, potential transcriptional targets will be further investigated to validate the differential expression, by investigating the expression of related genes and genetic interaction experiments.

Chapter 2. Materials and Methods

All reagents were purchased from Sigma Aldrich, unless otherwise stated.

2.1. General reagents

Many reagents were common to multiple protocols and were used throughout the work contained within this thesis. These general reagents are listed here. Other reagents which were specific to individual protocols are listed with the appropriate section below.

2.1.1. Phosphate buffered saline

Phosphate buffered saline (PBS) was prepared from tablets (Oxoid, BR0014). 10 tablets were dissolved in 1 litre of distilled water (dH_2O) and autoclaved before use.

2.1.2. RNase-free PBS

1 litre PBS was prepared as described above. This was then treated with 0.1% volume per volume (v/v) diethyl pyrocarbonate (DEPC) overnight and then autoclaved.

2.1.3. Paraformaldehyde

Fixation of all embryos was carried out in 4% weight per volume (w/v) paraformaldehyde (PFA) dissolved in DEPC-PBS with 7.5 mM sodium hydroxide (NaOH), unless otherwise stated.

2.2. Mouse lines

Throughout this study we used a number of mouse lines in the generation of mutant and control embryos between the ages of e7.5 and e15.5. Embryonic age was calculated based on the assumption that embryos were e0.5 at noon on the day of detection of the copulatory plug. All adult mice were kept in a 12-hour light/dark cycle. Wild type mice were purchased from Jackson Laboratories.

2.2.1. Tcfap2a^{LacZ}

The *Tcfap2a*-null allele, generated by the insertion of an internal ribosome entry site (IRES)-*LacZ* cassette into the coding sequence of this gene (Brewer *et al.*, 2002), was a gift from Prof. Trevor Williams (University of Colorado School of Medicine). This allele interrupts the final exon (exon 7) of the gene, causing a disruption of the DNA binding and dimerisation domains which are essential for AP-2α function. In addition, the

inclusion of the IRES-*LacZ* cassette into the gene allows the translation of β-galactosidase, under the control of the *Tcfap2a* promoter. In the presence of the substrate 5-Bromo-4-chloro-3-indolyl β-D-galactopyranoside (X-gal), those tissues expressing β-galactosidase will be stained blue, therefore also allowing the expression pattern of the gene to be monitored (see section 2.6).

The *Tcfap2a*^{LacZ} allele, from here on referred to as the *Tcfap2a*-null allele was crossed to wild type C57BL/6J mice for several generations in order to generate heterozygotes (*Tcfap2a*$^{+/-}$) on a congenic background. Heterozygotes were then crossed together in timed matings to generate homozygous null (*Tcfap2a*$^{-/-}$) embryos for downstream analysis.

2.2.2. Tcfap2a^{flox}

To further examine the importance of *Tcfap2a* in cardiovascular development, a conditional allele, *Tcfap2a*^{flox}, was also utilised. This mouse was also given to us by Prof. Trevor Williams. This allele includes two loxP sites inserted by homologous recombination upstream of exon 5 and downstream of exon 6 (Brewer *et al.*, 2004). In the presence of *Cre* recombinase, the loxP sites undergo recombination to remove the intervening exons.

2.2.3. Cre lines

In addition to the *Tcfap2a* alleles described above, a number of cre lines were also used to produce conditional deletions of *Tcfap2a*. These cre lines are listed in Table 2-1.

Table 2-1: Expression domains of Cre lines used in this project compared to *Tcfap2a.*

Expression domains	*Tcfap2a*	*Wnt1cre*	*Nkx2.5cre*	*Foxg1cre*	*PGKcre*	*Sox2cre*
SHF	×	×	✓	×	✓	✓
Myocardium	×	×	✓	×	✓	✓
Ectoderm	✓	×	✓	✓	✓	✓
Endoderm	×	×	✓	×	✓	✓
Mesoderm	×	×	×	×	✓	✓
NCCs	✓	✓	×	×	✓	✓
Reference(s)	Brewer *et al.*, 2002	Danielian *et al.*, 1998	Moses *et al.*, 2001	Hebert and McConnell, 2000	Lallemand *et al.*, 1998	Hayashi *et al.*, 2002

2.2.3.1. Wnt1cre

Cre recombinase under the control of a *Wnt1* enhancer (*Wnt1cre*; Danielian *et al.*, 1998) was used for conditional deletion of *Tcfap2a* from the NCCs. This cre line was created by random integration of the transgene into the genome. *Wnt-1* expression begins from e8.0, within the midbrain, and extends into the hindbrain and forebrain by e8.5. Expression continues in the derivatives of the cranial NC, with expression in the mesenchyme of the PAs observed from e9.25 (Echelard *et al.*, 1994). Activation of a reporter construct activated by *Wnt1cre*-mediated recombination was observed from e8.5 (Danielian *et al.*, 1998).

2.2.3.2. Nkx2.5cre

Nkx2.5cre is a 'knock-in' cre line, in which the *Cre* cDNA has been inserted directly into exon 2 of the *Nkx2.5* locus. This allows cre expression to be controlled directly by the endogenous gene; however, it results in the disruption of one allele of *Nkx2.5*, therefore reducing this gene to heterozygosity. This cre line is expressed within the cardiac crescent from e7.5. Expression continues in the myocardium during looping (e8.5-e9.0) and is also expressed in the ectoderm of the developing first PA from this time (Moses *et al.*, 2001). *Nkx2.5cre* was used to remove *Tcfap2a* from the PSE.

2.2.3.3. Foxg1cre

Foxg1cre is also a knock-in allele. This drives expression of cre from e8.5, within the anterior tip of the head folds and the underlying ectoderm. By e9.5, expression is observed in the PSE and by e10.5 throughout the foregut region (Hebert and McConnell, 2000). Therefore, this construct will remove *Tcfap2a* in the surface ectoderm of the PA region.

2.2.3.4. PGKcre

The *PGKcre* transgene was generated by cloning the *PGK-1* promoter upstream of the Cre gene and introduced by microinjection (Lallemand *et al.*, 1998). The transgenic construct was incorporated into the genome by random integration. Expression of this transgene is ubiquitous and will overlap with *Tcfap2a* in all tissues. The *PGK-1* locus becomes active from e3.5 (McBurney *et al.*, 1994), therefore, recombination of the *Tcfap2a* locus should occur long before endogenous *Tcfap2a* expression begins at e8.5 (Brewer *et al.*, 2002).

2.2.3.5. Sox2cre

The *Sox2cre* transgene was generated by the insertion of the Cre gene downstream of a 12.5 kb *Sox2* promoter sequence (Hayashi *et al.*, 2002). The transgene was microinjected into mouse pronuclei and was incorporated into the mouse genome by random integration. Expression of the *Sox2cre* was confirmed from e6.5 in all cells of the epiblast, but was excluded from extra-embryonic tissues. Therefore, this Cre line will conditionally delete *Tcfap2a* from all embryonic tissues, prior to activation of the *Tcfap2a* promoter.

2.2.4. Reporter lines

The expression pattern of *Wnt1cre* was examined using either a *LacZ* or enhanced yellow fluorescent protein (*EYFP*) construct introduced into the *Rosa26* locus ($R26R^{LacZ}$ (Soriano, 1999), $R26R^{EYFP}$ (Srinivas *et al.*, 2001)). These constructs contain a transcriptional stop sequence flanked by *loxP* sites, which is removed in the presence of Cre recombinase, therefore, allowing the expression of the LacZ and EYFP constructs in these tissues. The expression patterns of the Cre lines may then be visualised by X-gal staining for the expression of the LacZ construct (see section 2.6) in the $R26R^{LacZ}$ allele. Alternatively, recombination in $R26R^{EYFP}$ embryos was visualised using fluorescence immunohistochemistry on sectioned embryos (see section 2.5.5).

2.2.5. Dlx5-CreERT2

In order to investigate the potential genetic interaction between *Tcfap2a* and *Dlx5*, *Dlx5 Cre-ERT2* mice were purchased from Jackson laboratories (#010705). Homologous recombination was used to introduce the CreER cDNA at the translation initiation site of the *Dlx5* gene (Taniguchi *et al.*, 2011). This strain is, therefore, heterozygous for *Dlx5* and may be used in the generation of compound heterozygotes by breeding with $Tcfap2a^{+/-}$ mice. In this thesis, the *Dlx5 Cre-ER* mouse is used only as a null allele of *Dlx5* and will, therefore, be referred to as $Dlx5^{-}$ from here on.

2.2.6. Calculating genetic background

Throughout this thesis all mice were maintained on a C57BL/6J background. The genetic background of all mice used was between 93-99%. The genetic background of each embryo used in this work was calculated as the average of the genetic backgrounds of both parents. The genetic background of wild type mice was assumed to be 100% C57BL/6J. The genetic background of mice obtained from other groups,

which had been inbred onto a C57BL/6J background for numerous generations was presumed to be 99% C57BL/6J.

2.3. Genotyping

2.3.1. DNA extraction

DNA extraction of sample tissues was carried out using proteinase K digestion. The lysis buffer was prepared by diluting proteinase K to a final concentration of 600 µg/ml in proteinase K buffer (50 mM potassium chloride (KCl), 1.5mM magnesium chloride ($MgCl_2$), 10 mM Trizma base (tris) pH 8.5, 0.45% v/v Igepal® CA-630, 0.45% v/v Tween-20). This was added to the samples and incubated at 56°C for 2 hours, or until the sample had completely lysed. The samples were vortexed intermittently to ensure complete breakdown of the tissues and release of the DNA. Proteinase K was heat inactivated by incubating at 95°C for 10 minutes. The lysed sample was centrifuged at full speed for 1 minute to collect any debris and stored at 4°C until use.

The volume of lysis buffer prepared was dependant on the tissue to be lysed. For weaned mice, an ear punch was collected and lysed in 150 µl lysis buffer. For genotyping embryos at mid-embryogenesis (e8.0-11.5), the yolk sac was collected and lysis buffer volume was dependant on the size of the sample (see Table 2-2). For the genotyping of late-gestation embryos (e14.5-15.5) the left forelimb was collected for lysis.

Table 2-2: Volume of lysis buffer used in DNA extraction of various samples.

Sample to be lysed	Volume of lysis buffer
e7.5 extra-embryonic material	15 µl
e8.0 yolk sac	25 µl
e8.5 yolk sac	30 µl
e9.5 yolk sac	50 µl
e10.5 yolk sac	100 µl
e11.5 yolk sac	200 µl
e14.5/15.5 forelimb	400 µl
ear notch	150 µl

2.3.2. Polymerase chain reaction

Genotyping was carried out using the polymerase chain reaction (PCR) to identify the presence or absence of the gene of interest. All primers were designed by Dr Simon Bamforth or the lab responsible for generating the mouse strain and all PCR programmes have been optimised previously.

PCR reactions were carried out using GoTaq polymerase (Promega) and the associated buffer with the following reaction conditions: 1 unit GoTaq polymerase, 1x GoTaq reaction buffer (contains 1.5 mM $MgCl_2$), 0.25mM each deoxyribonucleotide triphosphate (dNTP) (Fisher), 0.5 µM forward primer, 0.5 µM reverse primer and 2 µl cell lysate prepared as above (section 2.3.1).

Samples were then incubated in a thermocycler for 35 cycles. The exact programme used for each primer pair was dependant on the size of the amplification product and the annealing temperature of the primers.

2.3.3. Gel electrophoresis

PCR products were analysed by gel electrophoresis. 1% w/v agarose (Lonza) was added to tris-acetic acid-ethylenediaminetetraacetic acid (EDTA) buffer (TAE) (40mM tris, 20mM acetic acid, 1mM EDTA) and heated to dissolve. Once the agarose solution had cooled, ethidium bromide (EtBr) was added to a final concentration of 0.5µg/ml. The agarose was poured into a cast and allowed to set before adding the PCR samples. PCR products were run alongside a GeneRuler™ 100 bp or 1 kb DNA ladder (Fisher Scientific) at 100 volts (V) for 30-60 minutes, until the bands had fully resolved. The gel was then imaged under UV light.

2.4. Embryo dissection

For those embryos collected at mid-gestation (e8.5-11.5), the general dissection procedure is described here; however, some applications required variations of this protocol. These variations are given in the descriptions of these applications. For embryos at late gestation the dissection procedure is described later (see section 2.7.1). Pregnant dams were sacrificed by cervical dislocation, and the uterus was removed and submersed in ice-cold PBS. Deciduates were removed from the uterus using vannas scissors and forceps (InterFocus). The yolk sac was removed and retained

for genotyping. Embryos were fixed in 4% PFA, unless otherwise stated. Fixation was carried out overnight for embryos aged e9.5-11.5 and for a minimum of 4 days for e15.5 embryos.

2.5. Histology

2.5.1. Wax embedding

Fixed embryos were briefly rinsed in PBS then dehydrated through a series of ethanol solutions at room temperature. Embryos were cleared in Histoclear (National Diagnostics, #HS-200), then a 1:1 solution of Histoclear:paraffin wax (VWR) at 60°C, before embedding in paraffin wax. The incubation times varied with the age of the embryos and are shown in Table 2-3.

Table 2-3: Dehydration and processing protocol for the wax embedding of fixed embryos.

	E9.5	E10.5	E11.5	E14.5	E15.5
50% Ethanol	30 minutes	30 minutes	1 hour	3 hours	3 hours
70% Ethanol x2	30 minutes 30 minutes	30 minutes 30 minutes	1 hour 1 hour	3 hours 3 hours	3 hours 3 hours
95% Ethanol	30 minutes	30 minutes	1 hour	3 hours	3 hours
100% Ethanol x2	30 minutes 30 minutes	30 minutes 1 hour	1 hour 1 hour	3 hours Overnight	3 hours Overnight
Histoclear x2	10 minutes 10 minutes	15 minutes 15 minutes	20 minutes 20 minutes	20 minutes 20 minutes	30 minutes 30 minutes
Histoclear/wax	15 minutes	20 minutes	20 minutes	1 hour	1 hour
Wax x3/4 (Heated: 60°C)	20 minutes 20 minutes 20 minutes	30 minutes 30 minutes 30 minutes	40 minutes 40 minutes 40 minutes	1 hour 1 hour 1 hour 1 hour	1 hour 1 hour 1 hour 1 hour

2.5.2. Sectioning

Embedded embryos were sectioned using a Leica RM 2235 microtome. Sections were cut at 8µm. For embryos at e9.5-11.5 embryos, were embedded in a coronal orientation and sections were stretched using a water bath at 37°C and collected on a glass microscope slide (VWR). Slides were dried for a few minutes on a hot plate (37°C) then transferred to a slide oven at 40°C for overnight drying. For embryos aged e14.5-15.5 embryos were embedded in a transverse orientation. Sections were stretched by placing onto a slide coated with water and heating on a hot plate, until all

water had evaporated. Once dry, slides were transferred to the 40°C oven overnight to dry, to ensure sections were firmly adhered prior to staining.

2.5.3. Haematoxylin and eosin staining

Haematoxylin and eosin staining was used to identify any morphological changes within embryos. Haematoxylin stains the cell nuclei purple, while eosin stains the cytoplasm pink.

Slides were submersed in Histoclear twice for 10 minutes each to remove wax from the sections. The sections were then incubated in 100% ethanol twice for 3 minutes, followed by rehydration through 90%, 70% and 50% ethanol solutions, and then washed in dH_2O for 2 minutes each. The sections were then stained in Harris' haematoxylin solution for 10 minutes. Excess haematoxylin was washed away with running water for 5 minutes, then slides were dipped in an acid alcohol solution (1% v/v hydrochloric acid (HCl), 70% ethanol) to remove the stain from all tissues except the nucleus and returned to the running water for a further 5 minutes. The slides were then incubated in eosin (Fisher Scientific) for 5 minutes, rinsed in running water and dehydrated by dipping in 50%, 70% and 90% ethanol. The slides were then transferred to 100% ethanol for 3 minutes, twice, and incubated twice in Histoclear for 10 minutes. Slides were mounted in Histomount (National Diagnostics) and dried overnight. Sections were imaged using a Zeiss Axioplan2 microscope and associated software.

2.5.4. Slide immunohistochemistry

Immunohistochemistry for platelet endothelial cell adhesion molecule-1 (PECAM-1; CD-31) was carried out on coronal sections of mutant and heterozygous embryos at stages e9.5, e10.5 and e11.5. Embryos were dissected as described above (section 2.4) and fixed in zinc fixative (BD Pharmingen) overnight. Embryos were embedded in paraffin wax and sectioned as described above (sections 2.5.1 and 2.5.2).

Slides were de-waxed in Histoclear, twice for 10 minutes each, followed by rehydration through an ethanol series (2 x 100%, 90%, 70%, 50%), for 2 minutes in each solution. Slides were equilibrated in PBS solution for 5 minutes, then incubated in 3% v/v hydrogen peroxide (H_2O_2) for 5 minutes. Slides were rinsed in dH_2O and Tris-buffered

saline with Triton-X 100 (TBS-TX; 100mM Tris-HCl, pH 7.5, 150mM sodium chloride (NaCl), 0.5% v/v Triton-X 100), followed by blocking in 10% v/v foetal bovine serum (FBS) in TBS-TX for 30 minutes.

The primary antibody, purified rat anti-mouse CD-31 (# 553370, BD Pharmingen) was prepared at a 1:50 dilution (final concentration of 0.01 µg/µl) in 2% FBS in TBS-Tx. 100 µl was applied to each slide, and covered with a parafilm coverslip, then incubated at 4°C in a humidified chamber overnight.

Following overnight incubation in primary antibody, the slides were washed in TBS-Tx then incubated for 1 hour in a humidified chamber at room temperature, in biotinylated rabbit anti-rat secondary antibody (Dako), prepared at 1:300 dilution in 2% FBS/TBS-Tx. The avidin-biotin (AB) complex (Vector) was prepared by the addition of 1 drop each of solutions A and B to 5ml of 50 mM Tris HCl, pH 7.5. Slides were washed in TBS-Tx, before the application of the AB complex . Following a 30 minute incubation with the AB complex, slides were washed again in TBS-Tx, then incubated in filtered 3,3'-diaminobenzidine (DAB) solution, prepared according to manufacturer's instructions for 30 minutes, or until brown staining developed. The reaction was stopped by placing the slides in PBS and the slides were then counterstained with methyl green (0.5% w/v methyl green, 0.1M sodium acetate pH 4.2), rinsed in dH_2O and butanol, washed in Histoclear (twice for 10 minutes each) and mounted in Histomount. Slides were imaged using a Zeiss Axioplan2 microscope.

2.5.5. Slide immunofluorescence

Embryos were collected at e10.5 and e11.5, fixed in 4% PFA, dehydrated through an ethanol series, embedded in paraffin wax in a coronal orientation and sectioned, as described above (sections 2.5.1 and 2.5.2). Slides were de-waxed in Histoclear for 5 minutes twice, then rehydrated through an ethanol series for 2 minutes in each solution and equilibrated in PBS. Antigen retrieval was performed using 0.01M citrate buffer (pH 6), heating in the microwave for 10 minutes and cooling at room temperature for 10 minutes then under running water for a further 10 minutes. For AP-2α immunofluorescence carried out by Kathleen Allinson, slides were immersed in citrate buffer in a pressure cooker at 80 kilo Pascals (kPa) for 5 minutes, followed by cooling as described above. The slides were then washed in PBS three times for 5

minutes each, before blocking in a 10% FCS in PBS solution. 100 µl of primary antibody in 2% FCS/PBS was added at the dilutions shown in Table 2-4. Each slide was covered with a parafilm coverslip and incubated overnight at 4°C in a humidifying chamber.

Primary antibody was removed by washing three times in PBS for 5 minutes each. The slides were then incubated in secondary antibodies diluted in 2% FCS/PBS for 1 hour at room temperature, in a humidified chamber. The secondary antibody corresponding to each primary antibody, and the dilution used are shown in Table 2-4.

Table 2-4 : Primary and secondary antibody concentrations used for immunofluorescence.

Primary antibody	Concentration	Secondary antibody	Concentration
Chicken anti-GFP (Abcam, ab13970)	1:100	Alexafluor 488 goat anti-chicken IgG (Invitrogen, A11039)	1:200
Mouse anti-α-smooth muscle actin (Sigma, A5228)	1:400	Alexafluor 594 donkey anti-mouse IgG (Invitrogen, A21203)	1:200
Mouse anti-AP-2α (3B5, santa cruz biotechnology sc-12726)	1:50	Alexafluor 594 donkey anti-mouse IgG (Invitrogen, A21203)	1:200
Cleaved Caspase3 (Asp175) antibody (9661, Cell Signalling Technology)	1:300	Alexafluor 594 donkey anti-mouse IgG (Invitrogen, A21203)	1:200
Anti-phospho-Histone H3 (Ser10) antibody (06-570, Millipore)	1:500	Alexafluor 594 donkey anti-mouse IgG (Invitrogen, A21203)	1:200

Slides were then washed three times in PBS for 5 minutes each before mounting in Vectashield with 4',6-diamidino-2-phenylindole (DAPI) (Vector laboratories LTD, H1500). Slides were analysed on a Zeiss Axioimager microscope, using the associated software.

2.5.6. Cell counting

Cell counting was performed on images of sections stained using the immunofluorescence technique described above (section 2.5.5). All cell counts were performed using ImageJ software (available from http://rsbweb.nih.gov/ij/) using the cell counter feature. Data was analysed in Microsoft Excel (Microsoft) to obtain average cell counts for each embryo and statistical analysis in the form of a student's

t-test was carried using the Prism 6 statistical package (available from http://www.GraphPad.com).

2.5.6.1. Apoptosis and proliferation

The apoptotic and proliferative index was calculated for the fourth PA only. Three control and three mutant embryos were examined for each process, with 1-3 images of the left and right fourth PAs being counted in each case. Images were cropped to 230 µm x 230 µm squares with the centre of the fourth PAA at the centre point of the image. Cell counts were obtained for the total number of cells, ectodermal cells, endodermal cells, NCCs (marked with anti-GFP antibody) and other cell types (endothelium and mesoderm). The average cell count for each of these tissues in each embryo was calculated, as was the average for each tissue in both the left and right fourth PA. These averages were compared and used in statistical analysis.

2.5.6.2. NCC density

To determine the density of cells within the fourth PA, three 100 µm x 100 µm squares were taken from each image analysed for apoptosis and proliferation (see section 2.5.6.1). The total number of cells and the number of NCCs within each image was counted and the average cell count for each image determined. The average number of cells for each PA (left and right) and the total number of cells for each embryo was then calculated and used for comparison and statistical analysis.

2.6. β-galactosidase staining

For whole mount β-galactosidase staining, transgenic mice were collected at e8.5-e10.5. Embryos were dissected in ice-cold PBS and lightly fixed in 0.2% v/v glutaraldehyde, 2 mM $MgCl_2$, 0.1 M phosphate buffer (77.4 mM sodium phosphate dibasic (Na_2HPO_4), 22.6 mM sodium phosphate monobasic (NaH_2PO_4), pH 7.3) for 20 minutes at room temperature. Embryos were washed in a detergent rinse (2 mM $MgCl_2$, 0.01% w/v sodium deoxycholate, 0.02% Igepal® CA-630, in 0.1 M phosphate buffer, pH 7.3) three times for 15 minutes each then the X-gal staining solution was added (0.1% w/v X-Gal, 5 mM potassium ferricyanide, 5 mM potassium ferrocyanide, 2 mM $MgCl_2$, 0.02% Igepal® CA-630, 0.01% sodium deoxycholate, 0.02 M Tris pH 7.3). Embryos were incubated in the staining solution in the dark, at room temperature

overnight with agitation. The following day, the staining solution was removed and embryos were rinsed in PBS several times before photographing.

2.7. Magnetic resonance imaging

Magnetic resonance imaging (MRI) was carried out on e15.5 embryos to identify morphological changes as an alternative to haematoxylin and eosin staining.

2.7.1. Dissection and processing

Embryos at e15.5 were collected and dissected in Hanks' balanced salt solution with 5mM EDTA, warmed to 37°C. The dissection procedure was performed on a heated mat to ensure that solutions and embryos were kept warm at all times. Embryos were dissected from the uterus, then the yolk sac was removed and discarded. The umbilical vessels were cut and embryos were allowed to bleed out. Care was taken to ensure that any clots were removed immediately to allow the embryos to bleed out fully, as the presence of blood limits the contrast in MRI scans. Embryos were washed twice in PBS, then the left forelimb was removed for genotyping and to allow easy identification of the left side of the embryo in analysis of the MRI images obtained. Slits were made in the skin beneath the forelimbs to allow sufficient penetration of the fixative. The embryos were then fixed in 4% PFA containing 4 µl/ml Magnevist® (gadopentetate dimeglumine, Gd-DTPA) for a minimum of 4 days at 4°C before loading into the MRI tube.

2.7.2. MRI tube preparation

MRI tubes were prepared as described previously (Bamforth *et al.*, 2012b). The MRI tube consists of a nuclear magnetic resonance tube (outer diameter 28mm; Fluorochem, UK) containing a teflon disk attached to a nylon rod to allow the embryos to be removed from the tube after scanning.

32 embryos (8 layers, 4 embryos per layer) were loaded into the MRI tube by embedding in agarose (1% agarose w/v in dH_2O, heated to dissolve) containing the contrast reagent Magnevist® (4µl/ml). The tube was sealed with a lid and parafilm to prevent the agarose from drying out and shipped on ice packs to Oxford for scanning. MRI scanning was carried out by Dr Jurgen Schneider (University of Oxford) and the embryos and images collected as a series of tagged image format (.tiff) files.

2.7.3. MRI data analysis and 3D reconstructions

The collected .tiff stacks can be analysed through AMIRA software (FEI Visualization Science Group). The voxel size used was: x-25.4, y-25.4, z-24.4. The .tiff stack for each layer of the MRI tube was opened separately and a transverse view through the embryos was analysed, using the removed left forelimb for orientation purposes. Once all embryos had been analysed for gross morphological changes, 3D reconstructions were produced.

The .tiff stack was cropped to include only the region of interest for the reconstruction, in order to minimise the file size. The labelling tools within the program were then used to label each structure of the heart for reconstruction. The hue, saturation and value levels for the colours used for each structure are shown in Table 2-5.

Table 2-5: Hue, saturation and value levels of all colours used in MRI reconstructions.

Structure	Hue	Saturation	Value
Aorta and aortic arch arteries	0.000	0.895	0.859
Pulmonary arteries/ ductus arteriosus	0.549	0.585	0.965
Trachea	0.376	0.161	0.949
Left ventricular lumen	0.041	0.804	0.800
Right ventricular lumen	0.667	0.506	1.000
Exterior surface of the heart	0.500	0.127	0.800
Background	0.611	0.000	0.000
Outside surface of the embryo	0.111	0.514	1.000

A 3D model of each structure may then be produced using the 'SurfaceGen' option with unconstrained smoothing. The unconstrained smoothing option allows us to create a 3D representation only.

2.8. Cloning

2.8.1. Restriction enzyme digest

All restriction enzymes, buffers and bovine serum albumen (BSA) were obtained from New England Biolabs. 1 µg plasmid DNA was digested in a 20 µl reaction mix containing: 20 units of restriction enzyme, 1x enzyme buffer, 1x BSA. The digestion mix was incubated at 37°C for 2 hours.

2.8.2. PCR purification

Purification of PCR and restriction digest reactions was carried out using a QIAquick PCR purification kit (QIAGEN), according to the manufacturer's instructions. Briefly, the sample to be purified was diluted in 5 volumes of the supplied buffer PB and then added to a QIAquick spin column and centrifuged at full speed to allow the DNA to adhere to the column surface. The column was washed by adding buffer PE, containing ethanol, and centrifuged again at full speed. The column was centrifuged a final time to ensure all of buffer PE had been removed then transferred to a fresh microcentrifuge tube for collection. The sample was eluted in 30 µl of buffer EB. To confirm the size of the purified sample, 5µl was added to 1 µl of 6x loading dye (Fermentas) for gel electrophoresis (see section 2.3.3).

2.8.3. NanoDrop spectrophotometry

Quantification of DNA samples was carried out using a NanoDrop spectrophotometer (Thermo Scientific). The NanoDrop channels were blanked using elution buffer and 1 µl of each sample was loaded onto the pedestals. Quantifications were given in ng/µl and quality was judged based on the absorbance at 260 nm divided by absorbance at 280 nm (260/280 value). A 260/280 value of 1.8 is considered high quality DNA.

2.8.4. Luria Bertani broth and Agar plate preparation

Luria Bertani (LB) broth was prepared with 171 mM NaCl, 1% w/v Tryptone (Oxoid) and 0.5% w/v yeast extract (Fisher) in dH_2O and autoclaved.

Agar plates were prepared by the addition of 1.5% w/v of Agar (Fisher) to LB broth and autoclaving. Agar was then cooled to 50°C and ampicillin was added to a final concentration of 50 µg/ml. The agar was then poured into petri dishes (20-25 ml per dish) and allowed to set in the presence of a flame.

2.8.5. Transformation

Transformations were carried out using Subcloning Efficiency™ DH5α™ chemically competent *Escherichia coli* (*E. coli*) (Invitrogen) according to the manufacturer's instructions. 1-10 ng of plasmid DNA was added to a 30 µl aliquot of competent cells and gently mixed, then incubated on ice for 30 minutes. Competent cells were heat-shocked for 20 seconds in a 42°C water bath to encourage uptake of the plasmid DNA, then returned to ice for a further 2 minutes. LB broth was preheated to 37°C and 970

µl was added to each vial of competent cells. The competent cells were then incubated at 37°C in a thermomixer for 60 minutes with agitation. The cells were then centrifuged at 3,000 x g for 10 minutes. The pellet was resuspended in 100 µl LB broth and then spread onto an agar plate and incubated at 37°C for 16 hours. After this time plates were stored at 4°C.

2.8.6. Miniprep of plasmid DNA

For miniprep of plasmid DNA, overnight cultures were prepared by inoculating 5ml of LB media containing ampicillin (50 µg/ml), with a single colony picked from an agar plate. Cultures were incubated at 37°C for 16 hours with agitation. The cultures were pelleted by centrifugation at 6,000 x g for 5 minutes at 4°C. The miniprep protocol was then carried out using a QIAprep Spin Miniprep kit (QIAGEN) according to the manufacturer's instructions. Briefly, samples were resuspended in 250 µl buffer P1, lysed in buffer P2 and then neutralised by the addition of buffer N3. The sample was centrifuged at 17,000 x g for 10 minutes to pellet cell debris and the supernatant was applied to a QIAprep spin column and centrifuged for 1 minute to allow binding of the plasmid DNA. The DNA was washed in buffer PB, then buffer PE, with centrifugation for 1 minute after each step. Plasmid DNA was eluted in 30 µl buffer EB.

2.8.7. Midiprep of plasmid DNA

Following transformation of competent *E. coli* cells and overnight incubation as described in 2.8.5 above, starter cultures were set up by inoculating 1ml of LB media containing 50 µg/ml of ampicillin with a single colony. Starter cultures were incubated at 37°C for 8 hours with agitation. Overnight cultures were then prepared in large flasks with a volume of 50 ml LB media containing 50 µg/ml of ampicillin. 100 µl of starter culture was added to each overnight culture, which were then incubated at 37°C for a further 16 hours, with agitation.

Cultures were transferred from flasks into 50 ml centrifuge tubes and centrifuged at 6,000 x g for 15 minutes at 4°C. The DNA was then extracted using a QIAGEN plasmid midi kit (QIAGEN), using the manufacturers recommended procedures. Briefly, the supernatant was discarded and the pellet was resuspended in buffer P1. The cells were lysed in buffer P2 for 5 minutes. Chilled neutralisation buffer (buffer P3) was added and the samples were then incubated on ice for 15 minutes. The samples were

transferred to a polypropylene centrifuge tube and centrifuged at 20,000 x g for 30 minutes at 4°C in a Sorvall Evolution RC Superspeed centrifuge. The supernatant was immediately removed and centrifuged again at 20,000 x g at 4°C for 15 minutes to remove further particulate material. The supernatant was then added to a supplied QIAGEN-tip 100, equilibrated using buffer QBT, and allowed to drain. The column was washed twice with buffer QC and allowed to drain fully. The plasmid DNA was then eluted in 5 ml of buffer QF. The DNA was precipitated by the addition of 0.7 volumes of isopropanol and centrifuged at 15,000 x g for 30 minutes at 4°C. The pellet was washed in 70% ethanol and centrifuged for a further 10 minutes at 15,000 x g at 4°C. The pellet was air-dried and redissolved in 100 µl Tris-EDTA (TE) buffer (10 mM Tris pH 8.0, 1 mM EDTA) and stored at -20°C.

The concentration of the plasmid DNA was determined by analysis on a NanoDrop spectrophotometer (see section 2.8.3).

2.8.8. DNA sequencing

Sequencing was performed to confirm that the correct plasmid DNA had been amplified. A 20µl volume containing between 30-100 ng/µl of plasmid DNA was sent to GATC biotech for sequence analysis. The sequence was returned in FASTA format and was analysed using a basic local alignment search tool (BLAST) (available online at: http://blast.ncbi.nlm.nih.gov/) to compare to all known sequences across the murine genome.

2.9. Whole mount *in situ* hybridisation

2.9.1. Probe preparation

Plasmid probes were gifts from Prof. Giovanni Levi (*Dlx5*) and Dr. Albert Basson (*Fgf8*). Plasmids were digested using the appropriate enzyme (Table 2-6) as described above (see section 2.8.1). Digested plasmid DNA was purified using a PCR purification method (see section 2.8.2), then quantified by spectrophotometry using a NanoDrop (see section 2.8.3).

Probes were labelled using a digoxygenin (DIG) RNA labelling kit (Roche) as follows: 1 µg linearised plasmid, 1x NTP labelling mix, 1x transcription buffer, 20 units of RNase

inhibitor, 40 units of polymerase (T7 or T3 (Roche) as in Table 2-6) in DEPC-H_2O. The reaction was incubated at 37°C for 2 hours.

Table 2-6: Restriction enzymes and RNA polymerases used in the preparation of WISH probes.

Probe	Enzyme for linearisation	RNA Polymerase
Fgf8 antisense	BamHI	T7
Fgf8 sense	KpnI	T3
Dlx5 antisense	EcoRI	T7
Dlx5 sense	KpnI	T3

The probe was extracted using lithium chloride (LiCl), with the addition of 250 µl of ice-cold 100% ethanol, 80 µl of DEPC-TE and 10 µl of 4M LiCl. The reaction was then incubated at -80°C for 2 hours or -20°C overnight.

Following this incubation the samples were centrifuged at full speed for 30 minutes at 4°C. The supernatant was removed and the pellet dried for 5-10 minutes at room temperature. The probe was dissolved in 100 µl DEPC-TE and 40 units of RNase inhibitor (Thermo Scientific) added, then stored at -80°C.

Probes were tested by electrophoresis on a 1% agarose gel with a 5 µl aliquot of probe mixed with 1 µl of loading dye and ran at 200V for 15 minutes. The high voltage allows the sample to run with minimal degradation of the RNA.

2.9.2. Embryo collection

Embryos were dissected at e9.5 as described above (see section 2.4), in ice-cold DEPC-PBS. All tools and equipment were treated with RNase Away (Fisher) to remove all traces of RNases that may degrade the RNA of interest. Embryos were fixed in 4% DEPC-PFA overnight, then rinsed in DEPC-PBS and dehydrated through a methanol series: 25%, 50%, 75% and 100% for 5 minutes each. The embryos were then stored at -20°C until required.

2.9.3. Whole mount *in situ* hybridisation

Three wild type (*Tcfap2a*$^{+/+}$) and three mutant (*Tcfap2a*$^{-/-}$) embryos at e9.5 (19-25s) were used to investigate the expression patterns of both *Dlx5* and *Fgf8*. Embryos were transferred to an RNase-free netwell filter (Corning) in a 12-well plate containing 100% methanol. Embryos were then rehydrated through 75%, 50% and 25% methanol

diluted in DEPC-PBT (DEPC-PBS containing 0.1% Tween-20, sterile filtered) and washed twice in DEPC-PBT. The embryos were then bleached in 6% H_2O_2 for 1 hour at room temperature. H_2O_2 was removed and embryos were rinsed in DEPC-PBT, three times, then treated with 10 µg/ml proteinase K for 15 minutes at room temperature. The enzyme reaction was stopped by washing in 2 mg/ml glycine and washing twice in DEPC-PBT. The embryos were fixed (0.2% glutaraldehyde, 4% PFA) for 20 minutes at room temperature and then rinsed in DEPC-PBT twice, then transferred to cryovials (thermo scientific) for hybridisation.

1ml of pre-hybridisation solution (50% v/v formamide, 5 x saline-sodium citrate solution (SSC) pH6, 0.1% Tween-20, 50 µg/ml heparin in DEPC-H_2O) was added to each vial and incubated at 70°C for 1 hour. The probe was diluted in hybridisation solution (50% formamide, 5x SSC pH6, 0.1% Tween-20, 50 µg/ml heparin, 50 µg/ml yeast transfer RNA (tRNA), 100 µg/ml salmon sperm DNA in DEPC-H_2O) and denatured at 100°C for 5 minutes . The pre-hybridisation solution was removed from the embryos and replace with hybridisation solution containing the correct probe and incubated overnight at 70°C with agitation in a hybridisation oven.

The following day, the hybridisation solution was removed and replaced with pre-warmed solution I (50% formamide, 4 x SSC, 1% w/v sodium dodecyl sulphate (SDS)). Embryos were washed twice, for 30 minutes each in solution I at 70°C. Embryos were then washed in a preheated 1:1 mixture of solution I:solution II (0.5M NaCl, 100 mM Tris pH 7.5, 0.1% Tween-20) for 10 minutes at 70°C, then washed a further 3 times in solution II for 5 minutes each at room temperature. Embryos were treated with 100 µg/ml RNaseA, diluted in solution II, twice for 30 minutes each at 37°C. Embryos were then washed in solution II at room temperate for 5 minutes, then in solution III (50% formamide, 4xSSC, 0.2% SDS) for a further 5 minutes at room temperature. The embryos were incubated twice for 30 minutes each in solution III at 65°C, then washed 3 times in Tris-buffered saline with Tween-20 (TBST) (50mM Tris pH 7.5, 150mM NaCl, 0.05% Tween-20). Embryos were transferred to glass vials for all subsequent steps. Embryos were blocked in 10% FBS, diluted in TBST for 2.5 hours at room temperature. The blocking solution was removed and replaced with 0.5µl/ml Anti-Digoxigenin-AP

Fab fragments (Roche) diluted in 1% FBS/TBST and embryos were incubated overnight at 4°C.

The antibody was removed and embryos were rinsed in TBST 3 times for 5 minutes each, then washed 5 times in TBST for 1 hour each with gentle agitation. Embryos were incubated in the final TBST overnight at 4°C. TBST was removed and embryos were washed 5 times for 10 minutes each in NTT solution (100 mM NaCl, 100 mM Tris pH9.5, 0.1% Tween-20). Embryos were then incubated in developing solution (20 µl/ml NBT/BCIP (Roche) in NTT) in the dark at room temperature to allow staining to develop. Once the development reaction was complete the embryos were washed in NTT twice for 10 minutes at room temperature, followed by a 10 minute wash in PBT pH 5.5 to stop the staining reaction and whiten embryos. Embryos were fixed in 0.1% glutaraldehyde in 4% PFA for 1 hour, then rinsed in PBS and photographed.

2.9.4. Sectioning

Embryos were sectioned following the whole mount *in situ* hybridisation (WISH) protocol by dehydrating through an ethanol series, embedding in wax and sectioning at 8 µm as described in section 2.5. Sections were counterstained in eosin only using the following method. Slides were de-waxed in Histoclear twice for 5 minutes each, washed in 100% ethanol twice for 1.5 minutes each, then rehydrated through an ethanol series of 90%, 70% and 50% ethanol for 1 minute each. Slides were washed in dH_2O for 1 minute then incubated in 1% eosin for 5 minutes. Following staining the slides were rinsed in running water to remove excess eosin then dehydrated through 50%, 70% and 90% ethanol, by dipping three times in each solution. The sections were incubated in 100% ethanol twice for 1.5 minutes then cleared in Histoclear twice for 5 minutes each before mounting in Histomount.

2.10. Pharyngeal arch dissections for quantitative PCR

2.10.1. Dissection

The pharyngeal arch region of both wild type (*Tcfap2a*$^{+/+}$) and mutant (*Tcfap2a*$^{-/-}$) embryos at e9.5 (18-25 somites) were collected for qPCR analysis. The embryos were collected in DEPC-PBS and kept on ice until dissected. Each embryo was removed from the deciduate and the yolk sac, with the yolk sac being collected for genotyping. A 27 gauge (G) needle was used to remove the PA region by cutting above the first PA and

below the heart (see Figure 2.1). The remainder of the embryo was discarded. The PA sample was collected in a sterile pasteur pipette and transferred to an RNase-free 1.5ml microcentrifuge tube, with any excess PBS being removed. The sample was immediately flash frozen in liquid nitrogen and stored at -80°C until RNA was extracted.

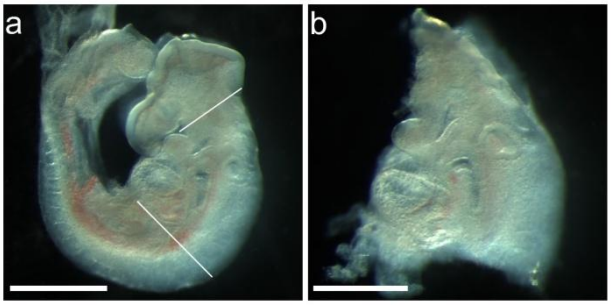

Figure 2.1: Dissection of the pharyngeal arch region in e9.5 embryos.
(a) e9.5 mutant embryo extracted from yolk sac. The lines indicate the region which was excised for RNA extraction. (b) The excised region. Scale bars = 1mm (a), 500 µm (b).

2.10.2. RNA extraction

500µl of TRIzol® reagent (Invitrogen) was added to each PA sample and incubated for 5 minutes to allow the nucleoprotein complex to dissociate. Homogenization was carried out by passing the sample through a 27G needle several times. 0.2 volumes of chloroform were added and the sample was shaken vigorously by hand, then incubated at room temperature for 2-3 minutes. Samples were centrifuged at 12,000 x g for 15 minutes at 4°C to allow phase separation of the samples components. 200µl of the upper aqueous phase, containing nucleic acids, was transferred to a fresh tube and an equal volume of RNase-free 70% ethanol added. The samples were mixed and then transferred to a PureLink™ RNA mini kit spin column (Life Technologies) and centrifuged for 15 seconds at full speed to allow binding of RNA to the column. The spin column was washed once in the supplied wash buffer 1 before on-column DNaseI treatment to remove any genomic DNA within the sample.

10 units of DNaseI were diluted in 1x DNase buffer in DEPC-H_2O to a total volume of 80 µl for each sample. The DNaseI mix was added to the spin column and incubated for 15 minutes at room temperature. The column was then washed again in wash buffer 1, followed by multiple washes in wash buffer 2 (contains ethanol). RNA was eluted from the column in 50 µl of the supplied RNase-free water. The quality and concentration of the eluted RNA was measured using a NanoDrop spectrophotometer

(section 2.8.3). Quality was determined using the 260/280 value, where optimal quality is determined by a 260/280 value of 2. Quality was also tested by running the samples on a 1% agarose gel at 200 V for 15 minutes. Total RNA was then used to synthesise complementary DNA (cDNA).

2.10.3. cDNA synthesis

cDNA synthesis was carried out using the High Capacity cDNA reverse transcription kit (Life Technologies). A 40 µl cDNA synthesis reaction contained: 500 ng RNA, 1 x Reverse transcriptase buffer, 1 mM each dNTP, 1 x random primers and 100 units reverse transcriptase. The cDNA synthesis reaction was carried out in a thermocycler with the following cycling conditions: 25˚C for 10 minutes, 37˚C for 2 hours, 85˚C for 5 minutes, 4˚C for 10 minutes. Synthesised cDNA was stored at -20°C until required.

2.10.4. Primer design

All qPCR primers were designed using the NCBI Primer-BLAST tool (available at: http://www.ncbi.nlm.nih.gov/tools/primer-blast), using the following parameters:

PCR product size	50-150 bp
Primer melting temperature (T_m)	Min: 57°C, Max: 70°C, Optimum: 60°C
Max T_m difference	1°C between primers
Exon junction span	Primer must span an exon-exon junction
Database	Refseq RNA (refseq_rna)
Organism	Mus musculus (taxid: 10090)
Splice variant handling	Allow primer to amplify mRNA splice variants

An accession number for each gene was obtained from the NCBI nucleotide database (available at: http://www.ncbi.nlm.nih.gov/nuccore) and input as the PCR template when designing primers. This allowed the Primer-BLAST tool to calculate the exon-exon boundaries so that one primer from each pair was designed to span an exon-exon junction. This, therefore, produced primers that were specific to the mRNA sequence of the gene and would be unable to bind to any contaminating genomic DNA. Where a single gene produced multiple transcripts, the accession number of the longest mRNA sequence was selected from the database. The splice variant handling parameter of the Primer-BLAST tool allowed us to design a single primer pair for binding to all

transcripts produced to get an overall impression of the activation of the genes promoter in the absence of *Tcfap2a*.

Table 2-7: Primer sequences and product sizes of all primers used in qPCR analysis.

Gene	Accession no.	Primer name	Sequence (5'- 3')	Product size (bp)
Housekeeping genes				
GAPDH	NM_008084	Gapdh fw	TGTGCAGTGCCAGCCTCGTC	80
		Gapdh rev	TGACCAGGCGCCCAATACGG	
Tcfap2 family genes				
Tcfap2a	NM_011547 NM_001122948	AP2a Ex6 fw	CCGATCCCAATGAGCAAGTGG	309
		AP2a Ex7 rev	TGCTTTTGGCGCTGTTGTCCG	
Tcfap2b	NM_009334	Tcfap2b fw	CGGCGTCCTCAGAAGAGCCAAAT	93
		Tcfap2b rev	CGCCTGCCCGCGGGTAAAT	
Tcfap2c	NM_001025305	Tcfap2c fw	TCGTGGAAGGTGAAGCCGTCCA	132
		Tcfap2c rev	TCCGCGTGGCCATCTCATTCC	
Neural crest markers				
Foxd3	NM_010425	foxd3 fw	TCGAGGAAGGCTGGTGAAGTGAGG	105
		foxd3 rev	CGAACTCTTGCGGTCCTCGACG	
Dlx5	NM_010056	dlx5 fw	GGCTACCCGGCCAAGGCTTATG	108
		dlx5 rev	TTCTTTCTCTGGCTGGCTGGTGG	
Snail2	NM_011415	Snai2 fw	CGCGCTCCTTCCTGGTC	187
		Snai2 rev	GCTGCCGACGATGTCCATAC	
Heart development genes				
Ccne2	NM_001037134 NM_009830	Ccne2 fw	TCTGTGCATTCTAGCCATCG	156
		Ccne2 rev	ACAAAAGGCACCATCCAGTC	
Smad7	NM_001042660	Smad7 fw 2	TCAACCCCGAGCTGGTGTGC	80
		Smad7 rev 2	GGAGTAAGGAGGAGGGGGAGACTCTAG	
Tgfb2	NM_009367	Tgfb2 fw 2	TGCTAACTTCTGTGCTGGGGCATG	126
		Tgfb2 rev 2	TCCTGGGACACACAGCAAGGG	
Fgf8	NM_010205 NM_001166361 NM_001166362 NM_001166363	Fgf8 all F	AGTTCGCGGCGCAGAGACAG	182
		Fgf8 all R	GCCGGCCCTTGCGGGTAAAG	
Fgf10	NM_008002	Fgf10 F	GAAGAACGGCAAGGTCAGCGGG	109
		Fgf10 R	GTTGCTGTTGATGGCTTTGACGGC	
Chd7	NM_001081417	Chd7 fw 2	TGCCACTAACGGGGTACAACAGC	85
		Chd7 rev 2	TTCATCCATAAGTGCACCATATGCCC	
Rara	NM_009024	Rara fw 2	CATCCCCTCGCTTCGAGCACC	187
		Rara rev 2	CGGAGGGGCCAGGTGGATTG	

Gene	Accession no.	Primer name	Sequence (5'- 3')	Product size (bp)
Rarb	NM_011243.1	Rarb fw 2	CCGCAGCATCAGCGCGAAAG	81
		Rarb rev 2	TGAATGAGAGGTGGCATTGATCCAGG	
Msx1	NM_010835	Msx1 fw 2	AGCTCTGCTGCCCTATACCA	202
		Msx1 rev 2	CTTGGCCTCTGCACCCTTAG	
Known Tcfap2a target genes				
Tbx20	NM_194263 NM_020496 NM_001205085	Tbx20 F	CGCCTGCAGCCTGGAAACGA	109
		Tbx20 R	TGACACGCGGATGGTGGGGA	
ErbB2	BC046811.1	ErbB2 fw	AACTGTGGTGGGCGTCCTGTTGT	130
		ErbB2 rev	GGCACGCCTCACCTCGGTCTC	
Acan	NM_007424.2	Acan fw	TACGGCGTGCGCCCATCATC	79
		Acan rev	TGGCGAAGAACACTTCCCCCTCA	
cMyc	NM_001177353.1	c-Myc fw	CCAGGCTCCGGGGAGGGAATTTT	143
		c-Myc rev	CGTCGTGGCTGTCGGGGTTTC	
cKit	NM_001122733.1	c-kit fw	CGGCACGGTGGAGTGTAAGGC	103
		c-kit rev	AGTGTGGGCCTGGATTTGCTCTTTG	
MMP-2	NM_008610.2	MMP2 fw	ACGTCACTCCGCTGCGCTTTT	83
		MMP2 rev	ATCTCCATGCTCCCAGCGTCCA	
VEGF-A	NM_001025250 NM_009505 NM_001025257	Vegfa fw1	CCAGGCTGCACCCACGACAG	171
		Vegfa rev1	CGCATCAGCGGCACACAGGA	
Sox10	NM_011437.1	Sox10 fw	TCACTACAAGAGTGCCCACCTGGA	134
		Sox10 rev	GCAGCTCTGTCTTTGGGGTGGTT	
Cited2	NM_010828.3	Cited2 fw 2	GAGCCCGCCTTCGGTGTTCC	158
		Cited2rev 2	GGCTCGGGAACTGCCCCATG	
Dlx family genes				
Dlx1	NM_010053.1	Dlx1 fw	TCGGTCAGCAGCCACGCGTCCA	113
		Dlx1 rev	CTCTTCTCGGAGTCCGCCCCTGGGT	
Dlx2	NM_010054.2	Dlx2 fw	GGGCCTCACCCAAACTCAGGTCAA	90
		Dlx2 rev	TCGGTGGGTATCTCGCCGCT	
Dlx3	NM_010055.3	Dlx3 fw	TTGCCTGCCCAGGACCCAGT	96
		Dlx3 rev	CGTTCGCGGCTTTCGGACCT	
Dlx4	NM_007867.4	Dlx4 fw	GCCACCCCCGGTCCTATTCC	150
		Dlx4 rev	GTGCCAGCTTCTCTGATTCTGCTTC	
Dlx5	NM_010056.2	Dlx5 fw3	CCAGCCAGCCAGAGAAAGAAGTGG	150
		Dlx5 rev3	GCAGGGCGAGGTACTGAGTCTTCT	
Dlx6	NM_010057.2	Dlx6 fw	GCGGGGACGACACAGATCAACAAAA	135
		Dlx6 rev	AGCGATGGTTTAAAGCCTGGAGCTG	

Gene	Accession no.	Primer name	Sequence (5'- 3')	Product size (bp)
Upstream activators of Dlx5				
Edn1	NM_010104	Edn1 fw	AGACCCCGCAGGTCCAAGCG	106
		Edn1 rev	CGACGCGCTCGGGAGTGTTGA	
ECE-1	NM_199307.2	ECE1 fw	GCCGCCCATGGTGAACGCTT	106
		ECE1 rev	CAAGGCGTTGGGTGAAGAGCGG	
Ednra	NM_010332.2	Ednra fw	TGTGGACAGGTACAGAGCAGTGGC	134
		Ednra rev	CGAAGCCGATTGCTTCCGGGAT	
Gnaq	NM_008139.5	Gnaq fw	ACCGTGTAGCCGACCCTTCCT	132
		Gnaq rev	GGCCCCCTACATCGACCATTCTGA	
Gna11	NM_010301.3	Gna11 fw	ACAATGAGAACCGCATGGAGGAGA	142
		Gna11 rev	TCGACCAAGTGTGAGTGCAGGA	
Gnas	NM_201618.1	Gnas fw	GGTGGCCAGCAGCAGCTACA	113
		Gnas rev	TGGTGCGCAGCCATCTGTTGT	
Gnai	NM_010305.1	Gnai fw	CCATGGGCTGCACATTGAGCG	132
		Gnai rev	ATTCCCCAGCACCCAGCAGC	
Downstream targets of Dlx5				
Cyp26a1	NM_007811.2	Cyp26a1 fw	TGGTGCTTCAGCGGAGGAAGTTT	121
		Cyp26a1 rev	ATGCGCCGCACATTATCCGC	
Cyp26b1 variant1	NM_175475.3	Cyp26b1.1 fw	GGGCTTGGGGCTTTGATGGCGGA	99
		Cyp26b1.1 rev	AGATTGCCTGGGGAGGCCTTGGCT	
Cyp26b1 variant2	NM_001177713.1	Cyp26b1.2 fw	CCCCTTCCACCTTCTATCGGCAATC	112
		Cyp26b1.2 rev	TCCTGGCACCCCTCGGAGAA	
Cyp26c1	NM_001105201.1	Cyp26c1 fw	TCGGCAACGGCGTAAGGTCC	75
		Cyp26c1 rev	CCCTGCAACCGTGGCACGAA	
Hand1	NM_008213	Hand1 fw 2	CGGAAAAGGGAGTTGCCTCAGCAG	83
		Hand1 rev2	CCGGTGCGCCCTTTAATCCTCTTC	
Hand2	NM_010402	Hand2 fw	CCAGCTACATCGCCTACCTC	163
		Hand2 rev	TTCTTGTCGTTGCTGCTCAC	
Isl1	NM_021459	Isl1 F	TGCCACCTAGCCACAGCACC	158
		Isl1 R	TGCCGCAACCAACACACAGGG	
Gbx2	NM_010262	Gbx2 F	GAGGCGGCAACTTCGACAAAGCC	190
		Gbx2 R	TCCTCCTTGCCCTTCGGGTCATC	

2.10.5. Quantitative PCR

2.10.5.1. Sample preparation

cDNA samples, prepared as above, were diluted 1:4 in dH_2O. Diluted samples were vortexed to ensure thorough mixing of the samples and briefly centrifuged. 2 µl of diluted cDNA was used in each quantitative PCR (qPCR) reaction.

2.10.5.2. Primer preparation

Primer stocks (Sigma) were diluted to a final concentration of 10 µM for use in the qPCR reactions. Each 10 µM primer mix was prepared with 10 µl forward primer, 10 µl reverse primer and 80 µl dH_2O. 1 µl of primer mix was added to an individual qPCR reaction. *Tcfap2b* primers were diluted to 5 µM using 5 µl forward primer, 5 µl reverse primer and 90 µl dH_2O, with 1 µl of primer mix being used in an individual reaction.

2.10.5.3. qPCR reactions

All qPCR reactions were performed on a 7900HT Fast Real-Time PCR system (Applied Biosystems) using SYBR®Green JumpStart™ Taq Ready Mix™ (Sigma). Each 10 µl reaction contained: 1 x SYBR Green mix, 1 x internal reference dye (Rox), 1 µM forward primer, 1 µM reverse primer and 2 µl diluted cDNA. Each reaction was carried out in triplicate on a 384-well plate (Greiner). The plate was centrifuged to collect all components of the reaction together in a Sorvall Evolution RC Superspeed centrifuge, using the SH-3000 rotor, for 4 minutes at 4,000 x g and 4°C. The plate was then inserted into the 7900 HT machine and the qPCR reaction was run using the programme shown in Table 2-8.

Table 2-8: qPCR programme used on the 7900 HT machine.

Temperature	Time		
95 °C	15:00		
95 °C	00:30		
60 °C	00:30	39	
72 °C	00:30	cycles	
79.5 °C	00:10		Data collection point
68 °C	00:10		Data collection point
99°C	00:10		Data collection point

2.10.6. Analysis

Data was analysed by the comparative cycle threshold (Ct) method using Microsoft Excel (Microsoft) (Schmittgen and Livak, 2008) and also the data analysis for real-time PCR (DART-PCR) excel spreadsheet method to ensure primer efficiencies were

comparable between target genes and sample groups (mutants vs controls) (Peirson *et al.*, 2003).

2.10.6.1. Comparative Ct method

The comparative Ct method of analysis requires data to be extracted in the form of Ct values. This is the number of reaction cycles required for level of fluorescence within each individual reaction to reach the threshold level set prior to the start of the reaction. Any Ct values within a triplicate which fell outside of 0.5 Ct values of each other were discarded as outliers and analysis was carried out with only two values.

Firstly, the average Ct value of the triplicate was calculated for each sample. This was then normalised to Glyceraldehyde 3-phosphate dehydrogenase (GAPDH), by subtracting the average Ct for GAPDH for each sample from the average Ct for the target gene of that sample. The ΔCt of each normalised value was calculated by 2 raised to the power of the negative of the normalised value:

$$\Delta Ct = 2^{-average\ Ct\ target\ gene - average\ Ct\ GAPDH}$$

This calculation is based upon the assumption of a 100% efficiency of the PCR reaction which would produce two copies of the gene at each cycle. The average ΔCt value for each sample group (control and mutant) was then calculated. The fold change in gene expression was calculated by dividing the ΔCt value of both control and mutant groups for each gene by the average ΔCt value for the control group. This allowed the value for all control groups to be maintained at 1 and all changes in expression in the mutant groups to be plotted relative to wild type expression. All data analysis and graphs were carried out using Microsoft Excel. Standard deviations were calculated using the raw ΔCt values for all samples and all genes for both groups and standard error was used for error bars on the graphs. The data was imported into the Prism 6 statistics package and statistical significance was calculated using a student's *t*-test.

2.10.6.2. DART-PCR

The use of the comparative Ct method described above assumes that efficiency of any PCR reaction is 100% and produces two copies of the target DNA per cycle of the reaction. However, an efficiency between 90-110% is generally considered acceptable

for using the comparative Ct method of analysis. The DART-PCR method (Peirson *et al.*, 2003) was used to calculate primer efficiencies for each target gene and the housekeeping gene GAPDH. This method uses the raw fluorescence data (ΔRn values) from the qPCR reaction to calculate how many copies of the target gene product are produced per cycle. The ΔRn value is calculated by normalising the fluorescence emission intensity of the reporter dye to that of the Rox dye and then subtracting the baseline level of fluorescence observed in the initial cycles of PCR when there is very limited change in fluorescence levels. The ΔRn values for each well were input into the DART-PCR spreadsheet and the primer efficiencies for both wild type and mutant groups were calculated and compared to ensure that the fold change calculated by the comparative Ct method was reliable and not the product of changes in the primer efficiency between these groups.

2.11. Reverse transcription PCR

Reverse transcription (RT)-PCR uses end point PCR on cDNA samples. All components of the RT-PCR reaction are as outlined in section 2.3.2 above, with the exception of DNA, which was replaced with varying volumes of cDNA. RNA extraction, cDNA synthesis and primer design were carried out as described above (see section 2.10), however regions of interest were specified for each primer pair designed to *Tcfap2a*.

2.11.1.PGKcre and Sox2cre

This method was used to investigate the transcripts produced by both *PGKcre* and *Sox2cre*-mediated deletions of *Tcfap2a*. Embryos were collected at e9.5 and stored for RNA extraction (see section 2.10.2). The primers used in the analysis of the *PGKcre* mutant embryos were GAPDH, *Tcfap2a, Tcfap2a* floxed and *Tcfap2a* common shown in Table 2-9. The *Tcfap2a* primers used in the qPCR analysis were initially used to investigate the wild type transcripts produced in the embryos. The *Tcfap2a* floxed primers bind either side of the floxed region and are therefore used to examine if this region has been successfully recombined in these mutants. The *Tcfap2a* common primers were designed to bind to all transcripts of *Tcfap2a*, including all splice variants and both mutant alleles. Analysis of *Sox2cre* mutant embryos used *Tcfap2a* floxed and GAPDH primers only.

2 µg of total RNA from each sample was used to synthesise cDNA. The cDNA was then diluted 1:10 and 2 µl were used in the RT-PCR reactions.

2.11.2.Wnt1cre

To investigate the recombination of *Tcfap2a* by *Wnt1cre* embryos were collected at e7.5, e8.0 and e8.5 for RT-PCR analysis. The primer pairs used in this analysis are shown in Table 2-9. The *Tcfap2a* floxed and common primers described above (see section 2.11.1) were used to examine *Tcfap2a* expression. Expression of *Wnt1cre* was examined using primers designed to the *Cre* cDNA construct. As these primers will bind both genomic DNA (gDNA) and cDNA a set of primers designed to *Cited2* which will also bind to gDNA were included in the analysis to exclude the possibility of gDNA contamination. Any gDNA contamination in these samples would result in a 636 bp band in addition to the 158 bp band observed for cDNA samples.

Table 2-9: Sequences and product sizes of primers used in RT-PCR reactions.

Gene	Primer name	Sequence (5'-3')	Product size (bp)
GAPDH	Gapdh fw	TGTGCAGTGCCAGCCTCGTC	80
	Gapdh rev	TGACCAGGCGCCCAATACGG	
Tcfap2a	AP2a Ex6 fw	CCGATCCCAATGAGCAAGTGG	309
	AP2a Ex7 rev	TGCTTTTGGCGCTGTTGTCCG	
Tcfap2a floxed	Tcfap2a ex3/4 fw	TTAAGAAAGGCCCCGTGTCCCTG	Wild type – 663 Recombined - 402
	Tcfap2a ex7 rev	TAACCGCTGCACACACCGCC	
Tcfap2a common	Tcfap2a ex3/4 fw	TTAAGAAAGGCCCCGTGTCCCTG	102
	Tcfap2a ex 4 rev	CGTTGGGGTTTACCACGCCAC	
Cre	S1X-A	GCATAACCAGTGAAACAGCATTGCTG	280
	S1X-B	GGACATGTTCAGGGATCGCCAGGCG	
Cited2	Cited2 fw 2	GAGCCCGCCTTCGGTGTTCC	158 (636 – gDNA)
	Cited2 rev 2	GGCTCGGGAACTGCCCCATG	

Four *Wnt1cre* positive and four *Wnt1cre* negative embryo samples were used at each stage. RNA extraction and cDNA synthesis was carried as described above (see section 2.10.5), with a few exceptions. The RNA from e7.5 embryos was eluted in 15 µl RNase-free water and 200 ng total RNA was used in a 20 µl cDNA synthesis reaction. 2 µl of cDNA was used in each RT-PCR reaction. For embryos at e8.0, RNA was eluted in 20 µl RNase-free water and 200 ng total RNA was used in a 20 µl cDNA synthesis reaction. For embryos at e8.5, RNA was eluted in 25 µl RNase-free water and 250 ng were used

in a 20 µl cDNA synthesis reaction. cDNA was diluted 1:2, and 2 µl were used in each RT-PCR reaction.

2.12. Western blotting

2.12.1. Sample collection

Embryos from a timed mating of *Tcfap2a*$^{+/f}$*;PGKcre* x *Tcfap2a*$^{f/f}$ animals were collected at e10.5. Embryos were dissected in ice-cold PBS. Mutant embryos (*Tcfap2a*$^{f/f}$*;PGKcre*) could be identified by an open neural tube at this stage. All embryos were flash frozen in liquid nitrogen and stored at -80°C until use. Yolk sacs were collected for genotyping.

2.12.2. Sample lysis

Whole e10.5 embryos were lysed in 300 µl of 1 x Laemmli buffer (2% SDS, 5% v/v β-mercaptoethanol (Merck), 10% glycerol, 0.05% w/v bromophenol blue (SLS), 62.5 mM Tris pH 6.8). The tissue was homogenised by passing through a 19G syringe several times, followed by passing through a 21G needle several times. Each sample was then heated at 95°C to denature the proteins within the sample for 5 minutes, followed by a 5 minutes centrifugation at full speed.

2.12.3. Polyacrylamide gel electrophoresis

Commercially available pre-cast gels (Mini-PROTEAN TGX Precast Gels, 10%; Bio-Rad) were used in all experiments to minimise variation between experiments. 10 µl of each sample was loaded into a well, and 9 µl of a protein standard (Life technologies) was run alongside for comparison. Samples were electrophoresed in a tank containing 1x running buffer (25mM Tris, 190 mM glycine 0.1% SDS, pH 8.3) at 180 V for 35 minutes or until the migration front had reached the end of the gel.

2.12.4. Protein transfer

A polyvinyl difluoride (PVDF) membrane was activated by immersion in 100% methanol for 30 seconds, then rinsed in dH_2O for 5 minutes and equilibrated in ice-cold transfer buffer (48 mM Tris, 39 mM glycine, 0.04% SDS, 20% methanol) for 20 minutes prior to transfer. Once the polyacrylamide gel had run completely it was removed from the plastic cast and placed onto the membrane. The gel and membrane were clamped together between with 2 sheets of blotting paper and a sponge on

either side and blotted at 100 V for 1 hour at 4°C. The transfer buffer was gently agitated with a magnetic flea throughout.

To ensure efficient transfer, proteins were visualised on the membrane using a ponceau staining technique. The membrane was removed from the transfer cassette and re-activated in methanol for 30 seconds. The membrane was then stained with ponceau staining solution (0.1% w/v ponceau-S, 5% v/v acetic acid) for 5 minutes and rinsed in 5% acetic acid to clear any background staining. The staining solution was then removed by rinsing several times in TBST (50 mM Tris, 150 mM NaCl, 0.1% Tween-20, pH 7.6).

2.12.5. Blocking and immunodetection

The membrane was blocked in 5% w/v milk powder, diluted in TBST, for 1 hour at room temperature with gentle agitation. The primary antibody, anti AP-2α (3B5, santa cruz biotechnology, sc-12726) was diluted 1:1000 in 5% milk/TBST blocking solution and incubated overnight at 4°C with gentle agitation. The following day the primary antibody was removed and the membrane washed 4 times in 5% milk/TBST for 10 minutes each then replaced with secondary antibody (polyclonal goat anti-mouse immunoglobulins/horse radish peroxidise, P0447) diluted 1:10,000 in 5% milk/TBST and incubated for 1 hour at room temperature. The membrane was washed a further 4 times in 5% milk/TBST then 4 times in TBST.

2.12.6. Development

For detection of the bound secondary antibody the SuperSignal West Dura Substrate (Thermo Scientific) was used. Solutions A and B were mixed in equal ratios and 2 ml were added to the membrane and incubated for 5 minutes. Excess substrate was drained from the membrane and the membrane wrapped in plastic and exposed to a sheet of X-ray film (Amersham Hyperfilm ECL, GE healthcare). The exposed film was then developed.

2.12.7. Bioinformatics

In order to determine the outcome of the mutations within the *Tcfap2a*^{LacZ} and *Tcfap2a*^{floxed} alleles on the protein produced, a bioinformatics approach was taken. The cDNA sequence was obtained from Ensembl (available online at: http://www.ensembl.org/index.html) as was the coding sequence of each exon

individually. The sequence of the recombined allele was recreated based on information from Brewer *et al*. (2004) and input into the GENESCAN web server (available online at: http://genes.mit.edu/GENSCAN.html) to determine if the removal of exons 5 and 6 had resulted a change in the position of the exon-intron boundaries. The protein sequence retrieved from GENESCAN was compared to the wild type protein sequence using a multiple sequence alignment tool (available online at: http://www.ebi.ac.uk/Tools/msa/clustalo). The ProtParam tool (available at: http://web.expasy.org/protparam) was also used to predict the size of any protein product that may be produced from this transcript.

2.13. India ink injections

To investigate the formation of the PAAs, embryos were collected at e10.5 (32-39s) for india ink injections. Dissections were carried out in ice-cold PBS as described above (section 2.4). The embryo was transferred to a petri dish containing 1% agarose (made up in dH_2O) and submersed in PBS. Embryos were pinned to the agarose from their right side, with one pin through the head and a further pin holding the tail in place, to expose the heart. India ink (pelikan, diluted 1:1 in dH_2O) was then injected into the left ventricle using a mouth pipette (Sigma) and a pulled glass pipette. The ink was forced into the PAAs by the pumping of the embryo heart. Images of the embryos from both right and left sides were taken for analysis.

Chapter 3. Investigating the role of *Tcfap2a* in the neural crest cells

3.1. Introduction

The preliminary data presented in the introduction chapter described the severe cardiovascular malformations observed in *Tcfap2a*$^{-/-}$ mutant mice on a C57BL/6J background (see section 1.5.2). The data obtained from a NCC-specific deletion of *Tcfap2a* on a 72.55% C57BL/6J background was also presented. This work indicated an increase in the levels of CCVM in comparison to that previously described (Brewer *et al.*, 2002; Brewer *et al.*, 2004). This chapter will investigate the penetrance of CCVM in a conditional deletion from the NCCs on a congenic C57BL/6J background. We also aim to further investigate the role that the genetic background has on the penetrance of the phenotype seen with the NCC-specific deletion of *Tcfap2a*, as variation between our data and that of Brewer *et al*. (2004), may be attributed to modifier loci on the altered genetic background affecting the observed phenotype.

3.1.1. Requirement of NCCs in PAA and heart development

The NCCs play important roles in the development of the mammalian heart. They migrate from the dorsal neural tube, through the caudal PAs and into the OFT. Once in the OFT, the NCCs are involved in the formation of the aorticopulmonary septation complex and in the septation of the interventricular septum. NCCs remaining in the PAs surround the PAAs and differentiate into the SMCs of the tunica media. The SMCs here are important in the ability of the vessel to withstand haemodynamic pressure as blood circulation begins, and also in supporting the PAAs during the subsequent remodelling stages (Kirby and Waldo, 1990; Hutson and Kirby, 2003). Reduction in NCCs, due to defective migration or cell death, or failure to differentiate into SMCs are key components in the development of PAA defects in many animal models (Lindsay and Baldini, 2001; Abu-Issa *et al.*, 2002; Calmont *et al.*, 2009) .

3.1.2. Cre/loxP recombination

First described in 1992, the Cre/loxP recombination system has been extensively used throughout developmental biology (Lakso *et al.*, 1992; Orban *et al.*, 1992). This technique utilises the enzyme cre recombinase, produced by the bacteriophage P1, which acts on short sequences termed 'loxP sites'. The enzyme causes recombination between two such sites, removing intervening sequences. These loxP sites can be

introduced into specific regions of a gene of interest to cause inactivation, by removal of important regions required for the function of the gene product. Alternatively, insertion of a floxed (flanked by loxP sites) 'stop' sequence upstream of a gene of interest, can be used to inactivate a gene in all tissues but that under investigation. The expression of the cre recombinase gene can be directed by the promoter of another gene (Figure 3.1a), allowing specific spatial and temporal activation of the cre enzyme, which therefore results in tissue-specific activation/inactivation of the gene of interest.

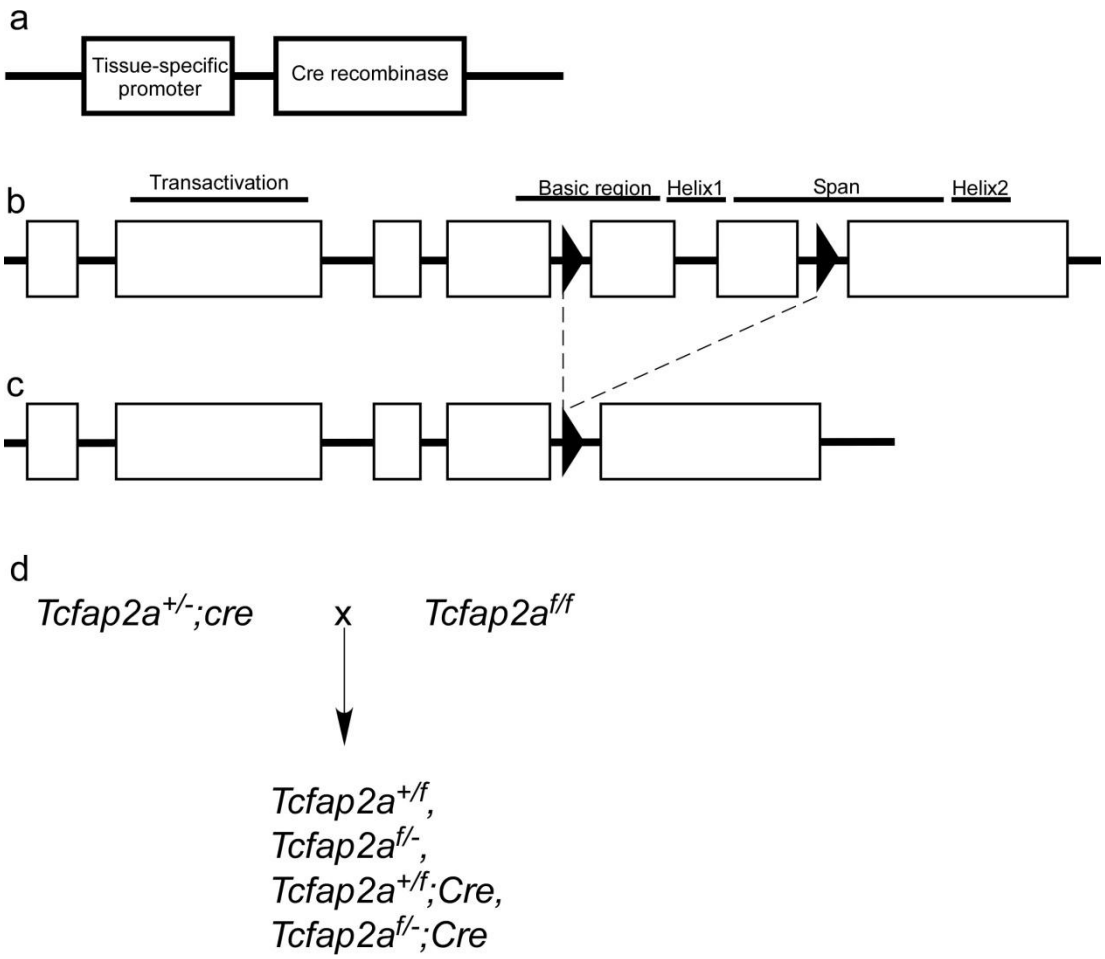

Figure 3.1: Tissue-specific deletion of *Tcfap2a*.
(a) A tissue-specific promoter drives the expression of the *Cre* recombinase gene, allowing recombination in only the desired tissues. (b) The structure of the floxed allele of *Tcfap2a*. The loxP sites (solid arrowheads) flank exons 5 and 6. (c) Cre-mediated recombination of the loxP sites removes exons 5 and 6. (d) A male heterozygous for *Tcfap2a* and carrying *Cre* driven by a tissue-specific promoter (*Tcfap2a*$^{+/-}$*;Cre*) was crossed to a female homozygous for the floxed *Tcfap2a* allele (*Tcfap2a*$^{f/f}$) to generate offspring which were heterozygous for *Tcfap2a* in all tissues, and are null in those tissues expressing cre (*Tcfap2a*$^{f/-}$*;Cre*). Embryos which were wild type in all tissues except those expressing *Cre* (*Tcfap2a*$^{+/f}$*;Cre*) were used as controls.

A floxed allele of *Tcfap2a* was generated by insertion of loxP sites within introns 4 and 6 of the *Tcfap2a* gene (Brewer *et al.*, 2004) (Figure 3.1b). Cre-mediated recombination between these sites results in the excision of exons 5 and 6 (Figure 3.1c), removing a

large portion of the basic region, important in DNA binding, and much of the HSH region of the dimerisation domain.

To generate tissue-specific deletions of *Tcfap2a*, the floxed allele was used in combination with the *Tcfap2a*-null allele. A cre-positive male heterozygous for *Tcfap2a* was crossed to a female homozygous for the floxed allele (Figure 3.1d) to generate mutant (*Tcfap2a*$^{f/-}$*;Cre*) and control (*Tcfap2a*$^{+/f}$*;Cre*) embryos.

In this study, we aimed to investigate the conditional deletion of *Tcfap2a* from the NCCs on a congenic C57BL/6J background. In addition, *Tcfap2a* is highly expressed within the PSE. We were, therefore, also interested in the role of *Tcfap2a* in this tissue. To investigate these tissues we used *Wnt1cre* to remove *Tcfap2a* from the NCCs and both *Foxg1cre* and *Nkx2.5cre* were used to inactivate the gene in the PSE.

3.1.2.1. Wnt1cre

Wnt1cre (Danielian *et al.*, 1998) was used to inactivate *Tcfap2a* within the NCCs. The *Wnt1* promoter becomes active at e8.0 with expression restricted to the midbrain. By e8.5, expression has extended caudally into the hindbrain and extended into the forebrain (Echelard *et al.*, 1994). The *Wnt1cre* transgene was generated by the insertion of the *Cre* cDNA downstream of the *Wnt1* promoter, therefore allowing *Wnt1*-driven activation of *Cre* in all NCCs. The transgene was electroporated into embryonic stem cells, allowing random integration of the construct. A line carrying a single construct was used to generate the *Wnt1cre* transgenic mouse strain. The expression of the *Wnt1cre* transgene was confirmed using a lineage tracing mouse strain and demonstrated that recombination had taken place within the midbrain by e8.5, less than 12 hours after the activation of the *Wnt1* promoter (Danielian *et al.*, 1998).

3.1.2.2. Nkx2.5cre

The *Nkx2.5cre* line was generated by introducing the *Cre* cDNA directly into the *Nkx2.5* locus by homologous recombination, producing a knock-in allele. The *Nkx2.5* promoter drives expression of *Cre* in the myocardium and the ectoderm and endoderm of the PAs, by e9.5 (Moses *et al.*, 2001). As *Tcfap2a* is not expressed within

the myocardium or endoderm (Brewer *et al.*, 2002), *Nkx2.5cre* can be used to disrupt *Tcfap2a* specifically within the PSE.

3.1.2.3. Foxg1cre

The *Foxg1cre* construct, like *Nkx2.5cre*, was also generated by homologous recombination into the *Foxg1* locus. Expression of *Cre* begins at e8.5 in the tip of the head folds and in the underlying ectoderm, the anterior neural ridge (ANR). By e8.75 expression has extended into the ectoderm that will come to cover the PAs. LacZ expression is seen in the PSE at e9.5 and extends into the foregut by e10.5 (Hebert and McConnell, 2000).

3.1.2.4. Wnt1cre-mediated deletions of Tcfap2a

Previously published data suggests that the deletion of *Tcfap2a* from the NCCs in mice on a black swiss background results in no cardiovascular anomalies (Brewer *et al.*, 2004). However, 43% of these mutants died before postnatal day (P) 1, due to inability to feed and respiratory distress. This was attributed to a cleft secondary palate, and embryos examined at e16.5 demonstrated that the palatal shelves elevate normally, but fail to elongate and fuse at the midline. Interestingly, a milder phenotype, in which incomplete fusion of the palatal shelves occurred, was also described in a number of mutants. These mutants survived in the immediate postnatal period, but failed to thrive, and died or were euthanized by P4 (Brewer *et al.*, 2004).

3.1.3. Genetic dissection in cardiovascular development

Genetic dissection is often used in models of cardiovascular development in an attempt to decipher which expression domains are responsible for each element of the phenotype. In some cases this can be a relatively simple task, in which a single Cre line is required to recapitulate the CCVM phenotype of the null mouse. However, in some cases it is not possible to dissect the individual expression domains of a gene, either due to the lack of specific cre lines, the complex genetic interactions between multiple tissue-types, or the gene of interest being expressed earlier than the cre lines available for that tissue. A number of cases in which genetic dissection has been used to investigate cardiovascular development, with variable outcomes are discussed below.

Gbx2$^{-/-}$ embryos have 39-50% incidence of heart defects, mostly affecting the development of the fourth PAAs, and a low incidence of OFT defects such as DORV and

OA (Byrd and Meyers, 2005; Calmont *et al.*, 2009). These defects have been attributed to disruptions of NCC migration into the PAAs at e9-9.5. However, as *Gbx2* is not expressed within the NCCs, the authors propose that *Gbx2* is important within the pharyngeal epithelia for the activation of signalling pathways required in NCC migration into the arches (Byrd and Meyers, 2005). Conditional deletion of *Gbx2* from the PSE, using AP-2α-IRESCre, resulted in a comparable level of fourth PAA defects to that seen in *Gbx2*$^{-/-}$ embryos, when examined at e10.5 by ink injection, suggesting that ectodermal expression of *Gbx2* is key to the NCC migration defects observed in *Gbx2*$^{-/-}$ embryos. The authors also demonstrate that these defects are the result of disruptions of the Slit/Robo pathway, involved in migration of the NCCs to the PAs (Calmont *et al.*, 2009).

Deciphering the tissue-specific requirements of *Tbx1* has proven much more difficult, however. The phenotype produced in *Tbx1*$^{-/-}$ embryos affects many areas of the embryos, including the OFT, interventricular septum, PAAs, thymus, parathyroids, ears and craniofacial development (reviewed in Lindsay, 2001; Scambler, 2010). As *Tbx1* is widely-expressed throughout the PA tissues and the SHF it is possible that each expression domain may contribute to different aspects of the phenotype. Additionally, haploinsufficiency of *Tbx1* results in thymus defects and hypoplasia of the fourth PAAs, adding to the difficulties associated with conditional removal of this gene. Therefore, a series of cre lines have been used to investigate the tissue-specific requirements of *Tbx1*, both in the context of null and heterozygous embryos.

Mutant embryos with a homozygous deletion in the endothelium and myocardium (using *Tie2cre* and *αMHCcre*, respectively) yielded no additional defects to those observed in *Tbx1*$^{+/-}$ embryos. However, conditional homozygotes using *Nkx2.5cre*, which is expressed within the pharyngeal endoderm, ectoderm and mesoderm in addition to the SHF, resulted in full recapitulation of the OFT defects and VSD observed in *Tbx1*$^{-/-}$ mutants. The authors describe a reduced and disorganised SMC layer surrounding the OFT in these mutants and propose that the reduced proliferative activity in the SHF is responsible (Xu *et al.*, 2004).

Further evidence that mesodermal expression of *Tbx1* is important for correct for OFT morphogenesis comes from crosses with *MesP1cre*, which is expressed in all

mesodermal derivatives including the endothelium. Conditional homozygotes in *MesP1cre*-expressing tissues exhibit 100% penetrance of PTA, VSD and PAA malformations. In addition, the segmentation of the pharynx is disrupted, resulting in the loss of the caudal PAs. Further defects affecting the migration of the NCCs into the PAs, disruptions of the NC-derived cranial ganglia and reduced proliferation of the PA mesenchyme, were also observed.

Reactivation of *Tbx1* within the mesoderm of mutant embryos was achieved through the introduction of a neomycin cassette, flanked by LoxP sites into the *Tbx1* locus. Null embryos, which were homozygous for this allele were produced and *Mesp1cre* was used to remove the neomycin cassette and reactivate mesodermal expression. This rescued the OFT and VSD phenotypes, but not the fourth PAA defects, suggesting other tissues are required in this malformation (Zhang *et al.*, 2006).

In order to address the tissue-specific requirements of *Tbx1* in PAA morphogenesis, a similar array of cre lines were used to produce conditional heterozygous embryos. Conditional deletions within the endothelium (*Tie2cre*) and mesoderm (*MesP1cre* and *Nkx2.5cre*) yielded no PAA malformations. However, removing *Tbx1* from the SHF, mesoderm, ectoderm and endoderm using *Foxg1cre* resulted in 42% fourth PAA hypoplasia. *Fgf15cre*, which is also expressed within the pharyngeal endoderm and ectoderm, was also used and PAA malformations were observed in 55% conditional heterozygotes, an almost complete recapitulation of the 60% penetrance of fourth PAA malformations observed in this genetic background. This suggests that *Tbx1* expression within the pharyngeal epithelia is required for correct PAA morphogenesis (Zhang *et al.*, 2005).

Further evidence for the role of epithelial expression of *Tbx1* in PAA development comes from conditional heterozygotes within the PSE (using AP-2α-IREScre), which resulted in 76% fourth PAA defects at e10.5, suggesting that the PSE is a major tissue for *Tbx1* expression in correct morphogenesis of the PAAs (Randall *et al.*, 2009).

In conclusion, mesodermal expression of *Tbx1* is required for proliferation in OFT morphogenesis and in correct fusion of the interventricular septum, while biallelic expression within the ectoderm is required in the development of the fourth PAA. In

addition the fourth PAA malformations within the *MesP1cre* mutants are likely to be the result of the loss of segmentation of the pharynx in these mutants, rather than suggesting a role of *Tbx1* in the mesoderm for PAA morphogenesis.

Despite a number of successes and the significant amount of knowledge gained from the use of cre lines to genetically dissect genes required for cardiovascular development, it is not always possible to understand the tissue-specific requirements of a gene of interest. An example of this is the genetic dissection of the AP-2 coactivator gene *Cited2*. *Cited2*-null mutations result in a number of cardiovascular defects including ASD, VSD, AVSD, DORV and PTA, with PAA defects such as IAA and RAA (Bamforth *et al.*, 2001). In addition, defects in left-right patterning were also observed on an altered genetic background (Bamforth *et al.*, 2004). Therefore, a series of genetic dissection experiments were designed in order to investigate the tissue-specific requirements for this gene. Removal of *Cited2* from the NCCs, using *Wnt1cre*, resulted in defects of the NCC-derived cranial ganglia in approximately 80% embryos, although no defects in NCC-migration were observed. Deletions in the mesoderm, using *Mesp1Cre* and *TCre*, resulted in cardiac septal defects in 16% and 21% embryos, respectively, with an additional 7% (1/14) of embryos having a left-right patterning defect and 71% with adrenal agenesis in the *TCre* mutants. Removal of *Cited2* from the entire epiblast using *Sox2cre,* however resulted in VSD and adrenal agenesis in all mutant embryos and cardiac laterality defects in 60% embryos. The authors conclude that *Cited2* is required in the epiblast during early stages of development for correct left-right patterning, with a secondary requirement in the mesoderm for cardiac septation (MacDonald *et al.*, 2008).

The examples presented above demonstrate both the advantages and disadvantages associated with the investigation of conditional mutants. Although in some cases the defects observed in null-mutants are relatively simple and the required tissues can be readily identified (e.g. *Gbx2*), other genes with more complex phenotypes require vast numbers of cre lines in order to infer which tissues are most important (e.g. *Tbx1*). In addition, for some genes (*Cited2*) it is not possible to distinguish between individual expression domains with currently available cre lines.

3.1.4. Effect of Genetic Background in Mice

The global deletion of *Tcfap2a* results in a fully penetrant cardiovascular phenotype, affecting the OFT, interventricular septum and PAAs. Both VSDs and OFT defects have been previously described in this model, however, the prevalence of PAA abnormalities was limited (Brewer *et al.*, 2002). The preliminary data described in the introduction chapter (see section 1.5.2) demonstrates full penetrance of PAA defects on a C57BL/6J background, which may be attributed to the change in genetic background.

Genetic background is a very important element in the phenotype of any mouse mutation and has been found in many cases to severely affect the manifestation of mutations in a gene of interest. In most cases modifying loci are mutated in specific backgrounds, and are phenotypically silent. It is only in the presence of another mutation, usually an experimentally-induced mutation in a gene of interest, that the effect of the modifying gene is visible.

The modifying gene generally has a function relevant to the phenotype which is being observed by the mutation in the gene which it is said to be modifying. Therefore, genes which modify the phenotype of a mutation in another gene are likely to be involved in similar processes or pathways to the gene of interest. However, in many cases the modifying gene is unknown, or multiple genes may be modifying the same phenotype generating greater variability.

3.1.5. Aims of chapter

The aim of this chapter is to investigate the role of *Tcfap2a* in the NCCs in the developing mouse cardiovascular system on a congenic C57BL/6J background. Previous work on *Tcfap2a*$^{-/-}$ embryos (Brewer *et al.*, 2002) demonstrates a fully penetrant cardiovascular phenotype consisting of a VSD and a malformation of the OFT, with limited prevalence of PAA defects. Further work by this group using a NC-specific cre line, *Wnt1cre*, has suggested that *Tcfap2a* is not required within the NCCs for correct cardiovascular development (Brewer *et al.*, 2004). However, our work on *Tcfap2a*$^{-/-}$ embryos demonstrates an increase in PAA defects (100% penetrant) to that seen by Brewer *et al.* (2002) on this altered background. In addition, preliminary data investigating *Tcfap2a*$^{f/-}$*;Wnt1cre* mutant embryos demonstrates 55% penetrance of

CCVM. Therefore, we wanted to examine the NC-specific deletion on this congenic C57BL/6J background to determine if the change in genetic background has had an effect on the NCCs. We also aim to investigate the role of the genetic background on the penetrance of the observed defects. Additionally, the role of another *Tcfap2a*-expressing tissue, the PSE, in modulating the phenotype will also be explored.

3.2. Results

3.2.1. Cleft palate in *Tcfap2a$^{f/-}$;Wnt1cre* embryos (72.55% C57BL/6J)

The study by Brewer *et al*. (2004) demonstrated that *Tcfap2a$^{f/-}$;Wnt1cre* mutants die in the immediate postnatal period, or soon after due to a cleft secondary palate. We, therefore, examined the *Tcfap2a$^{f/-}$;Wnt1cre* mutant embryos presented in the preliminary data (see section 1.5.2) for the presence of cleft palate. Of the 9 mutant embryos examined 3 were aged e14.5. During normal development the palatal shelves have elevated, elongated and begun fusion at this stage (Bush and Jiang, 2012). However, of 3 mutants and 1 control examined at this stage, all embryos showed failed elevation of the palatal shelves. This suggests a possible developmental delay in these embryos and they were excluded from further analysis.

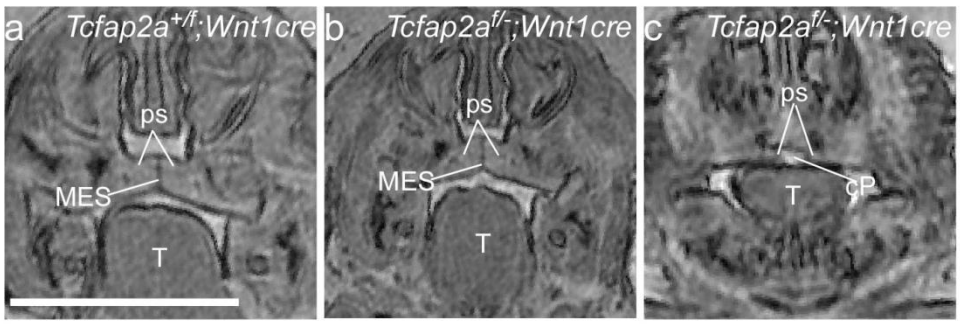

Figure 3.2: Palate development in *Tcfap2a$^{f/-}$;Wnt1cre* mutants.
Wild type (a) embryos show complete formation of the secondary palate, with the palatal shelves (ps) fused at the midline. 5/6 mutant embryos show normal palatal development (b), however, in one mutant the palatal shelves failed to fuse. T, tongue; ps, palatal shelves; cP, cleft palate; MES, midline epithelial seam. Scale bar = 2mm. (n=6)

Of the remaining e15.5 mutant embryos examined 5/6 showed normal palate development (Figure 3.2a-b). A single mutant embryo showed a failure in the fusion of the palatal shelves (Figure 3.2c). All embryos examined at this stage show evidence of the midline epithelial seam (MES), which would usually be apparent in only the most anterior regions. However, at e15.0 the MES is visible throughout the palate, again suggesting a mild developmental delay in these embryos, possibly due to differences in genetic background.

Overall, of the 6 *Tcfap2a*$^{f/-}$*;Wnt1cre* embryos examined at e15.5, only 1 (16.67%) showed any sign of cleft palate, indicating a significant reduction from that observed by Brewer *et al*., (2004).

3.2.2. Wnt1cre-mediated deletions of *Tcfap2a*

3.2.2.1. Expression patterns of Tcfap2a and Wnt1cre

To ensure efficient recombination between LoxP sites in the *Wnt1cre* mutants, we first chose to examine the expression pattern of both *Tcfap2a* and the *Wnt1cre* construct to confirm that *Wnt1cre* is active before the onset of *Tcfap2a* expression. *Wnt1cre* activation was examined using the R26R^{LacZ} reporter construct (see section 2.2.4) (Soriano, 1999). These transgenic mice allow for fate mapping of all cells in which *Wnt1cre* becomes activated. To determine the expression pattern of *Tcfap2a* we used the LacZ cassette knocked-in to the gene in the creation of the null allele.

Embryos were collected at e8.5-e10.5 and stained using the substrate X-gal to identify β-galactosidase activity. At early e8.5 (4-5 somites) a low level of *Tcfap2a* expression was apparent in a thin region of the midbrain (Figure 3.3a). At this stage, *Wnt1cre* expression is prominent throughout the midbrain region (Figure 3.3b). By e9.5 (22-24 somites), *Tcfap2a* expression can be seen throughout the first and second PAs and expression is becoming evident in the region where the caudal PAs (3-6) will develop (Figure 3.3c). *Wnt1cre* is strongly expressed throughout the head, and in both PAs and in the area that will give rise to the caudal PAs, at this stage (Figure 3.3d). At e10.5 *Tcfap2a* expression continues within the PAs. Expression is also visible in the limb buds at this stage (Figure 3.3e). At this time, *Wnt1cre* expression is visible throughout the head and PAs and extends along the dorsal midline into the tail (Figure 3.3f).

This demonstrates that the *Wnt1* promoter is active prior to e8.5, allowing the removal of the transcriptional stop sequence of the R26R^{LacZ} reporter construct, so that β-galactosidase can be produced. The expression of *Wnt1cre* begins before *Tcfap2a* at all stages, suggesting that efficient recombination of the *Tcfap2a*^{flox} allele by *Wnt1cre* would be possible, prior to the activation of the *Tcfap2a* promoter.

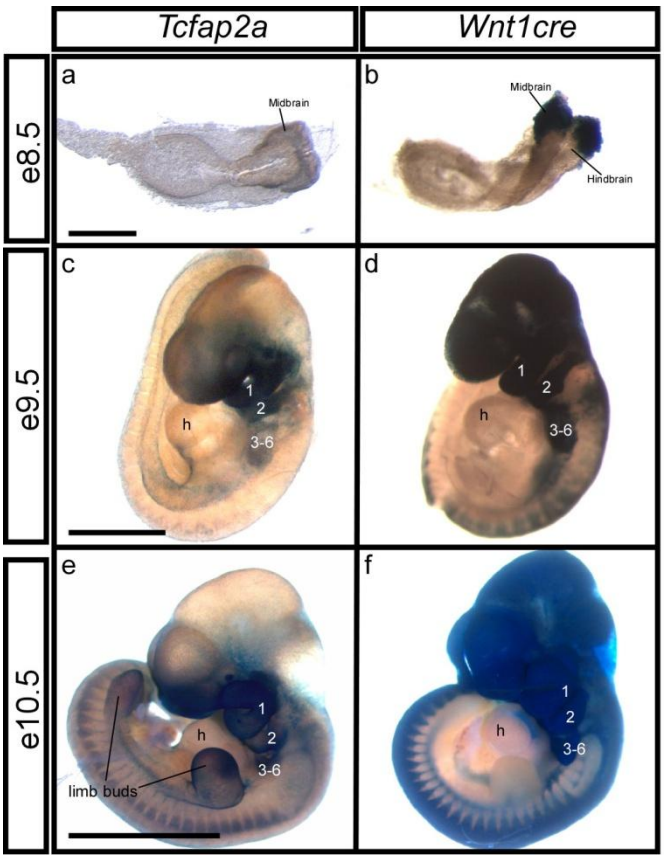

Figure 3.3: Comparison of the expression patterns of *Tcfap2a* and *Wnt1cre* during early development.
(a) Expression of *Tcfap2a* begins at e8.5 (5 somites) in a thin region of the midbrain. Scale bar = 500 µm. (b) At the same stage, Cre recombinase is active throughout the entire midbrain, with a sharp boundary between the midbrain and hindbrain. (c) By e9.5, expression of *Tcfap2a* has extended into the craniofacial region, throughout pharyngeal arches 1 and 2 and is beginning to be expressed in region which will come to form pharyngeal arches 3-6. Scale bar = 1mm. (d) *Wnt1cre* has been expressed throughout the entire head and within pharyngeal arches 1, 2 and 3-6. (e) At e10.5, *Tcfap2a* expression in the head is more restricted to the frontonasal region, and expression continues throughout the pharyngeal arches. LacZ expression is also visible in the limb buds. Scale bar = 2mm. (f) At this stage, *Wnt1cre* expression has extended along the dorsal midline through the trunk region and into the tail. Expression of these genes in the heart (h) is restricted to the NCCs of the OFT at the stages examined.

3.2.2.2. Wnt1cre-mediated deletion of Tcfap2a on a 94% C57BL/6J background

Both strains of mice (*Tcfap2a*$^{f/f}$ and *Tcfap2a*$^{+/-}$*;Wnt1cre*) were bred onto a C57BL/6J background for several generations, until the background reached approximately 94% C57BL/6J. Embryos were collected at e15.5, a stage at which cardiovascular development is complete. Examination of the dissected embryos revealed a reduction in the penetrance of exencephaly from that seen in the preliminary data. The majority of mutant embryos were indistinguishable from wild type animals in appearance, however, a small percentage showed an external phenotype. Exencephaly was observed in 5.26% (1/19) of *Tcfap2a*$^{f/-}$*;Wnt1cre* mutants examined (Figure 3.4b). A further 21% (4/19) of embryos showed a slight spinal curvature (Figure 3.4b), while the remaining embryos were wild type in appearance (Figure 3.4c).

Embryos were examined by MRI. The aligned .tiff stacks generated by this method were analysed with AMIRA software and used to create 3D representations of the observed cardiovascular phenotype (Figure 3.5). CCVM was observed in only 10.53% (2/19) of the examined mutant embryos. One embryo had a VSD and A-RSA (Figure 3.5c-d). Another embryo had a vascular ring (VR), which arises from the dorsal aorta passes behind the oesophagus, as an A-RSA would, however, this vessel joins to the ascending aorta. This would produce a completed ring, however, the aortic arch in this embryo contains an interruption and therefore, the VR is the only connection from the ascending aorta to the systemic blood flow (Figure 3.5e-f). The RSA forms normally in this embryo.

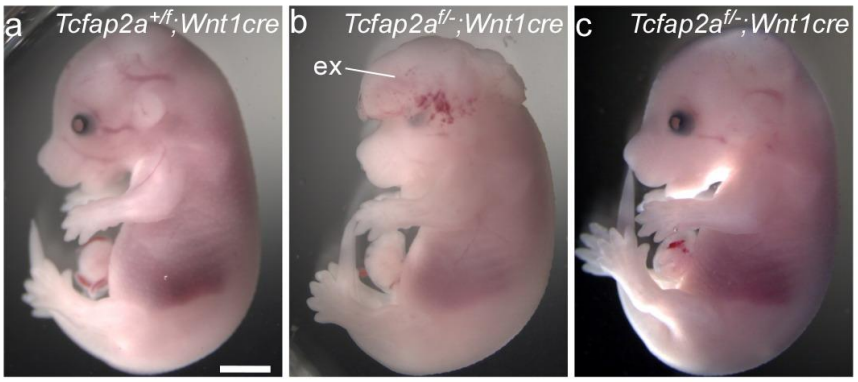

Figure 3.4: External phenotype of 94% C57BL/6J background *Tcfap2a$^{f/-}$;Wnt1cre* mutant embryos. *Tcfap2a$^{+/f}$;Wnt1cre* control embryos (a) show a normal external phenotype. One *Tcfap2a$^{-/f}$;Wnt1cre* mutant embryo had exencephaly (b), all other mutants appear as controls (c). Scale bar = 2 mm. (n = 19).

Histological analysis allows for a much higher resolution image than that provided by MRI analysis, and was therefore used to confirm the defects seen in the MRI data and to identify any subtle defects which could not be identified by MRI. The A-RSA in the first embryo was confirmed and can clearly be seen in the histological images as a protrusion from the dorsal aorta (Figure 3.6h). The VR was also confirmed. The series of sections in Figure 3.6 (i-l) show a vessel protruding from the dAo, much like the A-RSA in Figure 3.6 (h). This vessel then passes behind the oesophagus, and joins the ascending aorta. The brachiocephalic trunk, giving rise to the RSA and the RCC artery, develops normally from this vessel (seen in higher sections).

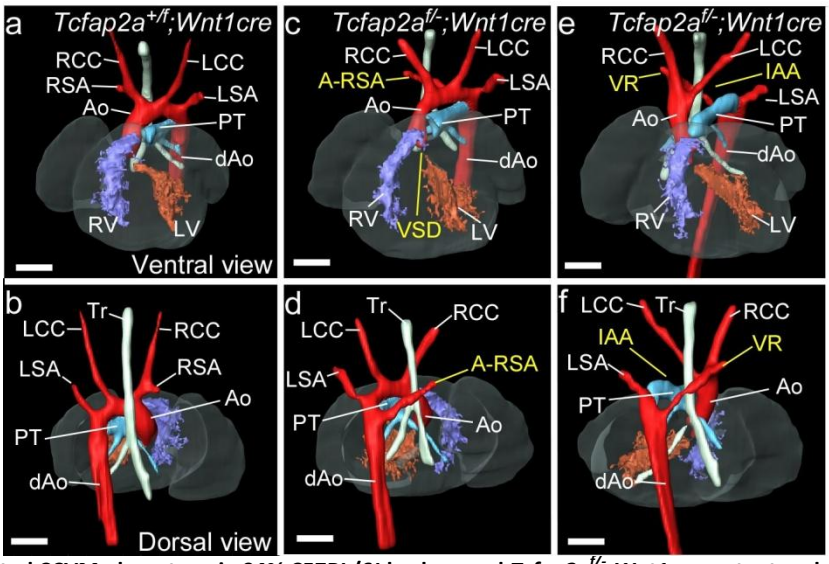

Figure 3.5: Limited CCVM phenotype in 94% C57BL/6J background *Tcfap2a$^{f/-}$;Wnt1cre* mutant embryos.
3D reconstructions of MRI data for *Tcfap2a$^{f/+}$;Wnt1cre* control (a-b) and *Tcfap2a$^{f/-}$;Wnt1cre* mutant hearts (c-f), from ventral (a, c, e) and dorsal (b ,d, f) views. One mutant had a VSD with an A-RSA (c-d). The other mutant had a IAA-B, with a VR joining the ascending aorta (Ao) to the systemic blood flow (e-f). Scale bar = 500 µm. (n = 19). RCC, right common carotid artery; RSA, right subclavian artery; Ao, aorta; Tr, trachea; LCC, left common carotid artery; LSA, left subclavian artery; PT, pulmonary trunk; dAo, dorsal aorta; RV, right ventricle; LV, left ventricle.

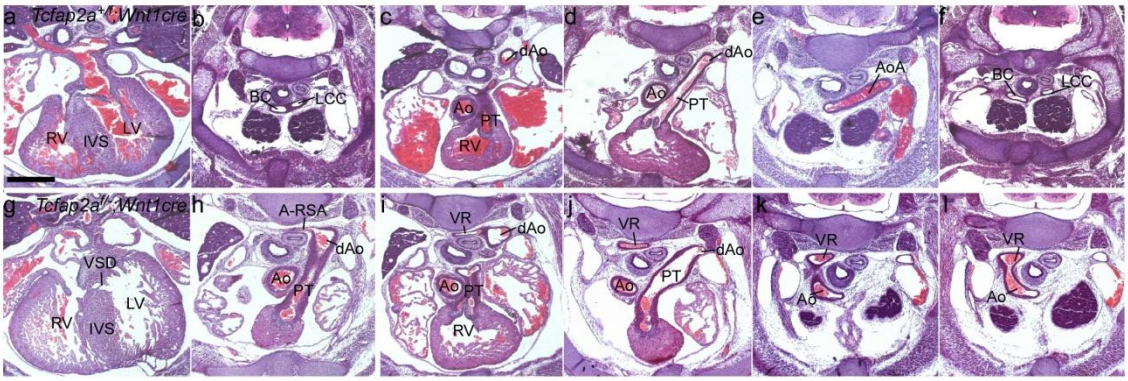

Figure 3.6: Histological analysis of CCVM in 94% C57BL/6J *Tcfap2a$^{f/-}$;Wnt1cre* mutants.
Haematoxylin and eosin-stained sections of *Tcfap2a$^{f/+}$;Wnt1cre* control (a-f) and *Tcfap2a$^{f/-}$;Wnt1cre* mutant (g-l) embryos. The mutant embryos are the same as those in the 3D reconstructions shown in Figure 3.5. In normal development an interventricular septum forms between the left and right ventricles (a). However, in one mutant embryo, a small interruption of this septum was seen, resulting in a VSD (b). Additionally, this embryo was also seen to have an A-RSA, with the right subclavian artery arising directly from the dorsal aorta (dAo) (h) instead of the brachiocephalic trunk (b). The remaining images are serial sections. In normal development, the pulmonary trunk arises from the right ventricle (RV) and forms the ductus arteriosus (DA) joining the dAo. The ascending aorta then joins to the dAo forming the aortic arch (AoA), which later gives rise to the left common carotid (LCC) artery and the brachiocephalic trunk (BC) (the base of both the right common carotid and the right subclavian arteries). In the mutant embryo (i-l) a vascular ring (VR) arises from the dAo (i), passes behind the oesophagus (j-k) and joins to the ascending aorta (l). Scale bar = 500 µm. (n = 19).

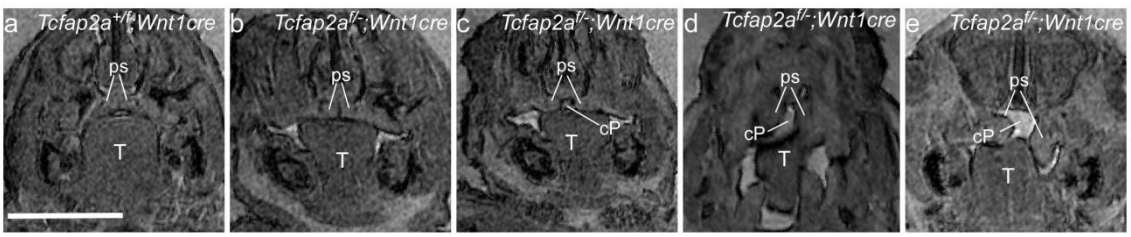

Figure 3.7: Identifying cleft palate in 94% C57BL/6J background *Tcfap2a$^{f/-}$;Wnt1cre* mutants.
Normal fusion of the palatal shelves as in*Tcfap2a$^{+/f}$;Wnt1cre* controls (a) was observed in 58% *Tcfap2a$^{f/-}$;Wnt1cre* mutant embryos (b). The remaining mutants had varying severities of phenotype, such as a failure in the fusion of the shelves (c), failure of the shelves to elongate (d) and failed elevation of one palatal shelf (e). Scale bar = 2mm. (n = 19).

This MRI dataset was also used to investigate the prevalence of cleft palate in these mutants. It was found that the majority (11/19, 58%) of mutant embryos had a fully formed palate as seen in controls (Figure 3.7a-b). In 10.5% (2/19) of mutant embryos examined the palatal shelves had elevated and elongated, but had failed to fuse at the midline (Figure 3.7c), while in another embryo the shelves had failed to elongate (1/19, 5.26%) (Figure 3.7d). A final class of cleft palate, which affected over 25% of mutant embryos (5/19, 26.3%), showed a failure in the elevation of the left palatal shelf, with the right palatal shelf being unaffected. Overall, 42% (8/19) of the embryos examined showed some malformation of the secondary palate.

To summarise, *Tcfap2a*$^{f/-}$*;Wnt1cre* mutant embryos on the high (94%) C57BL/6J background have a very low penetrance of CCVM (10.53%). Preliminary work on the *Wnt1cre* deletion of *Tcfap2a* revealed 55% penetrance of CCVM on a 72.55% C57BL/6J background. However, inbreeding further onto C57BL/6J (94%) has reduced the penetrance of defects. Therefore, altering the genetic background has affected the penetrance of CCVM in this line.

3.2.2.3. Wnt1cre-mediated deletion of Tcfap2a on a 72% C57BL/6J background

To further investigate the role of the genetic background in these mice, we attempted to recapitulate the penetrance of CCVM seen previously in the NCC-specific deletions, by outbreeding the *Tcfap2a*$^{+/-}$*;Wnt1cre* strain onto a CD1 background (Figure 3.8). Offspring from this cross would have a genetic background of approximately 50% C57BL/6J;50% CD1. *Tcfap2a*$^{+/-}$*;Wnt1cre* male offspring were then crossed with *Tcfap2a*$^{f/f}$ females (97% C57BL/6J). The embryos generated from these timed matings, therefore, had a genetic background which was approximately 75% C57BL/6J; 25% CD1.

This genetic background is similar to that used in the preliminary work (72.55% C57BL/6J), and we hypothesised that this background would increase the penetrance of CCVM to a level similar to that seen previously. 40% (4/10) of the mutants examined presented with exencephaly (Figure 3.9b), a pronounced increase in comparison to those embryos on the 94% C57BL/6J background, and more similar to that seen previously on the 72% C57BL/6J background (4/9, 45%). However, these mutant embryos were found to have no obvious cardiovascular malformations;

although one embryo had an unusual origin of the brachiocephalic trunk, arising directly from the ascending aorta (Figure 3.9h-l).

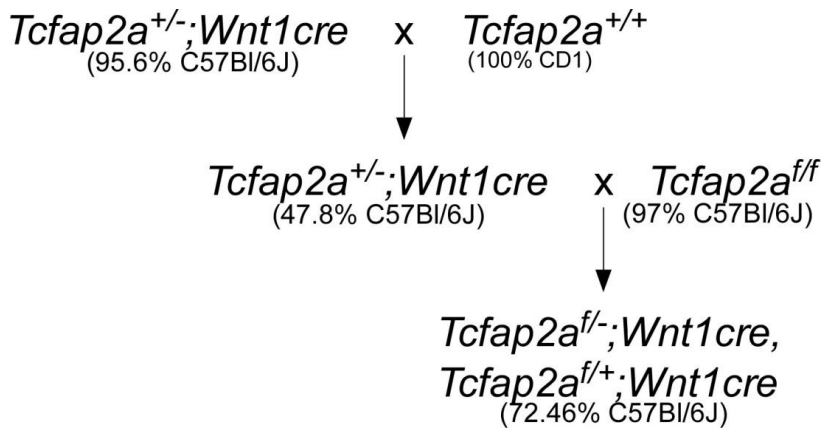

Figure 3.8: Breeding strategy for the generation of *Tcfap2a$^{f/-}$;Wnt1cre* mutant and *Tcfap2a$^{+/f}$;Wnt1cre* control embryos on a 72.5% C57BL/6J background.
The *Tcfap2a$^{+/-}$;Wnt1cre* male of 95.6% C57BL/6J background was bred to wild-type CD1 females. Offspring from this cross would be of a 47.8% C57BL/6J background. A male of genotype *Tcfap2a$^{+/-}$;Wnt1cre* from these litters was used in timed matings with *Tcfap2a$^{f/f}$* females from the congenic background. All resulting embryos of these matings were 72.5% C57BL/6J background. Other genotypes were produced in these crosses, but only those used in subsequent crosses or collected at embryonic stages for analysis are shown.

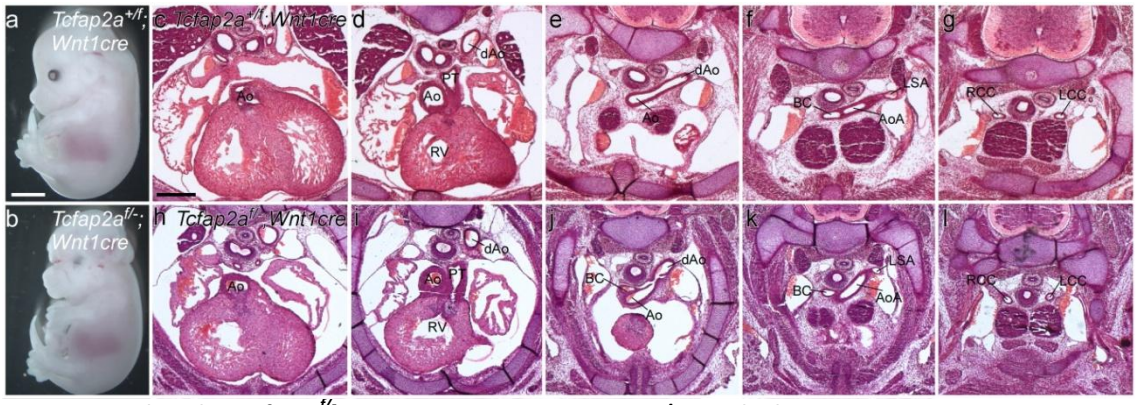

Figure 3.9: Outbreeding *Tcfap2a$^{f/-}$;Wnt1cre* mutants to 75% C57BL/6J resulted in no CCVM.
Control (a) and mutant (b) embryos were collected at e15.5. 4/10 (40%) mutants were found to show exencephaly (b). Serial sections of control (c-g) and mutant (h-j) embryos demonstrate that cardiovascular development in mutants occurs as in controls. One embryo had an aberrant origin of the brachiocephalic trunk (BC) (j). Scale bar = 2mm (a, b), 500 µm (c-l) (n=10).

As described above (see section 3.2.1), defects in the formation of the secondary palate were seen previously in *Tcfap2a$^{f/-}$;Wnt1cre* mutant embryos at e15.5. We therefore investigated the formation of the palate in these mutants. Of 9 embryos examined for CCVM, 3 were excluded due to developmental delay (aged e14.5). The 6 remaining mutants were analysed and compared to controls (Figure 3.10a). 33.33% (2/6) of embryos showed complete fusion of the palatal shelves (Figure 3.10b) as seen in controls. One embryo (16.67%) showed complete elongation of the palatal shelves, without fusion (Figure 3.10c), while 33.33% (2/6) showed incomplete elongation

(Figure 3.10d). In a further embryo (16.67%) the palatal shelf on the right had elevated, while the left shelf failed to do so (Figure 3.10e).

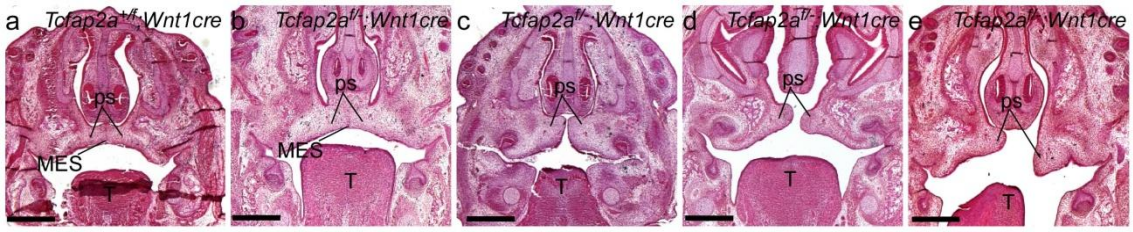

Figure 3.10: Identifying cleft palate in 72.46% C57BL/6J background *Tcfap2a$^{f/-}$;Wnt1cre* mutants.
(a) *Tcfap2a$^{f/+}$;Wnt1cre* control embryo with correct fusion of the palatal shelves. 2/6 *Tcfap2a$^{f/-}$;Wnt1cre* mutants also had complete fusion of the palatal shelves (b). One mutant embryos showed failed fusion of the palatal shelves (c), in two other mutants the palatal shelves had failed to elongate (d) and in another the left palatal shelf failed to elevate (e). Scale bar = 500 µm (n=10).

3.2.2.4. Summary and conclusions from Tcfap2a$^{f/-}$;Wnt1cre mutants

We have shown that the penetrance of CCVM in the NC-specific deletion of *Tcfap2a* is dependent on the genetic background. As summarised in Table 3-1, on the 72.55% C57BL/6J background there was a relatively high incidence of exencephaly and CCVM, but with low incidence of cleft palate. On the more congenic (94%) C57BL/6J background, the prevalence of both exencephaly and CCVM was reduced, while cleft palate is seen more often. In those embryos outbred to CD1 animals, the rate of exencephaly has increased closer to that seen in the original 72.55% C57BL/6J background, however CCVM had disappeared entirely, and the prevalence of cleft palate was higher than either of the previous crosses.

Table 3-1: Summary of phenotypes for *Tcfap2a$^{f/-}$;Wnt1cre* embryos on altered genetic backgrounds.

% C57BL/6J	72.55%	94%	72.46%
Other background	Mixed/129	Mixed/129	CD1
Exencephaly	45%	5.26%	40%
Cleft palate	16.67%	42.1%	66.66%
CCVM	55%	10.53%	0%
Phenotype	TGA, A-RSA, VSD	A-RSA, VSD, VR	No CCVM
Full descriptions	See sections 1.5.2 and 3.2.1	See section 3.2.2.2	See section 3.2.2.3

The reduced penetrance of CCVM in the NCC-specific deletion of *Tcfap2a* on a 94% C57BL/6J background is striking as on this background the global knockout showed 100% penetrance of VSD, OFT defects and fourth PAA defect. These defects are similar to those seen in NCC ablation in chicken embryos (Kirby, 1993), however, NCC-specific

loss of *Tcfap2a* yielded very low incidences of CCVM. This suggests that complex mechanisms of NCC patterning and regulation are in place which require signals from outside of the NC for NC development, and may indicate a further cell non-autonomous role of AP-2α on the NC.

3.2.3. *Tcfap2a* deletion from neural crest cells and surface ectoderm

As *Tcfap2a* is highly expressed in both the NCCs and the PSE, we wanted to investigate the possibility that the CCVM seen in the global knockout are the result of the removal of *Tcfap2a* from both tissues.

Previous work by our group has shown that *Tcfap2a* deletion using the ectodermally expressed cre lines, *Foxg1cre* and *Nkx2.5cre*, results in fully penetrant craniofacial defects. However, cardiovascular defects were seen only in very low numbers of these mutant embryos (Dr. Simon Bamforth, unpublished data). Therefore, as deletion from neither tissue individually can recapitulate the CCVM seen in the global mutants, we wanted to investigate the possibility that *Tcfap2a* is required in both tissues for correct cardiovascular development.

3.2.3.1. Breeding strategy

In order to investigate the role of *Tcfap2a* in both the NCCs and the PSE, complex cre lines, carrying both the NCC-specific *Wnt1cre* and one of the PSE-specific cre lines (PSE-cre) were generated (Figure 3.11). This was done by breeding *Tcfap2a*$^{+/-}$*;Wnt1cre* mice with *Tcfap2a* wild type mice carrying the PSE-cre of interest (*Tcfap2a*$^{+/+}$*;PSE-cre*). Once a complex cre male (*Tcfap2a*$^{+/-}$*;Wnt1cre;PSE-cre*) was created, he was bred with *Tcfap2a* floxed females to generate embryos with a conditional deletion of *Tcfap2a* in both the NCCs and the surface ectoderm of the PAs. Embryos with a tissue-specific deletion of *Tcfap2a* in either the NCCs or the PSE (*Tcfap2a*$^{f/-}$*;Wnt1cre* or *Tcfap2a*$^{f/-}$*;PSE-cre*) were used as controls to demonstrate that neither deletion alone gives fully penetrant CCVM.

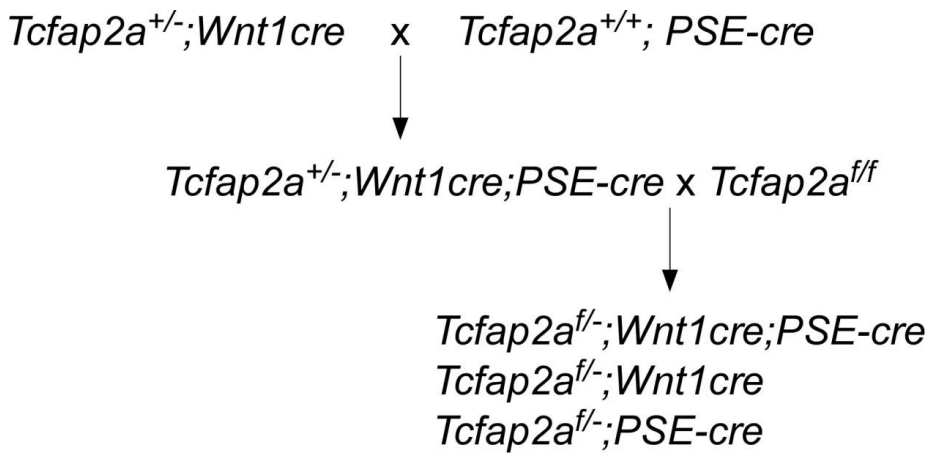

Figure 3.11: Breeding strategy for the generation of complex cre lines.
Tcfap2a$^{+/-}$*;Wnt1cre* stud male was bred with *Tcfap2a*$^{+/+}$ females carrying a cre line expressed in the pharyngeal surface ectoderm (PSE-cre), either *Foxg1cre* or *Nkx2.5cre*. Male offspring of the genotype *Tcfap2a*$^{+/-}$*;Wnt1cre;PSE-cre* were crossed to *Tcfap2a*$^{f/f}$ females and embryos were collected at e15.5. Mutant embryos had a tissue-specific deletion of *Tcfap2a* in both the NCCs and PSE (*Tcfap2a*$^{+/-}$*;Wnt1cre;PSE-cre*). Embryos with *Tcfap2a* deleted from only one of these tissues (*Tcfap2a*$^{f/-}$*;Wnt1cre* or *Tcfap2a*$^{f/-}$*;PSE-cre*) were used as controls.

3.2.3.2. Wnt1cre;Nkx2.5cre x Tcfap2a (97% C57BL/6J)

Nkx2.5 is most commonly known of as a cardiomyocyte-specific marker. However, the cre line is also known to be expressed within the surface ectoderm of the PAs, and it is here that the expression domain overlaps with that of *Tcfap2a*. Previous work by our group on *Tcfap2a*$^{f/-}$*;Nkx2.5cre* mutant embryos demonstrated a low level of CCVM (14%) in these embryos (Dr Simon Bamforth, unpublished data). A NCC-specific deletion using *Wnt1cre*, as discussed earlier, causes 10.53% penetrance of CCVM.

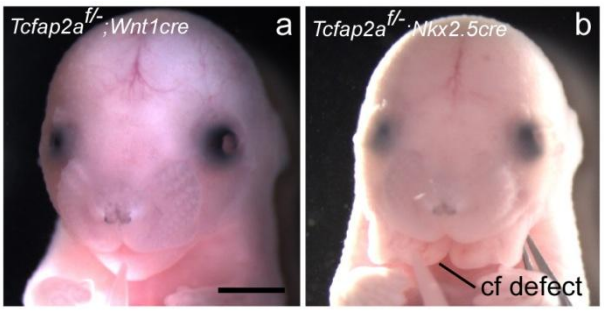

Figure 3.12: PSE-deletion of *Tcfap2a* by *Nkx2.5cre* results in lower jaw clefting.
(a) All *Tcfap2a*$^{f/-}$*;Wnt1cre* embryos show normal development of the craniofacial region. (b) Embryos carrying a tissue-specific deletion of *Tcfap2a* by *Nkx2.5cre* (either *Tcfap2a*$^{f/-}$*;Wnt1cre;Nkx2.5cre* or *Tcfap2a*$^{f/-}$*;Nkx2.5cre*) exhibit a craniofacial defect, caused by the failed fusion of the lower jaw at the midline. Scale bar = 2 mm. (n=6).

Tcfap2a$^{f/-}$*;Wnt1cre;Nkx2.5cre* mutant embryos were collected at e15.5. *Tcfap2a*$^{f/-}$*;Wnt1cre* or *Tcfap2a*$^{f/-}$*;Nkx2.5cre* littermates were used as controls. All *Tcfap2a*$^{f/-}$*;Wnt1cre;Nkx2.5cre* mutant and *Tcfap2a*$^{f/-}$*;Nkx2.5cre* control embryos show a mid-facial clefting in the lower jaw (Figure 3.12). However, histological examination of these embryos revealed no CCVM in any of the 6 mutants examined.

3.2.3.3. Wnt1cre;Foxg1cre x Tcfap2a (95.7% C57BL/6J)

Foxg1cre is also expressed in the surface ectoderm covering the PAs (Hebert and McConnell, 2000) and can be used in conjunction with *Wnt1cre* to remove *Tcfap2a* from both the PSE and NCCs.

A craniofacial defect affecting the frontonasal region was observed in all embryos of the genotypes *Tcfap2a$^{f/-}$;Wnt1cre;Foxg1cre* or *Tcfap2a$^{f/-}$;Foxg1cre* (Figure 3.13a-b). In addition 33% (2/6) of *Tcfap2a$^{f/-}$;Foxg1cre;Wnt1cre* embryos also presented with exencephaly (Figure 3.13, ex) as previously seen in the NC-specific deletion of *Tcfap2a*. This is also slightly higher level than seen in the NCC only conditional deletions of *Tcfap2a* (5.26%).

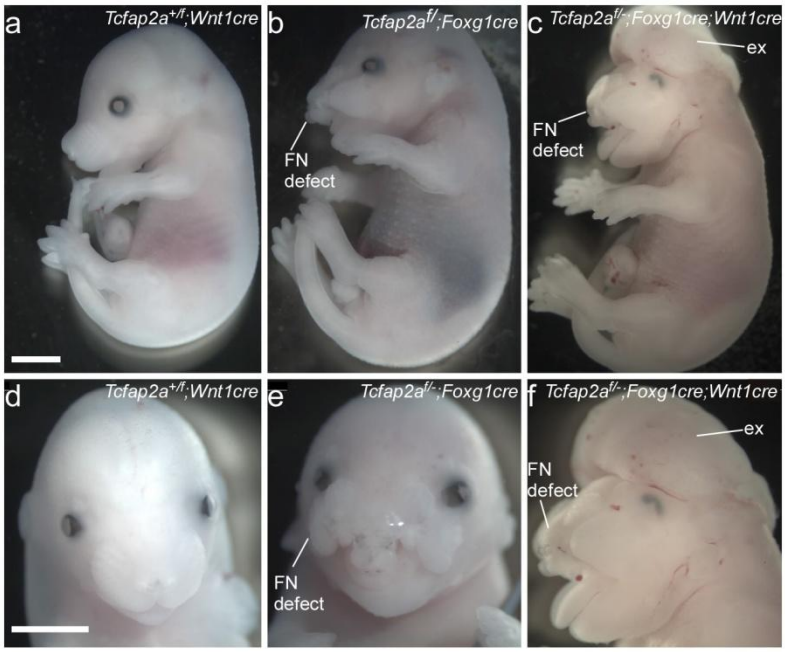

Figure 3.13: PSE-deletion of *Tcfap2a* by *Foxg1cre* results in frontonasal defects.
(a) *Tcfap2a$^{+/f}$;Wnt1cre* controls had normal craniofacial development. (b) All embryos with a PSE-deletion using *Foxg1cre* (*Tcfap2a$^{f/-}$;Foxg1cre* or *Tcfap2a$^{f/-}$;Wnt1cre;Foxg1cre*) develop a defect affecting the frontonasal region (FN defect). Some *Tcfap2a$^{f/-}$;Wnt1cre; Foxg1cre* embryos developed exencephaly (ex) in addition to the frontonasal defect. Scale bars = 2 mm (n=6 ,*Tcfap2a$^{f/-}$;Wnt1cre*; 5, *Tcfap2a$^{f/-}$;Foxg1cre*; 6, *Tcfap2a$^{f/-}$;Wnt1cre;Foxg1cre*).

Mutant and control embryos were sectioned and stained with haematoxylin and eosin and examined for cardiovascular defects. No cardiovascular defects were observed in either the *Tcfap2a$^{f/-}$;Foxg1cre* control or the *Tcfap2a$^{f/-}$;Foxg1cre;Wnt1cre* mutant embryos. However, an A-RSA was identified in a *Tcfap2a$^{f/-}$;Wnt1cre* control. Interestingly, anomalies relating to the thymus were also observed in these sections (Figure 3.14, Table 3-2).

In normal development, the two thymic rudiments develop from the third pharyngeal pouch endoderm and migrate downwards into their final position above the heart, as seen in the *Tcfap2a*$^{f/-}$*;Wnt1cre* controls (Figure 3.14a). However, in the *Tcfap2a*$^{f/-}$*;Foxg1cre* controls, only a single thymic rudiment migrates to this location. In 80% (4/5) of the embryos examined, the remaining thymic rudiment is on the left, with the right thymic rudiment being absent or ectopically placed. In 20% (1/5) of embryos the thymic rudiment had a central location. The removal of *Tcfap2a* from the NCCs in combination with the PSE exacerbated this phenotype further. *Tcfap2a*$^{f/-}$*;Foxg1cre;Wnt1cre* embryos showed a reduced number in which the right thymic rudiment was absent (2/6, 33.33%), but an increase in the number in which the rudiment was placed centrally (2/6, 33.33%). Additionally, a further 2/6 (33.33%) embryos were found to have no thymic rudiments present at this location, suggesting a complete failure of the thymic rudiments to migrate in these embryos.

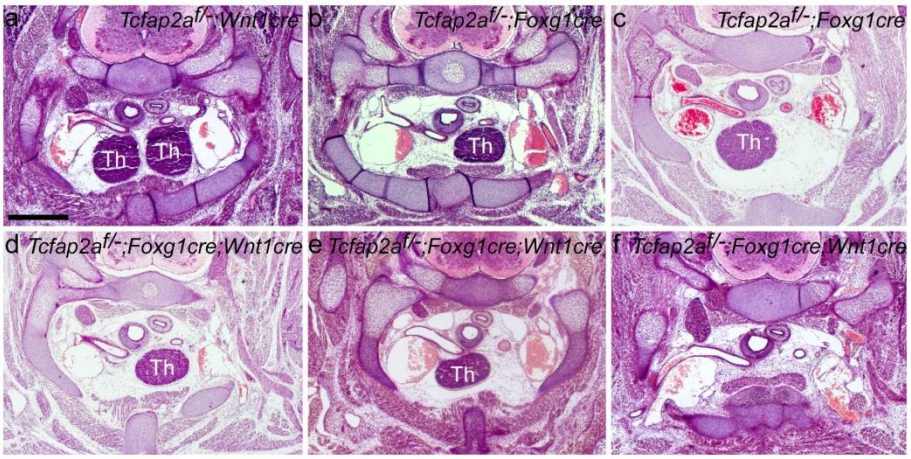

Figure 3.14: Absent thymus in embryos with a PSE deletion of *Tcfap2a* using *Foxg1cre*.
At e15.5 two thymic rudiments can be seen at the level of the brachiocephalic trunk in transverse sections. Thymus development is normal in *Tcfap2a*$^{f/-}$*;Wnt1cre* embryos (a). In embryos with a PSE-deletion using *Foxg1cre*, only one thymic rudiment is visible in the correct position, either on the left (b) or in a central location (c). *Tcfap2a*$^{f/-}$*;Wnt1cre;Foxg1cre* mutants also show these phenotypes (d-e), however, some mutants had no thymic rudiment (f). Th, thymic rudiment. Scale bar = 500 µm. (n = 6, *Tcfap2a*$^{f/-}$*;Wnt1cre*; 5, *Tcfap2a*$^{f/-}$*;Foxg1cre*; 6, *Tcfap2a*$^{f/-}$*;Foxg1cre;Wnt1cre*).

Table 3-2: Prevalence of thymus defects in *Tcfap2a*$^{f/-}$*;Foxg1cre* and *Tcfap2a*$^{f/-}$*;Foxg1cre;Wnt1cre* mutants.

	Tcfap2a*$^{f/-}$*;Foxg1cre **(n=5)**		***Tcfap2a*$^{f/-}$*;Foxg1cre;Wnt1cre*** **(n=6)**	
	No.	Percentage	No.	Percentage
Absent left	0	0	0	0
Absent right	4	80	2	33.33
Central	1	20	2	33.33
Both absent	0	0	2	33.33

In summary, all embryos with a PSE-deletion using *Foxg1cre* (*Tcfap2a$^{f/-}$;Foxg1cre* and *Tcfap2a$^{f/-}$;Foxg1cre;Wnt1cre*) exhibit a frontonasal defect and absent thymus. *Tcfap2a$^{f/-}$;Foxg1cre;Wnt1cre* mutant embryos also displayed exencephaly and an exacerbation of the absent thymus phenotype, with 33.33% (2/6) of embryos having bilaterally absent thymic rudiments. Of all the embryos examined, only a single embryo showed signs of CCVM, however this was in a *Tcfap2a$^{f/-}$;Wnt1cre* control (Table 3-3).

Table 3-3: Summary of defects observed in *Tcfap2a$^{f/-}$;Wnt1cre;Foxg1cre* mutant embryos and controls.

Genotype	n	FN defects	Exencephaly	Absent thymus		CCVM defects
				Unilateral	Bilateral	
Tcfap2a$^{f/-}$;Foxg1cre	5	100%	0%	100%	0%	0%
Tcfap2a$^{f/-}$;Wnt1cre	6	0%	0%	0%	0%	16% (1, A-RSA)
Tcfap2a$^{f/-}$;Foxg1cre;Wnt1cre	6	100%	33.33% (2)	66.67% (4)	33.33% (2)	0%

Those embryos with absent thymic rudiments (*Tcfap2a$^{f/-}$;Foxg1cre* or *Tcfap2a$^{f/-}$;Foxg1cre;Wnt1cre*) were re-examined to determine if the thymic rudiment was ectopically placed. It was found that the thymic rudiment appeared higher up in the embryo towards the head. In higher sections the thymic rudiment became misshapen and protruded from the skin.

3D reconstruction of *Tcfap2a$^{f/-}$;Foxg1cre* embryos imaged by MRI were made to determine the position of the protruding thymic rudiment from the skin. We found that the thymic rudiment protruded from the 'neck' region of the embryo (Figure 3.15).

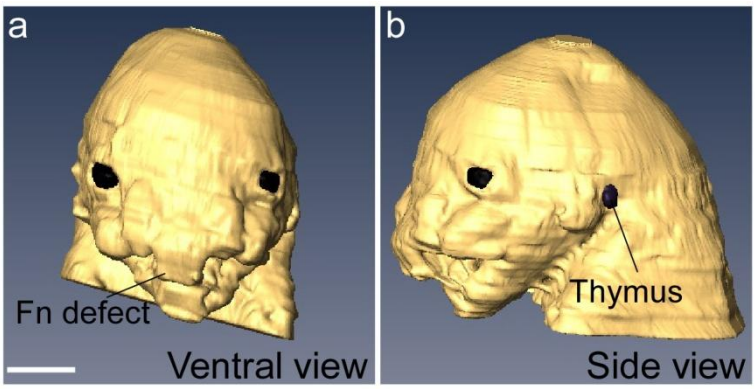

Figure 3.15: 3D reconstruction of the ectopic thymus defect in *Tcfap2a*$^{f/-}$*;Foxg1cre* mutant embryos.
(a) A ventral view of the reconstructions demonstrates the frontonasal defect (Fn) observed in all *Tcfap2a*$^{f/-}$*;Foxg1cre* mutant embryos. (b) A side view of the reconstruction demonstrates that the thymus arises from an ectopic position in the neck. Scale bar = 2mm.

3.3. Discussion

This chapter aimed to investigate the importance of *Tcfap2a* within the NCCs in the development of the mouse cardiovascular system in C57BL/6J mice. The preliminary data collected suggested that AP-2α was important in the NCCs for the development of the OFT, PAAs and interventricular septum. However, further examination on a congenic C57BL/6J background showed limited penetrance of this phenotype. We therefore went on to examine the effect of changing the genetic background in embryos with a NCC-specific deletion. This resulted in complete absence of CCVM, despite the appearance of an external phenotype (exencephaly was observed in 40% of embryos outbred to a CD1 background). To investigate the potential communication between the *Tcfap2a*-expressing tissues within the PAs (NCC-derived pharyngeal mesenchyme and PSE), we also carried out tissue-specific removal of *Tcfap2a* from both tissues simultaneously. Although this appeared to affect the development of other tissues (thymus and craniofacial region), no CCVM was observed in any of these complex mutant crosses.

3.3.1. Genetic Background

As described earlier in this chapter (see section 3.1.4), the genetic background of a mouse model can be highly influential in any phenotype resulting from genetic modification. These modifier loci are variations which arise in a specific strain of mice and persist in that background due to the lack of selective pressures. Modifier loci usually lay dormant until another gene in the same or related pathway is mutated. The modifier then becomes apparent in the manifestation of the phenotype.

The results shown here suggest that genetic background is important in the penetrance of the phenotype seen in *Tcfap2a* mutant mice. In the preliminary study, on a mixed background (72.55% C57BL/6J), an external phenotype was observed in 45% of mutants, and cardiovascular defects were seen in 55% of mutants. When these mice were inbred further onto a C57BL/6J background (94% C57BL/6J) the previously observed defects diminished considerably, to only 5.26% mutants with the external phenotype (exencephaly) and 10.53% with a CCVM. Following outbreeding of these mice onto a CD-1 background (75% C57BL/6J) the penetrance of exencephaly increased to 40%, however, there was no CCVM in these mutants. This suggests that the background of these mice is important in determining the presence or absence of an external phenotype and of CCVM in these crosses. For example, it is possible that a modifier locus which is required in the fusion of the neural tube is affected on a CD1 background, whereas, modifier loci involved in the role of *Tcfap2a* within the NCCs for cardiovascular development, are likely found on a mixed/129 background.

Work in many groups has demonstrated that variation of the genetic background in mice with *Tcfap2a* mutations cause alterations to the phenotype. Kohlbecker *et al*. (2002), demonstrated a variable penetrance of exencephaly in *Tcfap2a* heterozygotes (*Tcfap2a*$^{+/-}$). These mice were crossed from a 129/Sv strain to 129/Ola and collected at e13.5. At this stage 14% of heterozygous embryos showed exencephaly. However, this phenotype was no longer observed when the mice were bred to the Balb/c strain, suggesting that there may be modifier genes on the 129/Ola strain which affect the closure of the neural tube (Kohlbecker *et al.*, 2002). It is noteworthy that exencephaly was not observed in any of the heterozygotes examined here.

Furthermore, an effect of genetic background has also been described in mutant mice of both the AP-2 coactivator, *Cited2*, and another AP-2 family member *Tcfap2b*. *Cited2*$^{-/-}$ embryos inbred onto C57BL/6J displayed an increased penetrance of left/right patterning defects compared to that seen on the mixed background (Bamforth *et al.*, 2004). Additionally, mice with a homozygous deletion of *Tcfap2b* on a mixed 129S1/C57BL/6J background die at P1-2, from polycystic kidney disease (Moser *et al.*, 1997a). Whereas, breeding these mice onto a 129P2 background allowed mutant

embryos to survive up to 2 weeks of age, before dying from hypocalcaemia and polycystic kidneys (Moser *et al.*, 2003).

3.3.1.1. Effect of genetic background in Tcfap2a$^{f/-}$;Foxg1cre mutants

Interestingly, our study of PSE deletions of *Tcfap2a* is not the first. Brewer *et al*.(2004), also used *Foxg1cre* to delete *Tcfap2a* from the surface ectoderm, and found a substantially different phenotype. The *Tcfap2a$^{f/-}$;Foxg1cre* mutants presented in this chapter show a fully penetrant frontonasal defect. However, the same cross performed by Brewer *et al.*(2004), on a mixed 129/Black swiss background, presented with varying severities of ventral body wall defects. Some embryos showed only a mild exaggeration of an umbilical hernia, usually observed at e15.5, while others showed full omphalocele, reminiscent of that seen in *Tcfap2a$^{-/-}$* embryos.

As both the *Tcfap2a*-null and *Tcfap2a^{flox}* alleles used in this work are the same as those used by Brewer *et al*. (2004) the differences between the phenotype of these mutants are likely caused by changes in the genetic background. It is possible, that this altered genetic background causes changes in the expression pattern of *Foxg1,* which results in an alteration in the regions from which *Tcfap2a* is removed. This has been previously demonstrated for the strain (Hebert and McConnell, 2000). It is also possible that on an altered genetic background, the function of *Tcfap2a* is changed in such a way that removal from the PSE in one strain prevents fusion of the craniofacial processes, but in another background causes defects in the formation of the ventral body wall. A further possibility is that there are modifiers present on each genetic background that affect the presentation of each phenotype.

An extreme example of the effect of genetic background on an observed phenotype can be seen in mice with mutations of the EGF receptor (EGFR). On a CF-1 background these mice die at the peri-implantation stage (before e6.5), whereas on a 129/Sv background these embryos implanted into the uterine wall normally, but were unable to survive past mid-gestation (e12.5). Furthermore, outbreeding onto a CD-1 background allowed these mutants to survive for up to 18 days post-parturition. The authors attribute this to modifying loci within each genetic background (Threadgill *et al.*, 1995).

3.3.2. Cleft palate in *Tcfap2a$^{f/-}$;Wnt1cre* mutants

Brewer *et al.* (2004) previously described the conditional knockout of *Tcfap2a* in the NCCs, using *Wnt1cre*. The authors observed a number (17/39, 43%) of *Tcfap2a$^{f/-}$;Wnt1cre* neonates with insufficient elongation of the palatal shelves, resulting in a cleft palate. A further 7 mutants failed to thrive due to a milder cleft palate phenotype (Brewer *et al.*, 2004). We, therefore, examined the mutant embryos in our study for the presence of cleft palate. In the original study (72% C57BL/6J background), a single embryo with a mild form of cleft palate was found. Further breeding of these mice onto the C57BL/6J background increased the penetrance of cleft palate to 40% of all mutants examined. There was also an increase in the range of defects observed, with the most prevalent defect being the failure of the left palatal shelf to elevate. Additionally, outcrossing these mutants onto a CD1 background caused a further increase in the penetrance of cleft palate, with 66.66% of all mutants examined having a cleft palate (Table 3-4). Although the size of each study varies quite considerably, it does appear that there is an overall increase in the frequency and severity of the cleft palate phenotype across the three studies.

Table 3-4: Summary of palate phenotypes in *Tcfap2a$^{f/-}$;Wnt1cre* mutants.

	Genetic background of *Tcfap2a$^{f/-}$;Wnt1cre* mutants					
	72% C57BL/6J (mixed)		**94% C57BL/6J**		**72% C57BL/6J (CD1)**	
Phenotype	n=5	%	n = 19	%	n=6	%
Normal palate	4	80	11	57.9	2	33.3
Failed fusion	1	20	2	10.5	1	16.6
Failed elongation	-	-	1	5.2	2	33.3
Failed elevation (left)	-	-	5	26.3	1	16.6
Total	1	20%	8	40%	4	66.66%

It is interesting to note that in those embryos that show signs of failed elevation of the palatal shelves, only the left shelf was affected, with the right shelf elevating correctly. This phenotype was observed in 6 mutant embryos across two genetic backgrounds and suggests that the loss of *Tcfap2a* from the NCCs has a more severe effect on the left side of the embryo in relation to palate formation. It is also interesting to note that this phenotype was observed most frequently in those mutants on the congenic

C57BL/6J background. This suggests potential modifiers in this background that predispose these mutants to this apparently more severe clefting phenotype.

It should be clarified that although the failed elevation of the palate appears to be a more severe phenotype, Brewer *et al* .(2004) demonstrated even mutants with a mild phenotype, such as partial failure in fusion, were unable to survive after P0, therefore, it is likely that any form of palatal clefting in these mutants would result in postnatal lethality.

3.3.3. Ectopic thymus in *Tcfap2a$^{f/-}$;Foxg1cre* mutants

The thymus develops from two thymic rudiments, derived from the PA endoderm, which migrate to a position just above the heart and fuse at the midline. Ectopic thymus was identified in all *Tcfap2a$^{f/-}$;Foxg1cre* mutants examined. This phenotype was further exacerbated in the *Tcfap2a$^{f/-}$;Foxg1cre;Wnt1cre* double mutants, in which 2 of these embryos (33.33%) show no thymic rudiment present in the normal position. This suggests that there is an additive effect of *Tcfap2a* being removed from both these tissues simultaneously. The absent thymic rudiment was found to be ectopically placed and protruding from the neck.

There is much controversy over the role of the ectoderm in the formation of the thymus (reviewed in Manley and Blackburn, 2003). A dual-origin model for thymus development suggests that the distinct components of the thymus are derived from different tissues, with the cortical epithelium forming from the PA ectoderm and the medullary epithelium arising from the endoderm. However, many others suggest that the thymus arises solely from the endoderm of the pharyngeal pouch, with no contribution from the ectoderm. It is, therefore, interesting to note that *Tcfap2a* is not expressed within the pharyngeal endoderm, but is found within the ectoderm and NC-derived mesenchyme of the PAs (Brewer *et al.*, 2002). This may align with the dual-origin model, suggesting that *Tcfap2a* expression may be important within the PSE, in order for the PSE to form the cortical epithelium. However, although we did not investigate the structure and function of the thymus in our mutants, the thymus appears to be of normal size, suggesting that no component tissue is absent. Therefore, we postulate a role of *Tcfap2a* in the detachment of the thymic rudiment from the surface ectoderm and pharynx, which allows the thymic rudiments to migrate

to their final positions. It has been suggested that apoptosis is required for the endodermal pouch tissue to detach from the ectoderm and begin migration. As AP-2α has also been implicated in apoptosis, it is possible that AP-2α-mediated apoptosis is required to separate the naive thymic rudiment from the PSE. In the absence of *Tcfap2a* within the surface ectoderm, this detachment may not be possible, resulting in the thymus remaining attached to the ectoderm. As the embryo and the ectopically placed thymic rudiment grow, the new position of the thymic tissue may result in it being displaced by other developing structures. Therefore, the thymic rudiment becomes misshapen and protrudes externally.

The additive effect caused by the deletion of *Tcfap2a* in both the NCCs (*Wnt1cre*) and the ectoderm (*Foxg1cre*) suggests that *Tcfap2a* in the NCCs is also important in the development of the thymus. During development, the nascent thymic rudiment becomes surrounded by a layer of NCCs shortly after its formation from the interacting tissues of the pharyngeal pouch/cleft (Jiang *et al.*, 2000). This may therefore help to explain the additive effect caused by the loss of *Tcfap2a* from both tissues.

It is particularly interesting that a similar ectopic thymus phenotype to that described here has also been observed in patients with BOFS, caused by mutations in *TFAP2A* in human patients. In these patients the ectopic thymus is suggested to derive from the dermal layer of the skin in the neck and is therefore often described as a 'dermal thymus'. This particular phenotype appears to be unique to BOFS patients, and therefore to *TFAP2A* mutations. This therefore, suggests that the *Tcfap2a*$^{f/-}$*;Foxg1cre* mouse may be a unique model for further examination of this phenotype and determination of the molecular causes that result in the defect. It is also interesting to note that a number of ectodermal abnormalities are frequently described in BOFS patients, including hypodontia, prematurely grey hair and dysplastic nails (Milunsky *et al.*, 2008; Gestri *et al.*, 2009; Milunsky *et al.*, 2011).

The ectopic thymus in these patients is described, in clinical literature, as a 'tumour', or a 'scar-like lesion', which on resection of the tissue is found to be functional thymus tissue. The ectopic thymus in BOFS patients is often found on the right side of the neck, but most commonly appears bilaterally (Rizzo *et al.*, 1995; Bennaceur *et al.*, 1998; Hiraumi *et al.*, 2001; Drut and Galliani, 2003; Hiroshi *et al.*, 2006). This is

interesting as the *Tcfap2a*$^{f/-}$*;Foxg1cre* mutant mice most commonly show absence of the right thymic rudiment at the correct position, suggesting possibly conserved roles.

3.3.4. Craniofacial development in PSE-deletions of *Tcfap2a*

Nkx2.5cre and *Foxg1cre* were both used in this study to remove *Tcfap2a* from the surface ectoderm in conjunction with a *Wnt1cre*-mediated deletion from the NCCs. However, despite covering highly similar expression domains, each cre line gave different non-cardiac phenotypes. *Foxg1cre*-mediated deletion of *Tcfap2a* resulted in a craniofacial defect affecting the upper jaw and nasal region, with additional defects affecting the development of the thymic rudiments. The *Nkx2.5cre*-mediated deletion resulted in a lower jaw phenotype, which appeared to be the result of a failed fusion at the midline.

The vertebrate face forms from the frontonasal prominence, the lateral nasal prominence and the maxillary and mandibular components of the first PA (Figure 3.16 a-d). The frontonasal prominence goes on to form the philtrum of the lower lip and the primary palate. The lateral nasal prominence becomes the sides of the nose. The dorsal component of the first PA (the maxilla) gives rise to the sides of the middle and lower face and the secondary palate, while the ventral component (the mandible) forms the lower jaw. In the *Foxg1cre*-mediated deletion of *Tcfap2a*, the observed frontonasal defect appears to be caused by the failure of the frontonasal process to fuse with the maxillary component of the first PA. Whereas in the *Nkx2.5cre* mutants the defect is caused by a failed fusion of the mandibular components.

It is possible that this discrepancy between craniofacial defects is due to the slight differences in the expression patterns of the two cre lines within the maxillary and mandibular components of the first PA. It appears, from the literature, that *Nkx2.5cre* is expressed throughout the ectoderm of the mandibular component of the first PA, but not in the maxilla (Figure 3.16e). However, *Foxg1cre* appears to be expressed more strongly within the ectoderm of the maxillary component of first PA (Figure 3.16f). Therefore, *Tcfap2a* expression is required in the ectoderm of each of these first PA components in order for fusion to occur.

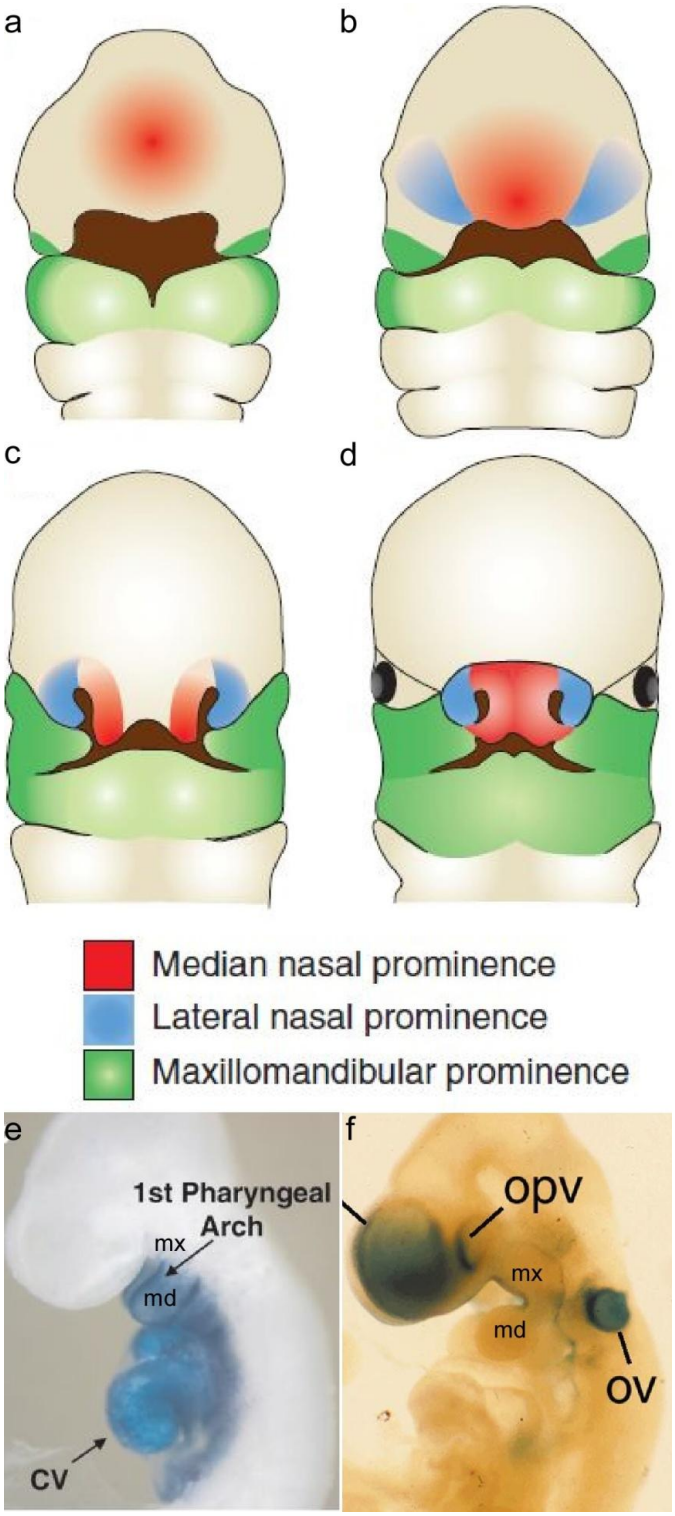

Figure 3.16: Craniofacial development in mouse embryos.
(a-d) The craniofacial region develops from three regions. The median nasal prominence (red) forms the primary palate, the philtrum and the middle of the nose. The lateral nasal prominence (blue) gives rise to the sides of the nose. The maxillomandibular prominence forms the lower jaw, the sides of middle and lower face and the secondary palate. (Figure taken from Helms *et al.*, 2005). (e) Lineage trace of *Nkx2.5cre*-expressing cells in an e9.5 embryo. Expression is observed in mandibular component of the first PA (md), with some expression in the maxilla (mx). Expression is also observed throughout the heart. (Figure taken from Moses *et al.*, 2001). (f) Lineage trace of *Foxg1cre*-expressing cells in an e9.5 embryo. Expression is observed in the maxillary component of the first PA (mx) with some expression in the mandibular component (md). Expression is also observed in the optic vesicle (opv) and the otic vesicle (ov). (FIgure taken from Hebert and McConnell, 2000). md, mandible; mx, maxilla; CV, Common ventricle.

Interestingly, the loss of fusion of the frontonasal prominence with the maxilla, as seen in the *Foxg1cre* mutants, is a cause of cleft lip, a phenotype which is highly prevalent in patients with *TFAP2A* mutations. Additionally, BOFS patients often have a dermal thymus, similar to the ectopic thymus phenotype also observed in *Foxg1cre*-mediated deletions of *Tcfap2a*. Therefore, it is plausible that BOFS is caused by mutations of *TFAP2A,* which are only manifesting in some tissues.

Defects affecting the development of the thymus were only identified in the *Foxg1cre* mutants, again suggesting differences between the expression of the PSEcre lines used in this study. It is possible that this is also due to differences in the expression patterns of these cre lines. However, as the thymic rudiments are derived from the third pharyngeal pouch endoderm, rather than any component of the first PA, it may be due to differences in the timing of expression of each cre line. *Foxg1cre* expression begins at e8.75, before the ectoderm has come to cover the PAs (Hebert and McConnell, 2000). *Nkx2.5cre* expression, however, is not observed in the pharyngeal ectoderm until e9.5 (Moses *et al.*, 2001). It is therefore possible that *Tcfap2a* is required within the surface ectoderm at some point before the expression of *Nkx2.5cre* begins, for correct thymus development.

3.4. Conclusions

The work presented in this chapter demonstrates that the role of *Tcfap2a* in cardiovascular development is very complex. The genetic dissection method used here has allowed us to identify the regions of *Tcfap2a* expression which are important in particular elements of the *Tcfap2a* phenotype. For example, it is clear that *Tcfap2a* deletion from the NCCs are important in correct fusion of the neural plates to form the neural tube, as *Wnt1cre*-specific deletion results in exencephaly with variable penetrance in these mutants. Also, *Tcfap2a*-deletion from the surface ectoderm results in the loss, or ectopic placement, of a single thymic rudiment. This, therefore, demonstrates a requirement for *Tcfap2a* in the PSE at this time. As the loss of the thymic rudiment was not observed in the *Nkx2.5cre* deletion this suggests that there is a narrow window between activation of these two cre lines, during which *Tcfap2a* is crucial in this tissue for thymic development. It would be interesting to investigate if loss of *Tcfap2a* in this tissue at an even earlier time-point would eradicate thymic development entirely.

In addition the loss of both thymic rudiments in some of the *Foxg1cre;Wnt1cre* double mutant embryos suggests that there may be a *Tcfap2a*-mediated interaction between the NCCs and surface ectoderm, which is required in thymus development. However, this phenotype had a lower penetrance than the single thymic rudiment loss seen in the *Foxg1cre* only deleted embryos, therefore suggesting that other factors are at work.

3.5. Further work

The histological staining of the *Tcfap2a*$^{f/-}$*;Foxg1cre;Wnt1cre* embryos demonstrates that the thymic rudiments have failed to migrate into their final position, remaining in a cervical position and protruding from the neck region. Furthermore, this phenotype appears closely related to the ectopic thymus defect observed in BOFS patients. However, during this study we were unable to confirm that the structure observed by histology was indeed the thymus. A good experimental test for this would be to use a marker of the developing thymus to stain the tissue. One such marker is Foxn1. Foxn1 is expressed in the thymic primordia and continues to be expressed throughout development and at least up to e14.5 (Manley and Blackburn, 2003; Boehm, 2008; Okubo *et al.*, 2011). Therefore staining using an anti-Foxn1 antibody would demonstrate that the observed tissue is of thymic origin. However, although a number of Foxn1 antibodies are commercially available, no account of their use in immunohistochemical procedures was identified within the literature. An alternative method would be to use slide *in situ* hybridisation on these specimens to confirm the thymic origin of the tissue. This has been performed for identifying ectopically placed thymic rudiments within mouse samples on many occasions. However, these samples were not prepared in an RNase-free environment, therefore, further embryos would need to be collected for this analysis.

Chapter 4. Recapitulating the *Tcfap2a*$^{-/-}$ phenotype using the *Tcfap2a*^{flox} line

4.1. Introduction

In the previous chapter we attempted to genetically dissect the function of *Tcfap2a* by conditional deletion from the NCCs and the PSE. We identified low penetrance of CCVM in the NCC-deleted mutants, which was not increased by simultaneous removal from the NCCs and PSE. Furthermore, it appears that the phenotype is dependent on genetic background. In this chapter we will attempt to recapitulate both the external phenotype and the cardiovascular defects of the *Tcfap2a*$^{-/-}$ global mutants using ubiquitously expressed cre lines. This will allow us to understand the low penetrance of CCVM observed in the conditional deletions described in the previous chapter.

4.1.1. Ubiquitously-expressed cre lines

Ubiquitously expressed cre lines, which are expressed in all tissues of the embryo, are very useful tools. They are often used in the validation of a newly generated floxed allele. Efficient recombination is likely to result in the recapitulation of the phenotype generated by a null allele. These lines are also often used to create a null line, by the deletion of the floxed region throughout the entire embryo. Heterozygotes carrying one wild type allele and one floxed-deleted allele may then be interbred to generate a null mutant. The ubiquitously expressed cre lines which will be used in this chapter are discussed below.

4.1.1.1. PGKcre

3-phosphoglycerate kinase (PGK) is an important enzyme in the glycolytic pathway and is therefore, expressed throughout all tissues of an organism. The *Pgk*-1 gene in mouse becomes active at e3.5 within the inner cell mass of the blastocyst, with additional expression in the trophectoderm in some embryos examined. By e7.5, expression is observed throughout all embryonic tissues, with particularly strong expression in the ectoderm. This pattern of expression is maintained at e8.5, with less intense expression within the trophectoderm being visible (McBurney *et al.*, 1994).

The *PGKcre* transgene was generated by the introduction of a cre cDNA downstream of the *Pgk-1* promoter. This construct was then introduced into pronuclei by microinjection, and allowed to randomly integrate into the genome. The efficiency of

cre-mediated recombination by this transgenic strain was then tested using southern blotting to indicate the loss of intervening sequences between two loxP sites. Efficient recombination was determined for multiple tissues, including the brain, kidneys, heart and liver (Lallemand *et al.*, 1998).

As with many cre lines, *PGKcre* is already active in the early stages of oogenesis and therefore, the cre recombinase protein may be passed from mother to offspring within the cytoplasm of the oocyte, a phenomenon termed 'maternal transmission'. Consequently, all offspring of a *PGKcre*-positive female will carry the enzyme, and recombination between flox sites, transmitted from the male, occurs at the zygote stage (Lallemand *et al.*, 1998).

4.1.1.2. Sox2cre

Sox2cre is an epiblast-specific cre line, which initiates recombination of LoxP sites within all cells of the embryo proper and excludes the extraembryonic ectoderm. The *Sox2cre* transgene uses a 12.5 kb portion of *Sox2* enhancer/promoter region to drive the expression of cre recombinase within the epiblast cells. Validation using the R26R^{LacZ} reporter construct demonstrated that Sox2cre is able to efficiently recombine LoxP sites throughout the embryo by e6.5 of mouse development. In addition, recombination also occurred within the epiblast derivatives of the extraembryonic ectoderm, including the yolk sac mesoderm and the amnion, while primitive endoderm derivatives, such as the visceral endoderm, do not undergo recombination. By e7.5 expression was evident in all three germ layers of the embryo and the epiblast-derived extraembryonic tissues, including the allantois, the amnion and the yolk sac mesoderm (Hayashi *et al.*, 2002).

Further validation using a sonic hedgehog (*Shh*) conditional allele demonstrated that *Sox2cre* was capable of recapitulating the null phenotype. Comparisons to *Mox2cre* (MORE) demonstrated that recombination with *Sox2cre* is more efficient, with MORE giving 33% of embryos with a milder phenotype, pertaining to incomplete recombination. It was also demonstrated that *Sox2cre* is activated earlier than MORE (Hayashi *et al.*, 2002).

This group went on to show that *Sox2cre*, like *PGKcre*, is inherited within the female germline, and is therefore transmitted to all offspring irrespective of their own genotype. As such, *Sox2cre* females mated to males carrying the R26R^{LacZ} construct produced litters in which β-galactosidase was activated in all embryos. Also, timed matings between a *Sox2cre* female and males homozygous for a conditional allele of *Smoothened* yielded 50% offspring with a null phenotype, instead of the expected 25%. Maternal expression of the cre, however, does result in efficient recombination in the early embryo (Hayashi *et al.*, 2003; Vincent and Robertson, 2003).

4.1.2. Tcfap2a mutant alleles

As described in the introduction chapter, *Tcfap2a* is composed of 7 exons, which contribute to 3 functional domains within the resulting protein. The transactivation domain encoded by exon 2 is the binding site for co-factors, which regulate the transcriptional activity of AP-2α. The DNA binding domain, consisting of a large number of basic amino acid residues, is encoded by portions of exons 4 and 5, while the helix-span-helix dimerisation domain is produced from the remaining segments of exon 5 and exons 6 and 7 (Williams and Tjian, 1991a; Williams and Tjian, 1991b) (Figure 4.1a).

The conditional allele used in the previous chapter was constructed by the addition of loxP sites flanking exons 5 and 6, which would therefore result in the removal of a large portion of both the DNA binding domain and the dimerisation domain of the protein (Figure 4.1c). The *Tcfap2a*^{LacZ} null allele was produced by replacing all but a single nucleotide of exon 7 with an IRES-LacZ cassette. This disrupts the dimerisation domain of the protein by removing much of the span region and the entire second α-helix (Figure 4.1b).

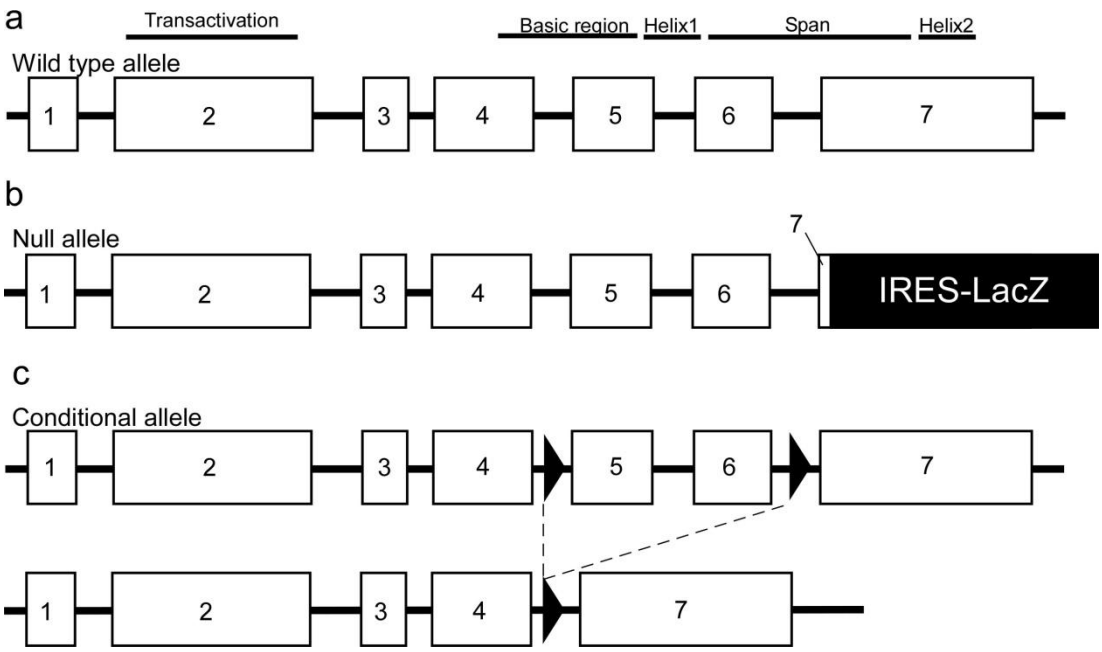

Figure 4.1: Structure of *Tcfap2a* alleles utilised in this thesis.
(a) Wild type *Tcfap2a* consists of 7 exons. The functional domain of the protein encoded by each exon is indicated above. (b) *Tcfap2a*-null allele. Exon 7, encoding a portion of the span domain and the second helix, has been removed and replaced with an IRES-LacZ cassette, producing a null allele. (c) Conditional (*Tcfap2α*^{flox}) allele. Exons 5 and 6 are flanked by LoxP sites (black triangles) (top panel), which are recombined in the presence of Cre recombinase (bottom panel). Numbers refer to exon number.

The function of each structural domain of the protein was determined through the use of *in vitro* assays assessing the consequences of a number of large deletions throughout the gene (Figure 4.2). DNA binding abilities were examined using an electrophoretic mobility shift assay (EMSA), while cross-linking or co-immunoprecipitation (co-IP) was used to investigate the dimerisation ability of each mutant construct. Mutations situated within exons 1-3 or the start of exon 4, were found to result in a protein which was capable of dimerisation and DNA binding, but had a reduced capacity to activate transcription. Mutations in the latter half of exon 4 or the start of exon 5, the regions which encode the basic DNA binding domain, results in a loss of DNA binding ability despite the protein being able to dimerise. Mutations within either of the α-helices causes the protein to lose the both dimerisation and DNA binding ability. Finally, mutations in the span region between the α-helices prevent the formation of homodimers, but allow heterodimer formation and DNA binding (Williams and Tjian, 1991a; Williams and Tjian, 1991b).

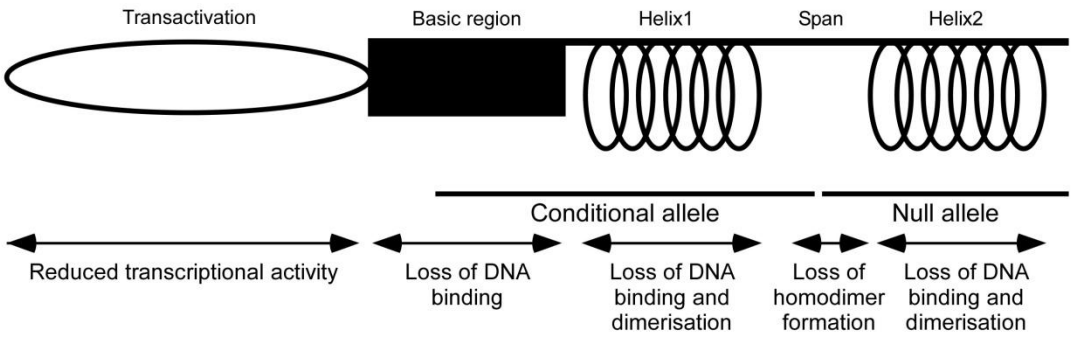

Figure 4.2: Functional consequences of deletions within AP-2α.
AP-2α contains a transactivation domain, a proline-rich basic domain and a helix-span-helix dimerisation domain. The functional consequences of mutations in these domains are indicated below. (Based on work by Williams and Tjian, 1991a; Williams and Tjian, 1991b)

Taking all of this information into consideration, it is therefore likely that any protein products of both the conditional and the null alleles will be non-functional, due to the disruption of large portions of the dimerisation domain, which will likely also result in an inability of the proteins to bind to DNA.

4.1.3. Aims of chapter

Tcfap2a expression is widespread throughout embryonic development, however, only two areas of *Tcfap2a* expression are likely to be involved in cardiovascular development, as discussed in the previous chapter. Deletion of *Tcfap2a* within the NCCs alone resulted in a low penetrance of cardiovascular defects (10.53%). In addition, deletion of *Tcfap2a* from both the NCCs and the PSE resulted in no CCVM.

We, therefore, wanted to understand the reasons for the low penetrance of cardiovascular defects in these conditional mutants. There are three possible explanations for this. The first is that *Tcfap2a* is not required within either the PSE or the NCCs for correct cardiovascular development. This, however, seems unlikely due to the importance of these tissues in PAA formation and remodelling and the high penetrance of PAA malformations in *Tcfap2α*$^{-/-}$ embryos. A second possibility is that these cre lines were not expressed at the appropriate time to allow efficient recombination of the *Tcfap2α*^{flox} allele.

A further possibility is that the *Tcfap2α*^{flox} allele is unable to recapitulate the phenotypes observed in the *Tcfap2α*$^{-/-}$ mutant embryos. As discussed above, the *Tcfap2a*-null and *Tcfap2α*^{flox} alleles vary in the exons which are disrupted. Therefore, it is possible that these differences affect the presentation of the phenotype in some

way. In this chapter, we will use a series of ubiquitously expressed cre lines in order to investigate the effect of these differences. In addition, this approach will allow us to understand the effect that the timing of the deletion has on the phenotype observed. All mutant embryos examined within this chapter have a genetic background of 97-98.3% C57BL/6J.

4.2. Results

4.2.1. Tcfap2a$^{f/f}$;PGKcre (97.22% C57BL/6J)

In order to investigate the consequences of a *PGKcre*-mediated deletion of *Tcfap2a* we first required a male of the genotype *Tcfap2a*$^{+/-}$*;PGKcre*. However, after several rounds of breeding yielded unsuccessful results, we generated an alternative breeding strategy as shown in Figure 4.3. A *PGKcre*-positive male was crossed to a female homozygous for the *Tcfap2a*^{flox} allele in order to generate a stud male of the genotype *Tcfap2a*$^{+/f}$*;PGKcre*. The floxed allele will undergo cre-mediated recombination so that the male is heterozygous for *Tcfap2a* in all tissues expressing *PGKcre*. This male was then crossed to further *Tcfap2a*$^{f/f}$ females in timed matings to generate offspring with a ubiquitous deletion of *Tcfap2a*.

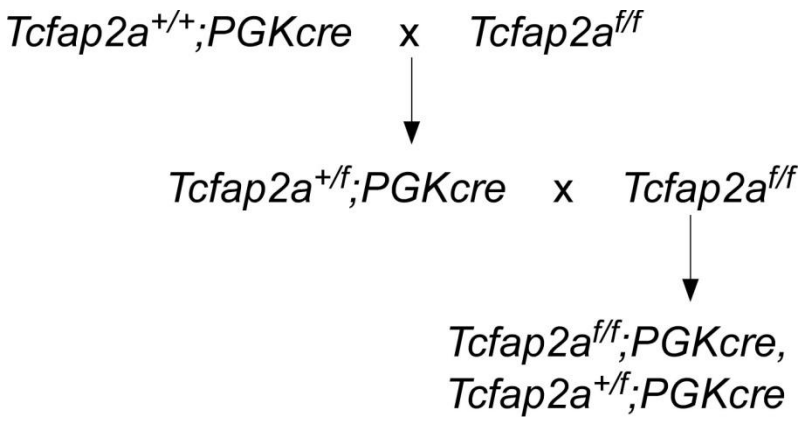

Figure 4.3: Breeding strategy for the generation of *Tcfap2a$^{f/f}$;PGKcre* mutant embryos.
A *Tcfap2a*$^{+/+}$*;PGKcre* male was crossed to *Tcfap2a*$^{f/f}$ females to generate a *Tcfap2a*$^{+/f}$*;PGKcre* stud male. The stud male was then further bred to *Tcfap2a*$^{f/f}$ females to generate *Tcfap2a*$^{f/f}$*;PGKcre* mutant and *Tcfap2a*$^{+/f}$*;PGKcre* control embryos for MRI analysis.

4.2.1.1. External phenotype

Mutant (*Tcfap2a*$^{f/f}$*;PGKcre*) and control (*Tcfap2a*$^{+/f}$*;PGKcre*) embryos were collected at e15.5. The external phenotype (Figure 4.4 b-d) clearly recapitulates the *Tcfap2a*$^{-/-}$ phenotype (Figure 1.11) and also displays variability, as was previously observed in the *Tcfap2a*$^{-/-}$ embryos (Dr Simon Bamforth, unpublished observations).

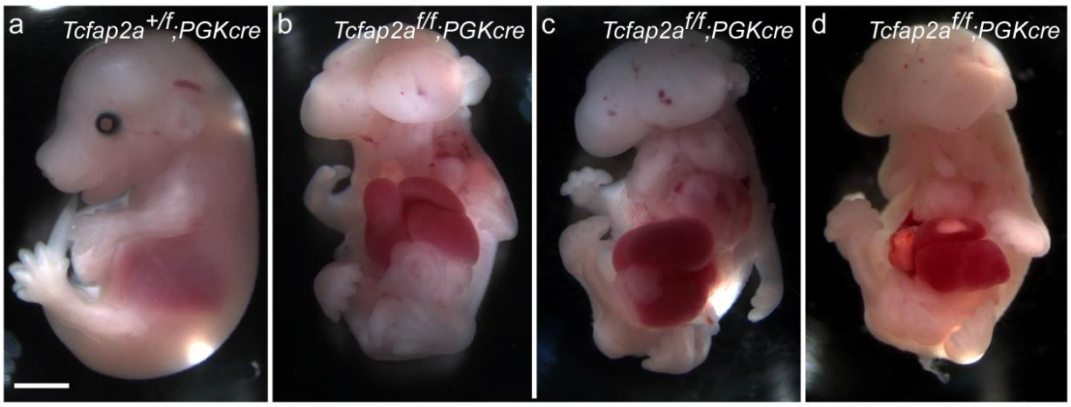

Figure 4.4: External phenotype in *Tcfap2a*$^{f/f}$*;PGKcre* mutant embryos.
(a) *Tcfap2a*$^{+/f}$*;PGKcre* control embryo. (b-d) *Tcfap2a*$^{f/f}$*;PGKcre* mutant embryos exhibit a variable phenotype, similar to that seen in *Tcfap2a*$^{-/-}$ mutant embryos. Scale bar = 2mm. (n=10).

4.2.1.2. Cardiovascular phenotype

The *Tcfap2a*$^{-/-}$ embryos presented with 100% penetrance of cardiovascular defects, characterised by a VSD, an OFT defect (TGA, OA or DORV) and defects of the fourth PAA derivatives (IAA, cAoA, CORSA, A-RSA). Therefore, the cardiovascular phenotype of the *Tcfap2a*$^{f/f}$*;PGKcre* mutant embryos was examined to confirm that these embryos showed full recapitulation of the *Tcfap2a*$^{-/-}$ mutant phenotype. Mutant and control embryos were examined by MRI, and 3D reconstructions were created. The results are summarised in Table 4-1.

The penetrance of fourth PAA defects in these mutants was very similar to that seen in the previous *Tcfap2a*$^{-/-}$ mutant embryos, with 50% (5/10) of mutant embryos having a defect affecting the left fourth PAA and 100% mutants having a right fourth PAA defect. The defects of the left fourth PAA included 20% (2/10) IAA-B, 20% cAoA and 10% hypoplastic aortic arch (hypoAoA, 1/10). The most common defect affecting the fourth right PAA was CORSA (70%, 7/10), with only 30% (3/10) of mutants with an A-RSA.

However, the remaining defects which were observed at 100% penetrance in the *Tcfap2a*$^{-/-}$ mutants appeared at very low levels in these mutants. Only 50% (5/10) of mutant embryos were found to have a VSD. In addition, the number and variety of OFT defects was also reduced. OA was found in 20% (2/10) of mutant embryos examined and the penetrance of DORV observed was also reduced to 20% (2/10). No TGA was observed in any of these mutant embryos.

Table 4-1: Prevalence of CCVM in *Tcfap2a*$^{f/f}$*;PGKcre* mutant embryos at e15.5 compared to *Tcfap2a*$^{-/-}$ embryos.

CCVM	Prevalence (n=10)	Summary	Prevalence in *Tcfap2a*$^{-/-}$	Summary for *Tcfap2a*$^{-/-}$
VSD	50%	VSD – 50%	100%	VSD – 100%
OA	20%	OFT defects - 40%	30%	OFT defects – 100%
DORV	20%		20%	
TGA	0%		50%	
IAA	20%	Left 4th PAA defects – 50%	30%	Left 4th PAA defects – 50%
cAoA	20%		20%	
Hypo AoA	10%		0%	
A-RSA	30%	Right 4th PAA defects – 100%	40%	Right 4th PAA defects – 90%
CORSA	70%		50%	
RAA	0%	No defects observed	10%	RAA with I-LSA – 10%
I-LSA	0%		10%	

Overall, of the 10 *Tcfap2a*$^{f/f}$*;PGKcre* mutant embryos examined, only 40% (4/10) exhibited the full phenotype as seen in the global deletion mutants (Figure 4.5c). A further 50% (5/10) of the mutant embryos presented only with defects of the PAA derivatives; with the ventricular septum and OFT being unaffected (Figure 4.5d-e). In addition, a single embryo was identified with a VSD and PAA defects, but with no OFT defect, suggesting that all three elements of the phenotype occur independently and that the VSD and OFT defects are not linked, with one being secondary to the other.

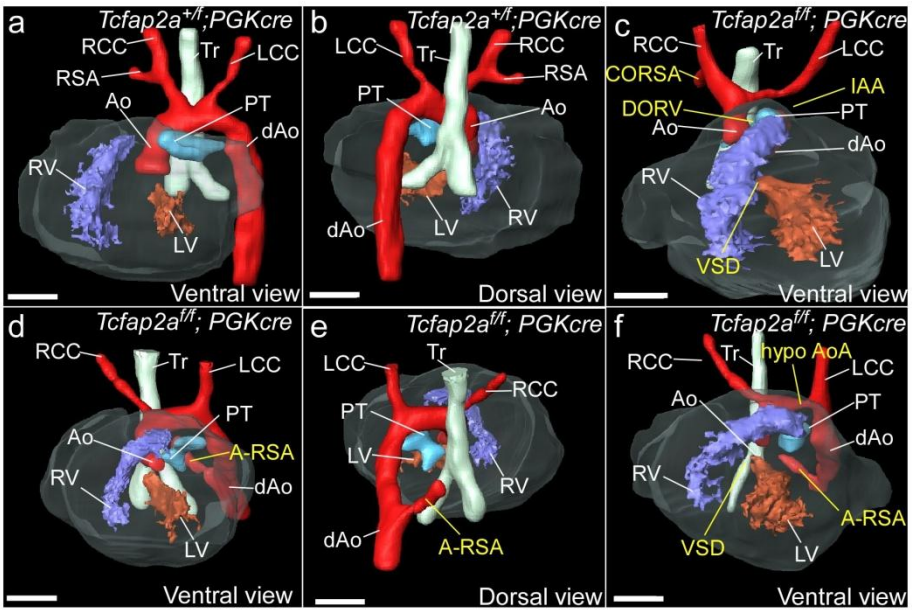

Figure 4.5: Deletion of *Tcfap2a* with *PGKcre* causes reduced penetrance of CCVM as compared to *Tcfap2a*$^{-/-}$ embryos.
(a, b) Control embryos from a ventral (a) and dorsal (b) orientation, showing normal development of the heart and aortic arch. Mutant embryos (c-f) show variable penetrance of the *Tcfap2a*-null CCVM phenotype. (c) Full phenotype consisting of a VSD, and OFT malformation (DORV) and defects of the derivatives of the fourth PAAs (IAA, CORSA). (d, e) Defects of the fourth PAAs only (A-RSA) from ventral (d) and dorsal (e) view. (f) VSD and fourth PAA defects (A-RSA and hypo AoA). RV, right ventricle; LV, left ventricle; Ao, aorta; PT, pulmonary trunk; RCC, right common carotid artery; LCC, left common carotid artery; RSA, right subclavian artery; LSA, left subclavian artery; Tr, trachea; dAo, dorsal aorta. Scale bar = 500 μm. (n=10).

Due to the poor resolution of the MRI images, embryos were also analysed by haematoxylin and eosin staining to identify more subtle defects and to confirm the defects identified by MRI analysis (Figure 4.6).

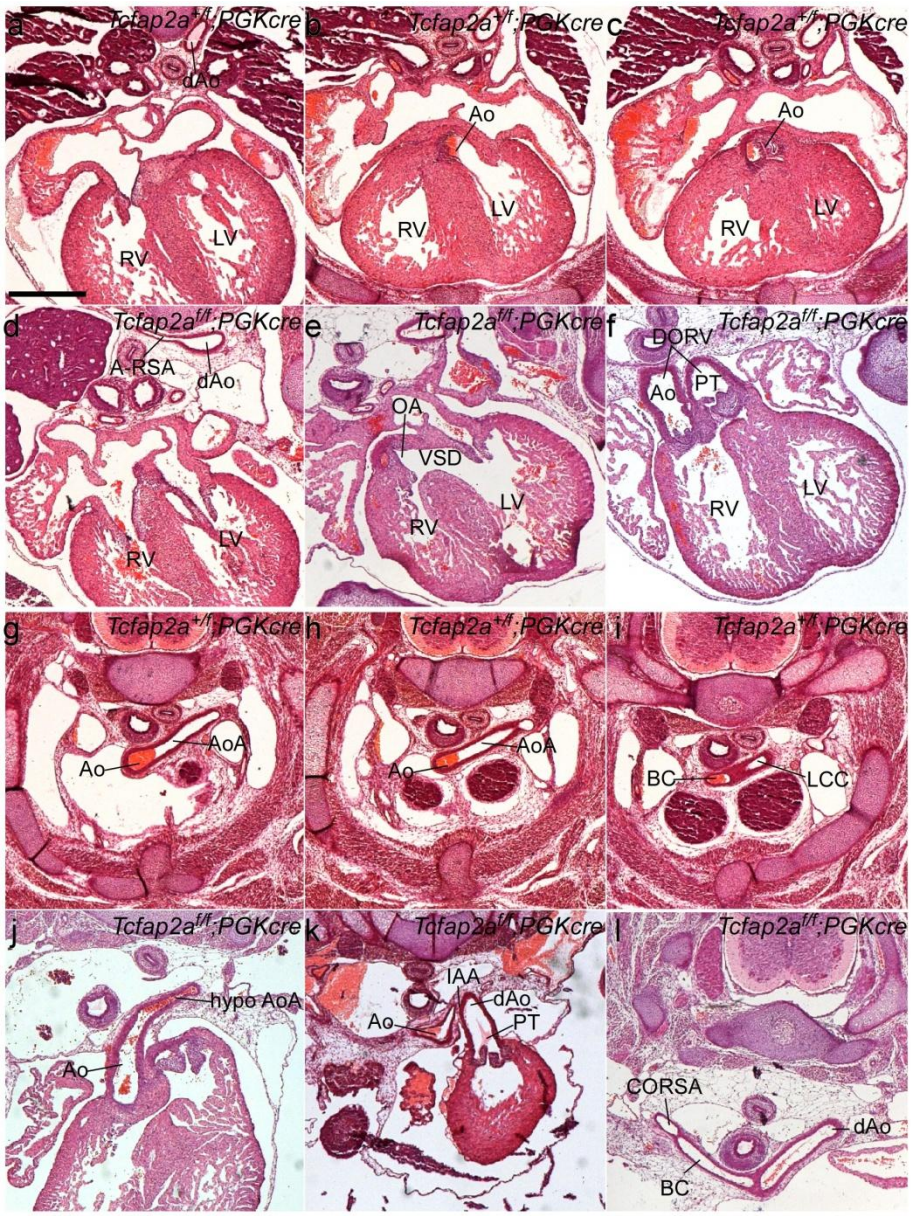

Figure 4.6: Histological sections confirm *Tcfap2a*$^{f/f}$*;PGKcre* phenotypes observed by MRI.
(a-c, g-i) *Tcfap2a*$^{+/f}$*;PGKcre* control embryos show normal cardiovascular development. (d-f, j-l) *Tcfap2a*$^{f/f}$*;PGKcre* mutant embryos with a variety of defects: (d) A-RSA, (e) VSD with OA, (f) DORV (j) hypoAoA, (k) IAA, (l) CORSA. BC, brachiocephalic trunk. Scale bar = 500 µm. (n=10).

4.2.1.3. Transcript analysis

As the levels of CCVM in the *Tcfap2a*$^{f/f}$*;PGKcre* mutants is variable we wanted to investigate if there was variable recombination efficiency between embryos from this cross. We collected *Tcfap2a*$^{f/f}$*;PGKcre* mutants at e9.5, a stage at which *Tcfap2a* is very strongly expressed, for RT-PCR analysis.

RNA was extracted from 2 wild type (*Tcfap2a*$^{+/f}$), 1 heterozygous (*Tcfap2a*$^{+/f}$*;PGKcre*) and 4 mutant (*Tcfap2a*$^{f/f}$*;PGKcre*) littermate embryos and used to synthesise cDNA for subsequent RT-PCR analysis. Samples from *Tcfap2a*$^{+/-}$ intercrosses were also used as controls and for comparison of the *Tcfap2a* expression levels: wild type (*Tcfap2a*$^{+/+}$),

heterozygous (*Tcfap2a*$^{+/-}$) and mutant (*Tcfap2a*$^{-/-}$) embryos. Strong expression of *Tcfap2a* was seen in both the *Tcfap2a*$^{+/+}$ and *Tcfap2a*$^{+/-}$ samples, with the *Tcfap2a*$^{-/-}$ lane being entirely devoid of any gene expression (Figure 4.7). Similar expression was seen for the *PGKcre* conditional deletion embryos with the wild type (*Tcfap2a*$^{+/f}$) and heterozygote (*Tcfap2a*$^{+/f}$;PGKcre) samples showing strong expression.

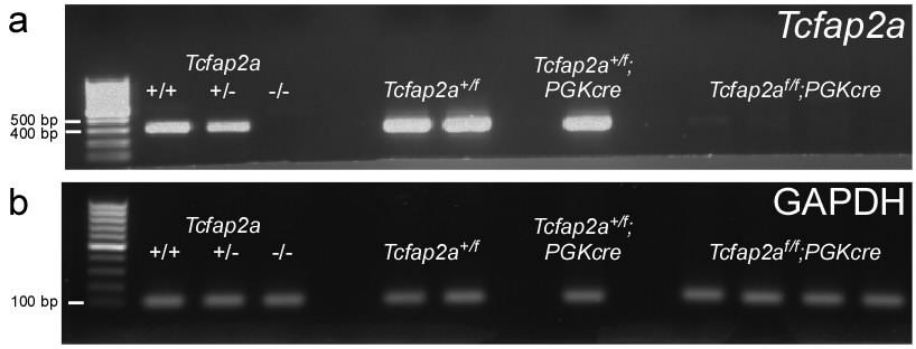

Figure 4.7: RT-PCR of *Tcfap2a* expression in *Tcfap2a*$^{f/f}$*;PGKcre* mutant embryos
(a) *Tcfap2a* expression in *Tcfap2a* control and mutant embryos. No *Tcfap2a* expression is observed in *Tcfap2a*$^{-/-}$ or *Tcfap2a*$^{f/f}$*;PGKcre* mutant embryos. (b) Glyceraldehyde 3-phosphate dehydrogenase (GAPDH) expression was also examined as a loading control.

The expression analysis described above was designed to investigate the expression of wild type *Tcfap2a* only. The primers used bind within exon 6 (removed in the recombined conditional allele) and exon 7 (removed from the null allele) and therefore will not bind to transcripts produced from either mutant allele. To determine if the floxed allele can produce a functional transcript, primers were designed within exons 4 and 7, which span the deleted region. These primers will generate a band of 663 bp in samples in which the floxed region remains, and a band of 402 bp in samples in which cre-mediated recombination has excised the sequence between the LoxP sites. RNA was collected from *Tcfap2a*$^{f/f}$*;PGKcre* mutants and *Tcfap2a*$^{+/f}$ controls and cDNA synthesised for use in the RT-PCR reactions. A *Tcfap2a*-null (*Tcfap2a*$^{-/-}$) sample was used as a negative control to demonstrate that no functional transcript was produced in these mutants.

In control samples we observed a single band of approximately 663 bp, which relates to the wild type transcript. In mutant samples a single band of approximately 402 bp was observed. This indicates that *PGKcre* has induced efficient recombination of the *Tcfap2a*^{flox} allele in these mutant embryos. As expected the *Tcfap2a*$^{-/-}$ negative control showed no product (Figure 4.8).

A further set of primers, binding within exons 3 and 4 and common to all *Tcfap2a* alleles, were used to determine if a transcript is also produced from the *Tcfap2a*-null allele. A 102 bp band was found in all samples at similar levels (Figure 4.8), indicating that a transcript is produced from each of the alleles.

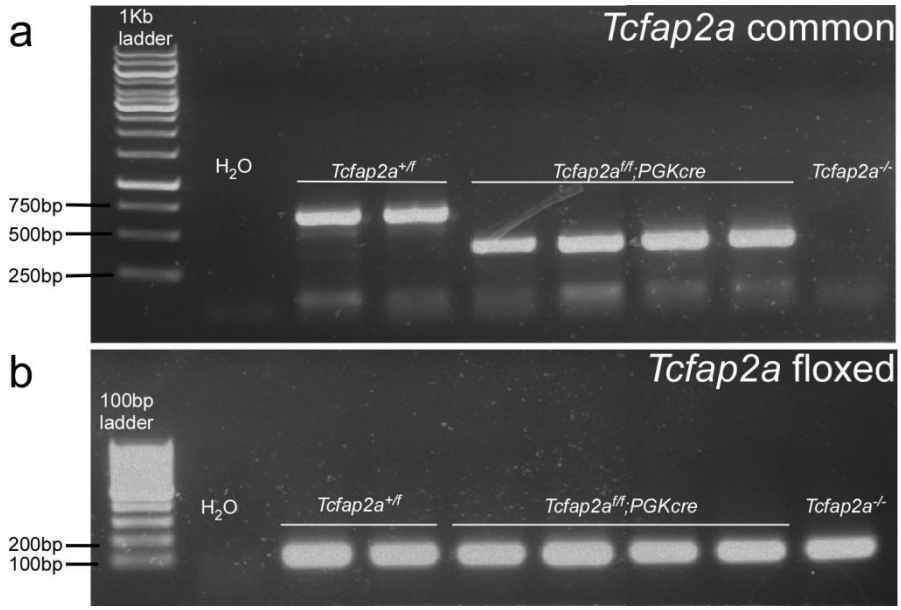

Figure 4.8: *PGKcre*-mediated recombination of *Tcfap2a*^{flox} allele.
(a) RT-PCR of control (*Tcfap2a*$^{+/f}$) and mutant (*Tcfap2a*$^{f/f}$*;PGKcre*) samples demonstrates efficient recombination between LoxP sites only in mutant samples. (b) RT-PCR using primers within exons 3 and 4 demonstrates that all samples contain a *Tcfap2a* transcript, even those of *Tcfap2a*-null embryos.

4.2.1.4. Protein analysis

As shown above, the recombined conditional allele is capable of producing a transcript which is not degraded and therefore could be translated into a protein with impaired function, which may account for the inability to completely recapitulate the *Tcfap2a*$^{-/-}$ CCVM phenotype using this allele. Therefore, we chose to investigate the changes in the protein sequence of the mutant allele using a bioinformatics approach.

First the coding sequence of each mutant allele was determined in order to infer the changes caused by the mutations. As described by Brewer *et al.* (2002) the insertion of the LacZ cassette into the null allele results in the loss of all but a single nucleotide of exon 7. As exon 7 has been shown to be important in DNA binding and dimerisation (Williams and Tjian, 1991a; Williams and Tjian, 1991b) (Figure 4.2) it is predicted that this allele will not produce a functional protein. The floxed allele contains loxP sites inserted into the introns flanking exons 5 and 6 (Brewer *et al.*, 2004). These exons also form part of the DNA binding and dimerisation domains and are therefore important

for the function of the protein (Williams and Tjian, 1991a; Williams and Tjian, 1991b) (Figure 4.2).

To confirm that the insertion of the loxP sites did not alter the exon-intron boundaries of the conditional allele the genomic DNA sequence for *Tcfap2a* was obtained from the Ensembl database and loxP sequences were inserted at the appropriate positions. The sequences between the two loxP sites was removed and the coding sequence was input into the GENESCAN web server. This server generated the amino acid sequence of the recombined transcript, which was compared to the wild type protein using a multiple sequence alignment tool. This revealed that the removal of exons 5 and 6 did not disrupt the open reading frame, but simply removed the amino acids coded for by these exons (Figure 4.9). Therefore, if a protein were to be produced from this allele, it would contain the same sequence as the wild type protein but without the portions of the sequence contributed by these exons.

```
Wildtype        MLWKLTDNIKYEDCEDRHDGTSNGTARLPQLGTVGQSPYTSAPPLSHTPNADFQPPYFPP 60
Recombined      MLWKLTDNIKYEDCEDRHDGTSNGTARLPQLGTVGQSPYTSAPPLSHTPNADFQPPYFPP 60
                ************************************************************

Wildtype        PYQPIYPQSQDPYSHVNDPYSLNPLHAQPQPQHPGWPGQRQSQESGLLHTHRGLPHQLSG 120
Recombined      PYQPIYPQSQDPYSHVNDPYSLNPLHAQPQPQHPGWPGQRQSQESGLLHTHRGLPHQLSG 120
                ************************************************************

Wildtype        LDPRRDYRRHEDLLHGPHGLGSGLGDLPIHSLPHAIEDVPHVEDPGINIPDQTVIKKGPV 180
Recombined      LDPRRDYRRHEDLLHGPHGLGSGLGDLPIHSLPHAIEDVPHVEDPGINIPDQTVIKKGPV 180
                ************************************************************

Wildtype        SLSKSNSNAVSAIPINKDNLFGGVVNPNEVFCSVPGRLSLLSSTSKYKVTVAEVQRRLSP 240
Recombined      SLSKSNSNAVSAIPINKDNLFGGVVNPNEVFCSVPGRLSLLSSTSKYKVTVAEVQRRLSP 240
                ************************************************************

Wildtype        PECLNASLLGGVLRRAKSKNGGRSLREKLDKIGLNLPAGRRKAANVTLLTSLVEGEAVHL 300
Recombined      PECLNASLLGGVLR---------------------------------------------- 254
                **************

Wildtype        ARDFGYVCETEFPAKAVAEFLNRQHSDPNEQVARKNMLLATKQICKEFTDLLAQDRSPLG 360
Recombined      ----------------------------------------RQICKEFTDLLAQDRSPLG 273
                                                        :******************

Wildtype        NSRPNPILEPGIQSCLTHFNLISHGFGSPAVCAAVTALQNYLTEALKAMDKMYLSNNPNS 420
Recombined      NSRPNPILEPGIQSCLTHFNLISHGFGSPAVCAAVTALQNYLTEALKAMDKMYLSNNPNS 333
                ************************************************************

Wildtype        HTDNSAKSSDKEEKHRK 437
Recombined      HTDNSAKSSDKEEKHRK 350
                *****************
```

Figure 4.9: Multiple sequence alignment of wild type and recombined protein sequences.
Multiple sequence alignment reveals that the removal of exons 5 and 6 does not disrupt the open reading frame of the protein. *, conserved residue; :, residues have similar properties.

Exons 5 and 6 contribute to the DNA binding domain, the first α-helix and a portion of the span domain. In the absence of these exons, the resultant protein would contain a

transactivation domain, some of the DNA binding domain, a portion of the span and the final α-helix. It is therefore possible that the recombined allele may produce a protein with some reduced function, which may cause the incomplete recapitulation of the *Tcfap2α*-null phenotype.

Therefore, we chose to investigate if the cre-recombined allele was capable of producing a protein product using western blotting. Wild type AP-2α has a molecular weight of 48 kDa. The removal of 87 amino acids in the cre-recombined allele will reduce the size of any resulting protein. Protein prediction software was used to predict the molecular weight of the protein produced from the *Tcfap2α*^{flox} allele. The molecular weight of this mutant protein would be 38.4 kDa

Heterozygous (*Tcfap2α*$^{+/f}$*;PGKcre*) and mutant (*Tcfap2α*$^{f/f}$*;PGKcre*) embryos were collected at e10.5 and lysed in denaturing conditions. Samples were run on a gel, transferred to a PVDF membrane and then detected using an anti-AP-2α antibody, which detects an antigen at the N-terminus of the protein. A 50 kDa band corresponding to wild type AP-2α was identified in the heterozygous controls (Figure 4.10), but absent from the mutant samples. Furthermore, no band corresponding to the predicted 38.4 kDa mutant protein was observed in the *Tcfap2α*$^{f/f}$*;PGKcre* mutant samples. The membrane was stripped and re-probed for γ-tubulin to control for difference in loading quantities.

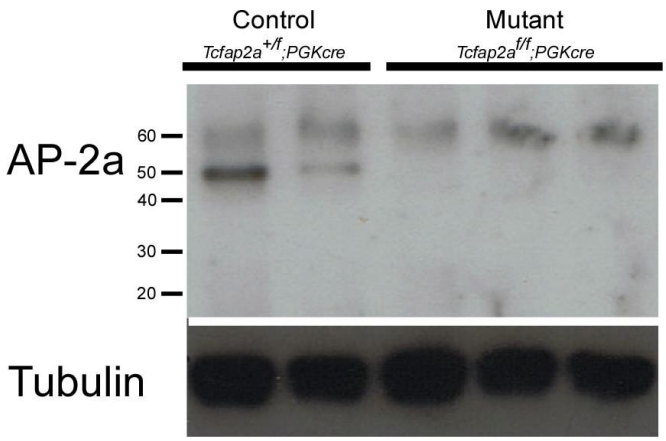

Figure 4.10: *PGKcre*-mediated recombination of the *Tcfap2a* conditional allele is unable to produce a protein product.
Western blot analysis of control (*Tcfap2a*$^{+/f}$) and mutant (*Tcfap2a*$^{f/f}$*;PGKcre*) embryos demonstrates the presence of wild type AP-2α (50kDa band) in control samples, which is not found in mutant samples. No further protein product relating to the recombined transcript is observed. The additional band at 60 kDa is due to non-specific binding of the antibody. A γ-tubulin antibody was used as a loading control.

We conclude that the deletion of exons 5 and 6 results in a non-functional protein, which is therefore degraded, and unable to cause the reduction in phenotype observed in the *Tcfap2a*$^{f/f}$*;PGKcre* mutant embryos.

4.2.2. *Tcfap2a*$^{f/-}$*;PGKcre* mutants (97.2% C57BL/6J)

After further rounds of breeding we were able to generate a stud male of genotype *Tcfap2a*$^{+/-}$*;PGKcre* for timed matings with *Tcfap2a*$^{f/f}$ females, through a breeding strategy similar to that described for the *Wnt1cre* male in the previous chapter. This will allow the results to be directly comparable. Embryos from this cross were collected at e15.5 and displayed an external phenotype identical to that of both *Tcfap2a*$^{-/-}$ and *Tcfap2a*$^{f/f}$*;PGKcre* mutant embryos examined previously. These embryos were examined by MRI for the presence of cardiovascular defects and 3D reconstructions were generated.

Of the 10 mutants examined 7 carried a VSD. 7 mutants also had OFT defects in the form of DORV. Although these phenotypes overlapped in most cases (6/7), one mutant had a VSD with no OFT defect, and a further embryo with DORV had a fully formed interventricular septum. No other OFT defects were observed in this dataset.

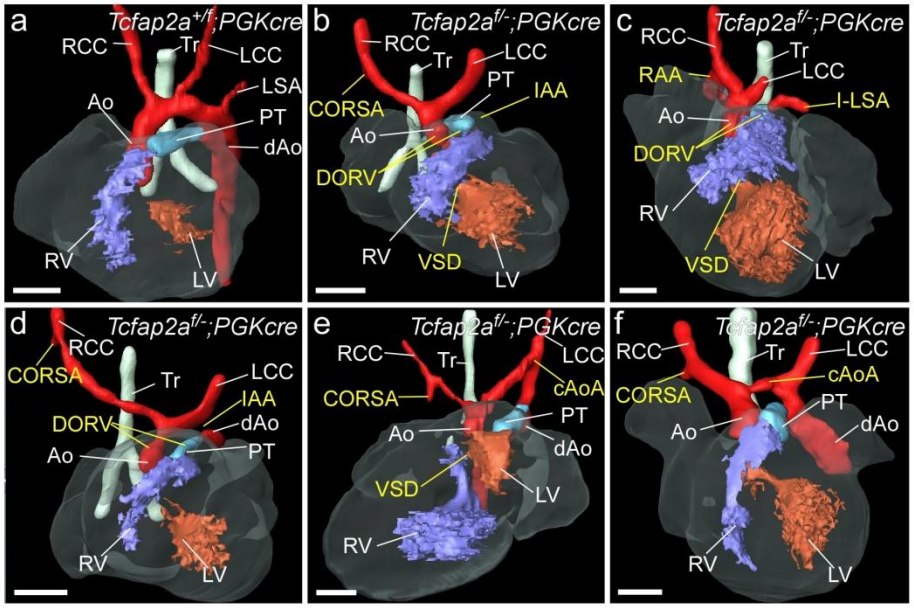

Figure 4.11: 3D reconstructions of the cardiovascular phenotypes in *Tcfap2a*$^{f/-}$*;PGKcre* mutant embryos. (a) control, (b) mutant with full phenotype (CORSA, IAA,VSD, DORV), (c) mutant with full phenotype (RAA and I-LSA, DORV, VSD), (d) OFT + PAA defects (CORSA, IAA, DORV), (e) VSD + PAA defects (VSD, CORSA, cAoA), (f) PAA defects only (CORSA, cAoA). Scale bar = 600 µm. (n=10).

Defects of the fourth left PAA were observed in 50% (5/10) of embryos. The most common of these defects was a cAoA, seen in 40% (4/10) embryos. Another embryo had an IAA. An RAA was also observed in 10% (1/10) of mutant embryos in this case. This defect was accompanied by an isolated left subclavian artery (I-LSA). CORSA was the only defect affecting the fourth right PAA in these embryos. This was observed in 90% (9/10) of embryos examined. These defects are summarised in Table 4-2 below.

Table 4-2: Prevalence of CCVM in *Tcfap2a*$^{f/-}$*;PGKcre* mutant embryos at e15.5 compared to *Tcfap2a*$^{-/-}$ embryos.

CCVM	Prevalence (n=10)	Summary	Prevalence in *Tcfap2a*$^{-/-}$	Summary for *Tcfap2a*$^{-/-}$
VSD	70%	VSD – 70%	100%	VSD – 100%
OA	0%	OFT defects - 70%	30%	OFT defects – 100%
DORV	70%		20%	
TGA	0%		50%	
IAA	10%	Left 4th PAA defects – 50%	30%	Left 4th PAA defects – 50%
cAoA	40%		20%	
Hypo AoA	0%		0%	
A-RSA	0%	Right 4th PAA defects – 90%	40%	Right 4th PAA defects – 90%
CORSA	90%		50%	
RAA	10%	RAA with I-LSA – 10%	10%	RAA with I-LSA – 10%
I-LSA	10%		10%	

Overall, these embryos had a slightly higher penetrance of VSD than that seen in the *Tcfap2a*$^{f/f}$*;PGKcre* mutant embryos (70% vs. 60%). An increased incidence of OFT defects was also observed, however, there was also a decrease in the range of OFT defects. In the previous *Tcfap2a*$^{f/f}$*;PGKcre* mutants, 40% of embryos had an OFT defect, which consisted of two cases of DORV and two incidences of OA. In this cross, we now see 70% incidence of OFT defects in the form of DORV only. Further, the variety of defects affecting the fourth PAAs is altered. In the previous PGKcre mutants we saw 50% left PAA defects (IAA, cAoA, hypoAoA) and 100% right fourth PAA defects (A-RSA, CORSA). In contrast, although in this cross we saw similar numbers of each PAA defect (50% left PAA, 90% right PAA) there were no incidences of A-RSA observed in these mutants, nor were there any cases of hypoplastic aortic arch.

4.2.3. Sox2cre (97.68% C57BL/6J)

As *PGKcre* deletion of *Tcfap2a* failed to recapitulate the phenotype observed in the global knockouts we chose to attempt to recapitulate the phenotype using a further ubiquitously expressed cre line, *Sox2cre*. Due to the difficulties we encountered in generating *Tcfap2a*$^{+/-}$*;PGKcre* stud males above, we employed two different breeding strategies in order to obtain either a *Tcfap2a*$^{+/-}$*;Sox2cre* or *Tcfap2a*$^{+/f}$*;Sox2cre* stud male. Once generated, these males were crossed to *Tcfap2a*$^{f/f}$ females in order to generate mutant embryos with a ubiquitous deletion of *Tcfap2a.*

4.2.3.1. Evidence of linkage between Sox2cre and Tcfap2a

Embryos from both breeding strategies were collected at e15.5 and their phenotypes and genotypes analysed. It became immediately apparent that there was a reduction in the number of mutant embryos collected in both crosses, compared to the expected mendelian ratios (see Table 4-3). As *Tcfap2a*$^{-/-}$ mutant embryos are able to survive to birth (Schorle *et al.*, 1996; Zhang *et al.*, 1996; Brewer *et al.*, 2002), this suggested that the loss of mutants is likely to be due to the *Sox2cre* transgene in these embryos. In addition, there was a reduction in the number of embryos of a 'wild type' (*Tcfap2a*$^{+/f}$) genotype obtained, suggesting that there may be genetic linkage between the *Sox2cre* transgene and the *Tcfap2a* locus.

Table 4-3: Frequency of each genotype obtained in breeding for a *Sox2cre* stud male.

Tcfap2a$^{+/-}$*;Sox2cre male*		*Tcfap2a*$^{+/f}$*;Sox2cre male*			
Genotypes	no. (%)	Genotypes	no. (%)	Total	Expected
Tcfap2a$^{+/f}$	16 (12.9%)	*Tcfap2a*$^{+/f}$	3 (16.7%)	19 (13.4%)	25%
Tcfap2a$^{f/-}$	50 (40.3%)	*Tcfap2a*$^{f/f}$	6 (33.3%)	56 (39.4%)	25%
Tcfap2a$^{+/f}$*;Sox2cre*	53 (42.7%)	*Tcfap2a*$^{+/f}$*;Sox2cre*	7 (38.9%	60 (42.25%)	25%
Tcfap2a$^{f/-}$*;Sox2cre*	5 (4%)	*Tcfap2a*$^{f/f}$*;Sox2cre*	2 (11.1%)	7 (4.9%)	25%
Total	124	Total	18	142	

The *Sox2cre* mouse is a transgenic line generated by random integration of the *Sox2cre* transgene into the genome at an undefined genetic locus. As this line was generated using wild type mice, if the transgene is in close proximity to the *Tcfap2a* locus then it will be linked to a wild type allele (Figure 4.12a). When a *Sox2cre* positive animal is bred with a *Tcfap2a*$^{+/-}$ mouse, both the *Sox2cre* transgene and the *Tcfap2a*-null allele will be transmitted to offspring equally, resulting in genotypes of the expected Mendelian ratios (Figure 4.12a). When the *Tcfap2a*$^{+/-}$*;Sox2cre* male is then crossed to a *Tcfap2a*$^{f/f}$ female, the *Sox2cre* transgene will co-segregate most often with the wild type allele (Figure 4.12b). Therefore, a recombination event during gametogenesis is required in order for the *Sox2cre* transgene to segregated with the *Tcfap2a*-null allele, producing the recombinant wild type (*Tcfap2a*$^{+/f}$) and mutant (*Tcfap2a*$^{f/-}$*;Sox2cre*) genotypes (Figure 4.12c).

A simple calculation can be used to calculate the genetic distance between the two loci in terms of centimorgans (cM). This distance is calculated based on the rate of recombination between the two loci. A total of 26 recombinant genotypes were obtained from a total of 142 embryos. Therefore, the recombination frequency is 18.3%, indicating that the distance between the two loci is 18.3 cM.

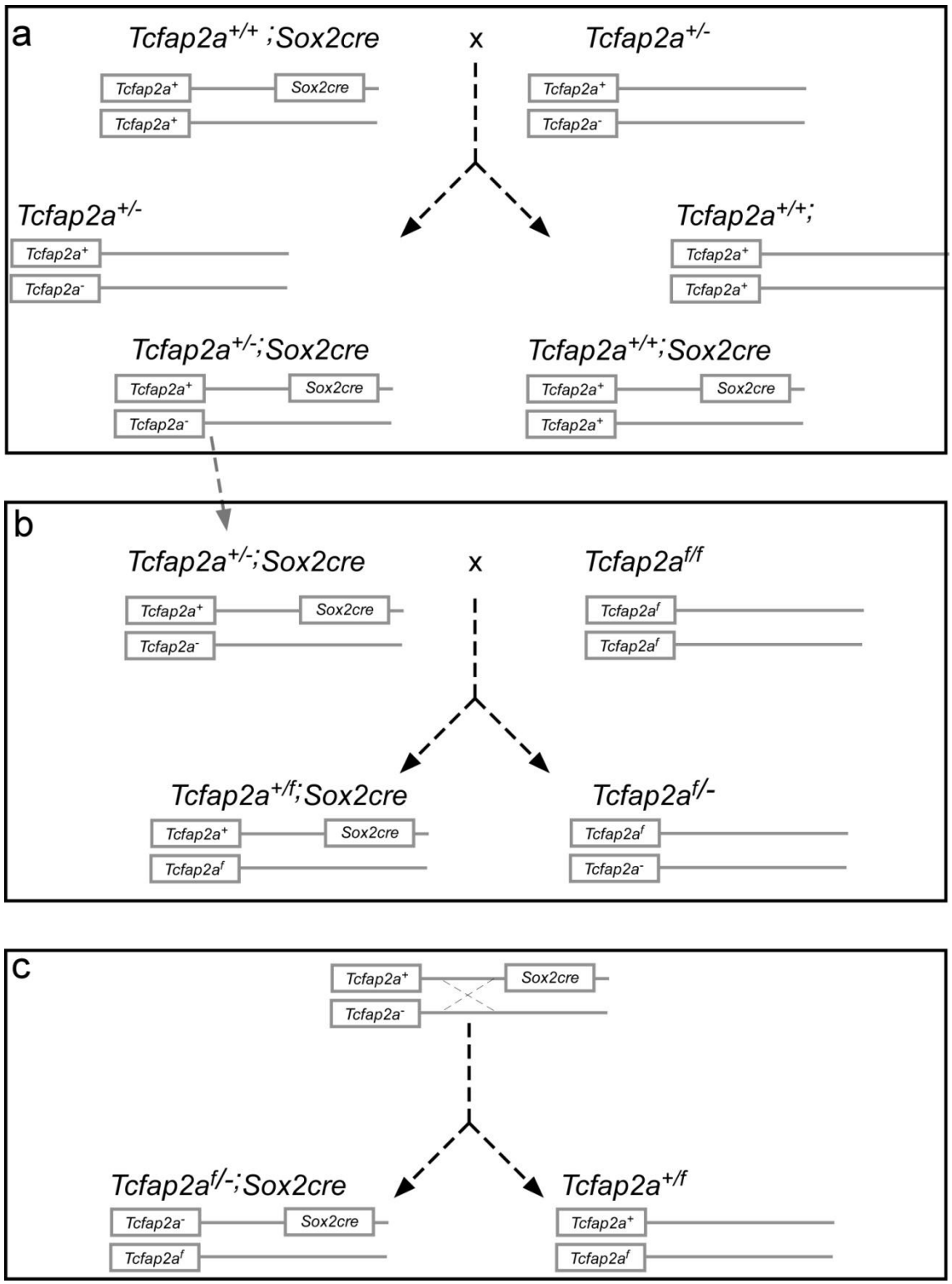

Figure 4.12: Segregation of allele in the breeding strategy designed to generate a *Sox2cre* stud male.
(a) Breeding a *Sox2cre*-positive male to a *Tcfap2a*$^{+/-}$ female results in the generation of four different genotypes. In each genotype the *Sox2cre* transgene is linked to a wild type allele of *Tcfap2a*. (b) Breeding *Tcfap2a*$^{+/-}$*;Sox2cre* offspring from the cross in (a) with a *Tcfap2a*$^{f/f}$ results in only two possible genotypes of offspring. (c) If recombination occurs in the region between the *Tcfap2a* locus and the insertion site of the *Sox2cre* transgene then *Sox2cre* may be linked to the *Tcfap2a*-null allele. This will then result in the recombinant genotypes shown.

4.2.3.2. Breeding strategy

In order to generate enough mutant embryos for analysis of cardiovascular development we chose to generate a 'recombinant' male of the genotype *Tcfap2a*$^{+/f}$*;Sox2cre*, in which the *Tcfap2a*^{flox} allele and *Sox2cre* transgene occur on the same chromosome. To generate this, a non-recombinant *Tcfap2a*$^{+/f}$*;Sox2cre* male was crossed to wild type C57BL/6J females. Any male offspring of this cross with the genotype *Tcfap2a*$^{+/f}$*;Sox2cre* will be a recombinant and has inherited both the *Tcfap2a*^{flox} allele and the *Sox2cre* transgene from the male (Figure 4.13).

Using this breeding strategy we were able to generate enough *Tcfap2a*$^{f/f}$*;Sox2cre* mutant embryos to analyse the cardiovascular phenotype by MRI. Further evidence of linkage between the *Tcfap2a* locus and the *Sox2cre* transgene was provided in the generation of these mutant embryos. The genotypes previously considered to be recombinant (*Tcfap2a*$^{+/f}$ and *Tcfap2a*$^{f/f}$*;Sox2cre*) were now obtained at much higher frequencies, similar to the frequencies previously seen with the non-recombinant genotypes (*Tcfap2a*$^{f/f}$ and *Tcfap2a*$^{+/f}$*;Sox2cre*). In addition those genotypes previously regarded as non-recombinant were now obtained at similar frequencies to the previously regarded as recombinant genotypes.

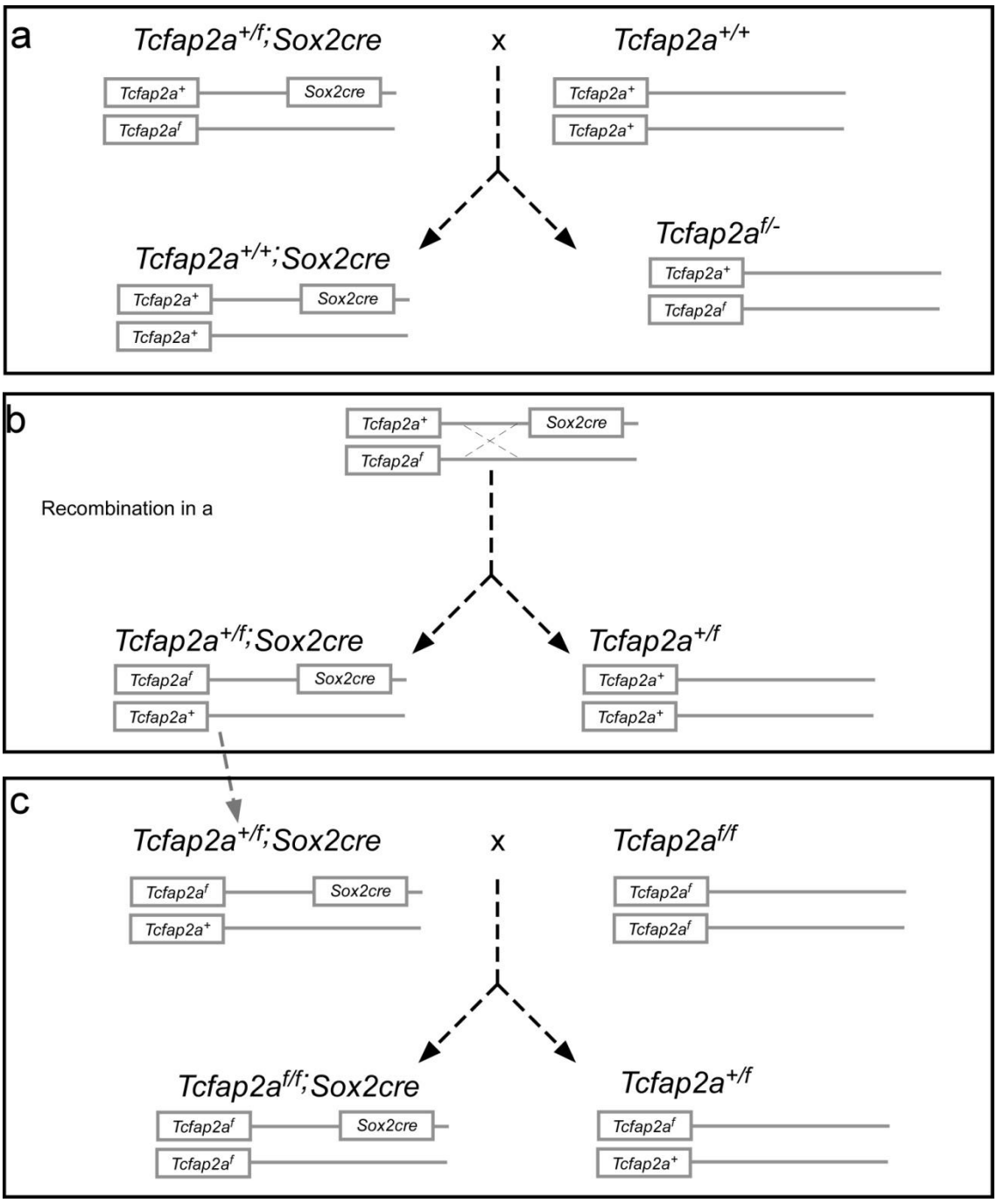

Figure 4.13: Breeding strategy for the generation of *Tcfap2a*$^{f/f}$*;Sox2cre* mutant embryos.
(a) A *Tcfap2a*$^{+/f}$*;Sox2cre* male was crossed to wild type C57BL/6J females. Due to the presumed linkage between the *Tcfap2a* locus and the *Sox2cre* transgene the majority of offspring from this cross will be of non-recombinant genotypes, as shown here. (b) If recombination occurs in (a) the *Sox2cre* transgene will be linked to the *Tcfap2a*^{f} allele, resulting in the recombinant genotypes shown. (c) Using recombinant male offspring of the genotype *Tcfap2a*$^{+/f}$*;Sox2cre* generated in (b), we can cross with *Tcfap2a*$^{f/f}$ females to produce offspring of the genotype *Tcfap2a*$^{f/f}$*;Sox2cre.*

4.2.3.3. External phenotype

Embryos were collected at e15.5 and examined for external malformations. The phenotypes observed in these mutant embryos conform to the external phenotype of *Tcfap2a*$^{-/-}$ mutant embryos (Figure 4.14).

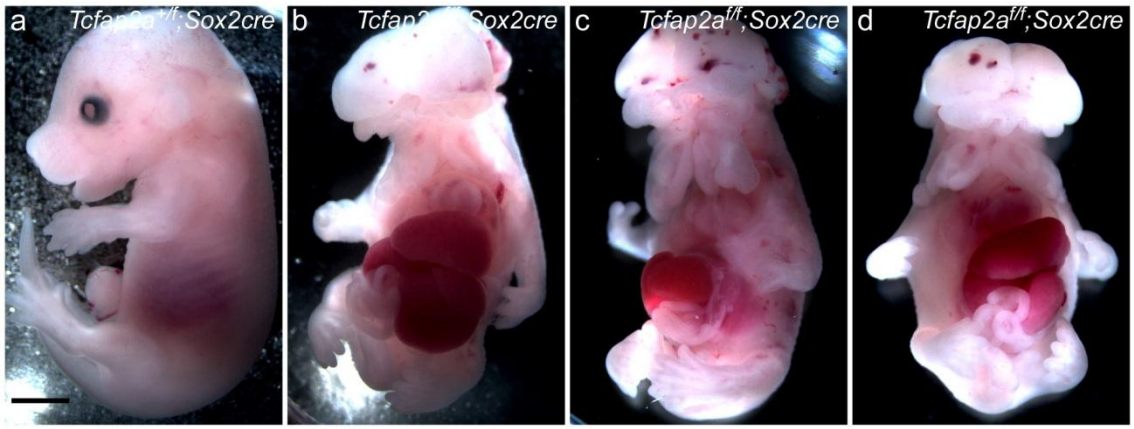

Figure 4.14: The external phenotype of *Tcfap2a*$^{f/f}$*;Sox2cre* mutant embryos phenocopies *Tcfap2a*$^{-/-}$ mutant embryos.
(a) Control (*Tcfap2a*$^{+/f}$*;Sox2cre*) embryo with normal external phenotype. (b-d) Mutant (*Tcfap2a*$^{f/f}$*;Sox2cre*) embryos with variable external malformations, which phenocopy *Tcfap2a*$^{-/-}$ mutant embryos. Scale bar = 2mm. (n=11).

4.2.3.4. Cardiovascular phenotype

Tcfap2a$^{f/-}$*;Sox2cre* mutant embryos were examined at e15.5 by MRI analysis. The phenotype of the *Tcfap2a*$^{-/-}$ mutants was not fully recapitulated in these mutant embryos. Of the 11 mutant embryos examined only 4 displayed the full CCVM phenotype seen in the *Tcfap2a*$^{-/-}$ mutants (Figure 4.15c-e). Other embryos carried variations of the full *Tcfap2a*$^{-/-}$ phenotype, including VSD with OFT malformation (1/11, 9.09%) (Figure 4.15f), VSD and PAA malformations (2/11, 18.18%), OFT defect and PAA malformations (1/11, 9.09%) (Figure 4.15g) and PAA malformations only (1/11, 9.09%) (Figure 4.15i). In addition, 2 of the mutant embryos had no CCVM at all (Figure 4.15j).

The most common OFT defect was OA, which occurred in 36.36% embryos (4/11), while DORV was seen in only 18.18% (2/11) of mutant embryos. TGA was not observed in any of the mutants in this dataset. The most common PAA malformation in this group was CORSA, which occurred in 45.45% (5/11) of mutant embryos. IAA (18.18%, 2/11), A-RSA (9.09%, 1/11) and cAoA (9.09%, 1/11) were also found in a small number of mutant embryos. A single embryo with a RAA was also identified. Interestingly, this RAA arose from a more cervical position along the brachiocephalic trunk suggesting a bilateral absence of the fourth PAAs, with persistence of the right carotid duct to connect the ascending aorta to the dorsal aorta. The penetrance of these defects is summarised in Table 4-4.

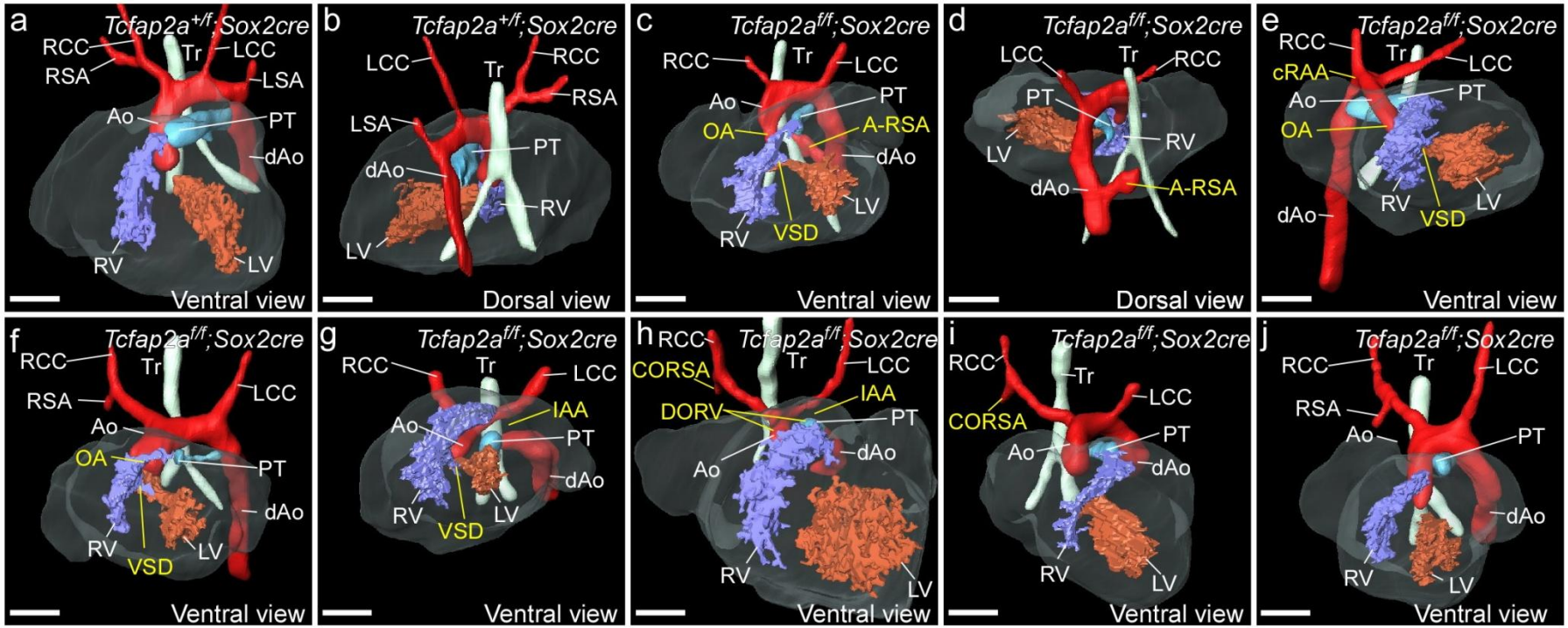

Figure 4.15: 3D reconstructions of the cardiovascular phenotype of *Tcfap2a$^{f/f}$;Sox2cre* mutant embryos.
(a-b) Ventral (a) and dorsal (b) views of a control (*Tcfap2a$^{+/f}$;Soxcre*) embryo heart with normal cardiovascular development. (b-g) Mutant *(Tcfap2a$^{f/f}$;Sox2cre*) embryos with various cardiovascular malformations: (c-d) Ventral (c) and dorsal (d) views of an embryo with the full phenotype consisting of a VSD, OFT defect (OA) and a PAA malformation (A-RSA); (e) Ventral view of an embryo with the full phenotype consisting of a RAA which appears at a more cervical position (cervical RAA, cRAA), a VSD and OA; (f) mutant embryo with VSD and OFT malformations (OA) only; (g) mutant embryo with a VSD and PAA malformations (IAA) only; (h) a mutant embryo with malformations of the OFT (DORV) and PAAs (IAA, CORSA) only; (i) a mutant embryo with defects of the PAAs (CORSA) only; (j) mutant embryo with no cardiovascular defects. Scale bar = 500 µm. (n=11).

Table 4-4: Prevalence of CCVM in *Tcfap2a*$^{f/f}$*;Sox2cre* mutant embryos at e15.5 compared to *Tcfap2a*$^{-/-}$ embryos.

CCVM	Prevalence (n=11)	Summary	Prevalence in *Tcfap2a*$^{-/-}$	Summary for *Tcfap2a*$^{-/-}$
VSD	54.54%	VSD – 54.54%	100%	VSD – 100%
OA	36.36%	OFT defects - 54.54%	30%	OFT defects – 100%
DORV	18.18%		20%	
TGA	0%		50%	
IAA	18.18%	Left 4th PAA defects – 27.27%	30%	Left 4th PAA defects – 50%
cAoA	9.09%		20%	
HypoAoA	0%		0%	
A-RSA	9.09%	Right 4th PAA defects – 54.54%	40%	Right 4th PAA defects – 90%
CORSA	45.45%		50%	
RAA	9.09%	RAA only – 9.09%	10%	RAA with I-LSA – 10%
I-LSA	0%		10%	

4.2.3.5. Transcript analysis

To exclude the possibility that *Sox2cre* does not cause efficient recombination between the loxP sites within the *Tcfap2a*^{flox} allele, embryos were collected at e9.5 for RT-PCR analysis. Whole RNA was extracted from these embryos and used to synthesise cDNA which was used in RT-PCR reactions. Using primers that span the floxed region we were able to determine that successful recombination of the loxP sites has occurred by e9.5 in *Tcfap2a*$^{f/f}$*;Sox2cre* mutant embryos, and no wild type transcripts were observed (Figure 4.16). We have already demonstrated that this recombined transcript is not translated to produce a protein product (see section 4.2.1.4).

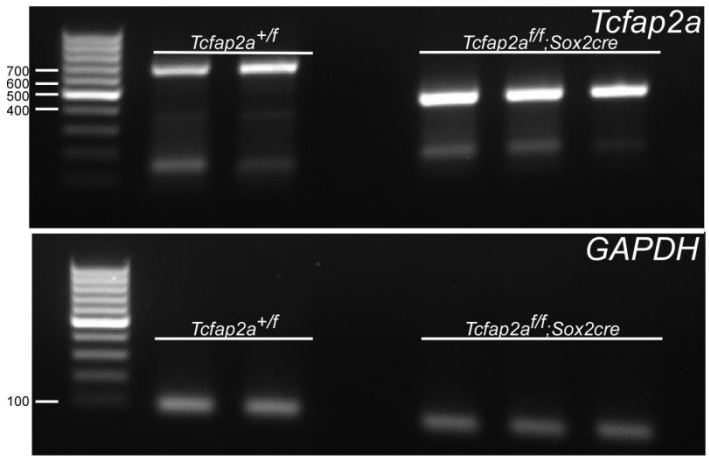

Figure 4.16: RT-PCR demonstrates efficient recombination of the *Tcfap2a*^{flox} allele by *Sox2cre*.
Top panel: *Tcfap2a* expression was investigated using primers spanning the floxed region and demonstrates a large (~663 bp) band in control (*Tcfap2a*$^{+/f}$*;Sox2cre*) embryos, corresponding to the wild type transcript. In mutant embryos (*Tcfap2a*$^{f/f}$*;Sox2cre*) a smaller band (~402 bp) was observed, corresponding to the product of a recombined allele.

4.2.4. *Tcfap2a*$^{+/\Delta}$ x *Tcfap2a*$^{+/\Delta}$ *(98.28%* C57BL/6J)

The use of both *PGKcre* and *Sox2cre* failed to recapitulate the phenotype observed in the *Tcfap2a*$^{-/-}$ embryos. The *Tcfap2a*$^{f/f}$*;PGKcre* and *Tcfap2a*$^{f/f}$*;Sox2cre* mutants differ from the *Tcfap2a*$^{-/-}$ mutants both in the timings of deletion and the exons which are removed by each mutation. To investigate if these factors were affecting the phenotype observed we generated *Tcfap2a*$^{\Delta/\Delta}$ mutants (where Δ or 'del' refers to the deletion of the recombined allele) by the intercrossing of mice with recombined alleles of *Tcfap2a*^{flox} (recombined by *Sox2cre*) (Figure 4.17). The *Tcfap2a*$^{+/f}$*;Sox2cre* stud male generated by the breeding strategy described above (see 4.2.3.2) was used to produce both male and female offspring of the genotype *Tcfap2a*$^{+/\Delta}$. These offspring were then intercrossed to generate*Tcfap2a*$^{\Delta/\Delta}$ mutant embryos.

4.2.4.1. External phenotype

Embryos were collected at e15.5 for MRI analysis. The external phenotype resembled that of the *Tcfap2a*-null mutant embryos and the other crosses described within this chapter (Figure 4.18).

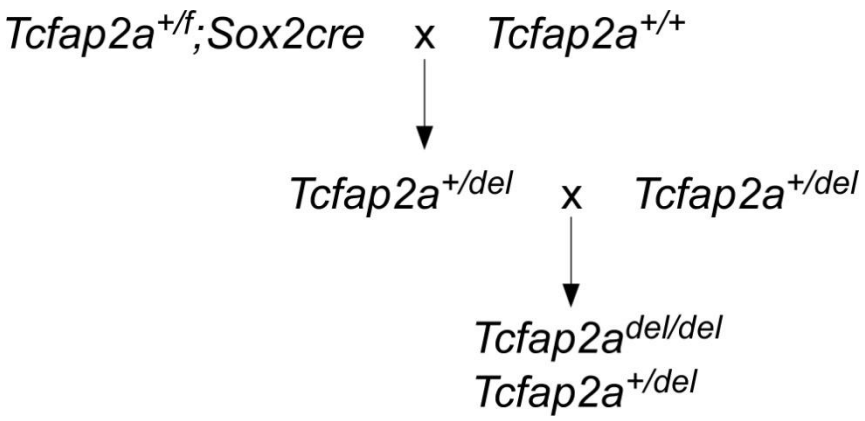

Figure 4.17: Breeding strategy for the generation of *Tcfap2a*$^{\Delta/\Delta}$ mutant embryos.
A *Tcfap2a*$^{+/f}$*;Sox2cre* male was crossed to wild type females to generate *Tcfap2a*$^{+/\Delta}$ mice in which the *Tcfap2a*^{flox} allele has been recombined by *Sox2cre*. *Tcfap2a*$^{+/\Delta}$ mice were intercrossed to generate *Tcfap2a*$^{\Delta/\Delta}$ mutant embryos.

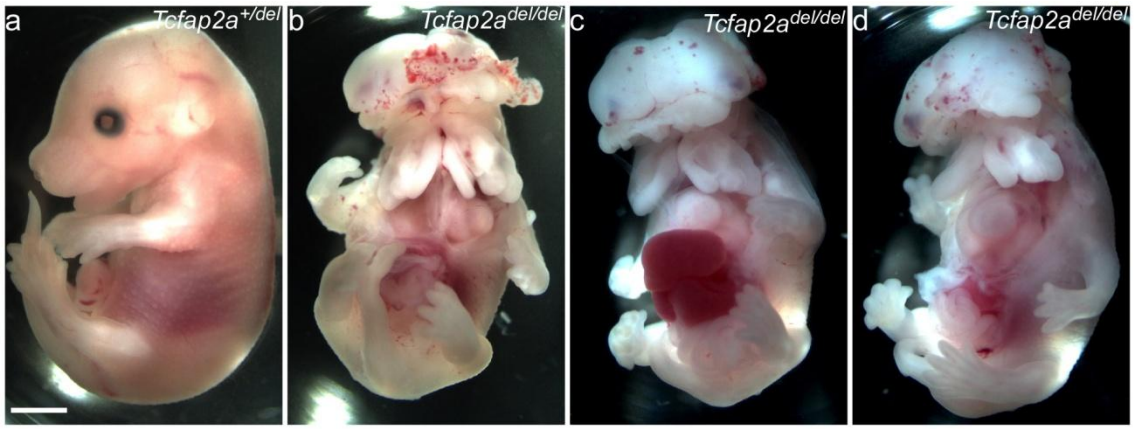

Figure 4.18: The external phenotype of *Tcfap2a*$^{\Delta/\Delta}$ mutant embryos recapitulates the phenotype of *Tcfap2a*$^{-/-}$ mutant embryos.
(a) Control (*Tcfap2a*$^{+/\Delta}$) embryo showing a normal external phenotype. (b-d) Mutant (*Tcfap2a*$^{\Delta/\Delta}$) embryos showing variable external malformations. Scale bar = 2mm. (n=12).

4.2.4.2. Cardiovascular phenotype

Mutant embryos from timed matings of *Tcfap2a*$^{+/\Delta}$ parents were collected at e15.5 for MRI analysis. As with the *Tcfap2a*$^{f/f}$*;Sox2cre* mutant embryos, these mutant embryos failed to recapitulate the cardiovascular phenotype observed with *Tcfap2a*$^{-/-}$ mutant embryos. Of the 12 mutant embryos examined only 3 (25%) had the full phenotype associated with *Tcfap2a*-null embryos (Figure 4.19b). A further 7 embryos (58.33%) had only PAA malformations (Figure 4.19d, f) and two further embryos (16.67%) had a VSD and OFT defect in the absence of PAA malformations (Figure 4.19c).

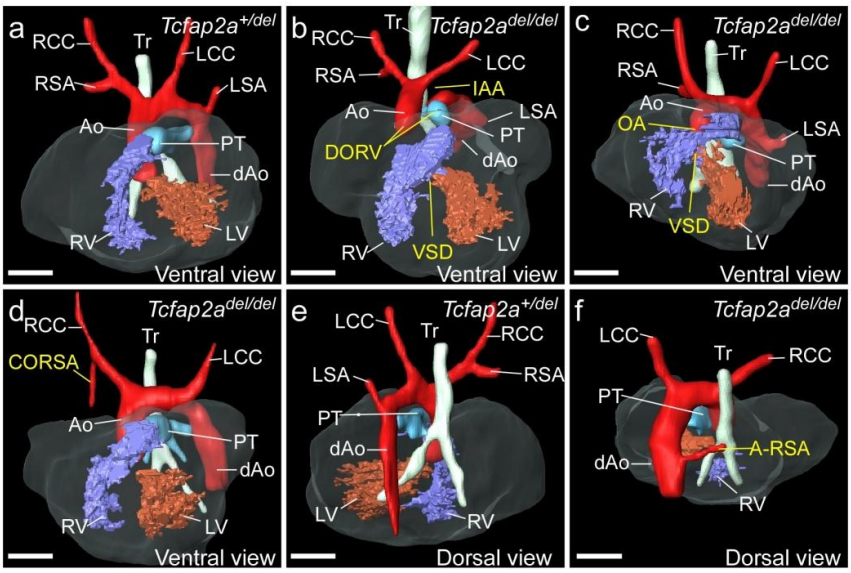

Figure 4.19: 3D reconstructions of the cardiovascular malformations observed in *Tcfap2a*$^{\Delta/\Delta}$ mutant embryos. (a) A ventral view of a control (*Tcfap2a*$^{+/\Delta}$) embryo showing normal cardiovascular development. (b-d) Ventral views of mutant (*Tcfap2a*$^{\Delta/\Delta}$) embryos with a variety of cardiovascular phenotypes: (b) A mutant embryo with the full phenotype of cardiovascular malformations consisting of a VSD, an OFT defect (DORV) and PAA malformations (IAA); (c) A mutant embryo with a VSD and OFT defect (OA) only; (d) a mutant embryo with PAA malformations only (CORSA). (e) A dorsal view of a control embryo with normal cardiovascular development. (f) A dorsal view of a mutant embryo with PAA malformations only (A-RSA). Scale bar = 500 µm. (n=12).

A VSD was observed in 41.67% (5/12) of mutant embryos. The observed OFT defects were OA and DORV, which occurred in 25% (3/12) and 16.67% (2/12) of mutant embryos respectively, and always in the presence of a VSD. PAA malformations occurred more commonly on the right (75%, 9/12) than the left (8.33%, 1/12), with the most common defect being CORSA (58.33%, 7/12). A-RSA (16.67%, 2/12) and IAA (8.33%, 1/12) occurred less often in these mutant embryos. None of these mutant embryos exhibited normal cardiovascular development (Table 4-5).

Table 4-5: Prevalence of CCVM in *Tcfap2a*$^{\Delta/\Delta}$ mutant embryos at e15.5 compared to *Tcfap2a*$^{-/-}$ embryos.

CCVM	Prevalence (n=9)	Summary	Prevalence in *Tcfap2a*$^{-/-}$	Summary for *Tcfap2a*$^{-/-}$
VSD	41.66%	VSD – 41.66%	100%	VSD – 100%
OA	25%	OFT defects – 41.66%	30%	OFT defects – 100%
DORV	16.67%		20%	
TGA	0%		50%	
IAA	8.33%	Left 4th PAA defects –8.33%	30%	Left 4th PAA defects – 50%
cAoA	0%		20%	
Hypo AoA	0%		0%	
A-RSA	16.66%	Right 4th PAA defects – 75%	40%	Right 4th PAA defects – 90%
CORSA	58.33%		50%	
RAA	0%	No defects observed	10%	RAA with I-LSA – 10%
I-LSA	0%		10%	

4.2.5. *Tcfap2a* and *Wnt1cre* expression analysis

The data collected from the above experiments demonstrates that the CCVM observed in *Tcfap2a*$^{-/-}$ mutant embryos cannot be fully recapitulated using the *Tcfap2a*^{flox} allele. However, the penetrance of CCVM observed in the NCC-specific conditional deletion was much lower than that observed here. We, therefore, wanted to investigate the timing of *Tcfap2a* and *Wnt1cre* expression to confirm the ability of this cre line to fully recombine the *Tcfap2a*^{flox} allele, before the *Tcfap2a* locus becomes active.

Embryos were collected at e7.5, e8.0 and e8.5 for analysis by RT-PCR. RNA was extracted from the samples and cDNA synthesis was carried out for use in RT-PCR reactions. Four cre-positive and four cre-negative samples were examined at each stage. To investigate the temporal expression of *Wnt1cre* within our embryos we used primers designed to bind within the *Cre* cDNA sequence of the expressed transcript. As these primers were not specific to the transcript and will also bind to genomic DNA, we used another primer pair, binding to *Cited2*, in order to distinguish between cDNA and genomic DNA contamination. These primers bind within exons 1 and 2 of the *Cited2* gene, and span a small intervening intron. Therefore, in the presence of genomic DNA contamination these primers will produce an additional larger band. To investigate *Tcfap2a* expression in these embryos we used primers spanning the floxed region (described in sections 4.2.1.3 and 4.2.3.5 above). This allowed us to determine both the timing of normal *Tcfap2a* activation, and whether the *Cre* transcript has been translated into a functional enzyme and induced recombination within the *Tcfap2a*^{flox} allele. GAPDH was used as a housekeeping gene.

At e7.5, neither *Tcfap2a* nor *Wnt1cre* are expressed, however, low levels of GAPDH expression were observed (Figure 4.20). By e8.0, expression of *Wnt1cre* is visible in cre-positive samples only. This product relates to the mRNA transcript, not the *Cre* cDNA within the genome, as the *Cited2* primers demonstrate that there is no contaminating genomic DNA within these samples. Expression of *Tcfap2a* is also observed at this stage and two bands, pertaining to the wild type and recombined transcript, were found in cre-positive sample 1. However, cre-positive sample 2 shows low levels of *Wnt1cre* expression in addition to only a single, wild type band for *Tcfap2a*. Although this result was only observed in a single sample, the sample in question was generated from an embryo of a younger age than the other samples (1

somite stage, compared to 3-4 somite stage embryos used for other samples). Therefore, it is possible that in this sample the *Tcfap2a* locus is already active, while the Cre transcript is still being translated. If this were the case it would allow some wild type *Tcfap2a* transcripts, and therefore wild type AP-2α protein, to be produced before the conditional removal of exons 5 and 6. By e8.5 *Wnt1cre* expression is reduced and both wild type and recombined bands are observed for *Tcfap2a*.

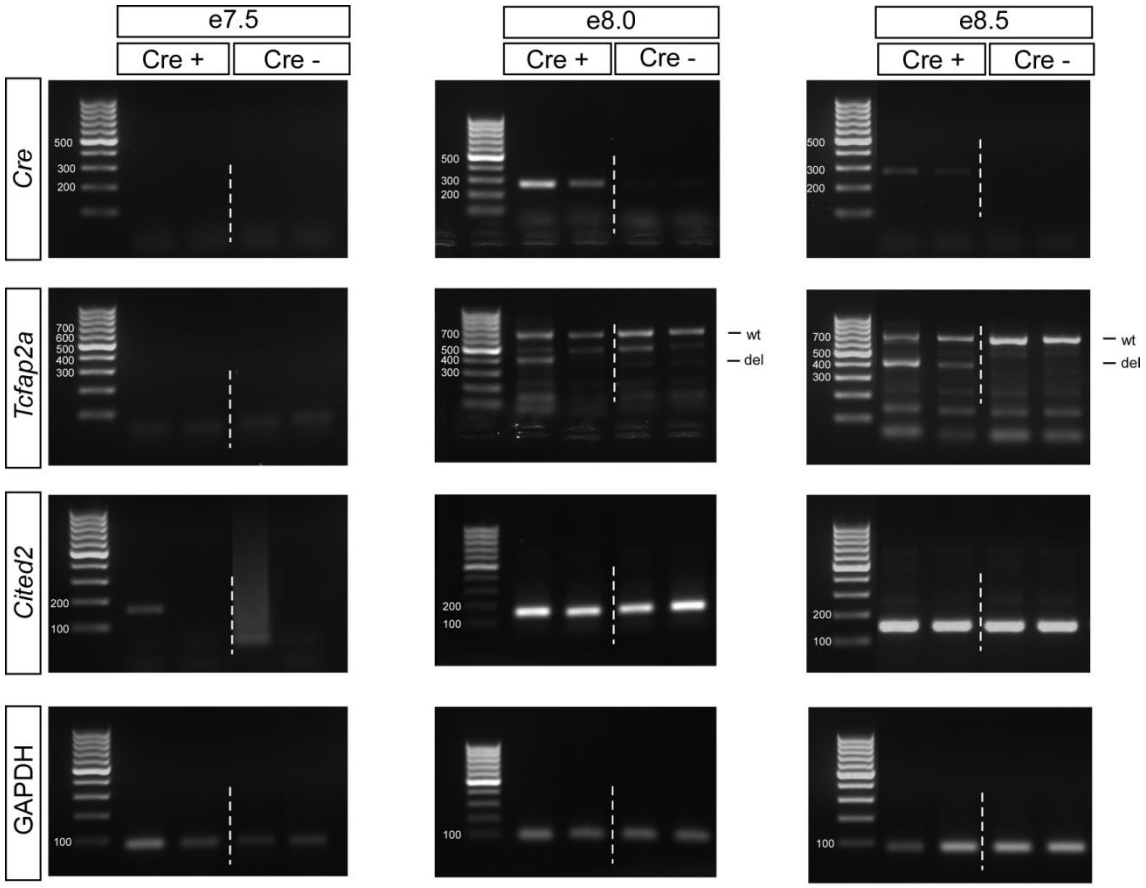

Figure 4.20: RT-PCR analysis of the temporal expression patterns of *Tcfap2a* and the *Wnt1cre* transgene. Expression of *Tcfap2a* and the *Wnt1cre* transgene was examined at e7.5 (left), e8.0 (middle) and e8.5 (right). Top panel: Expression of *Wnt1cre* transgene. Second panel: Expression of *Tcfap2a* wild type (663 bp) and recombined (402 bp) transcripts. Third panel: Expression of *Cited2* was examined to control for gDNA contamination. Bottom panel: Expression of GAPDH was examined as an internal control. Four cre-positive and four cre-negative samples were examined at each stage, representative images shown.

4.3. Discussion

In the previous chapter, we demonstrated the low penetrance of CCVM associated with conditional deletion from the NCCs, and the complete lack of CCVM in embryos with a conditional deletion from the NCCs and PSE. In this chapter we attempted to understand the reasons for this low penetrance. *Tcfap2a* is strongly expressed between e8.5 and e11.5 in various tissues of the developing mouse embryo. However, expression within tissues contributing to the developing cardiovascular system is

restricted to the NCCs and the PSE. Therefore, it is possible that the inability to recapitulate the cardiovascular defects observed in *Tcfap2a*$^{-/-}$ embryos in these crosses is the result of some intrinsic problems in the *Tcfap2a*^{flox} allele used here, or in the timings of expression of the tissue-specific cre lines examined in the previous chapter. Therefore, to address these questions, a series of ubiquitously expressed cre lines, which are expressed early in embryonic development, were used.

4.3.1. CCVM is not secondary to external malformations

Tcfap2a$^{-/-}$ embryos exhibit a very severe external phenotype characterised by anencephaly, a ventral body wall defect and severe craniofacial malformation (Schorle *et al.*, 1996; Zhang *et al.*, 1996; Brewer *et al.*, 2002). Each of these phenotypes may cause alterations to the haemodynamics of the developing embryo or allow the developing organs to be exposed to the external environment. It is therefore possible that the cardiovascular defects observed in *Tcfap2a*$^{-/-}$ mutant embryos are the result of the severe external malformations observed. As a very limited number of CCVMs were identified in the tissue-specific mutants, it is possible that the inability to recapitulate the cardiovascular phenotype was a result of the low penetrance of external phenotypes observed in these embryos.

PGK is a glycolytic enzyme and is therefore expected to be expressed at different levels in various tissues, owing to their different metabolic requirements (McBurney *et al.*, 1994). Examination of the mutant embryos collected revealed very similar external phenotype to that seen in the *Tcfap2a*$^{-/-}$ mutant embryos. However, MRI analysis of these embryos demonstrated that there were variations in the levels of CCVM observed in mutant embryos, despite the similarities between external phenotypes. This, therefore, suggests that the presence of CCVM is independent of the external malformations observed. Four different breeding strategies were employed throughout this chapter. Of the embryos examined under these four breeding strategies, less than half (39.5%, 17/43) had the full cardiovascular phenotype of the *Tcfap2a*$^{-/-}$ embryos described in the preliminary data (see section 1.5.1). Of those embryos failing to adhere to the full phenotype many different combinations of these defects were observed (Table 4-6). Approximately one third of mutant embryos (35%, 15/43) had only a PAA malformation. The remaining embryos had a variety of combinations of the phenotypes which occurred at low penetrance. Interestingly,

across the 4 different breeding strategies employed within this chapter, there were no cases in which either VSD or OFT defects occurred alone. In addition, these two phenotypes were found together in 46.5% (20/43) of mutant embryos. This indicates that these two elements of the phenotype may be linked by a common mechanism of development. However, less than 15% (13.95%, 6/43) of mutant embryos had only one of these phenotypes, in the presence of a PAA malformation. This suggests that the correct alignment of the OFT may be dependent on the formation of the interventricular septum or that the septation of the ventricles relies on correct OFT alignment. It has been previously suggested that in *Tbx1* mutant embryos the VSD phenotype is the result of PTA, in that the abnormal aorticopulmonary septum is unable to fuse to the forming interventricular septum (Arnold *et al.*, 2006). Although in our data the aorticopulmonary septum forms, but is simply misaligned, it is possible the phenotypes result from a similar mechanism. Additionally, NCC ablation in chicken embryos has also demonstrated that DORV and OA often occur in the presence of a VSD (Nishibatake *et al.*, 1987).

Table 4-6: Summary of the variety of CCVM observed in each mutant genotype examined in this chapter.

Genotype	*Tcfap2a*$^{f/f}$; *PGKcre*	*Tcfap2a*$^{f/-}$; *PGKcre*	*Tcfap2a*$^{f/f}$; *Sox2cre*	*Tcfap2a*$^{\Delta/\Delta}$	Total
Full phenotype*	4 (40%)	6 (60%)	4 (36.36%)	3 (25%)	17 (39.5%)
OFT and PAA defects	-	1 (10%)	1 (9.09%)	-	2 (4.65%)
VSD and OFT defects	-	-	1 (9.09%)	2 (16.67%)	3 (7%)
VSD and PAA defects	1 (10%)	1 (10%)	2 (18.18%)	-	4 (9.3%)
PAA defects only	5 (50%)	2 (20%)	1 (9.09%)	7 (58.33%)	15 (35%)
No CCVM	-	-	2 (18.18%)	-	2 (4.65%)

All numbers given above indicate the total number of embryos with each phenotype, with percentages given in brackets.
* The full phenotype is defined as a VSD, an OFT defect and a PAA malformation and was observed at 100% penetrance in *Tcfap2a*$^{-/-}$ mutant embryos.

In addition, analysis of *Tcfap2a*$^{f/f}$*;Sox2cre* mutant embryos revealed two embryos with normal cardiovascular development despite severe external malformations. Therefore it appears that the external malformations do not cause the cardiovascular phenotypes observed and that these phenotypes also occur independently. Further, one of the embryos from the *Tcfap2a*$^{\Delta/\Delta}$ dataset, which had a PAA defect, also exhibited a mild

ventral wall defect in comparison to other mutant embryos (see Figure 4.18b). This suggests that the external phenotype is completely independent of the cardiovascular phenotype.

4.3.2. The *Tcfap2a*^{flox} conditional allele

The *Tcfap2a*^{flox} allele was generated by the insertion of loxP sites within introns 4 and 6 of the *Tcfap2a* gene. In the presence of cre this results in the excision of exons 5 and 6. The work presented in this chapter demonstrates that both *PGKcre* and *Sox2cre* are able to successfully recombine the *Tcfap2a*^{flox} allele throughout the embryo by e9.5. However, western blotting revealed that this transcript failed to produce a functional protein by e10.5, therefore suggesting that any protein product from this allele is rapidly degraded and is therefore unlikely to be involved in any transcriptional processes.

The *Tcfap2a*-null allele was produced by the disruption of exon 7 of the *Tcfap2a* gene. We demonstrate in this chapter that the disruption of this exon does not prevent the production of a transcript; however, the ability of this transcript to be translated into protein was not investigated. Any protein resulting from this transcript would contain only approximately half of the dimerisation domain of the protein and is, therefore unlikely to be functional (Figure 4.21b). Sequence alignment of wild type and recombined transcripts revealed that any protein produced from the recombined allele would result in the removal of a portion of the basic DNA binding domain and the first helix and part of the span region of the dimerisation domain (Figure 4.21c). However, this transcript is not translated into a protein product.

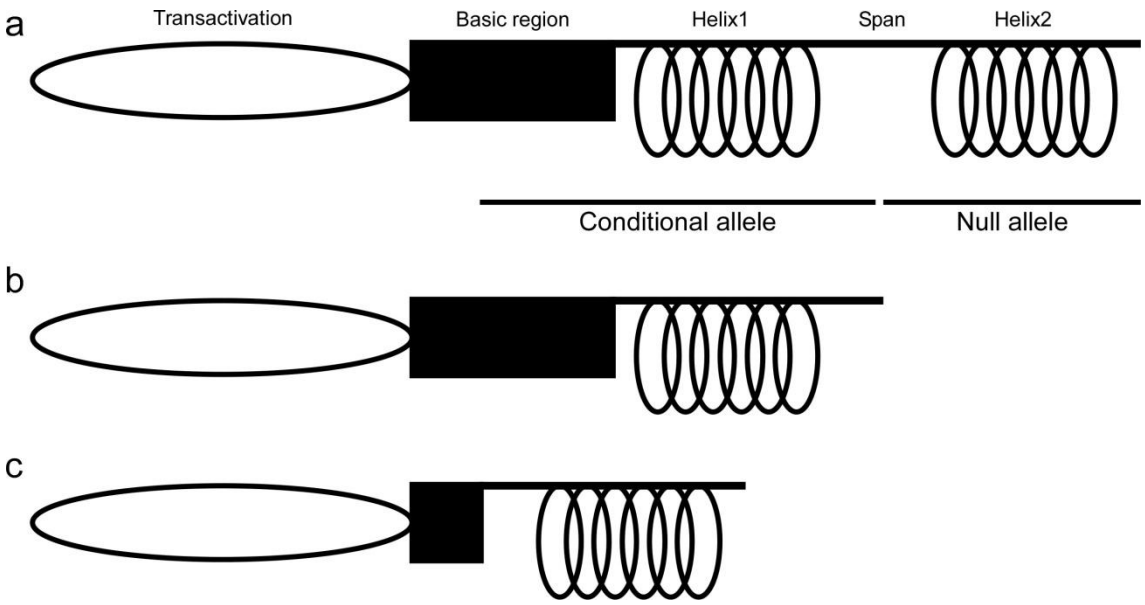

Figure 4.21: The structure of AP-2α protein products of the *Tcfap2a* alleles examined in this thesis.
(a)The structure of wild type AP-2α protein with the structural domains indicated. The regions disrupted by the conditional and null alleles are indicated below. (b) The structure of the protein product of the null allele. The insertion of a LacZ cassette into exon 7 removes part of the span region and the second helix of the dimerisation domain. (c) The structure of the protein product of the recombined conditional allele. Recombination between loxP sites results in removal of part of the basic DNA binding domain in addition to the first helix and part of the span region of the dimerisation domain.

Two previous *Tcfap2a*-null alleles have been produced to investigate the role of this gene in development (Schorle *et al.*, 1996; Zhang *et al.*, 1996). These null alleles varied from that produced by Brewer *et al.* (2002) in the positions of the mutations. Schorle *et al.* (1996) disrupted *Tcfap2a* by replacing exon 5 with a neomycin cassette, whereas Zhang *et al.* (1996) removed exon 6 and the first 3 nucleotides of exon 7 by a similar technique. Both mutations result in the same severe external phenotype observed here, however, these authors did not describe any cardiovascular defects in these mutants. Brewer *et al.* (2002) examined the cardiovascular defects of both the *Tcfap2a*-null allele, used within our work, and that produced by Zhang *et al.* (1996) and demonstrated complete penetrance of VSD and OFT defects, with a lower penetrance of PAA malformations. However, there were slight variations between the OFT phenotypes observed in each of these models. The OFT defect in the majority of embryos from these two models was DORV, however, the knock-out allele produced by Zhang *et al.* (1996) also resulted in 40% (2/5) of mutants with PTA. In addition, 60% (3/5) of these mutant embryos also had a malformation of the PAAs (IAA and A-RSA), whereas the knock-in allele created by Brewer *et al.* (2002) produced no mutant embryos with PTA and only a single mutant embryo with PAA malformations (A-RSA, 10%, 1/10) (Brewer *et al.*, 2002). Although the authors do not describe the genetic

background of the knock-out allele it is likely that both strains were maintained on a black swiss background and that this is not a factor in the variation of the phenotypes observed. Therefore, it is possible that the differences in the regions which are disrupted in the two alleles are the cause of the variations in the CCVM observed.

4.3.3. Conditional mutations of *Tcfap2a* are unable to recapitulate the null phenotype

Throughout this chapter a number of attempts have been made to recapitulate the phenotype observed in the *Tcfap2a*$^{-/-}$ mutant embryos, using various cre lines and breeding strategies. However, each strategy has proven unsuccessful. The conditional allele contains loxP sites within introns 4 and 6, which in the presence of Cre recombinase undergo recombination to excise the intervening sequence pertaining to exons 5 and 6. These exons encode a major part of the DNA binding and dimerisation domains of AP-2α and *in vitro* analysis has demonstrated that both functions are lost in mutant transcripts with deletions within these regions (Williams and Tjian, 1991a; Williams and Tjian, 1991b). It is therefore expected that upon efficient recombination this allele would behave as a null.

In this chapter we have demonstrated that both *PGKcre* and *Sox2cre* are capable of efficient recombination of the loxP sites within the *Tcfap2a*^{flox} allele by e9.5 of development. In addition, western blotting analysis failed to detect a protein product in these mutant embryos, suggesting that this transcript is incapable of translation or that any protein produced is rapidly degraded. As these embryos were collected at e10.5, a stage at which *Tcfap2a* is highly expressed, we would expect that any translated product would be visible in a western blot at this stage. It therefore appears that the recombined conditional allele does behave as a null allele in the sense that it results in no functional protein product.

However, recombination of this allele using two independent Cre lines failed to recapitulate the full cardiovascular phenotype observed in the global mutant embryos. One possibility for this discrepancy is the alteration in genetic background between the various lines under examination. However, this alteration is minor and unlikely to cause such severe changes to the cardiovascular phenotype. Another possibility is that recombination of the conditional allele within the genomic DNA is not complete by

e8.5, when *Tcfap2a* becomes active, but by e9.5 all alleles have been efficiently recombined. This would allow the synthesis of some functional protein product which may activate downstream targets, but has degraded by e10.5 when western blot analysis was carried out. However, the *Tcfap2a*$^{\Delta/\Delta}$ mutants, produced by intercrossing mice which were heterozygous for a *Sox2cre*-recombined conditional allele, show a similar penetrance of cardiovascular defects to that observed in the other ubiquitously deleted conditional mutants. This indicates that the reduced penetrance of cardiovascular defects observed in these mutant embryos are not the result of inefficient recombination of the cre enzyme or delayed activation of the cre gene.

It therefore appears that the discrepancies between the two models, the conditional mutant and the null-mutant are the result of intrinsic differences between the two alleles under investigation. The work presented within this chapter demonstrates that the cre-mediated recombination of the conditional allele results in no protein product. Therefore, it suggests that the issue lies with the *Tcfap2a*-null allele, used in the production of the global knock-out phenotype, upon which we have based our investigations. This allele incorporates a LacZ cassette into exon 7 of the *Tcfap2a* locus, which contains a portion of the HSH dimerisation domain required for the protein function. As discussed above, disruptions in this region result in abolishment of DNA binding and dimerisation activity of the resulting protein. It is therefore unlikely that this protein would be able to function as a transcription factor. It is also unlikely that this product can act as a conventional DN protein by dimerisation with the wild type protein to prevent wild type homo- or heterodimer formation and DNA binding activity. However, Buettner *et al.* (1993) characterised an alternatively spliced transcript consisting of the first five exons of the human *TFAP2A* gene only, which upon translation demonstrated DN activity. The authors demonstrate that the DN-AP-2α is incapable of binding to DNA or forming either homo- or heterodimers and proposed an indirect mechanism of inhibition, potentially mediated by additional factors provided by nuclear extracts in their experiments (Buettner *et al.*, 1993). These authors later described a mechanism of AP-2 inhibition termed 'transcriptional self-interference'. In this mechanism, overexpression of AP-2α results in a decrease in transcriptional activation due to the sequestration of coactivator molecules. AP-2

dimers bound to target genes do not receive the required coactivator molecules and are therefore unable to activate transcription (Kannan *et al.*, 1994).

We propose a similar mechanism is active in the *Tcfap2a*$^{-/-}$ mutant embryos in which coactivator molecules required for target gene transcription are unavailable to all members of the AP-2 family, resulting in downregulation of target genes of these transcription factors (Figure 4.22). It is interesting to note that of the four datasets investigated within this chapter, the *Tcfap2a*$^{f/-}$*;PGKcre* mutant embryos show the highest penetrance of CCVM. These mutant embryos show full recapitulation of the fourth PAA defects observed in *Tcfap2a*$^{-/-}$ mutant embryos and 70% penetrance of VSD and OFT defects. Overall, 60% of these mutant embryos recapitulate the full phenotype observed in the *Tcfap2a*$^{-/-}$ embryos. This suggests that the presence of the *Tcfap2a*-null allele is capable of modifying the phenotype in some way. Additionally, several authors have reported that whole gene deletions of *TFAP2A* in BOFS patients results in a milder phenotype to that seen in patients carrying missense mutations affecting only a few amino acids of the protein (Milunsky *et al.*, 2008; Gestri *et al.*, 2009; Milunsky *et al.*, 2011; LeBlanc *et al.*, 2013; Li *et al.*, 2013). Although, the phenotypes observed in BOFS are the result of heterozygous mutations within *TFAP2A*, it supports our suggestion that the presence of a mutant AP-2α protein is more deleterious than the complete absence of this transcription factor, as we see in the conditional mutants.

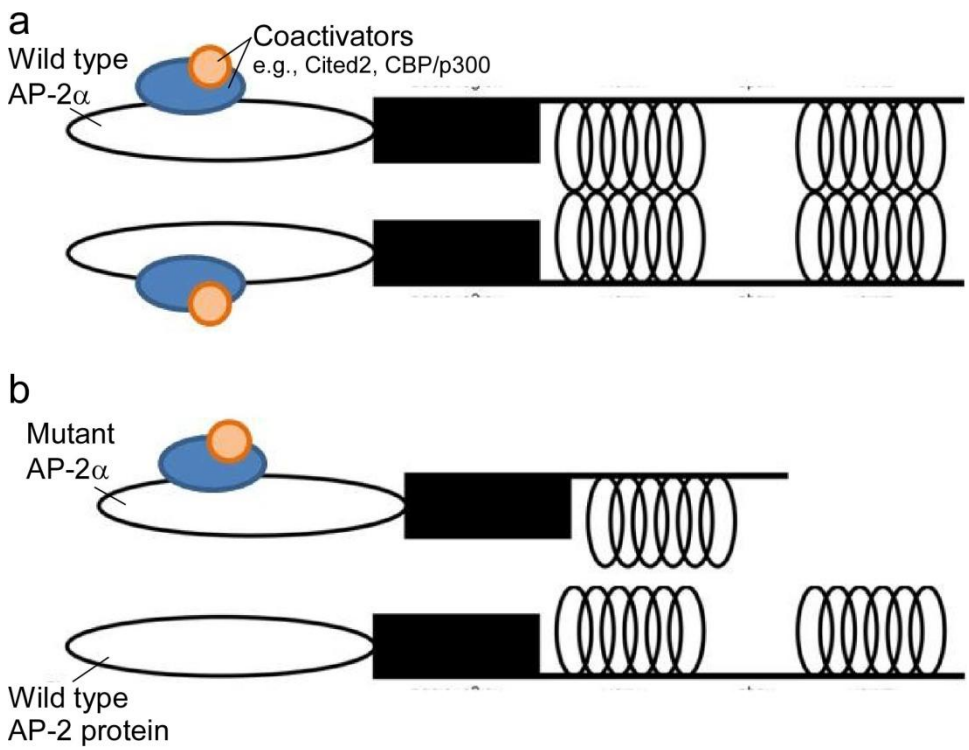

Figure 4.22: Model of transcriptional self interference in *Tcfap2a*-null allele.
(a) The wild type AP-2α protein forms dimers with other wild type AP-2 proteins and binds to coactivators molecules in order to activate transcription of target genes. (b) The mutant AP-2α protein produced from the *Tcfap2a*-null allele is unlikely to form dimers with any other AP-2 proteins. However, this protein may bind to and sequester coactivator molecules, preventing them from binding to wild type proteins to activate transcriptional targets.

4.3.4. Disadvantages of transgenic mouse lines

The random integration of transgenes into the murine genome creates numerous issues for geneticists. Although multiple copies of a single transgene may be integrated at various sites, this is usually controlled for using southern blotting techniques to select for embryonic stem cells with only a single copy of the transgene. However, other issues such as the location at which the transgene integrates and how this location impacts the expression of the transgene, are less readily controllable and the exact location of many transgenes within many mouse models remains unknown. For example, many cre lines become expressed in altered patterns due to the differential regulation by surrounding elements.

As shown in this chapter, the lack of information about the location of a transgene further impedes genetics research using mouse models. We demonstrated that *Sox2cre* is likely to have integrated into mouse chromosome 13, in close proximity to the *Tcfap2a* locus (approximately 18 Mb apart). Once it was identified that the two loci were in linkage disequilibrium, we were able to generate a viable breeding strategy in order to achieve our goals. However, if the location at which the transgene

had integrated was known prior to our investigation this would have guided our decisions on both which Cre lines to utilise and the appropriate breeding strategy for the generation of mutant embryos.

Despite these issues, the use of transgenic mouse lines remains a more viable option than cre lines which are 'knocked-in' to a locus, as many of these cre lines replace the gene at this locus (as is the case with the *Foxg1cre* and *Nkx2.5cre* lines used in the previous chapter). This can cause further difficulties as many of the genes used due to their specific expression within the developing heart, also have a role in the development of the cardiovascular system. This, therefore, can result in the insertion of the cre line acting to modify the phenotype that would potentially be observed. In these cases researchers need to be careful in interpreting results that may be the result of a genetic interaction between the two mutated loci rather that an effect of the deletion of the gene of interest in a specific tissue.

An alternative to the methodology for the generation of tissue-specific *Cre* lines, is to insert the *Cre* cDNA into the 3' untranslated region of the gene. This requires the use of an IRES cassette upstream of the cDNA, both of which are inserted into the gene, between the stop codon and the poly-adenylation signal. This allows Cre recombinase activity to be modulated by the promoter of the gene of interest, but does not interfere with the gene product. This technique was used in the creation of the *AP-2α-IREScre* and *Hoxa3-IREScre* lines (Macatee *et al.*, 2003).

4.3.5. PAA malformations in ubiquitous deletions of the *Tcfap2a* conditional allele

Although the conditionally null embryos described here failed to fully recapitulate the phenotype of the *Tcfap2a*$^{-/-}$ mutant embryos, the majority of mutant embryos do exhibit some form of PAA malformation. A total of 38 of the 43 mutant embryos (88.37%) examined in this chapter have some form of PAA malformation. This suggests that the PAAs may be more sensitive to deletions of *Tcfap2a* than other elements of the phenotype. It has previously been suggested that the PAA malformations of *Tbx1* mutants may be more susceptible to reduced levels of this gene than other cardiovascular malformations and heterozygotes show a range of PAA malformations (Baldini, 2006). PAA malformations in embryos in which the conditional

allele of *Tcfap2a* had been recombined using *Sox2cre* were much lower than those using *PGKcre*. Another possibility is that, as the phenotype of both *PGKcre* mutants is able to recapitulate the levels of PAA malformations in the *Tcfap2a*$^{-/-}$ mutant embryos, this may represent differences in the expression patterns of *PGKcre* and *Sox2cre*.

RAA has been observed twice in the mutant embryos examined within this chapter. This defect was also observed in one of the *Tcfap2a*$^{-/-}$ mutant embryos and was accompanied by an I-LSA. It is likely that each of these malformations are also associated with defects of the fourth PAAs. The loss of the left fourth PAA would cause the right fourth PAA to take its place, therefore resulting in a RAA. In this case, the right sixth PAA would persist to form the ductus arteriosus, the embryonic vessel connecting the pulmonary trunk directly to the aortic arch, and the left sixth PAA would be expected to regress, as is normal for the right sixth PAA in the left aortic arch. However, persistence of the left sixth PAA, accompanied by the loss of the fourth PAA on this side, could result in the left sixth PAA forming a connection between the pulmonary trunk and the seventh intersegmental vessel, therefore resulting in the I-LSA phenotype we observe here. Interestingly, the RAA observed in the *Tcfap2a*$^{f/f;}$*Sox2cre* mutant embryo also appeared to be in a more cervical position than would be normally expected. It is likely that this is due to the loss of both fourth PAAs, with persistence of the right carotid duct, as is normally observed in mutant embryos with a cervical left aortic arch. This phenomenon has been previously described in mouse embryos with mutations of the endothelin signalling pathway (Yanagisawa *et al.*, 1998a), therefore suggesting a possible common mechanism between these mutants and the defects observed in *Tcfap2a*$^{-/-}$ mutant embryos.

4.3.6. Temporal expression of *Wnt1cre*

The work presented within this chapter demonstrates that the conditional allele of *Tcfap2a* is incapable of recapitulating the phenotype observed in the *Tcfap2a*$^{-/-}$ mutant embryos. However, the number of PAA defects remains very similar between the two, as discussed above. Conditional deletion of *Tcfap2a* from the NCCs using *Wnt1cre* results in approximately 10% of mutant embryos with CCVM. Additionally, the defects observed affect the formation of the PAAs (A-RSA and vascular ring observed in these mutants). Therefore, it is tempting to propose that any conditional deletion is capable of recapitulating the majority of PAA malformations, providing that tissue is of

importance in the development of that structure. In this scenario, we would propose that the levels of PAA malformations observed in conditional deletion from the NCCs were representative of the effect of the deletion of *Tcfap2a* from this tissue. However, expression analysis presented in this chapter demonstrates that the *Tcfap2a* locus is activated prior to the *Wnt1cre* transgene. Therefore, it is possible that some wild type transcripts and therefore, wild type AP-2α protein, are produced within the NCCs before the *Wnt1cre* transgene is translated into cre recombinase and able to recombine the *Tcfap2a*^{flox} allele.

The preliminary data presented in the introduction chapter demonstrated that, on an alternative background, conditional deletion of *Tcfap2a* using *Wnt1cre* resulted in 45% CCVM, affecting the ventricular septum, OFT and PAAs. Therefore, it appears that altering the genetic background in these embryos may affect the time at which one or both of these loci are activated. A similar phenomenon, in which the expression pattern of *Foxg1cre* is affected upon altering the genetic background of the strain, has been described previously (Hebert and McConnell, 2000).

Interestingly, the work presented here may suggest that early expression of wild type *Tcfap2a* is important within the NCCs for correct formation and development of the PAAs. By e8.5, the *Wnt1cre* transcript has been translated and is capable of inducing recombination within the conditional allele. Therefore, it is likely that wild type AP-2α is required at e8.0 within the NCCS for PAA morphogenesis. It has previously been proposed that *Tbx1* expression as early as e7.5 is required for correct development of the PAAs. Removal of this gene from e8.5 onwards fails to recapitulate the PAA malformations observed in *Tbx1*$^{+/-}$ mice (Xu *et al.*, 2005). It is therefore, possible that *Tcfap2a* is required at a similar time for this process. However, the PAs have not yet begun to form at this stage and *Tcfap2a* expression is observed only within the NCCs at this time (Figure 3.3) (Brewer *et al.*, 2002). Therefore, it is likely that at this stage AP-2α is involved in the survival of the NCCs or delamination of these cells from the neural tube, which then results in a reduction of the number of NCCs migrating into the PAs and OFT later in development.

4.4. Conclusions

The work presented in this chapter demonstrates the issues relating to genetic dissection using mouse models. We have identified that the *Tcfap2a*^{flox} allele is unable to recapitulate the CCVM found in *Tcfap2a*$^{-/-}$ mutant embryos, through the use of two different cre lines and a germ line deletion. This work suggests an intrinsic difference between the *Tcfap2a*-null and *Tcfap2a*^{flox} alleles, potentially through a mechanism of transcriptional self-interference.

In addition, we have demonstrated the issue relating to transgenic mouse lines, both in their location and the alteration of expression patterns when the genetic background is altered. We also conclude that the low penetrance of defects observed in the previous chapter are the result of both the reduced ability of the *Tcfap2a*^{flox} line to recapitulate the phenotype of the *Tcfap2a*$^{-/-}$ embryo and the delayed expression of the *Wnt1cre* transgene.

4.5. Future work

Future work will focus on investigating the functional consequences of the *Tcfap2a*-null allele, to determine if this could indeed function to down regulate other AP-2 isoforms. Initial investigations would be to identify if a protein product is produced from this allele by western blotting. Subsequent work would then investigate the ability of this protein to form both homo- and heterodimers, bind DNA and activate transcription.

Chapter 5. Investigating the role of *Tcfap2a* in the development of the pharyngeal arch arteries

5.1. Introduction

5.1.1. *Tcfap2a* in cardiovascular development

In 1996, two studies were published investigating the role of *Tcfap2a* during mouse embryonic development (Schorle *et al.*, 1996; Zhang *et al.*, 1996). These studies demonstrated a severely abnormal external phenotype in mutant embryos, with defects of the sensory organs, cranial ganglia, craniofacial development, neural tube and ventral body wall.

In 2002, a further study was conducted, using a mutant allele which incorporated a LacZ cassette into the final exon of *Tcfap2a*, for the purpose of tracing *Tcfap2a* expression patterns. Work on this model and the previous mouse created by Zhang *et al*. (1996) identified an important role of *Tcfap2a* in cardiovascular development (Brewer *et al.*, 2002). It was found that *Tcfap2a*$^{-/-}$ mice show a fully penetrant cardiovascular phenotype, affecting the interventricular septum and OFT, with only 33% penetrance of PAA defects. In the majority of mutant embryos (13/15) the OFT defect observed was DORV, with a small number of these showing additional signs of a TOF phenotype, such as pulmonary atresia or stenosis. The remaining mutant embryos (2/13) had PTA, leading to the suggestion that *Tcfap2a* is required within the NCCs for correct cardiovascular development (Brewer *et al.*, 2002).

However, in addition to VSD and OFT defects observed by these authors, our group has demonstrated a fully penetrant PAA malformation phenotype in *Tcfap2a*$^{-/-}$ mutants, when further inbred onto a C57BL/6J background (see section 1.5.1), including IAA, A-RSA, CORSA and cAoA. Therefore, this congenic background may be used to investigate the role of *Tcfap2a* in PAA formation and remodelling.

5.1.2. Molecular processes of PAA development

The PAAs begin as five pairs of bilaterally symmetrical arteries, which remodel to form the mature mammalian aortic arch and associated vessels (see section 1.2.3). The processes through which these vessels form are still a point of controversy; however, studies in both mouse and zebrafish suggest that the most likely mechanism of

formation is vasculogenesis (Li *et al.*, 2012; Anderson *et al.*, 2008). Vasculogenesis is the process by which new vessels form from the aggregation of nascent endothelial cells (angioblasts) within the PAs, which then join to form a string of endothelium. Once this endothelium joins the ventral aorta to the dorsal aorta it begins to lumenise to form a PAA.

5.1.2.1. Vessel formation

The formation of blood vessels can be investigated using a number of different markers. The earliest known marker of the endothelial lineage is the VEGF receptor-2 (VEGFR2), which becomes expressed within the developing extraembryonic vasculature by e7.0 of mouse embryonic development (Yamaguchi *et al.*, 1993). A further marker of vessel endothelium is the platelet/endothelial cell adhesion molecule 1 (PECAM-1 or CD31), which is expressed by differentiated endothelium. Once the vessel has lumenised it becomes invested with NCCs, which differentiate into SMCs to support the vessels during remodelling.

5.1.2.2. Remodelling

PAA remodelling is an important process in the development of the mature aortic arch structure seen in neonatal mice. By e11.5, the formation of the bilaterally symmetrical PAA system, which will contribute to the mature aortic arch, is complete and the vessels begin to remodel. This remodelling process results in the regression of a number of vessels which are not required in the final aortic arch structure, such as the right sixth PAA, the α-segment of the right dorsal aorta and the γ-segments of the dorsal aortae (carotid ducts) on both left and right sides (Hiruma *et al.*, 2002) (see Figure 1.6). An important process in this regression is apoptosis. Apoptosis has been identified in the mesenchyme of the right dorsal aorta and right sixth PAA in mouse embryos, and surrounding the carotid ducts during development of the PAA system in rats (Molin *et al.*, 2002; Molin *et al.*, 2004). Reduced apoptosis in these sites, in *Tgfb2*$^{-/-}$ mutant embryos, results in a number of PAA remodelling defects. In addition, these authors also suggest a mechanism in which the regression of a specific vessel is the result of apoptosis in the absence of proliferation, which acts as a 'counter balance'. Therefore, both of these cellular processes are important in the development of correct PAA structure. The authors also demonstrate an increase in the levels of

apoptosis within the fourth PAAs, which are found to aberrantly regress in these mutants (Molin *et al.*, 2002).

5.1.3. Aims of chapter

The aim of this chapter is to investigate the role of *Tcfap2a* in the development of the PAAs. MRI data from our group demonstrates a fully penetrant cardiovascular phenotype in *Tcfap2a*$^{-/-}$ mutant embryos, affecting the development of the interventricular septum, the OFT and the PAAs.

Previous work has demonstrated the fully penetrant VSD and OFT defect phenotypes associated with *Tcfap2a* mutants (Brewer *et al.*, 2002). However, PAA malformations in these mutants were observed at very low levels (4/15, 26%). The MRI data collected by our group (see section 1.5.1) demonstrates a variety of defects affecting the development of the fourth PAAs in all embryos examined. It is likely that the change in genetic background from Black Swiss, used by Brewer *et al.* (2002), to C57BL/6J used by our group has resulted in the increased penetrance of these defects in our dataset. We, therefore, plan to exploit the fully penetrant PAA defects in our mutants in order to identify the role *Tcfap2a* plays in the development of these vessels.

The PAA malformations observed in *Tcfap2a*$^{-/-}$ mutant embryos may be classified as primary – occurring during the formation of the initial symmetrical PAA system – or secondary – occurring during the remodelling stages of the vessel. In order to classify these defects we will examine the development of the PAAs at e10.5, when the bilaterally symmetrical structure is fully formed. We will then further examine these defects by examining the molecular processes which contribute to the formation of the PAAs: endothelium development, SMC differentiation, apoptosis and proliferation. In addition, due to the issues we faced with the conditional deletion of *Tcfap2a* within the NCCs, we will also focus much of this work on understanding the effect that loss of *Tcfap2a* has on the NCCs in PAA development.

5.2. Results

5.2.1. Histological analysis of CCVM in *Tcfap2a*$^{-/-}$ mutant embryos *(93.45-95%* C57BL/6J)

The MRI data demonstrated high numbers of CCVM in the *Tcfap2a*$^{-/-}$ mutants (see section 1.5.1). However, due to the low resolution of the MRI images it was necessary to confirm the observed defects by histology. Embryos were embedded in paraffin wax and sectioned, then stained with haematoxylin and eosin.

Analysis of the sections confirmed the defects observed in the MRI data and 3D reconstructions. All mutant embryos have a VSD (Figure 5.1g, m) and OFT defect as discussed above. The most common OFT defect was DORV which was observed in 50% (5/10) of mutant embryos (Figure 5.1h). A further 30% (3/10) of mutant embryos had an OA (Figure 5.1n), which is one of the components of TOF. However, no other components of this defect were observed. The remaining 20% (2/10) of embryos had a TGA (Figure 5.1i), which has not been previously described in *Tcfap2a*$^{-/-}$ mutant embryos. In addition, in one mutant with DORV, the septation of the OFT was incomplete and therefore, could be considered as PTA.

There were also a number of defects relating to the derivatives of the fourth PAAs. Defects of the left fourth PAA were identified in 50% (5/10) of mutant embryos. Of these, 20% (2/10) have a cAoA (Figure 5.1j), while 30% (3/10) have an IAA (Figure 5.1p). In addition, defects of the fourth right PAA were also observed in 90% (9/10) of mutant embryos. A-RSA was observed in 40% (4/10) of mutant embryos (Figure 5.1k, l) and CORSA was identified in 50% (5/10) of mutants (Figure 5.1q). In addition, one of the embryos with A-RSA also had a RAA, which was accompanied by an I-LSA (Figure 5.1r). Overall, all examined embryos have a VSD, an OFT defect and a defect of one or both fourth PAAs (Table 5-1).

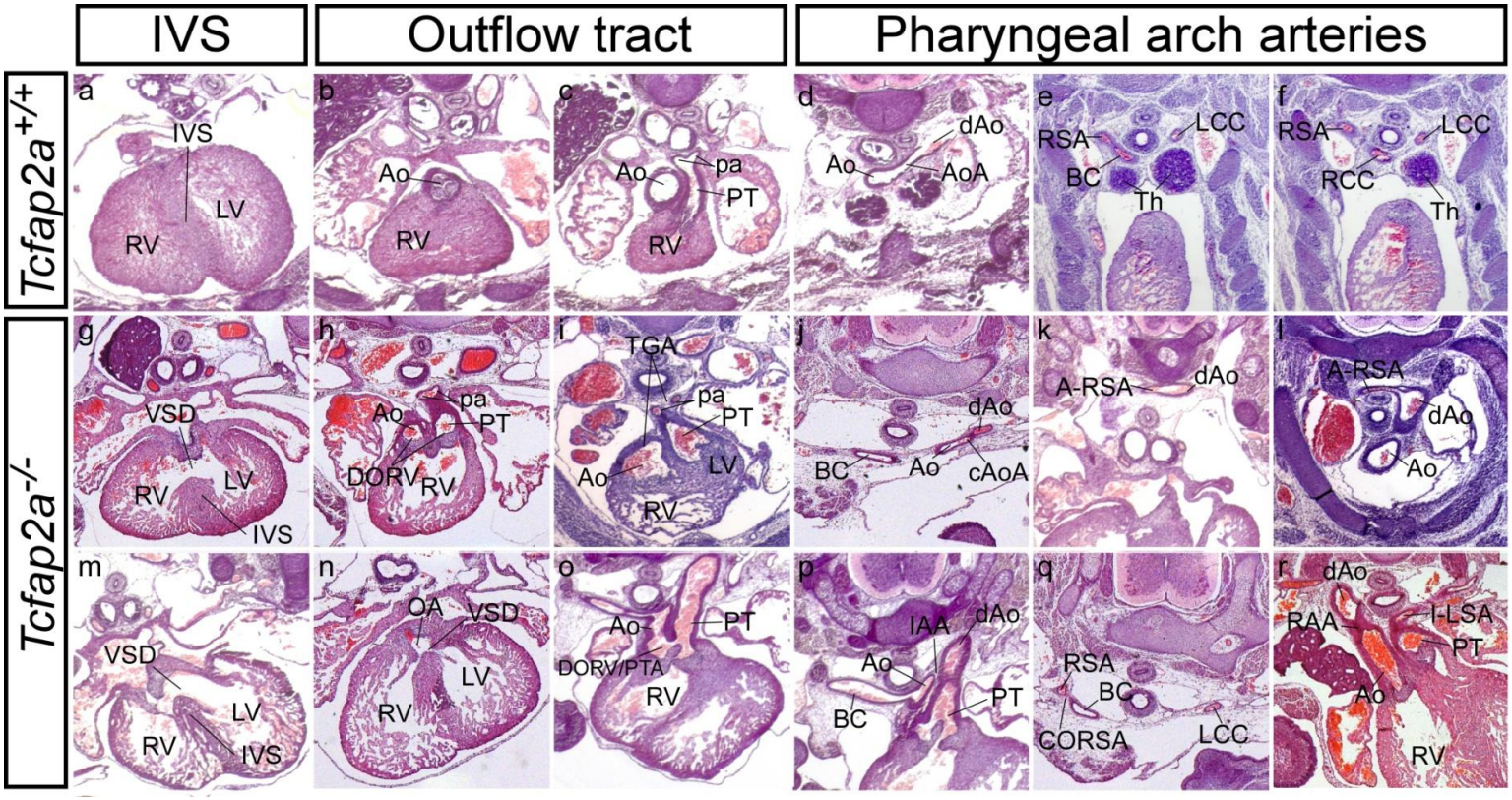

Figure 5.1: Histological sections confirm the *Tcfap2a*$^{-/-}$ phenotypes observed by MRI.
(a-f) Sections of a control (*Tcfap2a*$^{+/+}$) embryo, showing normal cardiovascular development. (a) Normal formation of an interventricular septum (IVS) between the left and right ventricles (LV, RV). (b, c) Normal OFT development, with the aorta (Ao) arising from the left ventricle (b) and the pulmonary trunk arising from the right ventricle. (d-f) Normal PAA development. (d) The ascending aorta joins the dorsal aorta (dAo) to form the aortic arch (AoA). (e) The aortic arch then gives rise to the left common carotid artery (LCC) and the brachiocephalic trunk (BC). (f) The brachiocephalic trunk bifurcates into the right common carotid artery (RCC) and the right subclavian artery (RSA). (g-r) Mutant (*Tcfap2a*$^{-/-}$) embryos have a number of cardiovascular malformations. (g, m) VSDs were observed in all mutant embryos. (h-i, n-o) All mutant embryos have an OFT malformation: (h) DORV, (i) TGA, (n) OA, (o) DORV with incomplete septum formation (partial PTA). (j-l, p-r) PAA malformations were observed in all mutant embryos: (j) cAoA, (k-l) A-RSA, (p) IAA, (q) CORSA, (r) RAA with I-LSA. RV, right ventricle; LV, left ventricle; IVS, interventricular septum; Ao, aorta; PT, pulmonary trunk; pa, pulmonary arteries; dAo, dorsal aorta; AoA, aortic arch; RSA, right subclavian artery; BC, brachiocephalic trunk; Th, thymus; LCC, left common carotid artery; RCC, right common carotid artery. (n=10).

Table 5-1: Prevalence of CCVM in *Tcfap2a*$^{-/-}$ mutant embryos examined by MRI and histology.

CCVM	Prevalence (n=10)	Summary
VSD	100%	VSD -100%
OA	30%	OFT defects – 100% (10/10)
TGA	30%	
DORV	50%	
IAA	30%	Left 4th PAA defects 50% (5/10)
cAoA	20%	
A-RSA	40%	Right 4th PAA defects 90% (9/10)
CORSA	50%	
RAA	10%	RAA with I-LSA -10%
I-LSA	10%	

5.2.2. Early PAA development

As demonstrated above, *Tcfap2a*$^{-/-}$ mutants on a congenic C57BL/6J background have an increased penetrance of fourth PAA defects to that described previously (Brewer *et al.*, 2002). In order to investigate the defects of the PAAs observed at e15.5 in *Tcfap2a*$^{-/-}$ embryos, we sought to understand the time at which these defects were arising. PAA development occurs in two stages: formation, the development of the bilaterally symmetrical pairs of vessels; and remodelling, the process which moulds these bilaterally symmetrical vessels into the mature aortic arch configuration that we observe at e15.5. If the defects observed are primary then a patent vessel will never form within the arch. If the defects are secondary to this, then the bilaterally symmetrical vessels will develop normally by e10.5, but will fail to remodel correctly during later stages.

We therefore, chose to investigate the development of the bilaterally paired vessels at e10.5, using India ink injections. India ink was injected into the left ventricle of control (*Tcfap2a*$^{+/-}$) and mutant (*Tcfap2a*$^{-/-}$) embryos (97% C57BL/6J) to reveal patent vessels. As the heart continues to pump, it forces the ink out of the heart via the developing OFT and into the PAAs. The control embryos display normal PAA development from the 34 somite stage onwards. The first and second PAAs have regressed, and the third and fourth PAAs are fully formed and are approximately equal sizes, with the sixth PAA beginning to form at this stage (Figure 5.2a-b). By the 37 somite stage the sixth PAAs

are fully formed (Figure 5.2c-d) and can be observed in all subsequent stages (Figure 5.2e-h).

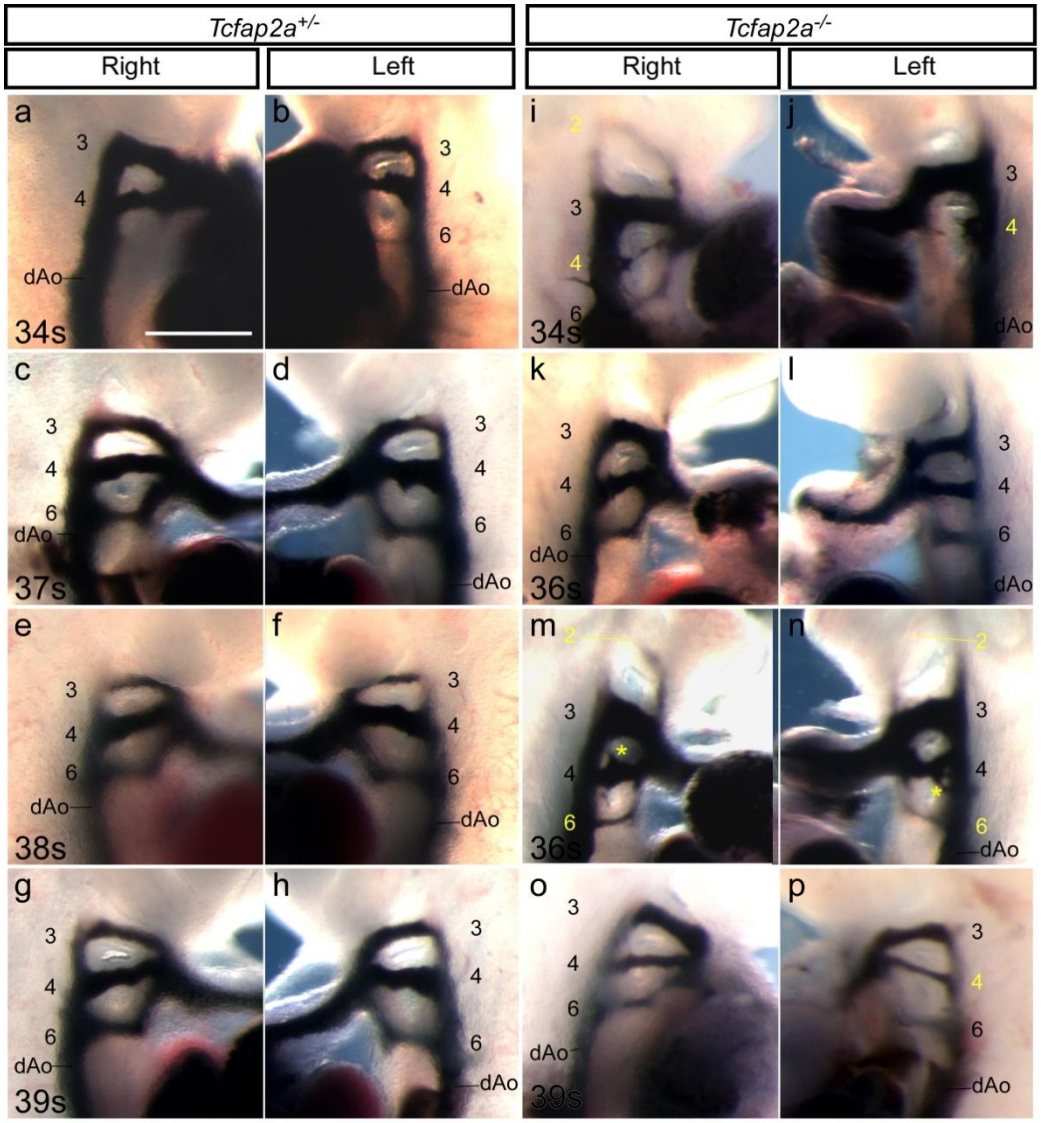

Figure 5.2: PAA formation is impaired at e10.5 in *Tcfap2a*$^{-/-}$ mutant embryos.
India ink injection of e10.5 control (*Tcfap2a*$^{+/-}$) (a-h) and mutant (*Tcfap2a*$^{-/-}$) embryos (i-p) to investigate PAA formation. (a, b) At the 34s stage the third and fourth PAA are fully formed in controls, but the formation of the sixth PAAs is delayed. By the 37s stage (c, d) and in all subsequent stages (e-h), the third, fourth and sixth PAA are fully formed and of equal sizes. In mutant embryos we observed a number of defects that were not observed in stage-matched controls including: (i) persistent second PAA, hypoplastic fourth PAA; (j) aplastic fourth PAA; (m, n) hypoplastic sixth PAA and abnormal branching around the fourth PAA (*), with persistent second PAA; (p) hypoplastic fourth PAA. In addition, some embryos had bilaterally (k, l) or unilaterally (o) normal PAA development. All images were taken at the same magnification. Scale bar = 500 µm. (n=10).

In mutant embryos, however, PAA formation is disrupted (Table 5-2). We observed a number of embryos with aberrant persistence of the second PAAs on both the left (2/10, Figure 5.2n) and right sides (3/10, Figure 5.2i, m), including one embryo at 39s, suggesting this is not merely the product of developmental delay. We also observed a high proportion of embryos with disruptions to the fourth PAAs, including both hypoplasia and aplasia (absence) of these vessels. These defects occur more

commonly, and are more severe, on the left side, with 20% (2/10) of embryos having a hypoplastic left fourth PAA (Figure 5.2p) and 30% (3/10) of embryos with an aplastic vessel (Figure 5.2j). Hypoplasia of the right fourth PAA was observed in 40% (4/10) of embryos (Figure 5.2i), with the remaining 60% developing normally. Defects of the sixth PAAs were also observed in the *Tcfap2a*$^{-/-}$ embryos. Hypoplasia of this vessel was observed in 40% (4/10, Figure 5.2i, m-n) of mutant embryos on both the left and right sides, with 30% embryos having bilaterally hypoplastic sixth PAAs. A further 10% (1/10) of embryos showed aplasia of the sixth left PAA (Figure 5.2j). In addition, a small number of mutant embryos showed branching of small vessels around the fourth PAAs. These additional vessels occurred on both the left (3/10, 30%) and right (2/10, 20%) sides. One mutant embryo was also found to have completely normal PAA development (Figure 5.2k, l).

Table 5-2: Summary of the PAA malformation in *Tcfap2a*$^{-/-}$ mutants at e10.5.

	Second PAAs		Third PAAs		Fourth PAAs		Sixth PAAs	
	Right	**Left**	**Right**	**Left**	**Right**	**Left**	**Right**	**Left**
Normal	7/10	8/10	10/10	10/10	6/10	5/10	6/10	5/10
Hypoplasia	-	-	-	-	4/10	2/10	4/10	4/10
Aplasia	-	-	-	-	-	3/10	-	1/10
Persistent	3/10	2/10	-	-	-	-	-	-
Total defects	30%	20%	0	0	40%	50%	40%	50%

5.2.3. Pharyngeal arch artery formation in *Tcfap2a*$^{-/-}$ *embryos* (97% C57BL/6J)

The data presented above demonstrates that the loss of *Tcfap2a* results in defective formation of the PAA, which contributes to the PAA malformations observed at e15.5. We, therefore, wanted to analyse the processes involved in PAA formation to understand why they were unable to form. The formation of the PAAs involves two main processes. The first is the formation of an endothelial tube, which then luminises to form the vessel. The second process involves the differentiation of the NCCs, within the PA mesenchyme, into SMCs which form the tunica media layer of the vessel to support it as it matures and remodels into the final aortic arch configuration.

5.2.3.1. Formation of the PAA endothelium in Tcfap2a$^{-/-}$ *embryos*

To visualise the formation of the endothelial layer of the PAAs, immunohistochemistry was used to stain coronal sections through *Tcfap2a*$^{+/-}$ control and *Tcfap2a*$^{-/-}$ mutant

embryos with an anti-PECAM-1 antibody. Embryos were collected at 3 stages (e9.5, e10.5 and e11.5) throughout the formation process to assess the ability of the mutant embryos to form the initial endothelial tube.

In control embryos at e9.5, the third PAA appears well formed and is fully invested with endothelium (Figure 5.3). The fourth PA is newly formed and the PAA within is apparent as aggregations of PECAM-1 positive endothelial cells (Figure 5.3c, c') or as small vessels budding-off from the dorsal aorta (Figure 5.3d'-f', arrows). Investigation of the mutant fourth PAAs indicates a similar pattern of PECAM-1 staining. In some embryos the fourth PAA has not yet formed within the PA (Figure 5.3g'-j'), however, others show a vessel budding-off from the dorsal aorta (Figure 5.3k'-l'). Therefore, it appears that the formation of the fourth PAA is unaffected at this time point.

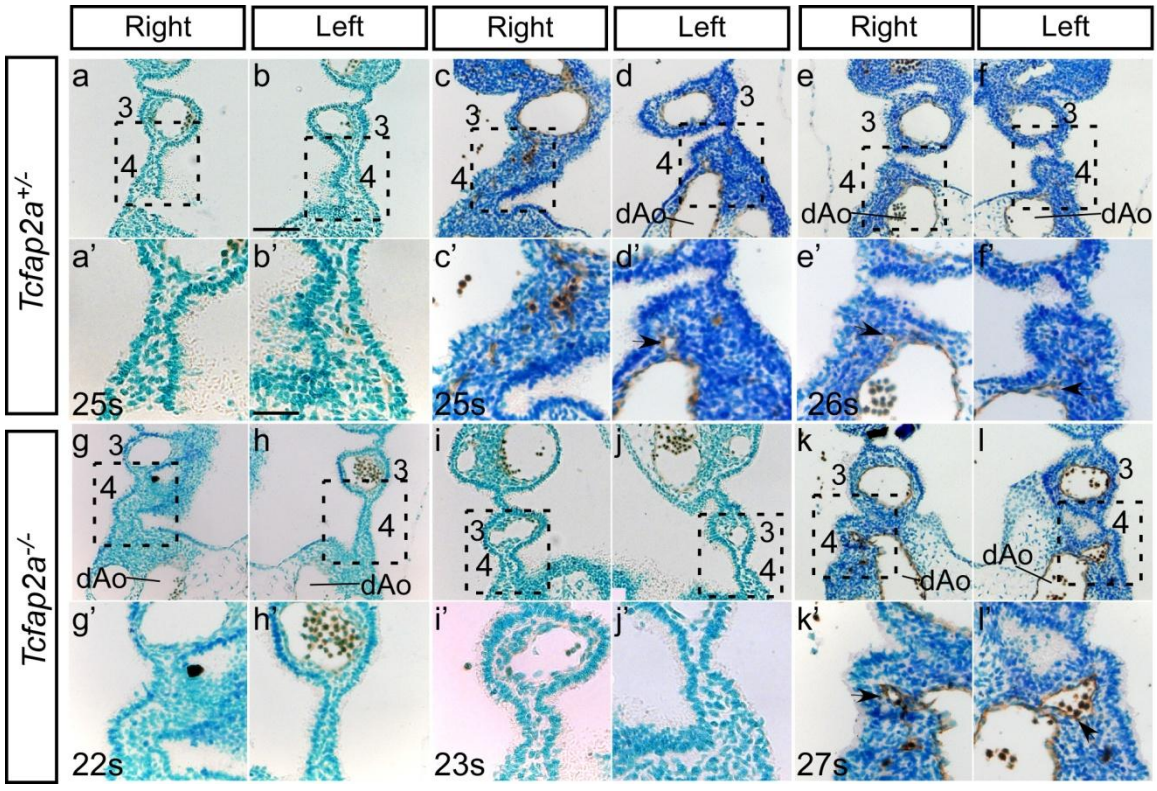

Figure 5.3: PECAM-1 staining of the pharyngeal arch arteries at e9.5.
Immunohistochemistry for PECAM-1 on coronal sections through the pharyngeal arch arteries of control (*Tcfap2a*$^{+/-}$) and mutant (*Tcfap2a*$^{-/-}$) embryos at e9.5. (a-f) The third PAAs of control embryos are well formed and invested with PECAM-1-positive endothelial cells. The fourth PAAs are beginning to emerge from the dorsal aorta in these embryos (arrows). (g-l) The mutant embryos appear similar to the controls, with the fourth PAA beginning to emerge from the dorsal aorta in the later stage embryos (arrows). Scale bar in a-l = 100 µm, scale bar in a'-l' = 50 µm. 3, third PAA; 4, fourth PAA; dAo, dorsal aorta. (n=3).

By e10.5 (29-33 somite stage), differences between the control and mutant embryos may be clearly identified (Figure 5.4). In the control embryos examined, the fourth

PAA had formed and fully lumenised, with a vessel diameter comparable to that of the third PAAs (Figure 5.4a-f). These vessels were also clearly invested with PECAM-1 positive endothelial cells (Figure 5.4a'-f'). However, in mutant embryos these vessels were delayed in their formation, with a reduced diameter and disorganised endothelial cells (Figure 5.4g-l). Although the vessel was misshapen, it is fully surrounded by PECAM-1 positive endothelial cells. In addition, the fourth PA in the mutant embryos is also reduced in size compared to that of littermate controls (Figure 5.4g'-l').

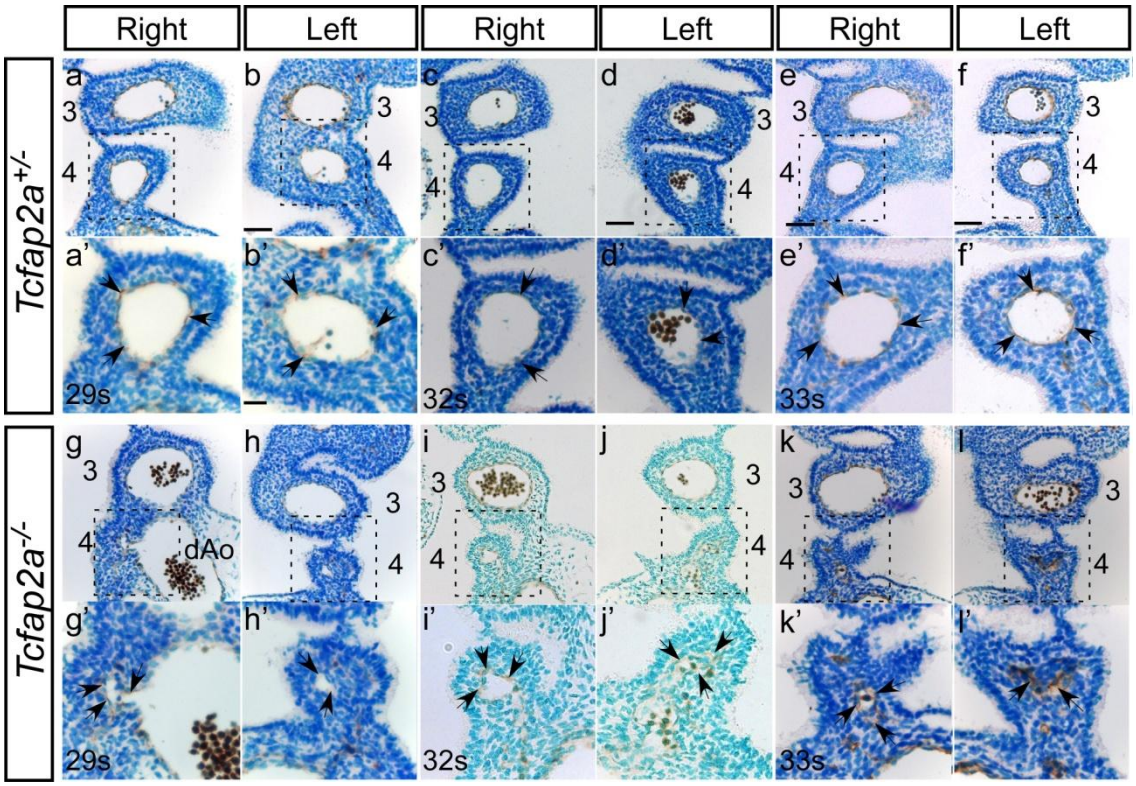

Figure 5.4: PECAM-1 staining of the pharyngeal arch arteries at e10.5.
Immunohistochemistry for PECAM-1 on coronal sections through the pharyngeal arch arteries of control (*Tcfap2a*$^{+/-}$) and mutant (*Tcfap2a*$^{-/-}$) embryos at e10.5. (a-f) The third and fourth PAAs of e10.5 control embryos appear fully invested with PECAM-1-positive endothelial cells. (a'-f') A higher magnification of the fourth PAA demonstrates that the vessel is well formed and invested with endothelium (arrows). (g-l) The third and fourth PAAs of mutant embryos. The third PAA appears well formed and is invested with endothelial cells. The fourth PAA endothelium appears disorganised. (g'-l') A higher magnification of the fourth PAA demonstrates that the vessel is disorganised, but contains endothelial cells (arrows). Scale bar in a-l = 50 µm, scale bar in a'-l' =20 µm. 3, third PAA;4, fourth PAA; dAo, dorsal aorta. (n=3).

By e11.5 the PAAs of control embryos are well formed and fully invested with PECAM-1-positive endothelium (Figure 5.5a-f). The third and fourth PAAs in mutant embryos are also invested with endothelium (Figure 5.5g-l). However, in some instances the vessel is small and misshapen (Figure 5.5k-l, k'-l').

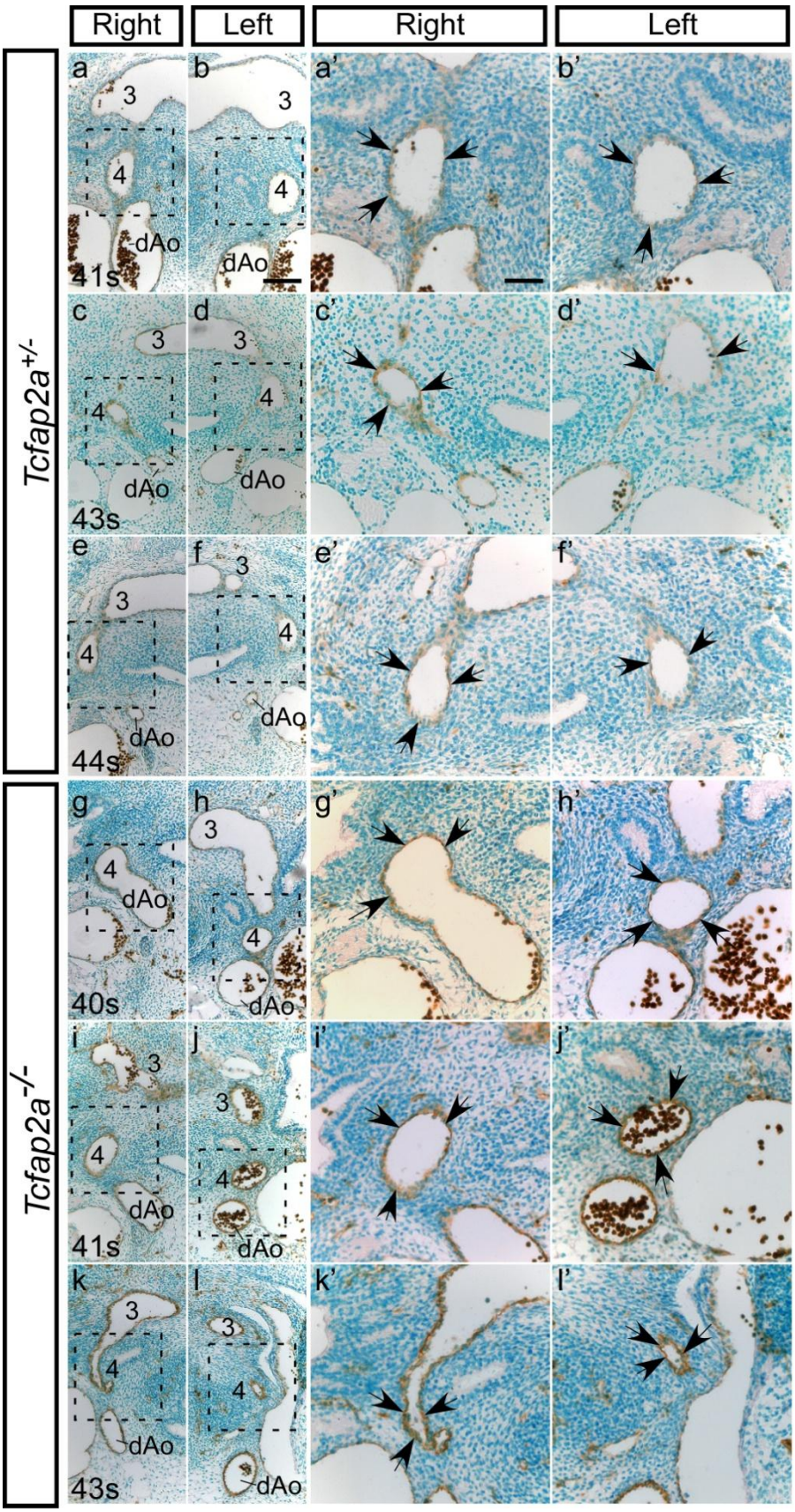

Figure 5.5: PECAM-1 staining of the pharyngeal arch arteries at e11.5.
Immunohistochemistry for PECAM-1 on coronal sections through the pharyngeal arch arteries of control (*Tcfap2a*$^{+/-}$) and mutant (*Tcfap2a*$^{-/-}$) embryos at e11.5. (a-f) The third and fourth PAAs of e11.5 control embryos appear well formed and invested with endothelium. (a'-f') Higher magnifications of the fourth PAAs in a-f. (g-l) The third and fourth PAAs of mutant embryos appear to be invested with endothelium. (g'-l'). Higher magnifications of the fourth PAAs in g-l. Scale bar in a-l = 100 µm, scale bar in a'-l' = 50 µm. Arrows, endothelial cells; 3, third PAA; 4, fourth PAA; dAo, dorsal aorta. (n=3)

5.2.3.2. Formation of PAA smooth muscle in Tcfap2a$^{-/-}$ mutant embryos

During PAA development, the NC-derived mesenchyme of the PAs surrounds the PAAs and differentiates into the smooth muscle lining of the vessel. The SMCs support the vessels as they remodel and also stabilise the vessels as the haemodynamic pressures increase. To investigate the formation of NC-derived SMCs around the PAAs of *Tcfap2a*$^{-/-}$ mutant mice, we crossed *Tcfap2a*$^{+/-}$*;R26R*$^{eyfp/eyfp}$ females to *Tcfap2a*$^{+/-}$*;Wnt1cre* males. The presence of *Wnt1cre* in the NCCs will cause the translational stop sequence situated between the R26R promoter and the EYFP gene to be excised, resulting in read-through from the promoter to EYFP only in the NCCs (see section 2.2.4). As the R26R promoter is constitutively active, the NCCs will continue to express EYFP throughout development, allowing us to trace the NCC lineage in these embryos.

Control (*Tcfap2a*$^{+/-}$) and mutant (*Tcfap2a*$^{-/-}$) embryos were collected at e10.5 and e11.5 and coronal section were stained with antibodies to α- smooth muscle actin (α-SMA) and green fluorescent protein (GFP), which marks both GFP and YFP expressing cells. This allowed the identification of SMCs derived from NCC.

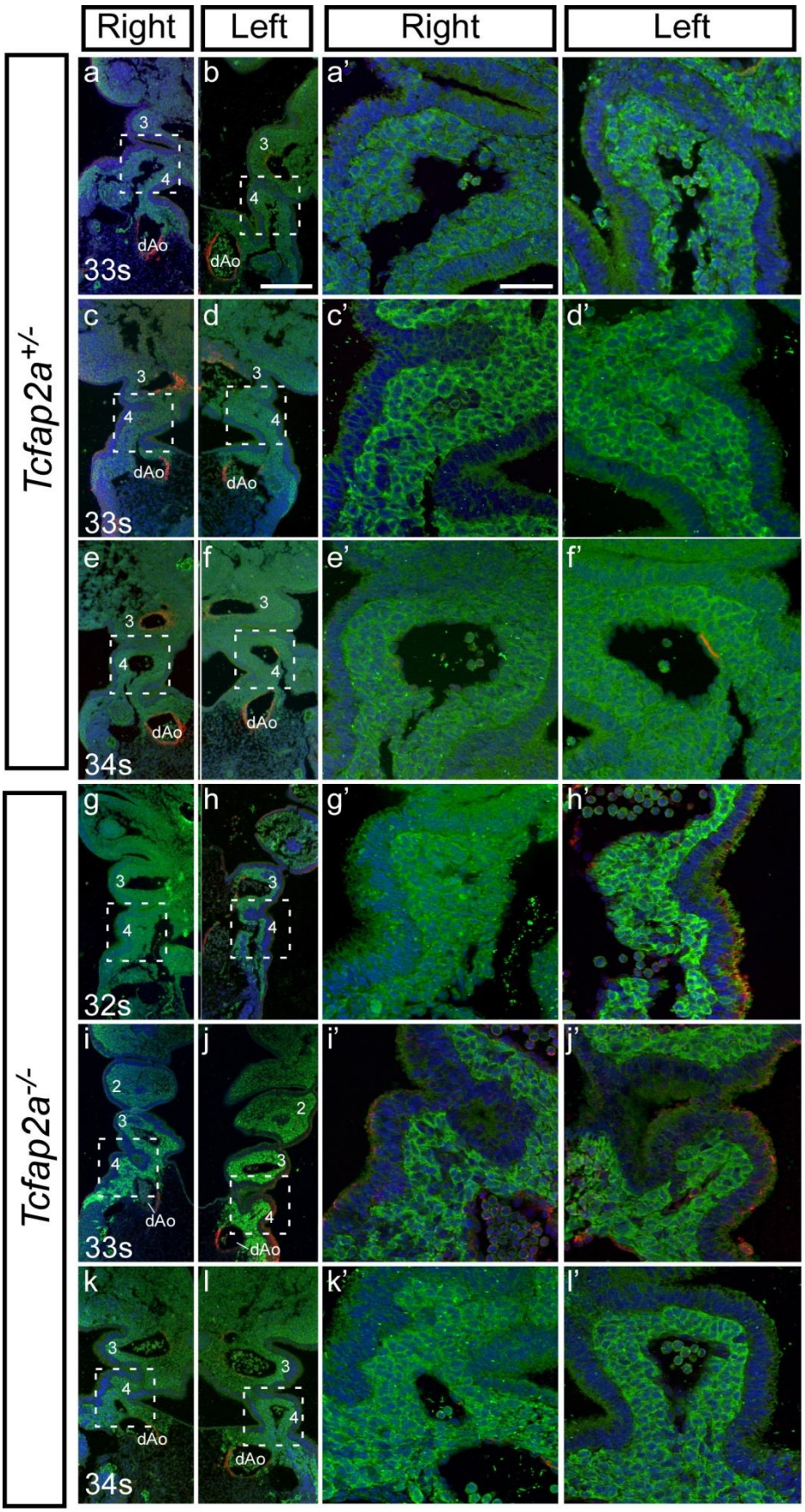

Figure 5.6: Distribution of NCC-derived smooth muscle cells in e10.5 *Tcfap2a*$^{-/-}$ mutant embryos.
NCC (green) and α-SMA (red) distribution in control (*Tcfap2a*$^{+/-}$) (a-f, a'-f') and mutant (*Tcfap2a*$^{-/-}$) (g-l, g'-l') embryos at e10.5. Control embryos have a large third and fourth PAs, invested with NCCs, but limited distribution of NCC-derived smooth muscle cells (orange) only in the third PAAs. Mutant embryos have a reduced fourth PA in comparison to the third. The fourth PA is invested with NCC, but no NCC-derived smooth muscle is observed. Scale bars = 200 µm (a-l), 50 µm (a'-l'). DAPI, blue; α-SMA, red; GFP, green. (n=3).

Even at early e10.5 stages (33 somites) the YFP-positive NCCs have fully invested the PAs in the control embryos (Figure 5.6a-f). The presence of NCC-derived SMCs is identified as orange staining, which was observed around the third PAAs only. No NCC-derived SMCs are observed around the fourth PAAs in either mutants or controls at this stage. Additionally, the smooth muscle surrounding the dorsal aorta is of non-NCC origin, as has been demonstrated previously in both mouse and chicken (Bergwerff *et al.*, 1998; Jiang *et al.*, 2000).

The mutant embryos also displayed a similar pattern of NCC migration to that seen in the controls, with the NCCs infiltrating the fourth PA (Figure 5.6g-l). As with controls, the fourth PAAs of the mutant embryos contain no NCC-derived SMCs. However, NCC-derived SMCs can be identified around the third PAAs, suggesting that *Tcfap2a*-deficient NCCs are able to differentiate into SMCs to support these vessels. In the mutant embryos, the fourth PAA appears reduced, compared to controls. This supports the defects we see at this stage in the PECAM-1-stained mutant embryos, again suggesting that the vessels are failing to form before this point. The PAs containing the reduced fourth PAAs also appear smaller than that of the control embryos in both cases.

By e11.5, we begin to see NCC-derived SMCs surrounding the fourth PAAs in control embryos (Figure 5.7a-f). However, in some embryos this expression is irregular and does not cover the full circumference of the vessel (Figure 5.7a'-b', e'-f'). In mutant embryos, however, the presence of NCC-derived SMCs is limited (Figure 5.7g-l) and mostly confined to the point at which the vessel arises from the dorsal aorta (Figure 5.7h', i', k'). The remainder of the vessel is completely devoid of NCC-derived smooth muscle. However, one mutant embryo had a normal left fourth PAA, with a complete layer of NCC-derived smooth muscle (Figure 5.7l').

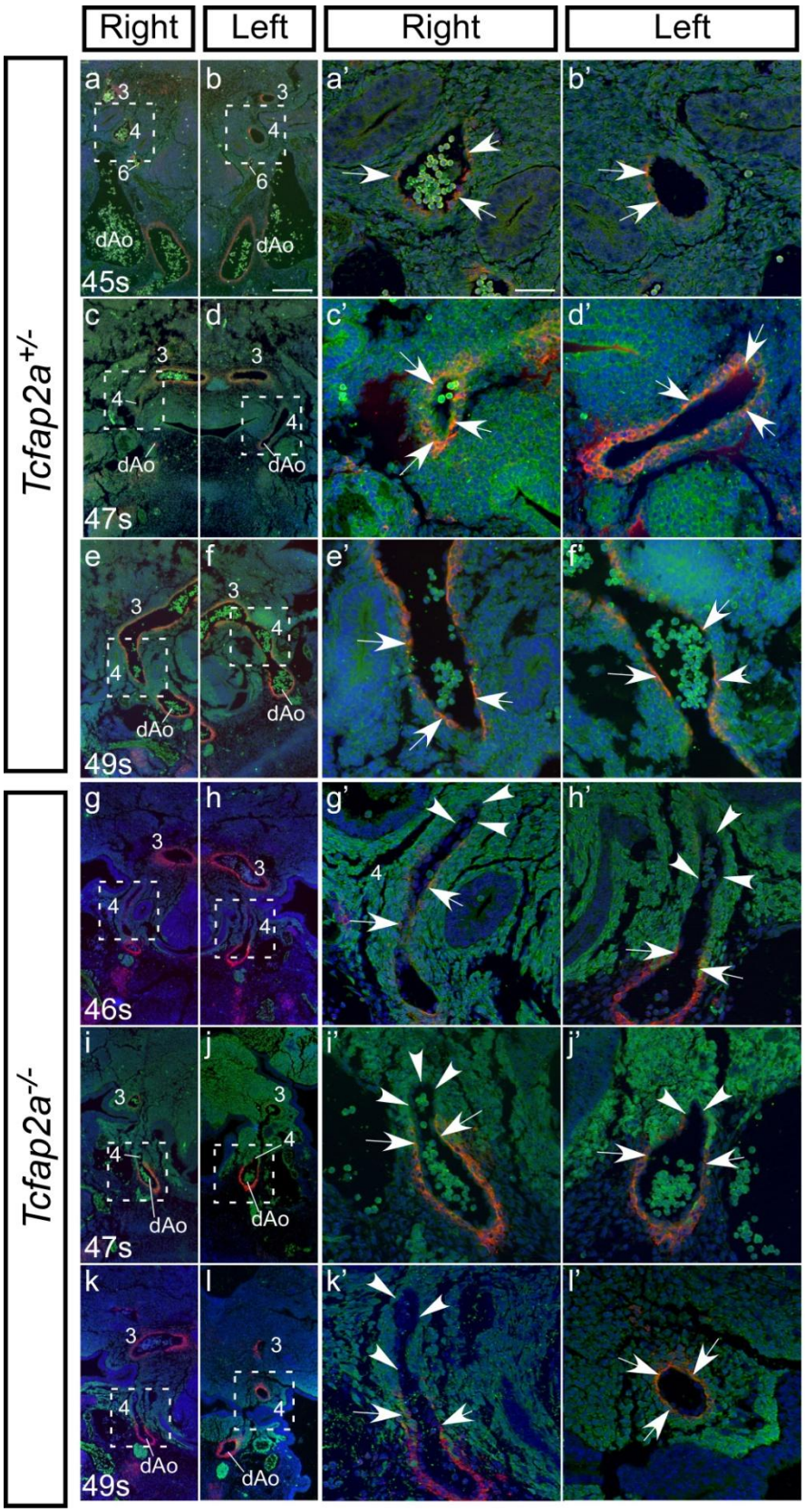

Figure 5.7: Distribution of NCC-derived smooth muscle cells in e11.5 *Tcfap2a*$^{-/-}$ mutant embryos.
NCC (green) and α-SMA (red) distribution in control (*Tcfap2a*$^{+/-}$) (a-f, a'-f') and mutant (*Tcfap2a*$^{-/-}$) (g-l, g'-l') embryos at e11.5. NCC-derived smooth muscle cells (orange, arrows) surround the third, fourth and sixth PAAs in control embryos (a-f, a'-f'). Mutant embryos appear to have comparable levels of smooth muscle cells surrounding the third PAAs, but reduced in the fourth PAAs (g-l). The fourth PAA in many mutant embryos is devoid of any smooth muscle cells (arrowheads) (g'-k'), although a single fourth PAA appeared to be fully invested with smooth muscle (l'). DAPI, blue; α-SMA, red; GFP, green. 3, third PAA; 4, fourth PAA; 6, sixth PAA; dAo, dorsal aorta. Scale bars = 200 µm (a-l), 50 µm (a'-l'). (n=3).

5.2.4. Apoptosis and proliferation *Tcfap2a*$^{-/-}$ embryos

To further understand the defects of the fourth PAAs in the *Tcfap2a*$^{-/-}$ mutants we chose to examine this region for changes in apoptosis and proliferation. Embryos were collected at e10.5 and stained using immunohistochemistry on coronal sections. An antibody to caspase3 was used to identify apoptotic cells, and phospho-histone H3 to detect proliferating cells. In particular, we were interested in investigating these processes within the NCCs. As shown above, the fourth PA at this stage is reduced in size, likely owing to a reduction in the NCC-derived mesenchyme within this structure. Therefore, in order to investigate this, the NCCs were again marked using the anti-GFP antibody, as described above.

5.2.4.1. Apoptosis

Examination of control embryos revealed a small number of apoptotic cells within the tissues of the fourth PA (ectoderm, endoderm and mesenchyme) (Figure 5.8a-f, a'-f'). Overall, the levels of apoptosis appeared to be consistent between each of these tissues. However, in the mutant embryos, there appeared to be an increase in the levels of apoptosis (Figure 5.8g-l, g'-l'). However, this was not confined to the NCCs as expected. Interestingly the highest levels of apoptosis were seen in the pharyngeal epithelia (ectoderm and endoderm).

In order to examine the changes in levels of apoptosis more thoroughly we employed cell counting techniques to quantify the amount of cell death in the tissues of the fourth PAs. When the number of apoptotic cells was compared within the entire fourth PA, we found a non-significant increase in the levels of apoptosis in mutants compared to controls (Figure 5.10a). To investigate this further, we examined the levels of apoptosis within each tissue of the fourth PAs. As *Tcfap2a* is highly expressed within the NCCs we examined the levels of apoptosis within this population and found that, although there appears to be an increase in the number of apoptotic cells in this population, this change is not significant. However, analysis of the ectoderm revealed an approximately 15% increase ($p = 0.0429$) in the number of apoptotic cells, suggesting that *Tcfap2a* in these cells is important in cell survival. As in the NCCs, the loss of *Tcfap2a* appeared to cause an increase in the numbers of apoptotic cells within the endoderm, which failed to reach statistical significance.

To further dissect the levels of apoptosis within the fourth PA of *Tcfap2a*$^{-/-}$ mutant embryos we compared levels in the left and right PAs. From the overall analysis we found that there was a statistically significant increase in the number of apoptotic cells within the fourth right PA (p = 0.0204), which was not seen in the left arch (Figure 5.10b). When further dissected into the individual tissue types, we again saw that the levels of apoptosis in the NCCs and endoderm of both arches was increased, but not statistically significant. However, the ectoderm of the fourth right PA had a very strong, statistically significant increase in the numbers of apoptotic cells (p = 0.0013).

5.2.4.2. Proliferation

In order to examine the levels of proliferation within these mutant and control embryos, coronal sections were also stained for an antibody against phospho-histone H3 (Figure 5.9). We identified that overall the levels of proliferation were variable between samples of the same groups. However, there appeared to be more proliferation in control embryos than in mutants.

To examine this further, we quantified the levels of proliferation within each tissue of the fourth arch and found that overall the levels of proliferation remained constant between control and mutant embryos. When comparing the levels of proliferation between the composite tissues, it appears that the level of proliferation within the NCCs is not altered between controls and mutants (Figure 5.10c). However, there does appear to be a generalised increase in the levels of proliferation within the ectoderm and decrease in the endoderm, neither of which were found to be statistically significant.

Comparison of the levels of proliferation between the left and right fourth PAs confirmed that there are no statistically significant changes between controls and mutants in the whole arch, the NCCs or the ectoderm. However, we identified a statistically significant (p = 0.0291) decrease in the levels of proliferation within the endoderm of the right PA (Figure 5.10d).

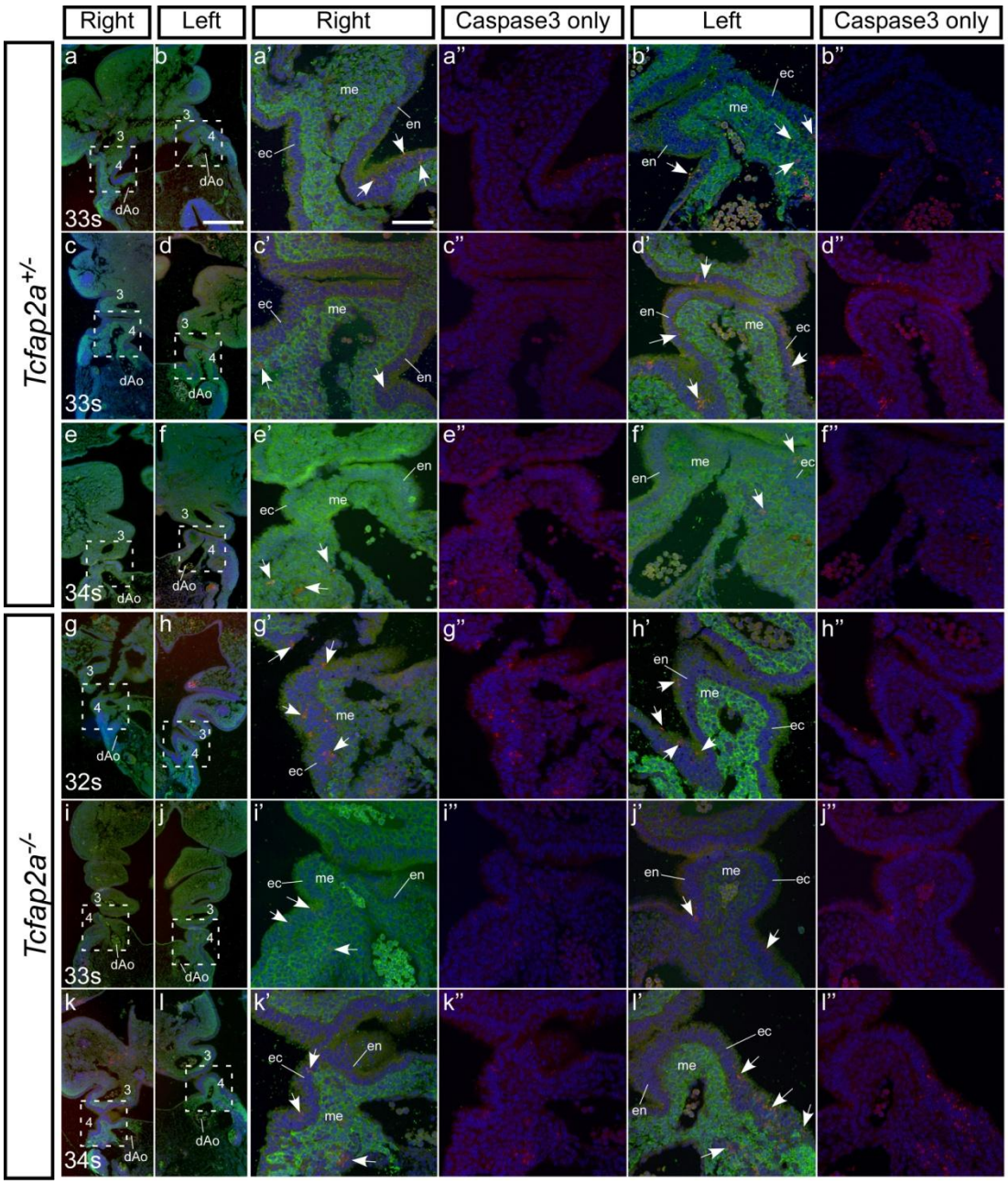

Figure 5.8: Expression of apoptosis marker in control and mutant fourth PAs at e10.5.
Coronal sections of control (*Tcfap2a*$^{+/-}$) and mutant (*Tcfap2a*$^{-/-}$) embryos stained with anti-caspase3 antibody. Control embryos (a-f) have low levels of apoptosis in all tissues examined. Examination of mutant embryos(g-l) reveals an increase in levels of apoptosis within the ectoderm of the fourth PAs. a'-l' show higher magnifications of the boxed regions in a-l. Arrows show apoptotic cells. a''-l'' show only caspase3 staining and DAPI, for clarity. ec, ectoderm; en, endoderm; me, mesenchyme. Scale bars = 200 µm (a-l), 50 µm (a'-l',a''-l''). DAPI, blue; GFP, green; caspase 3, red. (n=3).

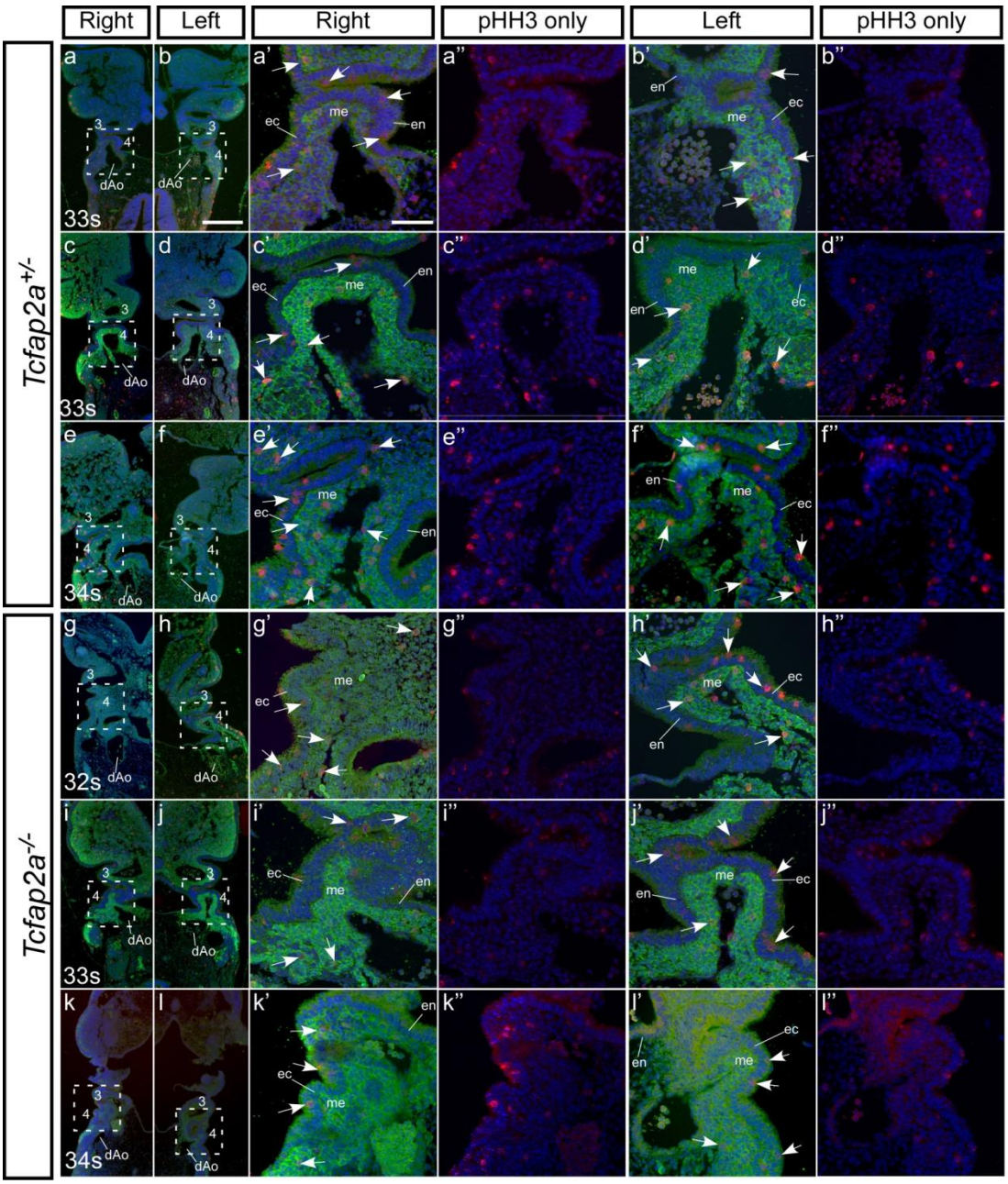

Figure 5.9: Expression of proliferation marker in control and mutant fourth PAs at e10.5.
Coronal sections of control (*Tcfap2a*$^{+/-}$) and mutant (*Tcfap2a*$^{-/-}$) embryos stained with anti-phospho-histone H3 antibody. Control embryos (a-f) have moderate levels of proliferation in all tissues examined. Examination of mutant embryos (g-l) appears to show a decrease in proliferation throughout all tissues. a'-l' show higher magnifications of the boxed regions in a-l. Arrows show proliferative cells. a''-l'' show only pHH3 staining and DAPI, for clarity. Scale bars = 200 µm (a-l), 50 µm (a'-l', a''-l''). DAPI, blue; GFP, green; pHH3, red. (n=3).

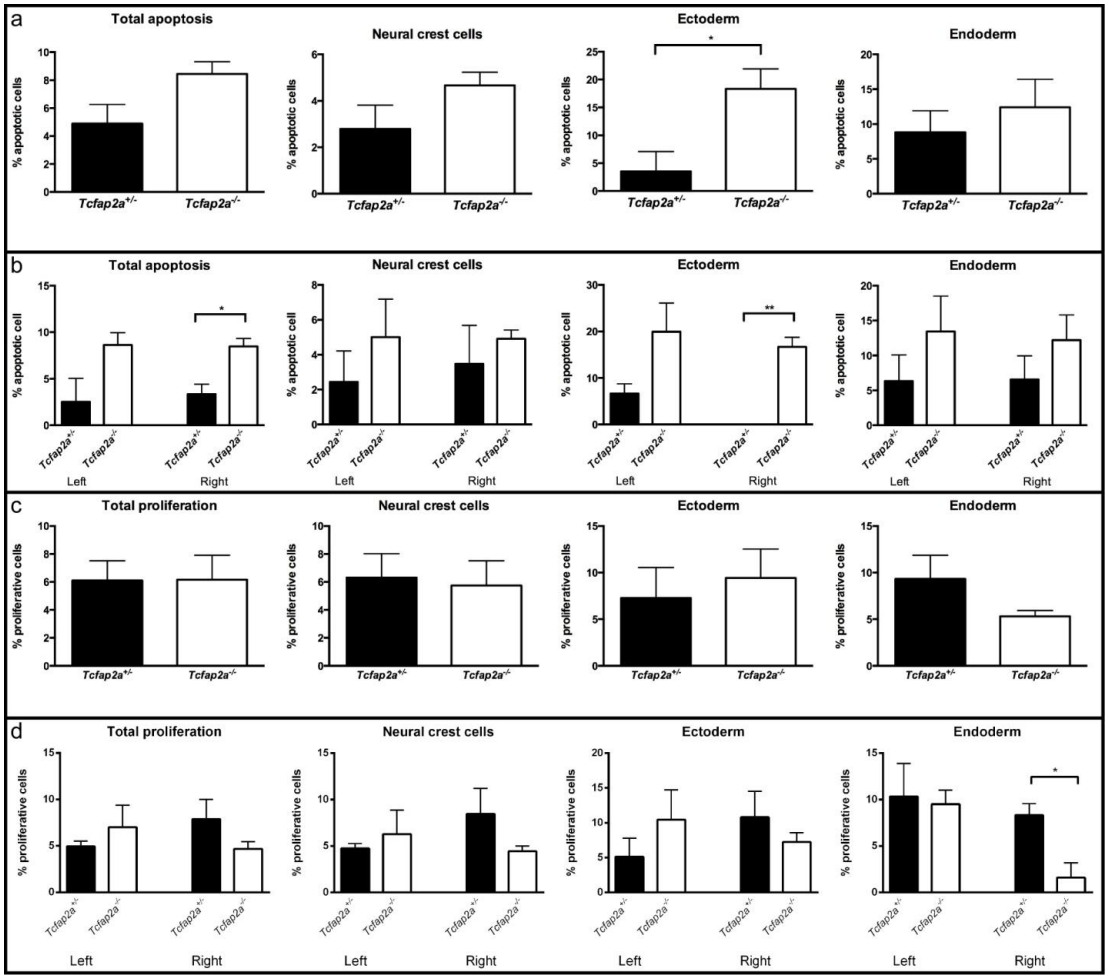

Figure 5.10: Quantification of apoptosis and proliferation within the tissue of the fourth PAs of control and mutant embryos.
Comparison of levels of apoptosis and proliferation between control (*Tcfap2a*$^{+/-}$) and mutant (*Tcfap2a*$^{-/-}$) embryos at e10.5. (a) Levels of apoptosis within both fourth PAs and the individual tissues: the NCCs, pharyngeal ectoderm and pharyngeal endoderm. (b) Levels of apoptosis within left and right PAs and each tissue individually. (c) Levels of proliferation within both fourth PAs and the individual tissues. (d) Levels of apoptosis within left and right PAs and each tissue individually. Error bars represent standard error of the mean (S.E.M). Statistical significance calculated by a student's *t*-test; *, $p < 0.05$; **, $p < 0.01$.

5.2.4.3. Neural crest cell numbers

We have identified that the fourth PAs in the mutant embryos appear smaller than that of the control embryos examined. By collating the data collected from both the apoptosis and proliferation studies we were able to determine the total numbers of NCCs within each PA at e10.5. Although there are limited numbers of NCC-derived SMCs surrounding the fourth PAA at this stage, it has been proposed that the NCCs may provide other roles in the maintenance of these vessels at this time (Waldo *et al.*, 1996).

We found a statistically significant decrease in the numbers of NCC within the fourth PAs between controls and mutants ($p = 0.0074$) (Figure 5.11a). Further, comparison of the left and right PAs show a generalised decrease in the numbers of NCCs in both arches, which reaches statistical significance only in the right PA ($p = 0.0417$) (Figure 5.11b). To confirm that the reduction of the total number of NCCs within each PA was not caused by a change in NCC density within the arch, we compared the density of total cells and NCCs within each PA. We found that neither the cell density of the entire PA region (Figure 5.11c), nor of the left or right PAs individually (Figure 5.11d), was significantly altered in mutants compared to control embryos. In addition, although on average the mutant PAs contained fewer NCCs per 100 μm^2 (Figure 5.11e), this was not significantly different. Furthermore, the NCC density was not significantly different in either of the PAs individually (Figure 5.11f).

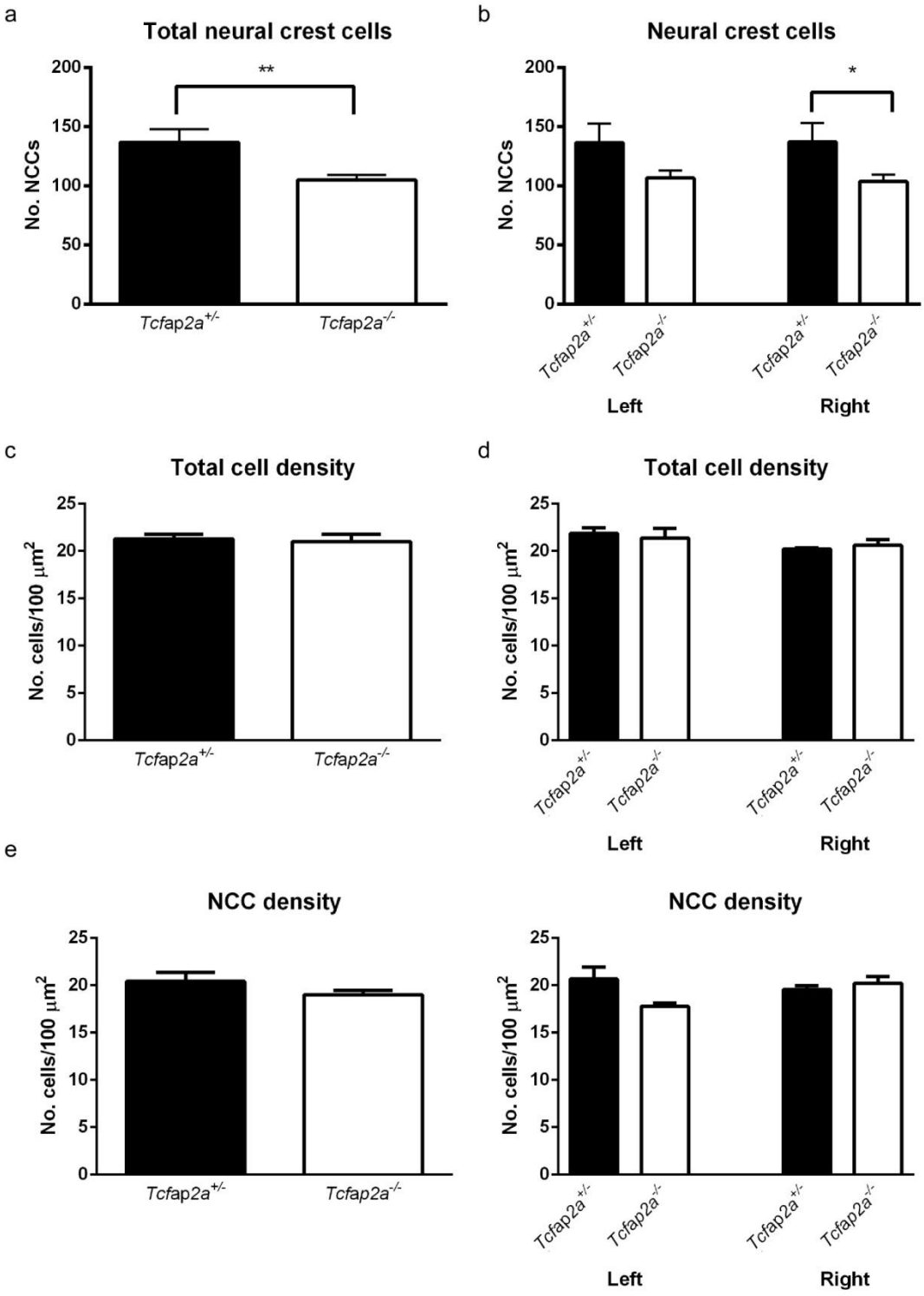

Figure 5.11: NCC number and density within the fourth PAs of control and mutant embryos.
Comparison of NCC density between control (*Tcfap2a*$^{+/-}$) and mutant (*Tcfap2a*$^{-/-}$) embryos. (a) Total number of NCCs within the fourth PA. (b) Number of NCCs within the left and right fourth PAs. (c) Total cell density within the fourth PAs. (d) Cell density within the left and right fourth PAs. (e) NCC density within the fourth PAs. (f) NCC density within the left and right PAs. Error bars represent S.E.M. Statistical significance calculated by a student's *t*-test; *, $p < 0.05$; **, $p < 0.01$.

5.3. Discussion

5.3.1. CCVM in *Tcfap2a*$^{-/-}$ *mutant embryos*

As discussed in the introduction, the cardiovascular defects of *Tcfap2a*$^{-/-}$ embryos have been explored previously, and demonstrated a fully penetrant cardiovascular phenotype consisting of VSDs and OFT malformations (Brewer *et al.*, 2002). In this chapter, and in the preliminary work presented in the introduction chapter (see section 1.5.1), we have demonstrated similar results, indicating that *Tcfap2a* is very important in the development of the OFT and interventricular septum. The OFT malformations observed in our work, however, vary from that seen in the previous study. Brewer *et al*. (2002) demonstrate a large number of mutant embryos, with DORV, and a small number of embryos with PTA. Our study, however, shows a reduction in the number of embryos with DORV and the appearance of other defects including TGA and OA.

In addition to those defects previously observed, we also identified a fully penetrant phenotype affecting the formation of the fourth PAAs, which were found at much lower levels in the previous study (Brewer *et al.*, 2002). Previous work on the cardiovascular malformations in *Tcfap2a*$^{-/-}$ embryos on a mixed/black swiss background, by Brewer *et al*. (2002), demonstrates PAA malformations in only 33% (5/15) embryos, which included A-RSA and IAA. This suggests that the prevalence of CCVM in *Tcfap2a*$^{-/-}$ mice changes with genetic background. Interestingly, we also identified a number of PAA malformations, which were not previously described in *Tcfap2a*$^{-/-}$ mutant embryos, including CORSA and cAoA. It is possible that in histological examination, these defects may have been overlooked. However, the use of MRI and 3D reconstructions allowed us to identify these subtle defects. Therefore, we have generated a model in which the PAA defects previously described in these embryos, can be examined thoroughly.

5.3.2. A dual role for AP-2α in PAA morphogenesis?

The data presented within this chapter clearly demonstrates a role for *Tcfap2a* in PAA morphogenesis. At e15.5 *Tcfap2a*$^{-/-}$ embryos show a variety of malformations affecting the fourth PAAs, which are fully penetrant. These defects most commonly affect the right fourth PAA (90% embryos), with the left fourth PAA being less commonly affected (50% embryos).

To further understand the role of *Tcfap2a* in PAA morphogenesis, mutant embryos were examined at e10.5 using India ink injection methods. At this stage, the formation of the caudal PAAs is complete but remodelling has not yet begun. At this time defects were observed in both fourth PAAs, with the left PAA being hypoplastic or aplastic in 50% mutant embryos and the right PAA in only 40% mutant embryos (Table 5-3). This suggests that the defects of the fourth left PAA in *Tcfap2a*$^{-/-}$ mutant embryos are the direct result of this vessel failing to form. In addition, the remodelling defects associated with this arch, which result in the persistence of the left carotid duct and the appearance of a cAoA, occur secondarily to the abnormal formation of this vessel.

Table 5-3: Comparison between PAA abnormalities observed at e10.5 and e15.5.

	E10.5	**E15.5**
Left fourth PAA	5/10 (50%)	5/10 (50%)
Right fourth PAA	4/10 (40%)	9/10 (90%)

The defects observed in the right fourth PAA at e10.5, however, are not consistent with a role for AP-2α solely in the formation of the vessel. Between the formation of the vessel at e10.5 and complete development of the cardiovascular system by e15.5 we see a two-fold increase in the number of right fourth PAA abnormalities (Table 5-3). Overall, this work suggests that *Tcfap2a* has a dual role in the development of the right fourth PAA: an initial role during the formation of the vessel followed by a further role in the remodelling of the vessel to form the RSA.

It is likely that the remodelling defects of the *Tcfap2a*$^{-/-}$ mutant fourth PAAs are the result of a NCC defect, that prevents the differentiation of these cells into smooth muscle, which supports the vessel throughout the remodelling process. Indeed, at e11.5, we find that the majority of fourth PAAs examined were sparsely invested with NCC-derived smooth muscle. It is therefore expected that these vessels would collapse shortly after this stage due to the increased haemodynamic pressure.

The role of the NCCs within the PAs prior to smooth muscle differentiation is not well documented; however, it has been proposed that in quail embryos the NCC-derived mesenchyme provides support to the nascent PAA (Waldo *et al.*, 1996). The ablation of the NCCs in these embryos results in a severe reduction in the size of the PA and

causes significant impact on the development of the artery therein. The vessel was found to become irregularly shaped and wider than normal in some regions, whilst hypoplastic or collapsed in others. The authors propose that the initial formation and lumenisation of the vessel occurs independently of NCC involvement, however, the NCC-derived mesenchyme within the arch is required to maintain the correct structure of the PAA. Additionally, the majority of defects in these vessels occur prior to the formation of the NCC-derived smooth muscle of the tunica media, suggesting that the NCCs may be responsible for the deposition of extracellular matrix proteins, which are required to support the vessel throughout its development.

We, therefore, propose a similar scenario in the formation of the fourth PAAs in *Tcfap2a*$^{-/-}$ mutant embryos. At e10.5, we observe a reduction in the number of patent fourth PAAs forming, in comparison to control embryos, while immunohistochemistry of embryos at this stage revealed a reduction in the number of NCCs within the mutant PAs. Although this reduction was only found to be statistically significant in the right PA, the number of NCCs within the left PA was similarly reduced. Therefore, it is possible that the reduction in the number of NCCs within the fourth PA at this stage is responsible for the loss of these vessels, due to the lack of mesenchymal support or deposition of extracellular matrix.

The increased number of fourth PAA defects between e10.5 and e15.5 is intriguing, and suggests a specific pathway within the right PA is being disrupted in these embryos. We have demonstrated that the right fourth PA has a statistically significant reduction in the number of NCCs and the levels of proliferation within the endoderm, while the levels of apoptosis within the surrounding ectoderm are significantly increased. Further investigations are required to identify the effect of these defects on the development of the right fourth PAA, however, it is likely that these factors explain the remodelling defects observed within the right PAA, which are not found in the left PAA.

5.3.3. Defects are specific to the fourth pharyngeal arch arteries

The PAA defects observed in the *Tcfap2a*$^{-/-}$ embryos examined appear to be specific to the fourth PAA. At e10.5, we observe defects affecting the development of the second, fourth and sixth PAAs, however, by e15.5 only defects of the fourth PAA are observed.

In particular, these defects appear to affect the formation of the RSA, which is derived from the fourth right PAA. Kutche and van Mierop (1984) propose three routes which the RSA can follow in cases where the fourth PAA fails to develop correctly. The most common defect of the RSA was A-RSA, followed by CORSA and finally, in rare cases, I-RSA (see Figure 1.9 in introduction chapter). In the *Tcfap2a*$^{-/-}$ mutants we observe both A-RSA and CORSA phenotypes, in approximately equal ratios. Although we do not observe any incidences of I-RSA, it is interesting to note that in the case of the single embryo with a RAA, the LSA arises from the pulmonary trunk. It is therefore likely that this phenotype results from a similar mechanism.

This study examined the presence of RSA malformations in human infants with an interruption of the aortic arch and found that two thirds (66%) of infants with an IAA also carried RSA defects (Kutsche and Van Mierop, 1984). Therefore, suggesting a common mechanism which results specifically in defects of the fourth PAAs. However, in *Tcfap2a*$^{-/-}$ mutant embryos, there was a much greater incidence of RSA malformations than defects of the aortic arch, therefore suggesting that defects of the RSA are not dependent on an IAA. Rather, it is likely that the subtle, potentially asymptomatic RSA defects are more readily identified in patients with a severe aortic arch malformation.

It is interesting to speculate that the fourth PAAs are more susceptible to genetic insult that that of the other caudal PAAs. Indeed, there are many examples in the literature of PAA defects as a result of fourth PAA malformations. Of particular interest are the endothelin and TGFβ2 signalling pathways, which result in similar malformations to those observed here. Mutation in members of the endothelin signalling pathway often result in the persistence of the carotid ducts in the absence of the left or right fourth PAAs (Yanagisawa *et al.*, 1998a). In addition, mutations in *Tgfb2* often result in PAA abnormalities such as IAA, A-RSA, hypoplasia of the aortic arch and aberrant persistence of the right dorsal aorta (Bartram *et al.*, 2001). Furthermore, it has previously been suggested that the aberrant persistence of PAA segments, such as the carotid ducts (resulting in CORSA and cAoA) and the right dorsal aorta (which results in A-RSA) are the result of a reduction in the levels of apoptosis within the smooth muscle lining of these vessels (Molin *et al.*, 2004). Therefore, although we did not

investigate the levels of apoptosis within these regions, it is likely that altered levels of apoptosis are the cause of their persistence. Further investigations are required to examine the apoptosis in this region, however, it may indicate an overall deregulation of basic cellular processes in *Tcfap2a*$^{-/-}$ mice.

The CORSA phenotype has also been identified in the Df1 mouse model of 22q11DS (Lindsay *et al.*, 1999), and in children with the 22q11DS mutation. One study shows that the malformation was found in greater than 60% of the patients examined and suggest that this phenotype may be specific to the syndrome (Rauch *et al.*, 2002).

The failure in the correct formation of the fourth PAAs, however, may be a result of their natural composition. It has been shown that these vessels have reduced α-SMA deposition in the tunica media layer of the vessels, leading to reduced stability of these arteries (Bergwerff *et al.*, 1999). These authors also demonstrated reduced α-SMA deposition in the derivatives of these vessels at later stages of development: in segment-B of the aortic arch and at the point where the brachiocephalic bifurcates into the RSA and the RCC arteries. Therefore, it is possible that minor perturbations in the development of this PA are sufficient to destabilise the vessel, causing them to become hypoplastic or collapse.

5.3.4. Other abnormalities of the PAAs at e10.5

Ink injections were used to investigate how the PAA defects observed at e15.5 relate to the development of the early PAA system. In control embryos at e10.5, the bilaterally symmetrical PAA system is fully developed and consists of three caudal PAA of approximately equal size. However, at this time a number of mutant embryos were seen to have aberrant persistence, hypoplasia or aplasia of the second, fourth and sixth PAAs.

By e15.5, defects of the second and sixth PAAs are no longer observed. It is possible, therefore, that these defects are the result of developmental delay in the mutant embryos. As there is no evidence for the persistence of the second PAAs into later life (e15.5) it is likely that the failure of these vessels to regress by e10.5 is due to a delay in the development of the PAA system in these mutants. A further possibility is that the defects of the caudal PAAs (4 and 6) result in the persistence of the second PAAs as

a secondary effect, due to increasing haemodynamic pressure. Conversely, the hypoplasia of the sixth PAAs may result in the persistence of the second PAAs, in order to maintain the blood flow from the developing heart. Whatever the cause of these defects, it appears that it is corrected at some later point, allowing the second and sixth PAAs of the *Tcfap2a*$^{-/-}$ mutants to develop normally by e15.5.

Defective formation of the sixth PAAs was confined to hypoplasia in the majority of cases. However, a single embryo was identified at e10.5 with aplasia of the sixth left PAA. This vessel contributes a major part of the ductus arteriosus to the mature aortic arch system, and therefore it is likely that the inability of this vessel to form would result in the loss of the ductus arteriosus. In addition, this embryo also has an absent left fourth PAA, which may be the result of a developmental delay, as the embryo in question was only 34 somites. However, it is interesting to speculate that aberrant loss of both the fourth and sixth PAAs on the left may be the cause of the RAA phenotype observed in only a single embryo of the 10 examined. In this scenario, the loss of the sixth left PAA would likely result in a right-sided ductus arteriosus. This would result in an increase in the levels of blood flow through the right side of the PAA system, which in collaboration with the loss of the fourth left PAA is likely to result in the formation of the RAA. Interestingly, Yashiro *et al.* (2007) demonstrated that ligation of the left sixth PAA in wild type embryos resulted in the persistence of the right sixth PAA in approximately half of the embryos examined. In addition, in those embryos with a patent right sixth PAA, the right dorsal aorta was often found to have a greater diameter than the left, indicating the importance of haemodynamics in the development of the PAA system.

A further interesting finding from this work was the appearance of small branching vessels around the fourth PAA in mutant embryos. These vessels were identified in both the left and right PAs, in 30% and 20% embryos, respectively. It is possible that these vessels are the collateral channels described by Bamforth *et al.* (2012a), which connect the fourth and sixth PAA. However, these channels were identified in wild type embryos from e11.5 onwards. Our work demonstrates the presence of these vessels in mutant embryos at e10.5. In addition, a similar phenotype was observed in *Gbx2*$^{-/-}$ mutant embryos (Calmont *et al.*, 2009). It is likely that these malformations are

a further result of the increase in blood pressure, causing new vessels to sprout in order to keep up with the increased blood flow.

5.3.5. NCC migration in *Tcfap2a*$^{-/-}$ mutant embryos

As discussed above, many of the malformations of the PAAs in *Tcfap2a*$^{-/-}$ mutant embryos can be attributed to defects of the NCCs. The NCCs differentiate into the smooth muscle layer surrounding the PAAs, a process which we have shown to be disrupted in *Tcfap2a*$^{-/-}$ mutant embryos. In addition, the NCCs are responsible for forming the mesenchymal tissue of the PA, which is then able to support the vessels during early development. Therefore, the reduction in the number of NCCs in the PAs by e10.5 is likely to cause the formation defects, through reduced mesenchymal support of the vessels.

Despite, the importance of the NCCs in the development of the heart and PAAs, and the high levels of *Tcfap2a* within this tissue, defects in NCC development and migration have not previously been described in *Tcfap2a*$^{-/-}$ mutant embryos. In fact, examination of NCC migration has previously been suggested to be normal (Brewer *et al.*, 2002; Zhang *et al.*, 1996). However, previous analysis has concentrated on the localisation of the NCCs. Here, we present the first study quantifying NCCs migrating into the PA region, and identify that this process is disrupted in *Tcfap2a*$^{-/-}$ mutant embryos. Although, the reduction in the number of NCCs observed is subtle, it is possible that this deficit results in the defective formation and remodelling of the fourth PAAs in these embryos. In addition, we have demonstrated that the levels of apoptosis and proliferation are not significantly disrupted in these mutant embryos, therefore, suggesting that the NCC deficit within the fourth PA is the result of the inability of NCCs to migrate into the arches, rather than loss of these cells following migration.

5.3.6. The role of PA epithelium in PAA morphogenesis

Overall it appears that the loss of *Tcfap2a* is important in cell survival and proliferation within the fourth PAs. Our data demonstrates alterations in the levels of both apoptosis and proliferation in the epithelia of the fourth PAs. We show a significant increase in the levels of apoptosis within the ectoderm of the right fourth PA at e10.5, accompanied by a significant decrease in the levels of proliferation within the endoderm of this arch. This suggests that the remodelling of the fourth right PAA into

the RSA requires signals from the surrounding epithelia which help to support and maintain the vessel or aid in NCC differentiation into SMCs. Although the levels of both cellular processes remain unaffected in the NCCs, there was a reduction in the numbers of NCCs within the fourth PAs at e10.5. It is, therefore, possible that the changes in these cellular processes result in a decrease in the number of epithelial cells within the right PA. This in turn would cause a reduction in the level of signalling from these tissues, which aid in the migration of the NCCs into the PAs. It has been shown that signalling from the ectoderm is important in the migration of the NCCs into this region, and loss of this signalling results in PAA defects (see section 1.3.4.2). The reduced number of epithelial cells in this region may cause a reduction in the numbers of NCCs migrating into the area and, therefore, the number of cells available to differentiate into SMCs at a later time.

5.3.7. Advantages and disadvantages of this study

The work presented within this chapter has focussed on the formation and development of the PAAs in *Tcfap2a*$^{-/-}$ mutant embryos. In order to investigate this process, a number of techniques were employed. The formation of these vessels was investigated using ink injection, a vascular filling technique, in addition to immunohistochemistry. Vascular filling methods are commonly used to identify patent vessels within the developing embryo, which is then used to infer if a vessel has formed correctly. However, this does not accurately determine the formation of a vessel. The PAAs form through the aggregation of angioblasts into an endothelial string, which then luminises to form a vessel. The vascular filling methods are only able to investigate the lumenisation step of this process. In this study, however, we have complemented this technique with the use of immunohistochemistry to determine if the endothelium of the vessel forms correctly.

Chapter 6. Identification of transcriptional targets of AP-2α in cardiovascular development

6.1. Introduction

The work presented throughout this thesis demonstrates the importance of *Tcfap2a* in cardiovascular development. However, the target genes of this transcription factor in cardiovascular development remain unknown. In this chapter we will investigate the downstream targets of AP-2α in PAA development, in order to further understand the role of this transcription factor in this process.

6.1.1. Transcriptional targets of AP-2α

Much of the work which has deduced putative targets of AP-2α has been carried out to further understand the role of this transcription factor in cancer progression and development. However, a number of these genes have been implicated in processes relevant to cardiovascular development. This work has identified significant involvement of AP-2α in basic cellular processes such as proliferation, apoptosis and differentiation, which play major roles in cardiovascular development.

VEGF is an important gene in tumour angiogenesis and has been shown to be a downstream target of AP-2α in cancer (Gille *et al.*, 1997). This gene is pivotal in both angiogenesis and vasculogenesis, and is therefore integral to the formation of the vasculature of the developing embryo. This suggests that downregulation of this gene in *Tcfap2a*$^{-/-}$ embryos may prevent PAA formation. *VEGF* mutations result in severe malformations of the PAAs, including IAA, double aortic arch and persistence of the carotid duct segments of the dorsal aorta. In addition, TOF was also observed in mouse embryos with mutations of the dominant VEGF^{164} isoform (Stalmans *et al.*, 2003). Many of these phenotypes have been described in *Tcfap2a*$^{-/-}$ mutants, suggesting that *VEGF* is a viable candidate for AP-2α-mediated regulation in PAA development.

MMP-2 is involved in the degradation of a number of ECM proteins (Shapiro, 1998). In the developing chicken embryo its expression begins in the NCCs after migration from the neural tube into the PAs. It has been suggested that this expression may be involved in the remodelling of the PAAs (Cai *et al.*, 2000).

Further, the AP-2 family has been associated with the negative regulation of the T-box transcription factor, TBX20 in patients with TOF. RT-PCR of atrial and ventricular biopsies from patients with TOF demonstrated higher levels of *TBX20* than in controls with VSDs, while expression of AP-2 family genes was reduced. In addition, constructs of *TFAP2A, -B* and *–C* were able to downregulate *TBX20* in a dose-dependent manner (Hammer *et al.*, 2008). This, therefore, suggests a role for AP-2 family genes and *TBX20* in the presentation of TOF in patients.

Therefore, AP-2α can be implicated in the activation of a number of genes which are important in cardiovascular development. However, despite these links and the importance of *Tcfap2a* in cardiovascular development, the transcriptional targets of AP-2α in cardiovascular development have never been investigated.

6.1.2. Aims of chapter

The *Tcfap2a* gene encodes the transcription factor AP-2α, which has an important role in cardiovascular development. We demonstrated in the previous chapter that, by e10.5, PAA formation is impaired in *Tcfap2a*$^{-/-}$ mice. As discussed above, many genes have been suggested as downstream targets of AP-2α in cancer, some of which also have roles in cardiovascular development. However, none of these genes have been validated as the cause of CCVM in *Tcfap2a*$^{-/-}$ mutants.

In this chapter we aim to understand the effect of the loss of *Tcfap2a* at the transcriptional level, in order to further characterise the role of this transcription factor in cardiovascular development. To do this we will examine the expression levels of a number of previously identified AP-2α target genes within the PA region of control and mutant embryos. In addition, we also aim to investigate the expression levels of a number of genes key to cardiovascular development, each of which contains AP-2 binding sites within the promoter region.

The identification of any potential downstream targets will require further validation, through the use of *in situ* hybridisation and genetic interaction studies. This will also be presented here.

6.2. Results

6.2.1. Transcript analysis of the pharyngeal arch region in *Tcfap2a*$^{-/-}$ embryos

In order to investigate the effect of *Tcfap2a* deletion on the expression of potential target genes in the PA region, wild type (*Tcfap2a*$^{+/+}$) and mutant (*Tcfap2a*$^{-/-}$) embryos were collected at e9.5 for qPCR analysis. This stage is immediately prior to fourth PAA morphogenesis (Hiruma *et al.*, 2002) and will therefore allow us to understand the transcriptional changes occurring in mutant embryos at this time, in order to prevent correct vessel formation. The PA region was dissected and retained for RNA extraction (see section 2.10.1).

A candidate gene approach was used to select target genes. As *Tcfap2a* is highly expressed in the NCCs at the stage of interest and due to the importance of the NCCs during PAA development, a number of target genes were selected based on expression within the NCCs. Two such genes are *Tcfap2b* and *Tcfap2c*, members of the AP-2 family, which overlap with *Tcfap2a* expression patterns in the NCCs. A number of NCC markers were also investigated to identify any transcriptional changes occurring in this population of cells at this time. In addition, we also examined the expression levels of putative *Tcfap2a* target genes, and genes known to be involved in cardiovascular development, in the context of the *Tcfap2a*$^{-/-}$ PA region. Analysis was conducted using the comparative Ct method, with results being normalised to the housekeeping gene GAPDH.

Firstly, a qPCR reaction was performed to examine *Tcfap2a* expression, using primers that bind within exons 6 and 7. As the null allele replaces exon 7 with a LacZ cassette, these primers will be unable to bind to mutant transcripts. As expected, we found that *Tcfap2a* expression was reduced to less than 0.08% of wild type expression levels (p <0.0001), indicating that no wild type transcripts are produced (Figure 6.1a).

Examination of *Tcfap2b* and *Tcfap2c* expression in *Tcfap2a*$^{-/-}$ mutant embryos demonstrates a marginal, but statistically significant increase in the levels of both genes in comparison to wild type controls (Figure 6.1a). *Tcfap2b* expression was increased by 11% of wild type expression (p = 0.0379), while *Tcfap2c* was increased by almost 14% (13.79%, p=0.0452).

A number of genes associated with CCVM, which contain AP-2 binding sites within their promoter region, were also examined (promoter analysis carried out by Dr Simon Bamforth). Some of these genes, (retinoic acid receptors α and β (*Rara, Rarb*) and cyclin E2 (*Ccne2*)) appeared to be upregulated in *Tcfap2a*$^{-/-}$ mutant embryos, suggesting a possible repressive effect of AP-2α on these genes. However, upon statistical analysis none of these were found to be significant. Other genes (*Smad7*, *Chd7* and *Fgf8*) appear to be downregulated in *Tcfap2a*$^{-/-}$ mutant embryos. Of these, only one was statistically significantly reduced in *Tcfap2a*$^{-/-}$ mutant embryos. *Fgf8* was reduced to approximately 78% (p = 0.0233) wild type expression in mutants (Figure 6.1b) and therefore is a potential downstream target of AP-2α.

Interestingly, analysis of known *Tcfap2a* target genes yielded no statistically significant changes between wild type and mutant embryos. Three of these genes (*cMyc*, *ErbB2* and *Acan*) appeared to be marginally reduced, however, failed to reach statistical significance. *Sox10* appeared to be upregulated in mutant embryos. However, the large error bars associated with this result, likely due to the high Ct values in the qPCR analysis, prevented this gene from reaching statistical significance.

A number of known NCC markers were also examined. As *Tcfap2a* is highly expressed in the NCCs, we wanted to examine the effects of loss of *Tcfap2a* on this population of cells as a whole. However, only one of these genes was affected in our analysis. *Dlx5* was significantly downregulated (p = 0.0069) in *Tcfap2a*$^{-/-}$ mutant embryos, while the other NCC markers, *Foxd3* and *Snail2* show no differential expression between wild type and mutant samples. This suggests that *Dlx5* may be a direct target of *Tcfap2a* within the PA region.

The qPCR analysis presented here suggests two possible downstream target genes of *Tcfap2a* in the PA region. *Fgf8* is expressed within the PSE, where it has been shown to be important for correct PAA development (Abu-Issa *et al.*, 2002). *Dlx5* expression is activated in the post-migratory NCCs at around e9.5, and is known to be required in the PAs for correct craniofacial development (Acampora *et al.*, 1999; Depew *et al.*, 1999). However, *Dlx5* has not previously been implicated in cardiovascular development.

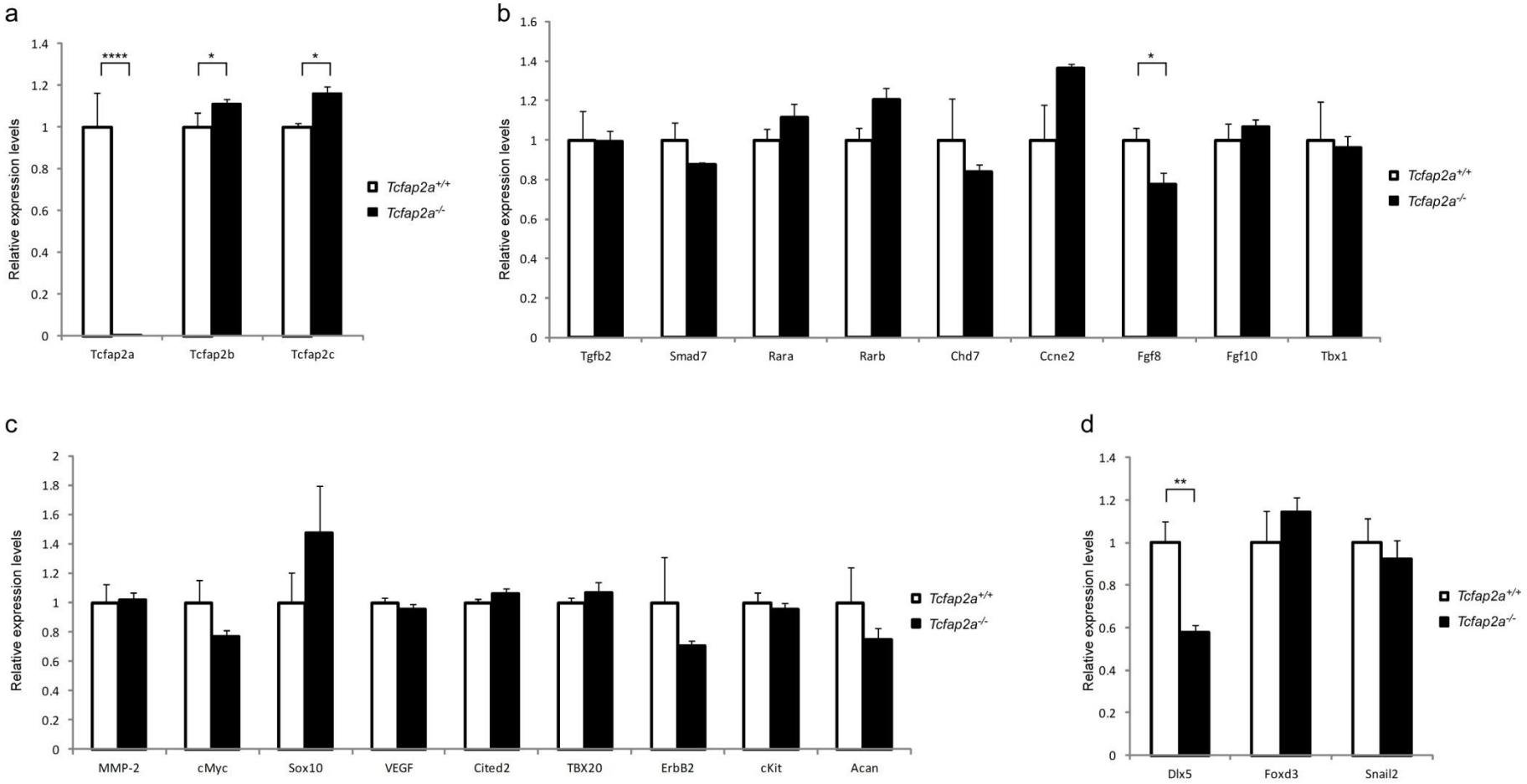

Figure 6.1: Quantitative RT-PCR of potential downstream targets of AP-2α in *Tcfap2a*$^{-/-}$ mutant pharyngeal arch at e9.5 relative to wild type controls.
(a) Expression of AP-2 isoforms expressed within the murine NCCs. (b) Expression of genes with a known role in cardiovascular development. The genes examined have a conserved AP-2 binding site within their promoter. (c) Expression levels of known AP-2α target genes with functions in cardiovascular development. (d) Expression levels of neural crest markers in mutant pharyngeal arch tissue. Statistical significance determined using a student's *t*-test; *, p <0.05. **, p <0.01. ****, p <0.0001. Error bars indicate S.E.M.

6.2.1.1. In Situ hybridisation of candidate genes

The qPCR analysis shown above suggests that *Fgf8* and *Dlx5* may be downstream targets of AP-2α. Therefore, WISH was used to validate the results obtained from qPCR and investigate the spatial changes in expression of these genes.

Sense and antisense probes to *Fgf8* and *Dlx5* were prepared by labelling with DIG. At e9.5, *Fgf8* expression was similar to that described previously (Ohuchi *et al.*, 1994). Expression was observed at the midbrain-hindbrain border, the future olfactory bulb, within the endoderm of the caudal PAs and within the first PA, in all wild type embryos examined (Figure 6.2a). Examination of *Tcfap2a*$^{-/-}$ mutant embryos reveals that the expression pattern within the head and pharyngeal endoderm is conserved between wild type and mutant embryos, however, ectodermal expression within the first PA appears disrupted (Figure 6.2b). *Fgf8* is strongly expressed in both the maxillary and mandibular components of the first PA and is restricted to the ectoderm (Vitelli *et al.*, 2002) (Figure 6.2c). In *Tcfap2a*$^{-/-}$ mutant embryos, however, expression in the distal portion of the mandibular component of the first arch is lost, and expression in the more proximal portion is reduced (Figure 6.2d). Expression within the maxilla does not appear to be affected. The pattern of staining in the olfactory bulb appears reduced as the craniofacial processes have not fused (Figure 6.2e).

Expression of *Dlx5* at e9.5 was found to be similar to that previously described (Acampora *et al.*, 1999). In wild type embryos, strong expression was identified in the otocyst and the PA region (Figure 6.3a) at e9.5. Expression in *Tcfap2a*$^{-/-}$ mutant embryos, however, appears reduced in both regions (Figure 6.3b). At higher magnifications it is apparent that *Dlx5* is strongly expressed within the first and second PAs. Weaker expression was also observed in the third PA and the developing fourth and sixth PAs (Figure 6.3c). Mutant embryos, however, show reduced expression within the first and second PAs and expression in the caudal PAAs appears completely diminished (Figure 6.3d).

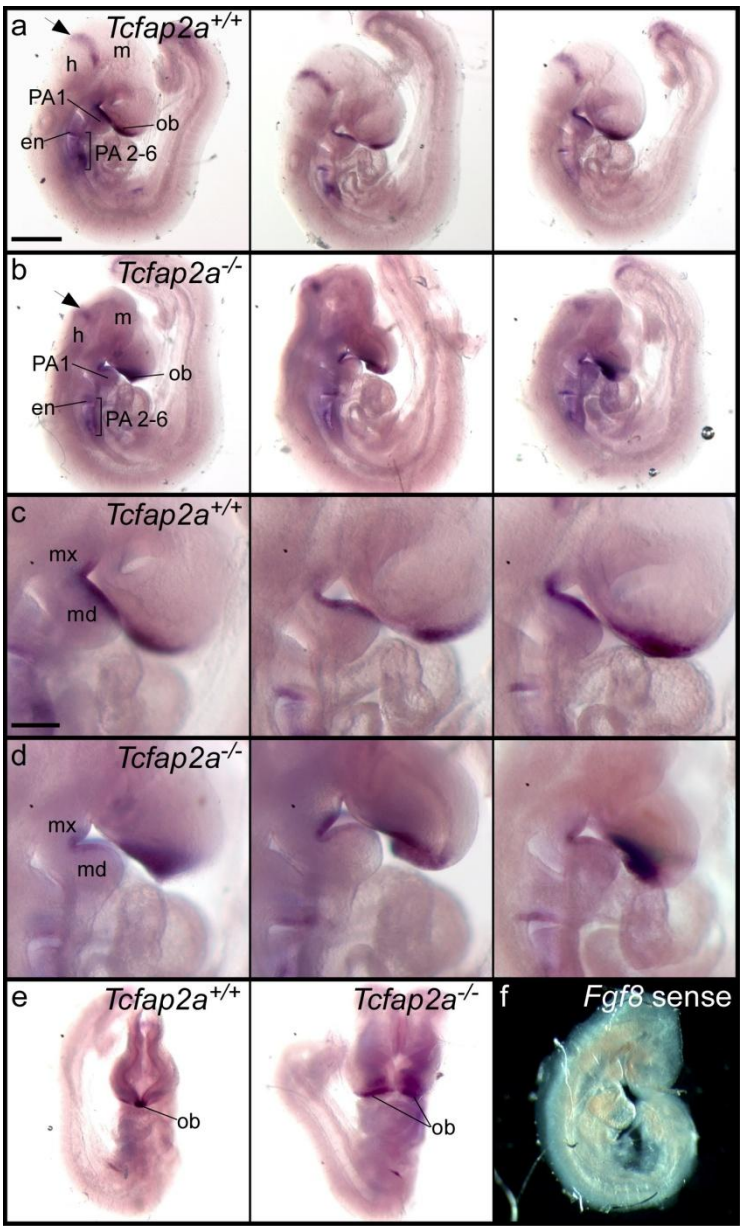

Figure 6.2: *Fgf8* expression is reduced in the first pharyngeal ectoderm in *Tcfap2a*$^{-/-}$ mutant embryos.
WISH of *Fgf8* expression in *Tcfap2a*$^{+/+}$ control (panels a and c) and *Tcfap2a*$^{-/-}$ mutant (panels b and d) embryos at e9.5. (a) Expression of *Fgf8* in wild type control embryos is observed at the border of the midbrain and hindbrain (arrow), in the future olfactory bulb (ob), the ectoderm of the first pharyngeal arch (PA1) and the endoderm (en) of the caudal PAs (PA 2-6). (b) Expression of *Fgf8* in mutant embryos. Expression in the midbrain/hindbrain border is diminished due to the open neural tube. Expression in the first pharyngeal arch ectoderm is reduced in the mutant embryos. All other expression domains remain unaffected. (c) Higher magnification images of wild type embryos shown in panel a. Strong expression is visible within the future olfactory bulb and the ectoderm of the mandibular (md) and maxillary (mx) components of the first pharyngeal arch. (d) Higher magnification images of *Tcfap2a*$^{-/-}$ mutant embryos shown in panel b. *Fgf8* expression is diminished in the distal part of the mandibular component of the first pharyngeal arch and is reduced in the proximal part of the mandible. Expression also appears altered in the future olfactory bulb. (e) Frontal views of wild type and mutant embryos demonstrating that the change in expression patterns within the future olfactory bulb are the result of the failure of the craniofacial processes to fuse. (f) *In situ* hybridisation of *Fgf8* sense probe demonstrates no non-specific staining in the absence of the antisense probe. Scale bars = 1 mm (a-b, e-f), 500 μm (c-d). (n=3).

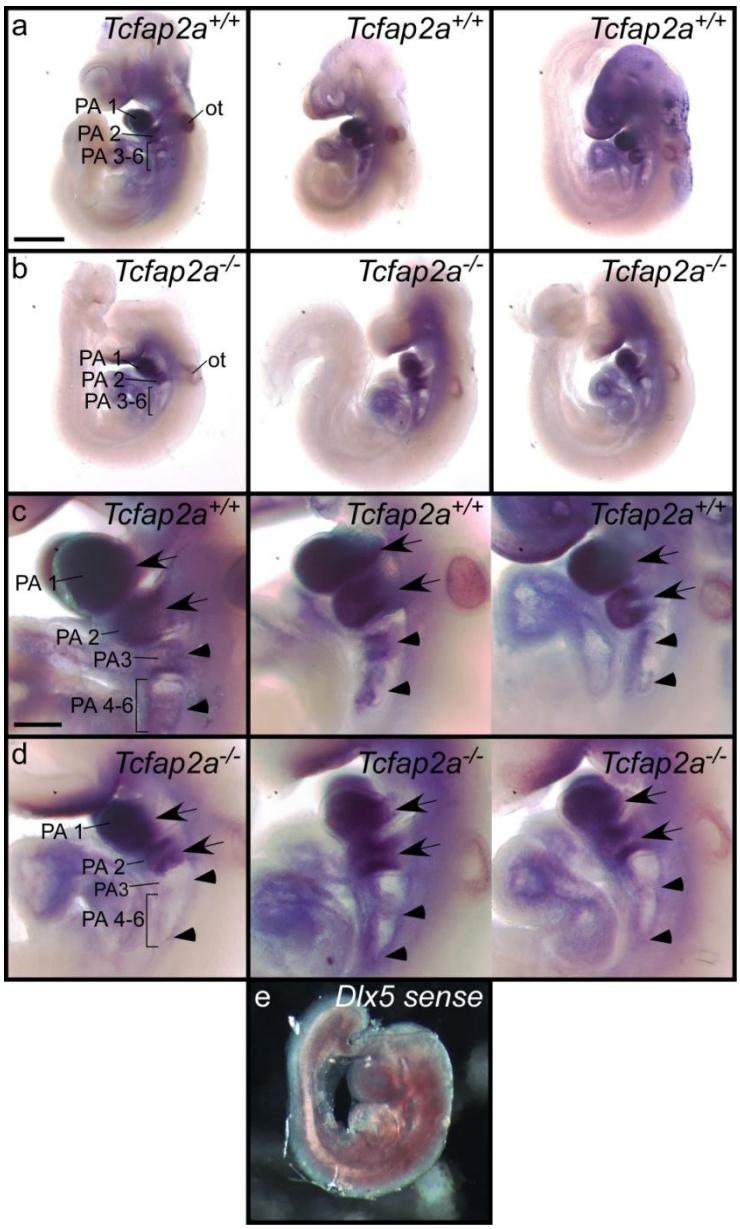

Figure 6.3: *Dlx5* expression is reduced within the pharyngeal arches in *Tcfap2a*$^{-/-}$ mutant embryos.
WISH of *Dlx5* expression in *Tcfap2a*$^{+/+}$ control (panels a and c) and *Tcfap2a*$^{-/-}$ mutant (panels b and d) embryos at e9.5. (a) Control embryos showing *Dlx5* expression in the otocyst (ot) and pharyngeal arches (PA) 1-6. (b) *Dlx5* expression in *Tcfap2a*$^{-/-}$ mutant embryos appears reduced in the otocyst and PAs. (c) Higher magnification of the embryos in panel a. Strong expression is observed in the first and second PAs (arrows). Weaker expression is also observed in the third PA and in the forming fourth and sixth PAs (arrowheads). (d) Higher magnification of the embryos in panel b. Expression of *Dlx5* in the first and second PAs appears marginally reduced (arrows, compare to panel c), while expression in the caudal pharyngeal arches is almost completely lost (arrowheads, compare to panel c). (e) *In situ* hybridisation using a *Dlx5* sense probe demonstrates no non-specific binding of the probes. Scale bars = 1mm (a-b, e), 500 µm (c-d). (n=3).

To confirm the loss of *Dlx5* expression within the caudal PAs, embryos were sectioned in a coronal orientation (Figure 6.4). This analysis demonstrates that *Dlx5* expression within the first PA of wild type and mutant embryos is comparable (Figure 6.4a-b, e-f). However, expression within the more caudal PAs (2-4) appears strongly reduced within the pharyngeal mesenchyme only (Figure 6.4c-d, g-h).

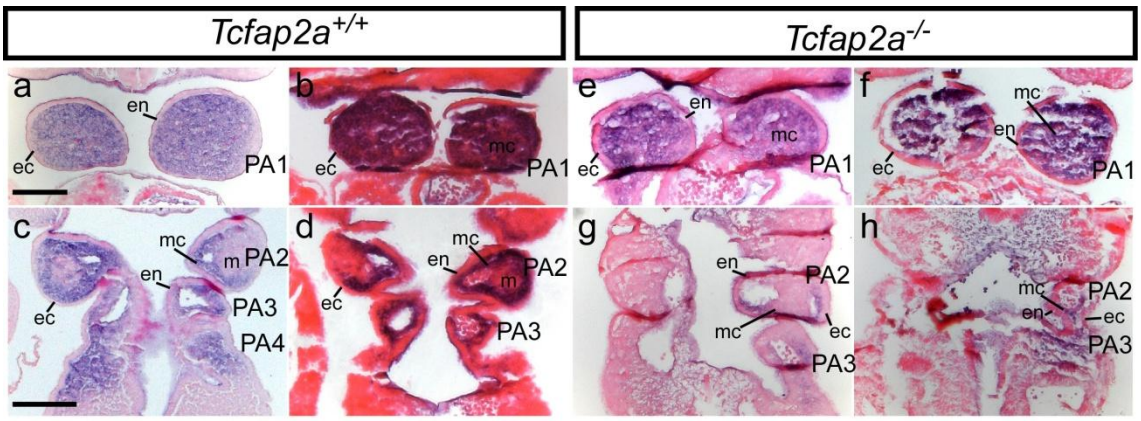

Figure 6.4: *Dlx5* expression is reduced within the caudal PAs.
Coronal sections through *Tcfap2a*$^{+/+}$ control (a-d) and *Tcfap2a*$^{-/-}$ mutant (e-h) embryos following WISH (purple staining) and counter-stained with eosin (pink). Expression of *Dlx5* within the first PA (PA1) appears comparable between controls (a-b) and mutants (e-f). Expression within the caudal PAs (PAs 2-4) is severely reduced in mutant embryos. (g-h) compared to controls (c-d). N=3, representative images shown. Scale bars = 100 µm. PA, pharyngeal arch; en, endoderm; ec, ectoderm; mc, mesenchyme; m, mesoderm. (n=3).

Fgf8 and *Dlx5* were selected for further analysis as they were significantly downregulated in the qPCR analysis shown above. Validation of this change in expression by WISH has revealed that *Fgf8* expression is strongly reduced in the ectoderm of the mandibular component of the first PA. However, it is unlikely that reduced expression of the signalling factor in this region, which is primarily involved in craniofacial development, would result in the severe cardiovascular malformations observed in *Tcfap2a*$^{-/-}$ mutant embryos. It is likely that the reduced expression of *Fgf8* is involved in the presentation of the craniofacial phenotypes.

Dlx5 however, shows a downregulation throughout the NCC-derived mesenchyme of the caudal PAs, which support the PAAs that remodel into the mature aortic arch. This suggests that *Dlx5* may be a target of *Tcfap2a* within the NCCs and reduced expression of this gene may result in the PAA abnormalities observed in *Tcfap2a*$^{-/-}$ mutant embryos.

6.2.2. Co-localisation of *Dlx5* and *Tcfap2a*

The work described above demonstrates that *Dlx5* is downregulated in the PA region of *Tcfap2a*$^{-/-}$ mutants at e9.5. To confirm that *Dlx5* may be a direct target of AP-2α, we wanted to confirm that both genes are expressed in the same tissues within the PA. AP-2α distribution was analysed by immunohistochemistry and compared to expression of *Dlx5* in coronal WISH sections.

Dlx5 is strongly expressed in the mesenchyme of the first and second PAs (purple staining, Figure 6.5a), with all other pharyngeal tissues (endoderm, ectoderm and mesoderm) being devoid of staining. Expression was also observed within the mesenchyme of the third PA and within the presumptive fourth PA region. *Tcfap2a* expression was identified within the pharyngeal mesenchyme of each of the PAs, and in the surrounding surface ectoderm (Figure 6.5b). Therefore, both genes are expressed within the NCC-derived pharyngeal mesenchyme at e9.5. The apparently reduced levels of expression in the more caudal PAs is likely caused by incomplete migration of the NCCs into these arches at this time.

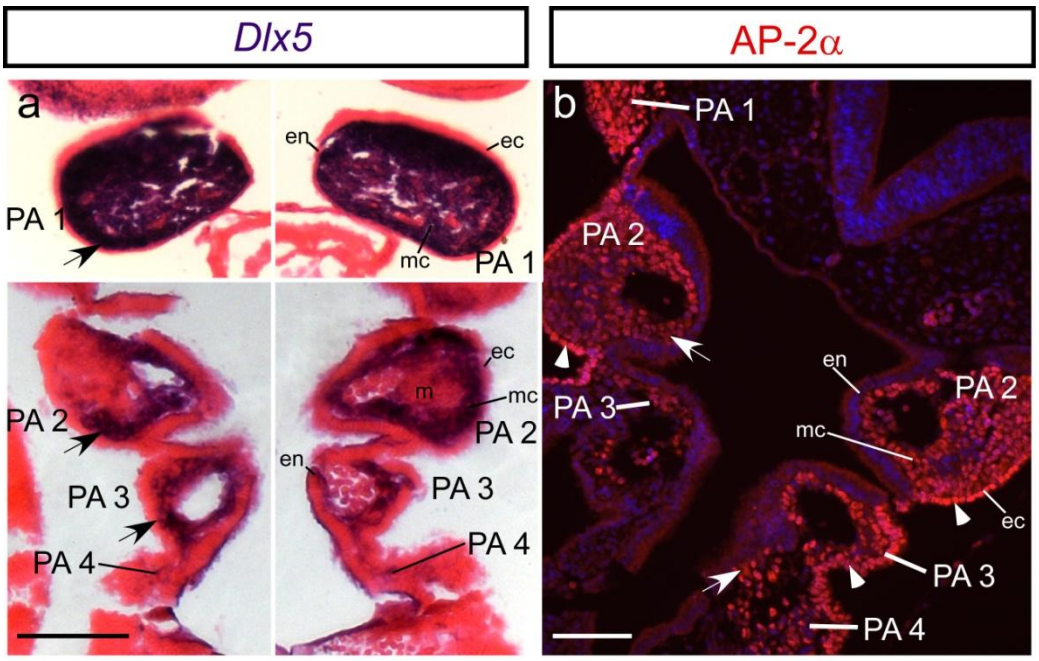

Figure 6.5: Colocalisation of *Dlx5* and AP-2α within the pharyngeal arches at e9.5.
Expression of *Dlx5* (a) and AP-2α (b) in wild type (*Tcfap2a*$^{+/+}$) e9.5 embryos. (a) Coronal sections through an embryo stained for *Dlx5* antisense probe using WISH (purple). Sections were counterstained with eosin (pink). Arrows denote expression within the NC-derived mesenchyme. (b) Immunofluorescence on coronal sections showing the localisation of *Tcfap2a* expression (red, *Tcfap2a*; blue, DAPI). Image kindly provided by Kathleen Allinson. Arrows denote expression within the NC-derived mesenchyme, arrowheads denote expression within the PSE. Scale bars = 100 µm. PA, pharyngeal arch; en, endoderm; ec, ectoderm; mc, mesenchyme; m, mesoderm.

6.2.3. Transcriptional activation of *Dlx5* pathways

The data presented above suggests that *Dlx5* may be a direct downstream target of AP-2α within the NCC-derived pharyngeal mesenchyme. To further investigate the nature of the potential AP-2α-mediated regulation of *Dlx5*, we used qPCR to examine the expression levels of other genes within the *Dlx5* pathway.

The members of the *Dlx* family are highly homologous and are found as inverted tandem repeats within the genome, often with shared enhancer elements between

the two genes (Merlo *et al.*, 2000). To investigate the potential role of *Tcfap2a* in the activation of all *Dlx* family genes, primers were designed to each of the known mouse paralogs of *Dlx.* An additional set of primers to an alternative region of *Dlx5* were also designed to further validate the downregulation of this gene.

Dlx1 and *Dlx2* show marginal changes in expression (84% and 91% wild type expression levels, respectively) in *Tcfap2a*$^{-/-}$ mutants compared to wild type controls (Figure 6.6a). *Dlx3* and *Dlx4* expression was reduced further (70% and 45% respectively), however, did not reach statistical significance. *Dlx5* and *Dlx6*, however, were both significantly reduced in *Tcfap2a*$^{-/-}$ mutants with expression decreased to 54% and 45%, respectively (p = 0.0002 and p = 0.001). This suggests that AP-2α regulation of the Dlx family is specific to *Dlx5* and *Dlx6*.

Expression of *Dlx5* and *Dlx6* is known to be controlled by the endothelin signalling pathway in the patterning of the first and second PAs in craniofacial development (Jeong *et al.*, 2008). The Endothelin-1 gene (*Edn1*), which encodes the ET-1 signalling molecule, and the endothelin converting enzyme (*ECE-1*) are expressed within the PA epithelium (ectoderm and endoderm) and the paraxial mesoderm of the PA. The converted ET-1 molecule is released from the epithelia/mesoderm and received by the ET_A receptor (encoded by *Ednra*) within the PA mesenchyme. As *Tcfap2a* is expressed within both the pharyngeal ectoderm and the NCCs it is possible that AP-2α is regulating *Dlx5* and *Dlx6* indirectly by activation of either *Edn1* or *ECE-1* in the ectoderm, or *Ednra* or a downstream g-protein in the mesenchyme. To test this hypothesis, primers were designed to each of these genes, and qPCR analysis in wild type and mutant embryos carried out.

There were no significant differences between wild type and mutant embryos in the expression levels of *Edn1*, *ECE-1* or *Ednra* (Figure 6.6b). Additionally, the expression levels of the g-proteins examined (*Gnaq*, *Gna11*, *Gnas* and *Gnai*) were also consistent between wild type and mutant embryos. This suggests that AP-2α is activating *Dlx5* and *Dlx6* independent of the endothelin signalling pathway, or that *Tcfap2a* is an intermediate step between the endothelin pathway and *Dlx5/6*.

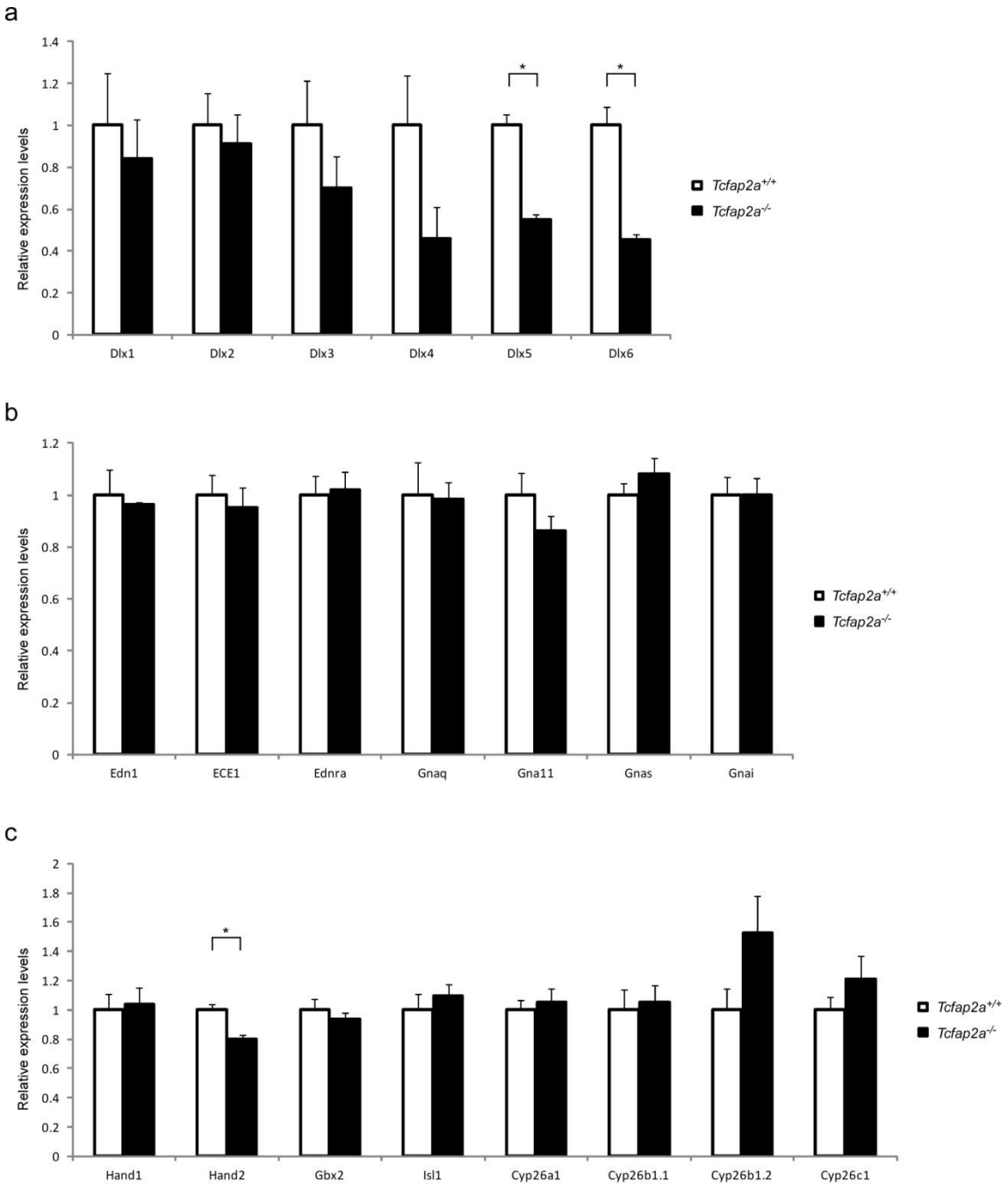

Figure 6.6: Quantitative RT-PCR of genes associated with *Dlx5* in *Tcfap2a*$^{-/-}$ mutant pharyngeal arch at e9.5 relative to wild type.
(a) Expression levels of Dlx family genes in the *Tcfap2a*$^{-/-}$ mutant pharyngeal arch. (b) Expression levels of upstream activators of Dlx5. (c) Expression levels of Dlx5 downstream targets.

Although the potential role of either *Dlx5* or *Dlx6* in cardiovascular development has never been examined, a study of *Dlx5/6*$^{-/-}$ double mutant embryos, has revealed a number of downstream targets, which have known roles in cardiovascular development, including *Gbx2*, *Cyp26a1*, *Hand1* and *Hand2* (Jeong *et al.*, 2008). *Gbx2* and *Cyp26a1* are thought to be 22q11DS modifying genes based on genetic interaction

studies, downregulation of these genes in *Tbx1*$^{-/-}$ mice and complementary expression patterns (Roberts *et al.*, 2006; Calmont *et al.*, 2009).

To investigate the effect of *Tcfap2a* loss and the reduced expression of *Dlx5/6* on *Dlx5/6* target genes, primers were designed to *Hand1, Hand2, Isl1, Gbx2* and the three murine Cyp26 genes: *Cyp26a1, Cyp26b1* and *Cyp26c1*. As *Cyp26b1* produces 2 transcripts which could not be examined using a common pair of primers, primers were designed to each transcript individually. These transcripts appear in the analysis as *Cyp26b1.1* and *Cyp26b1.2*.

Figure 6.6c shows the expression levels of these genes in *Tcfap2a*$^{-/-}$ mutants compared to wild type controls. The majority of these genes showed only marginal changes, which were not statistically significant. However, *Hand2* was downregulated to approximately 80% of wild type expression in *Tcfap2a*$^{-/-}$ mutant embryos (p = 0.0052). Interestingly, *Cyp26b1* variant 2 expression was increased by 50% in the mutant embryos, however, the high Ct values for this variant resulted in an increase in variability and therefore prevented this result from reaching statistical significance.

The data presented above suggests that AP-2α is responsible for specific regulation of both *Dlx5* and *Dlx6*, and that this regulation is independent of the endothelin signalling pathway. In addition, most common targets of *Dlx5* and *Dlx6* were not found to be downregulated in *Tcfap2a*$^{-/-}$ embryos, despite a reduction in expression of both *Dlx5* and *Dlx6* to approximately 50% of wild type expression. However, *Hand2* exhibited a statistically significant downregulation to 80% wild type levels.

6.2.4. *Tcfap2a* x *Dlx5* genetic interaction study (98.8 – 99.3% C57BL/6J)

To investigate a potential genetic interaction between *Tcfap2a* and *Dlx5*, *Tcfap2a*$^{+/-}$ females were crossed to *Dlx5-CreERT2* male mice, to generate compound heterozygotes. This cre line was produced by direct insertion of the CreERT2 cDNA into the *Dlx5* locus, resulting in a null allele. Therefore, this male is heterozygous for *Dlx5* and this genotype will be referred as *Dlx5*$^{+/-}$ throughout the remainder of this chapter.

6.2.4.1. External phenotype

Tcfap2a$^{+/-}$*;Dlx5*$^{+/-}$ compound heterozygotes and *Dlx5*$^{+/-}$ control embryos were collected at e15.5 for external examination and MRI analysis of cardiovascular defects. Of 10 *Tcfap2a*$^{+/-}$*;Dlx5*$^{+/-}$ embryos examined only a single embryo exhibited an external phenotype in the form of exencephaly (Figure 6.7b). The remaining compound heterozygotes and control embryos did not differ from wild type in appearance (Figure 6.7c).

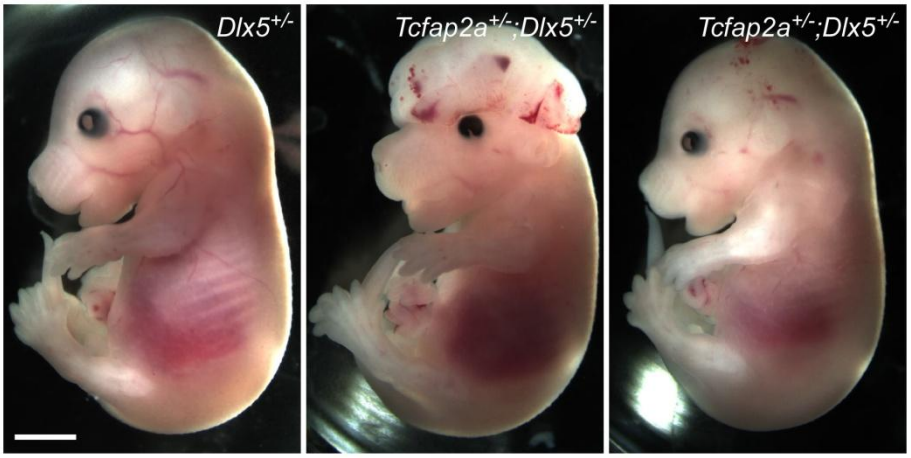

Figure 6.7: External phenotype of *Tcfap2a*$^{+/-}$*;Dlx5*$^{+/-}$ compound heterozygotes.
(a) Control (*Dlx5*$^{+/-}$) embryo showing normal external phenotype. (b) Compound heterozygous embryo with exencephaly. (c) Compound heterozygous embryo with normal external phenotype. Scale bar = 2mm. (n=10).

6.2.4.2. MRI analysis

Compound heterozygotes and control embryos were examined by MRI analysis at e15.5. Examination of each of these embryos identified normal cardiovascular development throughout all of the embryos analysed. In addition, *Dlx5*$^{-/-}$ mutant embryos exhibit exencephaly and cleft palate (Acampora *et al.*, 1999; Depew *et al.*, 1999). These phenotypes have previously been described in *Tcfap2a*$^{-/f}$*;Wnt1cre* conditional mutant embryos (see section 3.2) (Brewer *et al.*, 2002). Therefore, the palate was examined in the *Tcfap2a*$^{+/-}$*;Dlx5*$^{+/-}$ compound heterozygote and found to develop normally. In addition, the development of the thymic rudiments also appeared normal. Therefore, it is likely that more complex crosses will be required in order to fully investigate the genetic interaction of these two genes *in vivo*.

6.2.5. *Dlx5/6* double mutant embryos

Investigation of the *Tcfap2a*$^{+/-}$*;Dlx5*$^{+/-}$ compound heterozygotes did not reveal any cardiovascular defects. However, both *Dlx5* and *Dlx6* were reduced to approximately 50% of expression in our transcript analysis. Therefore, it is possible that *Dlx6* acts in a

redundant manner when *Dlx5* is reduced in our compound heterozygotes. Embryos were collected at e15.5 by Professor Giovanni Levi (Paris, France) and sent to us for analysis.

6.2.5.1. External phenotype

The external phenotypes of these embryos were examined and several malformations were identified. The most common phenotype was a hox-like transformation of the lower jaw, which results in the lower jaw forming as a mirror image of the upper jaw, which has been previously described (Beverdam *et al.*, 2002). This phenotype was identified in 85.7% (6/7) of mutant embryos (Figure 6.8d, i). Exencephaly was observed in 57.14% (4/7) of mutant embryos examined (Figure 6.8d-e). The *Dlx5/6*$^{-/-}$ mutant mice have been previously described as a model for split hand-foot malformation (SHFM) (Merlo *et al.*, 2002) and therefore, the hind limbs were examined for the presence of this phenotype. Defects of the left hind limb were identified in 42.85% (3/7) of mutant embryos, and the right hind limb was also affected in 42.85% (3/7) of mutant embryos. Defects of the hind limbs were identified bilaterally in two mutant embryos and unilaterally in two, with three others showing no signs of malformations of the hind limb. The defects affecting this appendage varied between embryos, with some mutant embryos showing the full SHFM-like phenotype (Figure 6.8c, g), while others showed syndactyly of digits 2-3, with a reduced 'split' between digits 3 and 4 (Figure 6.8d, h). Additionally, some embryos had a curled tail (28.57%, 2/7) (Figure 6.8d) and one embryo (14.29%) was found to have a protruding liver (Figure 6.8e, i) reminiscent of the ventral body wall defects in *Tcfap2a* mutant embryos. One further embryo also had a small eye in comparison to controls (Figure 6.8c).

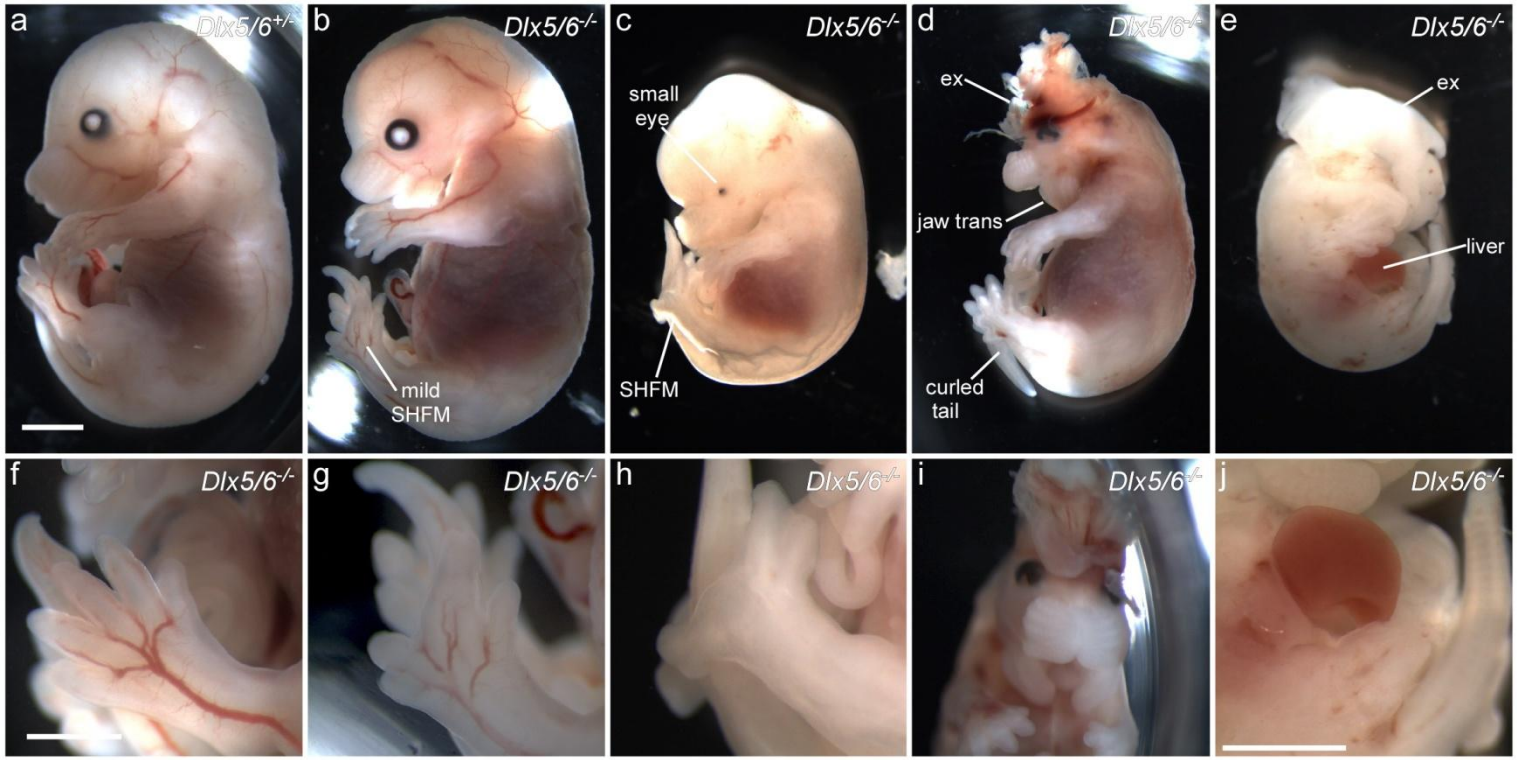

Figure 6.8: External phenotype of *Dlx5/6*$^{-/-}$ double mutant embryos.
(a) *Dlx5*$^{+/-}$ control embryo showing normal external phenotype. (b-j) *Dlx5/6*$^{-/-}$ mutant embryos with variable malformations. (b) Mutant embryo with mostly normal external phenotype showing a mild SHFM phenotype and jaw transformation. (c) Mutant embryo with severe SHFM phenotype and a small eye. (d) Mutant embryo with exencephaly (ex), jaw transformation (jaw trans) and a curled tail. (e) Mutant embryo with exencephaly and protruding liver. (f) The hind limb of a mutant embryo showing normal morphology. (g) The hind limb of the mutant embryo shown in (b) showing syndactyly of digits 2 and 3 and a split between digits 3 and 4. (h) The hind limb of the mutant embryo in (c) showing a complete SHFM phenotype. (i) A frontal view of the mutant embryo shown in (d) demonstrating the transformation of the lower jaw. (j) The protruding liver of the embryos shown in (e). Scale bars = 2mm (a-e), 1 mm (f-h), 2mm (j). (n=7).

6.2.5.2. CCVM phenotype

Dlx5/6$^{-/-}$ mutant embryos were collected at e15.5 for MRI analysis. However, two of the embryos were too young for MRI analysis (e14.5) and were examined by histology (Figure 6.9). At this stage in the control (*Dlx5/6*$^{+/-}$) embryo the interventricular septum had formed normally, separating the right and left ventricles (Figure 6.9a). Of the two mutant embryos examined by this method, one had developed a normal interventricular septum (Figure 6.9b) while the other had a small VSD (Figure 6.9c).

A further five mutant embryos were examined by MRI. No cardiovascular or thymus defects were observed in these embryos. However, examination of the palate revealed a severe clefting phenotype (Figure 6.10b-f), which was not observed in control embryos (Figure 6.10a).

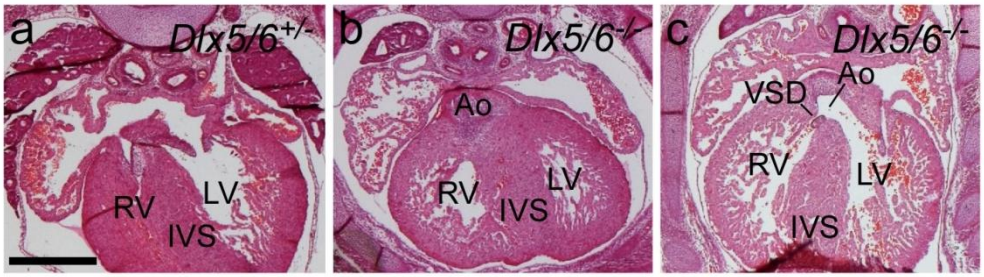

Figure 6.9: Cardiovascular phenotype of *Dlx5/6*$^{-/-}$ mutant embryos.
Ventricular septum formation in control (*Dlx5/6*$^{+/-}$) and mutant (*Dlx5/6*$^{-/-}$) embryos. (a) Control embryo showing normal formation of the interventricular septum (IVS) between the right (RV) and left ventricles (LV). (b) Mutant embryo with normal IVS formation. (c) Mutant embryo with small VSD. Ao, aorta. Scale bar = 500 µm. (n=2).

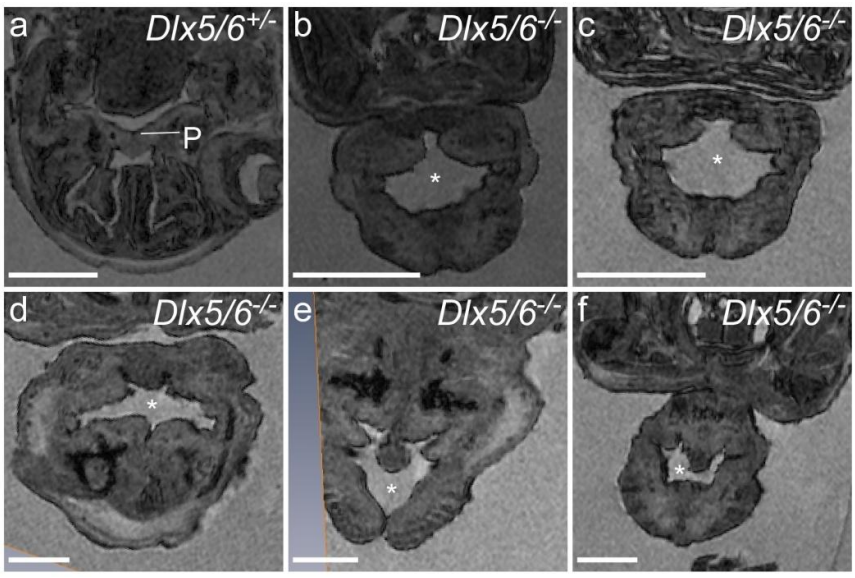

Figure 6.10: Palate formation in *Dlx5/6*$^{-/-}$ mutant embryos.
(a) Control (*Dlx5/6*$^{+/-}$) embryos show normal palate development (P). (b-f) Mutant (*Dlx5/6*$^{-/-}$) embryos show and almost complete absence of palate development (*). Scale bar = 100 µm. (n=5).

6.3. Discussion

6.3.1. Transcript analysis

Tcfap2a encodes the transcription factor AP-2α. Although it is clear that AP-2α is important for cardiovascular development, the transcriptional targets involved in this process are not understood. This chapter aimed to elucidate the downstream target genes of AP-2α in fourth PAA morphogenesis.

Firstly, we examined the expression of other AP-2 isoforms expressed within the NCCs. Both *Tcfap2b* and *Tcfap2c* encoding the transcription factors AP-2β and AP-2γ, respectively, are expressed within the NCCs during development (Chazaud *et al.*, 1996; Moser *et al.*, 1997b). There is significant homology between the different members of the AP-2 family of transcription factors, in particular within the DNA binding basic region encoded by exon 5 (Oulad-Abdelghani *et al.*, 1996). This allows the members of the AP-2 family to share a consensus binding sequence, although each will bind to a specific sequence with variable affinities. Therefore, the increase in expression levels of *Tcfap2b* and *Tcfap2c* in *Tcfap2a*$^{-/-}$ PA region may suggest some functional redundancy between these isoforms, within the NCCs. Interestingly, mutations of *TFAP2B* in humans (Satoda *et al.*, 2000) and *Tcfap2b* in mice (Zhao *et al.*, 2011) result in PDA, suggesting a role for AP-2β in cardiovascular development. *Tcfap2c*$^{-/-}$ mice, however, die at e9.5 due to deficiencies in trophoblast development (Werling and Schorle, 2002) and therefore, no similar studies have been possible.

Other genes were selected due to their involvement in cardiovascular development. The promoter regions of these genes were scanned for potential AP-2α binding sites, and those genes with the strongest or highest number of binding sites were selected for transcriptional analysis. A number of these genes, such as *Tgfb2*, *Chd7* and *Tbx1* have important roles in fourth PAA development (Lindsay *et al.*, 2001; Molin *et al.*, 2002; Randall *et al.*, 2009). *Tgfb2*$^{-/-}$ mice often have CORSA or cAoA as a result of aberrant regression of the fourth PAAs and persistence of the carotid ducts. The aberrant loss of the fourth PAAs in these mutants is accompanied by an increase in apoptosis in the surrounding mesenchyme. Additionally, the persistence of the right dorsal aorta is accompanied by a significant reduction in the levels of apoptosis surrounding these vessels (Molin *et al.*, 2002).

A number of genes such as *ErbB2*, *VEGF* and *Tbx20*, which have been previously identified as *Tcfap2a* targets (Bosher *et al.*, 1995; Gille *et al.*, 1997; Hammer *et al.*, 2008) have known roles in cardiovascular development. We therefore aimed to ascertain if the misregulation of these genes in the absence of *Tcfap2a* were likely to be causative of the observed phenotypes. We found very limited changes in the expression of any of these genes, with *ErbB2* being reduced to ~70% (but not reaching significance) in the mutants, while *VEGF* and *Tbx20* remained constant between controls and mutants. As the role of *ErbB2* during cardiovascular development is mostly restricted to ventricular trabeculation (Lee *et al.*, 1995) and no trabecular defects are observed in *Tcfap2a*$^{-/-}$ mutants, it stands to reason that this gene would not be affected in our mutants. It is therefore likely that *Tcfap2a* regulation of *ErbB2* is specific to other cell and tissue types.

6.3.2. *Fgf8* as a downstream target of AP-2α

The qPCR analysis presented in this chapter demonstrates a reduction of *Fgf8* expression to 78% of wild type expression levels within the PA region of *Tcfap2a*$^{-/-}$ mutant embryos. This marginal reduction in expression levels is likely due to the almost complete loss of expression within the mandibular component of the first PA ectoderm, as demonstrated by WISH. While, it seems that loss of expression from this region is not required for cardiovascular development, it may be responsible for elements of the craniofacial phenotype observed in *Tcfap2a*$^{-/-}$ mutant embryos. Additionally, our analysis has focussed on the PA region at e9.5. However, AP-2α may be involved in the regulation of *Fgf8* at different time points and in various regions of the body.

Fgf8 hypomorphic mutants show a number of cardiovascular defects similar to that seen in *Tcfap2a*$^{-/-}$ mutants, such as VSDs, DORV, IAA and abnormalities of the RSA (Abu-Issa *et al.*, 2002). In addition, genetic dissection techniques have demonstrated that loss of *Fgf8* within the pharyngeal ectoderm, recapitulates the fourth PAA malformations of the *Fgf8* hypomorphs (Macatee *et al.*, 2003). Therefore, it is possible that the loss of *Tcfap2a* expression within the surface ectoderm at later stages, results in a reduction in *Fgf8* expression in the caudal pharyngeal ectoderm. This may then be involved in the PAA malformations observed in *Tcfap2a*$^{-/-}$ mutant embryos.

In addition, *Fgf8* expression is also known to be required in limb development, another area which is affected in *Tcfap2a*$^{-/-}$ mutant embryos. At e9.5, the forelimb bud is only just beginning to form and this region was not included in our qPCR analysis. However, the work presented here suggests that *Fgf8* may be a downstream target of AP-2α in the developing mouse embryo and it would therefore be interesting to investigate the effect that loss of *Tcfap2a* has on the expression of this gene throughout the embryo as a whole.

6.3.3. *Dlx5* as a downstream target of AP-2α

Dlx5 was significantly downregulated in *Tcfap2a*$^{-/-}$ mouse embryos at a stage immediately before the formation of the fourth PAA and is coexpressed with *Tcfap2a* in the post-migratory NCCs of the PAs. Although a role for *Dlx5* in cardiovascular development has not yet been investigated, we postulated that the PAA defects observed in *Tcfap2a*$^{-/-}$ embryos are the result of the downregulation of *Dlx5* and/or its downstream targets.

Dlx5 expression begins at e8.25 in the ANR, and extends into the first PA by e9.0. By e10.5 expression has extended to the NCC-derived mesenchyme of PAs 1-4. Additionally, Dlx5$^{-/-}$ embryos show varying penetrance of exencephaly (12% -28%, dependant on genetic background) and cleft palate (88%) (Acampora *et al.*, 1999; Depew *et al.*, 1999), both of which are observed in *Wnt1cre*-mediated deletions of *Tcfap2a* (see section 3.2) (Brewer *et al.*, 2004). This suggests that *Dlx5* down regulation may be partially responsible for the external phenotypes in *Tcfap2a* mutants.

We propose that *Dlx5* is a direct downstream target of AP-2α within the NCCs. Our analysis of *Tcfap2a*$^{+/-}$*;Dlx5*$^{+/-}$ compound heterozygotes revealed a single embryo with exencephaly. This suggests that these genes may be involved in a similar pathway required for neural tube closure. However, on some genetic backgrounds *Tcfap2a*$^{+/-}$ heterozygous embryos have a low penetrance of exencephaly (Kohlbecker *et al.*, 2002) and therefore, the presence of the defect in *Tcfap2a*$^{+/-}$*;Dlx5*$^{+/-}$ embryos may be the result of *Tcfap2a* heterozygosity. Examination of the palate and thymus, the development of which are affected in *Tcfap2a*$^{-/-}$ mutant embryos and conditional deletions from the NCCs and PSE, revealed that both structures develop normally.

Additionally, no cardiovascular malformations were observed in any of the compound heterozygote embryos examined and neonates of this genotype survive at least the initial postnatal period.

Therefore, it appears that if *Dlx5* is a downstream target of AP-2α, we will require more complex genotypes in order to identify the role in cardiovascular development. In addition, the high levels of homology between the members of the *Dlx5* family may result in redundancy. We have demonstrated, through qPCR analysis, that the expression levels of *Dlx1-4* are not significantly affected by the loss of *Tcfap2a*. However, the expression of *Dlx1* and *Dlx2* appear marginally reduced, while the expression of *Dlx3* and *Dlx4* are more strongly reduced. Therefore, it is possible that the loss of *Tcfap2a* results in an overall downregulation of the *Dlx* family, which collectively result in the external malformations observed in the *Tcfap2a*$^{-/-}$ mutant embryos. In addition, our qPCR analysis revealed that both *Dlx5* and *Dlx6* are reduced to approximately 50% wild type expression levels in *Tcfap2a*$^{-/-}$ mutant embryos. Therefore, it is possible that *Dlx6* is able to act redundantly to *Dlx5* in our compound heterozygotes.

In addition, Jeong *et al.* (2008) demonstrate that the expression of *Dlx3* and *Dlx4* is disrupted in *Dlx5/6* mutant embryos. Therefore, it is possible that the downregulation of the other members of the *Dlx* family in *Tcfap2a*$^{-/-}$ mutant embryos is due simply to the reduced expression levels of both *Dlx5* and *Dlx6.*

6.3.4. *Dlx5* and *Dlx6* as downstream targets of AP-2α

Members of the *Dlx* gene family appear as paired clusters of genes within the genome, with shared enhancer elements in the intergenic region. Therefore, genes within each cluster (*Dlx1/2*, *Dlx3/4* and *Dlx5/6*) often have similar functions and target genes and are therefore thought to act redundantly to each other.

Dlx5 and *Dlx6* are capable of redundancy in target gene regulation. Jeong *et al*. (2008) performed an extensive analysis examining the regulation of downstream targets in *Dlx5/6*$^{-/-}$ mutant embryos. This study focussed on genes involved in craniofacial development, however, a number of genes that were differentially regulated in these mutants are also relevant to cardiovascular development. For example, *Gbx2*, *Hand1*

and *Hand2* were significantly downregulated in *Dlx5/6*$^{-/-}$ mutant embryos, while *Cyp26a1* was upregulated in comparison to wild type controls (Jeong *et al.*, 2008).

Both *Gbx2* and *Cyp26a1* are thought to be modifiers of the 22q11DS phenotype observed in *Tbx1* mutant mice. *Gbx2* mutant mice have unilateral hypoplasia/aplasia of the fourth PAAs as a result of defective NCC migration. Additionally, crossing *Gbx2* heterozygotes to *Tbx1* heterozygotes exacerbates the fourth PAA phenotype caused by *Tbx1* haploinsufficiency (Calmont *et al.*, 2009). *Cyp26a1* encodes a retinoic acid catabolist, which is downregulated in *Tbx1*$^{+/-}$ mice. Further, chemical inhibition of all Cyp26 isoforms (Cyp26a1, Cyp26b1 and Cyp26c1), in developing chicken embryos phenocopy the defects observed in 22q11DS (Roberts *et al.*, 2006). The SHF marker *Isl1* has also been suggested as an indirect target of *Dlx5* in inner ear development (Sajan *et al.*, 2011). Although *Tcfap2a* is not expressed within the SHF it has recently been proposed that *Isl1* is expressed within a small subset of NCCs which go on to infiltrate the cardiac OFT cushions and form the smooth muscle lining of the great vessels (Engleka *et al.*, 2012). *Hand* (Heart and neural crest derived)-1 and *Hand2* are also important transcription factors in cardiovascular development (Srivastava *et al.*, 1997).

The qPCR analysis presented here revealed that only *Hand2* is differentially regulated in *Tcfap2a*$^{-/-}$ mutant embryos. This is likely due to the incomplete knockdown of *Dlx5* and *Dlx6* expression in these mutants, and suggests that *Hand2* is more sensitive to the expression levels of *Dlx5* and *Dlx6* than other targets. WISH of *Hand2* expression on *Dlx5/6*$^{-/-}$ mutant embryos demonstrates a strong reduction in expression, however, the gene expression is not completely diminished (Jeong *et al.*, 2008). Therefore, in *Tcfap2a*$^{-/-}$ mutant embryos, where both *Dlx5* and *Dlx6* are only reduced to 50% wild type expression levels, it is not surprising that *Hand2* levels are only modestly reduced.

Double knock-out mice, with a deletion of both *Dlx5* and *Dlx6* show a homeotic transformation of the lower jaw, with the lower jaw being a mirror-image of the upper jaw (Beverdam *et al.*, 2002). These mice also show a split foot phenotype, in which the third digit fails to form correctly (Merlo *et al.*, 2002). Mutations in these genes have also shown to be linked with this phenotype in human patients SHFM (Crackower *et al.*, 1996). These patients have defects in the third digit of both the hands and feet,

however, Dlx5/6$^{-/-}$ mutant mice show this phenotype only in the hind limb (Merlo *et al.*, 2002).

Defects of the hind limbs were identified in 42.85% (4/7) of the *Dlx5/6*$^{-/-}$ embryos examined in this chapter. The phenotypes were variable between each mutant and between each limb in some mutants. This phenomenon has been reported in cases of SHFM in humans (reviewed in Duijf *et al.*, 2003). In addition, one embryo appeared to have a unilateral syndactyly of digits 2 and 3. Interestingly, this phenotype has been observed at low penetrance in BOFS patients with whole gene deletions of *TFAP2A* (Gestri *et al.*, 2009; Murray *et al.*, 2013). Microphthalmia, the appearance of a small eye, was identified in a single *Dlx5/6*$^{-/-}$ mutant embryo and is often found as part of the BOFS phenotype and was also described in *tfap2a* mutant zebrafish (Gestri *et al.*, 2009). Further, mental retardation, low-set ears, limb abnormalities and cleft lip/palate have also been described in patients with SHFM (reviewed in Duijf *et al.*, 2003). Therefore, it is possible that both *Dlx5* and *Dlx6* are downstream targets of AP-2α in mice, and that this regulation is conserved in humans and contributes to elements of the BOFS phenotype.

SHFM has been linked to 5 different chromosomal locations and patients are designated as SHFM1-5, dependant on the loci affected. SHFM1 and SHFM5 patients have deletions of members of the *Dlx* family of genes, and a number of these affected individual also have congenital heart defects (Elliott and Evans, 2008). Of these patients, 10% of SHFM1 (affecting *Dlx5/6*) patients and 47% of SHFM5 (affecting *Dlx1/2*) were found to have CCVM. These defects include a number of ASDs and VSDs, in addition to lower levels of TGA, PDA and total anomalous pulmonary venous return.

6.3.5. AP-2α regulates *Dlx5* and *Dlx6* in an endothelin-independent manner

Dlx5 and *Dlx6* are activated by the endothelin signalling pathway within the PAs, through a signalling cascade which results in the activation of the I56i intergenic enhancer element that lies between the two genes (Park *et al.*, 2004). ET-1 is a signalling molecule secreted by the PSE and the vascular endothelium and is received by the ET_A receptor expressed in the NCCs.

As *Tcfap2a* is expressed within the PSE and NCCs, it is possible that AP-2α may be regulating any one of these genes, resulting in reduced expression of both *Dlx5* and *Dlx6*. Therefore, we examined the expression of each of these genes and a small number of g-protein α-subunit genes (*Gnaq*, *Gna11*, *Gnas* and *Gnai*) by qPCR analysis, to identify any differential expression.

We found that the endothelin signalling pathway is not disrupted in *Tcfap2a*$^{-/-}$ mutant embryos, suggesting that the differential expression of *Dlx5/6* in *Tcfap2a*$^{-/-}$ mutant embryos is due to direct activation of these genes by the transcription factor AP-2α. In addition, it suggests a novel, endothelin-independent mechanism of activation of these genes.

The endothelin pathway is important in cardiovascular development and mutations in any element of this pathway results in severe CCVM. Mutations in *Edn1*, *ECE-1* or ET_A result in a number of cardiovascular defects affecting the development of the interventricular septum, the OFT and the PAAs (Kurihara *et al.*, 1995; Clouthier *et al.*, 1998; Yanagisawa *et al.*, 1998a). In addition, the first and second PAAs and the carotid ducts often persisted in these mutants (Yanagisawa *et al.*, 1998a). The similarities between the phenotypes of the endothelin mutants and *Tcfap2a*$^{-/-}$ embryos suggest a common pathway.

In addition, reports have also demonstrated cardiovascular defects in embryos with mutations of the α-subunits of the g-proteins examined here. Simultaneous knock-down of *Gnaq* and *Gna11* results in mouse embryos with a common ventricle (Offermanns *et al.*, 1998). Further, analysis of downstream targets of the ET_A receptor in these mutants demonstrated that expression of *Dlx3*, *Dlx6, Hand1* and *Hand2* were almost completely lost in these mutants, while *Dlx5* was not examined (Ivey *et al.*, 2003).

We hypothesised that *Dlx5* and *Dlx6* were the common denominators that link the similar cardiovascular phenotypes observed between the endothelin pathway mutants and those of *Tcfap2a*$^{-/-}$ embryos. However, examination of cardiovascular development in *Tcfap2a*$^{+/-}$*;Dlx5*$^{+/-}$ compound heterozygotes revealed no defects. In addition, no CCVM was identified in *Dlx5/6*$^{-/-}$ double mutant embryos, therefore

suggesting that *Dlx5* and *Dlx6* are not required for correct cardiovascular development. Severe malformations of the palate were identified in the *Dlx5/6*$^{-/-}$ mutants, however, suggesting that the reduced expression of these genes within the NCCs may contribute towards the cleft palate phenotype observed in *Tcfap2a*$^{f/-}$*;Wnt1cre* mutant embryos.

6.3.6. Advantages and disadvantages of this study

This study has been carried out to investigate the potential transcriptional targets of the transcription factor AP-2α in fourth PAA development. In this study, we collected only the PA region of embryos to prevent any changes being diluted out by expression in other regions of the developing embryo. This allowed us to focus only on the gene expression changes involved in PA and cardiovascular development. This principal is supported by the strong reduction in *Fgf8* expression within a small part of the region under investigation, which led to an overall reduction in expression to approximately 80%. It is likely that if we had produced RNA using the entire embryo, that this minor change would not have reached statistical significance. The avoidance of the dilution of changes in gene expression levels could have been further improved by targeting specific tissues of *Tcfap2a* expression, such as the NCCs and PSE. However, dissecting out these tissues alone would prove very technically difficult. A further approach would be to use fluorescence-activated cell sorting (FACS) to select only tissues expressing the cre line of interest. However, the genetic dissection of *Tcfap2a* did not reveal a specific tissue in which *Tcfap2a* was required. In addition, these approaches would result in much lower levels of RNA and therefore dramatically increase the number of embryos required.

The use of qPCR was chosen over microarray to allow for a more specific choice of candidate genes. This approach allowed us to validate all genes as potential targets in advance, through literature searches and by examining the promoter regions for AP-2 binding sites.

A further disadvantage of this study is that the gene expression profile was examined only at e9.5, in order to elucidate the targets of AP-2α in fourth PAA development. At this time point we identified only 2 candidates for further analysis. However, it is possible that at different time points other candidate genes may have been differentially regulated.

6.4. Further work

The work presented above suggests that *Dlx5* and *Dlx6* are downstream targets of the transcription factor AP-2α in PA and cardiovascular development. However, this work is not without limitations (as discussed above).

Disappointingly the genetic interaction study between *Tcfap2a* and *Dlx5* did not result in a cardiovascular phenotype. Therefore, it would be interesting to examine further crosses between these two strains to investigate their interaction.

The expression levels of many of the *Dlx* family members were reduced in *Tcfap2a*$^{-/-}$ mutant embryos. Therefore, it would be interesting to investigate any changes in expression patterns by WISH of these genes to determine if they are affected in the caudal PAs. It would also be interesting to investigate the expression patterns of the other AP-2 family genes. *Tcfap2b* and *Tcfap2c* were both found to be significantly upregulated in this analysis, potentially to compensate for the loss of *Tcfap2a* in a redundant manner. Therefore, WISH analysis of these genes in *Tcfap2a* mutant embryo would allow us to understand where these changes take place.

Analysis of target genes by qPCR at e9.5 yielded few potential downstream effectors of AP-2α. However, this study was focussed specifically on the formation of the fourth PAA, which forms only one part of the *Tcfap2a*$^{-/-}$ phenotype. Therefore, further investigations are required to determine the role of *Tcfap2a* in the formation of the interventricular septum and the OFT.

Chapter 7. Final Discussion

7.1. Introduction

Tcfap2a has an important role in cardiovascular development, and absence of this gene results in severe CCVM. However, the mechanisms through which CCVM occurs in *Tcfap2a*$^{-/-}$ mutant mice have not yet been elucidated. This thesis provides the first extensive study of the role of *Tcfap2a* in cardiovascular development.

Although, we have been unable to provide definitive answers as to the function of *Tcfap2a* in cardiovascular development, we have identified a number of possible mechanisms which are disrupted in the absence of this gene. Work in this thesis provides the first insight into defects of NCC migration within *Tcfap2a* mutants. Further, we have identified possible downstream target genes, which may be involved in the defects identified in the mutant embryos.

In addition, a number of extracardiac defects, affecting craniofacial development, neural tube and body wall closure and the correct development of the thymic rudiments, have also been identified in these mutants. Here we have provided insight into potential tissue-specific dysregulation of *Tcfap2a* in the appearance of a number of these defects.

7.2. PAA malformation in *Tcfap2a*$^{-/-}$ mutant embryos

In this thesis we describe a number of mutant embryos with malformations of the PAAs. The *Tcfap2a*$^{-/-}$ mutant embryos on a congenic C57BL/6J background have a fully penetrant PAA phenotype, contrary to the previously published work on this model (Brewer *et al.*, 2002). In addition, the defects observed in the NCC-specific deletion of *Tcfap2a* affected the PAA system only. Furthermore, although the ubiquitously expressed cre lines (*PGKcre* and *Sox2cre*) failed to fully recapitulate the phenotype observed in *Tcfap2a*$^{-/-}$ mutant embryos, almost 90% of these embryos showed some form of PAA malformation, affecting the fourth PAAs. Therefore, it appears that, at least on the background examined here, *Tcfap2a* expression is highly important in the development of the PAAs. In addition, the fourth PAAs seem to be particularly susceptible to genetic defects and a number of mutants have been discussed throughout this thesis in which the development of the fourth PAA is disrupted (*Tbx1*,

Chd7, *Fgf8*, *En1*, *ECE1*, *Ednra*, *Gbx2* (Kurihara *et al.*, 1995; Clouthier *et al.*, 1998; Yanagisawa *et al.*, 1998a; Lindsay *et al.*, 2001; Abu-Issa *et al.*, 2002; Byrd and Meyers, 2005; Calmont *et al.*, 2009; Randall *et al.*, 2009). It is possible that these defects are the result of the absence of SMCs lining a small portion of the fourth PAAs in mice (Bergwerff *et al.*, 1999). A wild type embryo is able to survive, without any malformations of the fourth PAAs, in spite of this absent portion of smooth muscle. However, in the presence of mutations of a gene which is important in the development of this vessel, the vessel is unable to persist and therefore collapses. This theory, however, does not account for the fact that in many embryos with a mutation in one of these genes, the defects are visible from e10.5. Data presented in this thesis demonstrates that the fourth PAA does not become invested with SMCs until later (approximately e11.5). Therefore, the reduced level of smooth muscle within the fourth PAA cannot account for defects observed before this time. It is likely that the PAA defects observed within these mutants are the result of the reduced investment of NCC within the PAs, which is required to support the vessel before SMC differentiation occurs (Waldo *et al.*, 1996).

This suggests that the role of *Tcfap2a* in PAA development lies within the NCCs, and that in the absence of this transcription factor, the NCCs are unable to migrate into the fourth PA in sufficient numbers. However, signalling from the PSE is important in migration of the NCC into the PAs (see section 1.3.4.2) and it is therefore possible that the defective NCC migration that we observe in *Tcfap2a*$^{-/-}$ mutant embryos, is a consequence of the increased levels of apoptosis in the PSE, which reduces the number of cells and therefore the levels of signalling between the two tissues. As *Fgf8* expression is reduced in the first PA of *Tcfap2a*$^{-/-}$ mutant embryos at e9.5, it is possible that this gene is also under the regulation of *Tcfap2a* within the PSE of the caudal arches at later stages. *Fgf8* hypomorphs display a number of PAA malformations similar to that observed in *Tcfap2a*$^{-/-}$ mutant embryos (Abu-Issa *et al.*, 2002), which can be recapitulated by tissue-specific removal from the PSE (Macatee *et al.*, 2003). A further possibility is that *Tcfap2a* is required for cell survival. Apoptosis was examined at e10.5 in these mutant embryos. At this stage *Tcfap2a* is no longer expressed in the NCCs, but continues to be expressed within the PSE (Brewer *et al.*, 2002). Therefore,

the reduced numbers of NCCs within the fourth PA at e10.5 may be the result of increased cell death within this population at e9.5.

7.3. Genetic background

A common theme throughout this thesis is the effect of the genetic background on the phenotypes observed. The change in genetic background from that used by Brewer *et al*. (2002) to that used by our group revealed an important increase in the levels of PAA malformations, which allowed us to examine the mechanisms resulting in these defects. In addition, we have also demonstrated that the penetrance of CCVM, cP and neural tube defects observed in the NCC-specific mutant embryos differ, dependant on the genetic background of the mutant embryo.

This phenomenon has previously been described in work on the Df1 mouse model of 22q11DS. This work demonstrates that approximately 50% of heterozygous embryos have some form of CCVM on a C57BL/6J background, which was reduced to 16% of embryos on 129SvEv background. This pattern was also mirrored in the prevalence of thymus malformations in these mutants (Taddei *et al.*, 2001).

An extreme example of alterations in genetic background can be seen in mice with mutations of the EGFR. On a CF-1 background these mice die at the peri-implantation stage (before e6.5), whereas on a 129/Sv background these embryos implanted into the uterine wall normally, but were unable to survive past mid-gestation (e12.5). Furthermore, outbreeding onto a CD-1 background allowed these mutants to survive for up to 18 days post parturition (Threadgill *et al.*, 1995).

Therefore, this work highlights the importance of using a defined genetic background when investigating mouse models. In addition, it is also important to accurately report the genetic background so that others can interpret the role of the genetic background more accurately. Unfortunately, due to the time required to produce an inbred strain, and the increased research costs associated with this, it is not always feasible.

7.4. Redundancy

We have demonstrated that the *Tcfap2a*^{flox} allele is unable to recapitulate the cardiovascular malformations observed in the *Tcfap2a*$^{-/-}$ mutant embryos, suggesting

that the *Tcfap2a*-null allele has a DN effect on the other AP-2 isoforms. In addition, qPCR of the mutant PA region demonstrated a small, but statistically significant increase in the level of other AP-2 family genes in the absence of *Tcfap2a*. This suggests that there may be some redundancy between these isoforms.

It has previously been proposed that the phenotypes observed upon mutation of these isoforms are too divergent to indicate functional redundancy (Hilger-Eversheim *et al.*, 2000; Eckert *et al.*, 2005). Embryos with mutations in *Tcfap2a* have severe morphological defects affecting limb, kidney, eye and cranial ganglia development, and exhibit an open neural tube and open ventral body wall in addition to severe craniofacial malformations and die at birth (Schorle *et al.*, 1996; Zhang *et al.*, 1996; Brewer *et al.*, 2002). *Tcfap2b*$^{-/-}$ embryos, however, are able to survive for up to 2 weeks after birth, before dying from polycystic kidney disease and hypocalcaemia (Moser *et al.*, 1997a; Moser *et al.*, 2003). *Tcfap2c*-null embryos die in early embryogenesis due to a failure of gastrulation, resulting in growth retardation by e7.5 and embryos are reabsorbed by e9.5 (Werling and Schorle, 2002).

However, analysis of the amino acid composition of AP-2α, -β and -γ demonstrated high levels of homology between the three isoforms, with the greatest protein identity within the basic domain and the first helix of the HSH motif (AP-2α and AP-2β - 97%, AP-2α and AP-2γ - 99%, AP-2β and AP-2γ – 96%) (Oulad-Abdelghani *et al.*, 1996). This high homology in the DNA binding domain suggests the proteins are capable of binding to and activating many of the same target genes.

In addition, these genes also exhibit overlapping expression domains. From e8.0 *Tcfap2b* expression is observed in the lateral head mesenchyme, the neural folds and the extraembryonic trophoblast. This pattern overlaps with that of early NCCs (Moser *et al.*, 1997b). At e9.0 both genes are detected in the PSE, midbrain, hindbrain and spinal cord. This pattern continues at e10.0, with additional expression in the facial mesenchyme, dorsal root ganglia and the first PA. From e11.0 expression of the two isoforms begin to diverge as *Tcfap2b* expression becomes more intense in the midbrain, *Tcfap2a* expression is no longer detected (Moser *et al.*, 1997b).

Tcfap2c in the mouse is expressed in the neural plate, surface ectoderm and extraembryonic tissue at e7.5. By e8.0-8.5 expression is also seen in the premigratory and migrating NCCs. Later expression can be seen in the facial mesenchyme, surface ectoderm and nasal and oral epithelium. Expression is also seen in the progress zone of the limb bud (Chazaud *et al.*, 1996).

In zebrafish, *tfap2a*, is the only isoform expressed within the NCCs, however, all three isoforms are co-expressed within the surface ectoderm (Knight *et al.*, 2005). However, double knock-down studies have been conducted, that suggest AP-2α may act redundantly with AP-2β and -γ in processes such as craniofacial skeleton development and NCC maintenance. Knock-down of *tfap2b* in *low* zebrafish demonstrated severe defects in all pharyngeal cartilages, suggesting that AP-2α and AP-2β work together within the PSE to induce development of the NCC-derived skeletal elements. Transplantation of ectoderm from wild-type embryos into these double mutant embryos resulted in partial rescue of the pharyngeal cartilage phenotype (Knight *et al.*, 2005).

Double knock-out of *tfap2a* and *tfap2c* results in the absence of pigmentation and PA cartilage (Li and Cornell, 2007). In addition, knock-down of *tfap2c* in *low* zebrafish demonstrated a reduction of *foxd3* expression in pre-migratory NCCs, suggesting that *tfap2a* and *tfap2c* are required together in the maintenance of the NC (Hoffman *et al.*, 2007).

In addition to the evidence of redundancy in zebrafish embryos, the phenotypes observed in humans with mutations in these genes also show a number of similarities. Human *TFAP2B* has been identified as the gene responsible for Char syndrome, an autosomal dominant disease characterised by PDA, facial malformations and anomalies of the fifth digit of the hand. This disease has been found to be the result of the production of a DN protein product (Satoda *et al.*, 2000). Therefore, it is possible that some of the phenotypes identified in these embryos, such as facial dysmorphism and limb abnormalities are the result of a DN effect on *TFAP2A,* resulting in some overlap between Char syndrome and BOFS. Furthermore, a 4.5 Mb deletion containing *TFAP2C* (20q13.2-13.3) has been identified. The patients displayed pre- and

postnatal growth retardation, hypotonia and facial dysmorphism (Genevieve *et al.*, 2005).

Therefore, it appears that there is sufficient evidence from studies of both mouse and zebrafish development, in addition to phenotypic data from patients, to suggest that at least these three members of the AP-2 family are capable of acting in a redundant manner. In addition, the overlapping expression within the surface ectoderm and NCCs suggests that these three genes may function redundantly to activate the same target genes in PAA development.

7.5. Branchio-oculo facial syndrome

The tissue-specific deletions of *Tcfap2a* presented within this thesis demonstrate a number of more subtle phenotypes, which could not be identified within the *Tcfap2a*$^{-/-}$ mutant embryo. These phenotypes include cleft palate, craniofacial malformations and thymus defects, many of which are reminiscent of BOFS.

BOFS is a syndrome which results from *TFAP2A* mutations in humans. This disease consists of a branchial, ocular and facial phenotype – as the name suggests – however, there are also a multitude of defects observed at varying degrees within these patients. A number of BOFS patients present with defects affecting the development of the limbs, such as syndactyly, kidney abnormalities, including polycystic kidneys, and a small number of cardiovascular abnormalities. Interestingly, one of these patients presented with TOF (Reiber *et al.*, 2010). In addition, Brewer *et al*. (2002) described two cases of potential TOF in *Tcfap2a*$^{-/-}$ mice. Although, this malformation was not found in our work, we identified a number of embryos with VSD and OA, in the absence of the further phenotypes characteristic of TOF. Furthermore, *TFAP2A* has been associated with the regulation of *TBX20* in a group of patients presenting with TOF (Hammer *et al.*, 2008). *TBX20* was found to be significantly upregulated in cardiac biopsies of TOF patients, although no mutations were seen in this gene. *TFAP2A, -B* and *–C* were found to negatively regulate the *TBX20* gene, and *TFAP2C* levels were significantly reduced in the cardiac biopsies of TOF patients, suggesting a possible role of *TFAP2C* in the TOF phenotype by de-regulation of *TBX20*.

Despite the strong evidence of CCVM in mouse mutants of *Tcfap2a*, the prevalence of these defects in BOFS patients is remarkably low, with only 3 reported cases of cardiovascular malformations to date (of approximately 100 patients). However, it is likely that much of this is due to the nature of the mutations present in BOFS patients. CCVM is identified in all mouse embryos homozygous for a large deletion of the *Tcfap2a* gene. The mutations in patients are heterozygous, and most commonly affect only a small number of nucleotides. Therefore, it is likely that those BOFS patients with CCVM also have mutations at a modifying locus that further affects the phenotype. Due to the severity of defects observed in *Tcfap2a*$^{-/-}$ mouse embryos, it is likely that an infant with homozygous mutation would be unable to survive to term, or would die in the immediate postnatal period.

Furthermore, echocardiography to examine the heart is only requested by physicians in cases where a patient is suspected of impaired cardiac function (Milunsky *et al.*, 2011), therefore, the cardiovascular phenotype is unknown in approximately 50% of patients. In addition, in patients with more subtle malformations, such as those affecting the formation of the RSA, it is unlikely that an impaired cardiac function would be detected. For example, the presence of an A-RSA, which was identified in a number of *Tcfap2a*$^{-/-}$ and *Tcfap2a*$^{f/-}$*;Wnt1cre* mutant embryos in this thesis, usually presents as dysphagia. It is, therefore, unlikely that echocardiography would be carried out in this instance, suggesting many more BOFS patients may have CCVM, than are currently reported in the literature.

More commonly identified malformations in BOFS patients include cleft lip and thymus malformations, both of which are identified upon tissue-specific removal of *Tcfap2a* from the ectoderm using *Foxg1cre*. We identified, a fully penetrant frontonasal defect in *Tcfap2a*$^{f/-}$*;Foxg1cre* mutant embryos, which is reminiscent of some of the more severe facial malformations in BOFS patients. Of the 41 BOFS patients analysed by Milunsky *et al.* (2011), only 6 had no defects of the lip, while another was described with an abnormal philtrum. Nine patients were identified with a complete bilateral cleft lip, while a further 10 patients exhibited a unilateral cleft lip. The remaining patients had pseudo clefts of the lip, which are reminiscent of a badly repaired cleft lip. Therefore, the *Tcfap2a*$^{f/-}$*;Foxg1cre* mutant mice may offer a unique model for the

examination of many of the facial phenotypes observed in BOFS patients. In addition, a number of patients presented with cleft palate in addition to the cleft lip discussed above (10/41 patients analysed by Milunsky *et al.* (2011)). This phenotype was observed at varying levels in all the embryos with a tissue-specific deletion of *Tcfap2a* from the NCCs. This, therefore, suggests some involvement of the NCCs in the phenotypes described in BOFS patients. Furthermore, as discussed in chapter 3 (see section 3.3.3), the thymus defects observed in the *Tcfap2a*$^{f/-}$*;Foxg1cre* mutant embryos are similar to that identified in BOFS patients, and are further exacerbated by the additional removal of *Tcfap2a* from the NCCs. The tissue-specific deletion presented here, therefore, may provide a unique mouse model for the investigation of the phenotypes observed in BOFS patients.

7.6. Findings in relation to initial aims

The work presented has addressed the aims set out in the Introduction chapter, as follows:

7.6.1. To investigate the role of *Tcfap2a* within the NCCs on a congenic C57BL/6J background.

The preliminary data collected demonstrated a 55% penetrance of CCVM in *Tcfap2a*$^{f/-}$*;Wnt1cre* mutant embryos, on a 72.55% C57BL/6J background. In this thesis, we set out to examine these mutant embryos on a more congenic background (94% C57BL/6J). We identified a reduction in the levels of CCVM observed in these *Tcfap2a*$^{f/-}$*;Wnt1cre* mutant embryos on a 94% C57BL/6J background, compared to a 72% C57Bl/6J background. In addition, we also identified a number of other phenotypes, which were affected by the change in genetic background, including cleft palate and exencephaly. The prevalence of cleft palate was higher in *Tcfap2a*$^{f/-}$*;Wnt1cre* on a 94% C57BL/6J (40%, compared to only 20% on a 72% C57BL/6J background), whereas the prevalence of exencephaly was reduced from 45% (72% C57BL/6J) to 5% (94% C57BL/6J). This suggests that the role of *Tcfap2a* in the NCCs is not restricted to cardiovascular development, but also is involved in the correct formation and fusion of the palatal shelves and neural tube.

7.6.2. To investigate the role of genetic background in the variation of CCVM observed.

In addition to investigating the NCC-specific deletion of *Tcfap2a* on a congenic background, we also outbred these mutant embryos to a CD1 background. This allowed us to further investigate how the genetic background affects the defects observed in *Tcfap2a*$^{f/-}$*;Wnt1cre* mutant embryos. We found no CCVM in these mutant embryos. However, we identified that the phenotypes varied considerably between each of the backgrounds examined. While the prevalence of CCVM in this background was completely diminished, the levels of cleft palate were higher than on either of the previously examined backgrounds (66.66%). In addition, the rate of exencephaly in this background was similar to that observed in the preliminary data (40% compared to 45% in the preliminary data). This suggests that modifier loci are present on each of the three backgrounds examined, which result in altered prevalence of each of the phenotypes examined. For a summary see Table 3-1.

7.6.3. To investigate the role of *Tcfap2a* in PAA formation and remodelling.

In chapter 5, we conducted a thorough examination of the PAA defects observed in *Tcfap2a*$^{-/-}$embryos. Embryos were examined between stages e9.5-11.5 to identify the timing and etiology of the fourth PAA defects observed at e15.5. We determined that only approximately 50% of the defects of the right fourth PAA observed at e15.5 were the result of a primary failure in the formation of the vessels by e10.5. In addition, we suggest that these primary defects are caused by the reduced number of NCCs within the PA region, which support the vessel as it forms. The remaining 50% of defects of the right fourth PAA are likely to result from the loss of smooth muscle deposition around the vessels by e11.5.

7.6.4. To investigate potential transcriptional targets of *Tcfap2a* in cardiovascular and PAA development.

This thesis investigated transcriptional changes in a number of potential AP-2α target genes and identified *Fgf8* and *Dlx5* as putative downstream targets. These genes were further investigated to identify spatial changes in expression patterns. We propose that *Dlx5* is a target of AP-2α in a pathway that is likely to be independent of endothelin-1 signalling. We further identified that *Dlx6* and the *Dlx5/6* downstream target, *Hand2*, are significantly downregulated in *Tcfap2a*$^{-/-}$ mutant embryos at e9.5. Interbreeding of *Tcfap2a*$^{+/-}$ and *Dlx5*$^{+/-}$ mice failed to produce any relevant phenotypes,

however, *Dlx5/6*$^{-/-}$ mutant embryos showed a complete failure in palate formation. Therefore, it is possible that the cleft palate phenotype identified in *Tcfap2a*$^{f/-}$*;Wnt1cre* mutant is related to a reduction in the expression of both *Dlx5* and *Dlx6* in the NCCs.

7.7. Model of *Tcfap2a* function in cardiovascular development.

For the purpose of cardiovascular development *Tcfap2a* is only expressed in the NCCs and PSE (Figure 7.1). Therefore, the role of the protein product in regulating cardiovascular development is likely to lie in these tissues. Our qPCR analysis suggests that AP-2α is involved in the regulation of *Dlx5*, *Dlx6*, *Fgf8* and *Hand2*. Of these four genes, only *Fgf8* is expressed in the PSE, while *Dlx5*, *Dlx6* and *Hand2* are expressed within the NC-derived mesenchyme of the PAs. *Dlx5* and *Dlx6* are activated by the endothelin signalling pathway, which originates from the PSE. However, the expression levels of the genes involve in endothelin signalling pathway are unaffected in *Tcfap2a*$^{-/-}$ mutant embryos at e9.5. Therefore, regulation of *Dlx5/6* by AP-2α is likely to occur in the NC-derived PA mesenchyme, and be independent of Endothelin-mediated regulation of these genes; although we cannot rule out the possibility that *Tcfap2a* is activated by $G\alpha_{q/11}$, which then leads to activation of *Dlx5/6*. In addition, the down regulation of *Hand2* is likely due to the reduced levels of *Dlx5/6* activation in these mutant embryos. This does not, however, affect the expression of other *Dlx5/6* targets, such as *Gbx2*, *Hand1* and *Cyp26a1*.

In addition, our data suggests that AP-2α is capable of regulating *Fgf8* in the PSE. Although, the WISH experiment suggests that this regulation occurs only within the first PA, it is likely that AP-2α is capable of activating *Fgf8* expression in the more caudal arches at later stages. In this case, the reduced expression of *Fgf8* in the PSE may be a contributing factor to the reduced number of NCCs migrating into the fourth PA. FGF8 signals from the PSE are received by the FGF receptors FGFR1 and FGFR3, within the NCCs, which then signals the cells to migrate into the PAs (see section 1.3.4.2). In this model, AP-2α is responsible for activating *Fgf8* in the PSE. In the absence of AP-2α, FGF8 signals are reduced or diminished, causing a reduction in the numbers of NCCs migrating into the PA region. This results in the PAAs not being supported during development and therefore collapsing.

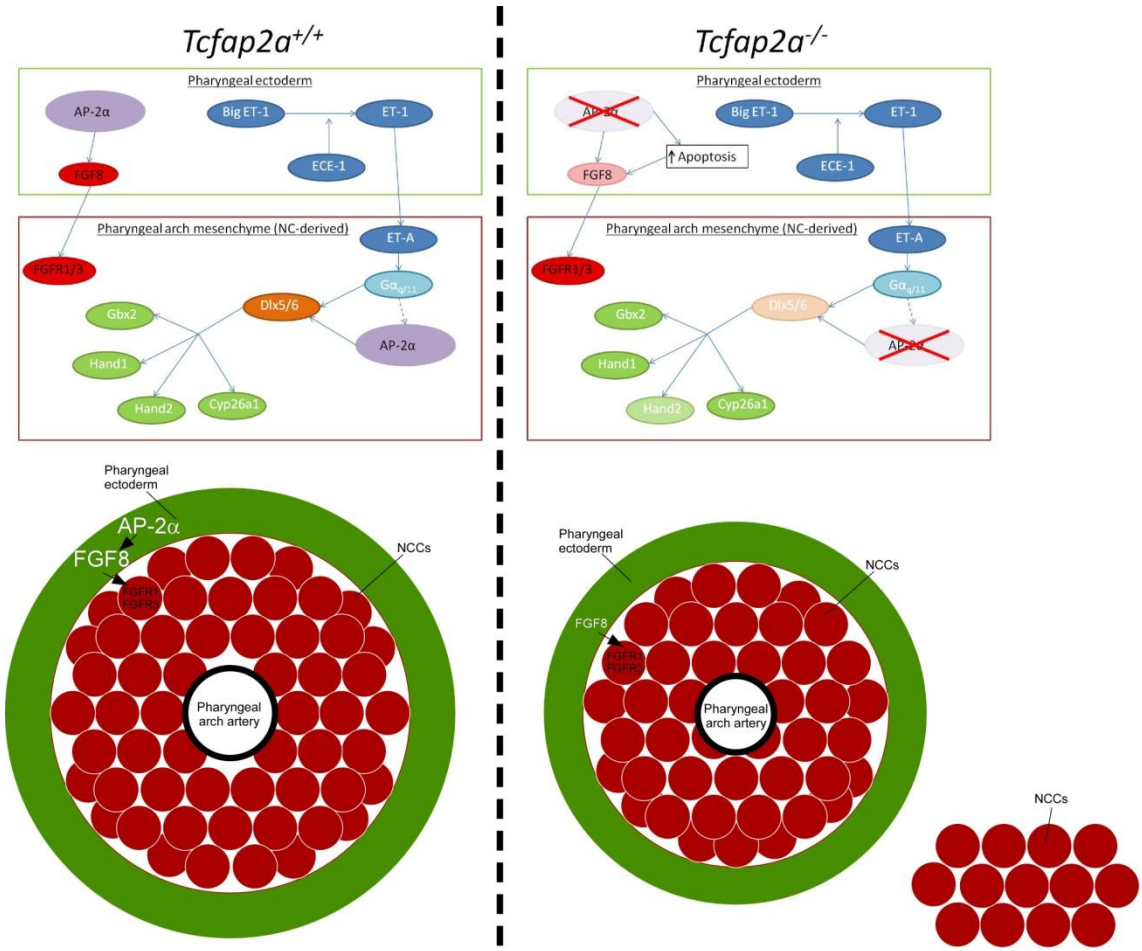

Figure 7.1: Model of *Tcfap2a* function in cardiovascular development.
In a wild type embryo, *Tcfap2a* is expressed and translated within both the ectoderm and NCCs of the PA region. The data presented within this thesis suggests that AP-2α is capable of regulating *Fgf8* expression within the PSE and *Dlx5/6* within the NCCs. In turn, *Dlx5/6* then activate a number of further downstream targets. In addition, FGF8 signals to FGFR1 and FGFR3 within the NCCs and assists in the migration of the NCCs into the PA. In *Tcfap2a*$^{-/-}$ mutant embryos, *Fgf8* expression is reduced in the PSE, which is likely to result in a reduction in the levels of FGF8 signalling to FGFR1 and FGFR3 in the NCCs. In addition, the increase in the levels of apoptosis within the PSE is also likely to have an impact on *Fgf8* expression levels. Loss of AP-2α in the NCCs results in a decrease in the levels of *Dlx5/6*, which also causes a reduction in *Hand2* expression, without affecting other *Dlx5/6* targets. The reduced signalling between FGF8 and FGFR1/3 also impacts on the migration of the NCCs into the PA region, resulting in fewer NCCs migrating into the PA region. This causes the PA to be smaller and reduces the amount of support the PAA receives from the surrounding cells. As a result, the PAA fails to form a patent vessel and collapses.

7.8. Further work

Although this thesis addresses a number of questions relating to the role of *Tcfap2a* in both cardiovascular development and craniofacial development, some further experiments could complement the work presented here.

7.8.1. PAA defects in *Tcfap2a*$^{-/-}$ mutant embryos

The work presented in this thesis suggests that the PAA defects result from a reduction in the number of NCCs within the PA region. It appears that the reduction in NCC number is due to the increase in the levels of apoptosis within the PSE, which in turn would cause a reduction in the levels of signalling between the PSE and the NCCs,

which aid in their migration. However, this could not be definitively proven using the data acquired here. Therefore, further experimentation would be necessary to determine if this was, in fact, the case.

Initial experiments would focus on lineage tracing of the NCCs, using the R26R^{EYFP} construct in conjunction with *Wnt1cre*, in whole mount and in sections. Alternatively, WISH or whole mount immunohistochemistry of a NCC marker, such as *Sox10* (which was unaffected in the transcriptional target analysis) may be used. This would allow us to determine if the NCCs are halted at some point along their migratory pathway, or if the initial delamination of NCCs in disrupted, preventing the cells from migrating to their final locations. Lineage tracing should be carried out at several stages between e8.5-e10.5, to determine when the migratory defect is occurring. If the migration of the NCCs is disrupted in the circumpharyngeal region, it may again suggest that the signalling from the PSE to the NCCs is disturbed in these mutant embryos. If this were the case, it would be important to examine the pathways involved in this process, and to determine how the signalling is disturbed. Immunohistochemistry could be used for this purpose. Examination of FGF8 and other FGF family members would be important, as both the qPCR and WISH data suggests that *Fgf8* is a putative downstream target of AP-2α. Additionally, it would also be important to examine the expression of the receptors of these signalling molecules within the NCCs, to determine if the NCCs are capable of receiving the secreted signals. The receptors to be examined would be FGFR1 and FGFR3, however, other receptors and alternative signalling pathways may also be examined.

If the results of the lineage tracing experiments do not suggest that NCC migration is being inhibited in any way, it would be possible that the NCCs are dying *en route* to the PA region, or even prior to delaminating from the neural tube. In this instance, whole mount terminal deoxynucleotidyl transferase dUTP nick end labelling may be appropriate, to determine if the NCCs are undergoing cell death, therefore reducing the numbers available to migrate into the PAs. Again, examination of various stages between e8.5-e10.5 would be necessary, to determine when cell death is occurring. Alternatively, further immunofluorescence staining using the pHH3 and caspase3 antibodies at these stages would also be possible. This would allow the

proliferation/apoptosis indices to be calculated, and would therefore allow for statistical examination of these processes.

7.8.2. Downstream targets of AP-2α

The qPCR analysis carried out has suggested two new, putative, target genes of AP-2α: *Dlx5* and *Fgf8*. However, further experimentation is required in order to validate these genes as downstream targets. Although *Fgf8* expression was significantly reduced at e9.5 in *Tcfap2a*$^{-/-}$ mutant embryos, WISH suggested that the changes in spatial expression of this gene is not likely to affect cardiovascular development. However, it is possible that reduced expression of *Fgf8* at later stages is responsible for some of the PAA defects observed in *Tcfap2a*$^{-/-}$ mutant embryos. Therefore, the expression levels of this gene at e10.5 and e11.5 should also be examined by qPCR, and complemented with further WISH at these stages. In addition, downstream targets of FGF8 should also be examined. WISH should also be used to validate the results obtained by qPCR for *Dlx6*, *Hand2*, *Tcfap2b* and *Tcfap2c*. It would also be interesting to repeat the qPCR examination at various other stages between e10.5-15.5 to identify any roles these genes may have in other processes during cardiovascular development.

Following on from the qPCR analysis and subsequent validation by WISH, it would be important to determine if the putative targets are directly activated by AP-2α. This could be confirmed using a luciferase assay, which would require the cloning of a region of the promoter of the gene of interest into a luciferase expression vector and examining the levels of promoter activation upon the addition of AP-2α. Alternatively, chromatin immunoprecipitation may also be used to determine if AP-2α is capable of binding directly to the promoter region of a gene of interest.

Although the *Tcfap2a*$^{+/-}$*;Dlx5*$^{+/-}$ compound heterozygote embryos did not show any cardiovascular phenotypes, it is possible that more complex mutants are required in order to produce a phenotype. It will therefore be important to examine embryos of the genotype *Tcfap2a*$^{+/-}$*;Dlx5*$^{-/-}$ to understand if completely knocking-out *Dlx5*, in the presence of only a single *Tcfap2a* allele, will result in a cardiovascular phenotype. It is likely, due to the severity of the *Tcfap2a*$^{-/-}$ external phenotype, that embryos of the genotypes *Tcfap2a*$^{-/-}$*;Dlx5*$^{+/-}$ and *Tcfap2a*$^{-/-}$*;Dlx5*$^{-/-}$ will prove difficult to examine for either external defects or cardiovascular malformations. However, if there are no

further defects in the *Tcfap2a*$^{+/-}$*;Dlx5*$^{-/-}$ mutant embryos, then these other genotypes should also be examined.

7.8.3. Craniofacial development and BOFS

Tcfap2a$^{f/-}$*;Foxg1cre* mutant embryos on a C57BL/6J background were shown in this thesis to have a frontonasal defect reminiscent of the cleft lip phenotype that is often observed in BOFS patients. Therefore this may present an interesting model for understanding the causes of the craniofacial defects seen in patients. Initial studies would investigate the levels of apoptosis and proliferation within the first PA, to determine if the failure of the maxillary component of the first PA to fuse with the frontonasal prominence is due to a problem in the size of the maxilla.

In addition, ectopic placement of the thymic rudiments was also described in these mutant embryos. This resembled the dermal thymus phenotype of BOFS patients, therefore, further suggesting that the *Tcfap2a*$^{f/-}$*;Foxg1cre* mutant embryos may also be a viable model for investigating this phenotype. To investigate this further, it would first be important to confirm that the tissue thought to be ectopic thymus is in fact thymic tissue. This may be possible using slide ISH with a *Foxn1* probe. This was not possible in the initial study as the tissue was not processed in an RNase-free environment. Therefore, more embryos should be collected at e15.5 for this purpose. Once it is confirmed that this is in fact thymus tissue, it would be interesting to follow the formation of the ectopic thymus through development, from e9.5 to e15.5. *Tcfap2a*$^{f/-}$*;Foxg1cre* mutant embryos and *Tcfap2a*$^{+/f}$*;Foxg1cre* control embryos would be examined using *Foxn1* slide ISH at each of the stages, to determine when the development of the thymus deviates from the normal processes, in the mutant embryos. Furthermore, as discussed in section 3.3.3, it is likely that the ectopic placement of the thymic rudiments is due to the failure of the endodermal tissue to separate from the pharyngeal ectoderm. Therefore, the levels of apoptosis between these tissues should also be compared. For this purpose, embryos would be collected at e12.5, as this is the time at which the thymic rudiments sever their connection with the pharynx (Manley and Blackburn, 2003), sectioned and immunohistochemistry using the caspase3 antibody would be performed and quantified.

In addition to the experiments described above, it would also be interesting to investigate the transcriptional changes occurring in the tissues concerned. To investigate the expression changes occurring in the formation of the frontonasal defects, it would be possible to extract the first and second PA region from mutant (*Tcfap2a*$^{f/-}$*;Foxg1cre*) and control (*Tcfap2a*$^{+/f}$) embryos. The candidate genes for analysis would be selected by identifying mutants with similar phenotypes, or genes known to be involved in the formation of the craniofacial processes. Additionally, depending on the results of the apoptosis study described above, genes may also be selected due to their involvement in basic cellular processes, such as apoptosis, proliferation and differentiation.

7.8.4. Transcriptional self-interference

We proposed in chapter 4 that the lack of phenotype observed when using the *Tcfap2a*^{flox} allele, compared to the *Tcfap2a*-null allele, was a result of transcriptional self-interference in the *Tcfap2a*$^{-/-}$ mutant embryos. However, further investigations are required in order to confirm this hypothesis. Initially, it will be important to ascertain if a protein is produced by the *Tcfap2a*-null allele, using western blotting. If a protein product is produced, it will then be important to determine if this truncated protein is capable of interfering with the function of other AP-2 isoforms. In order to examine this, a luciferase assay could be carried out. This would require the production of a construct identical to that of the null transcript. This construct may then be used in a luciferase assay to investigate the potential inhibitory effect of the construct on a wild type *Tcfap2a* construct. A control experiment containing only the wild type construct would also be carried out, for comparison. It would also be interesting to attempt a rescue experiment, in which higher levels of the necessary co-activator molecules are added to the assay, in order to demonstrate that the reduced activity is due to the mutant protein sequestering the co-activators available within the cell. Furthermore, repeating these experiments using wild type *Tcfap2b* and *Tcfap2c* constructs would allow us to confirm that the *Tcfap2a*-null allele is capable of inhibiting these isoforms through the process of transcriptional self-interference.

7.9. Conclusions

The data presented in this thesis demonstrates the importance of *Tcfap2a* in cardiovascular development. In particular we have demonstrated a role for this gene

in the development of the fourth PAA. Furthermore, we have presented data to suggest the possibility of redundancy between AP-2α and other AP-2 isoforms, AP-2β and –γ. This work also clearly demonstrates the importance of genetic background in working with mouse models.

Appendix A. Primer sequences and conditions for PCR genotyping.

Tcfap2a alleles

Tcfap2a wild type

Primer name	Primer Sequence	Product size (bp)
Tcfap2a wt fw1	GACTGGCCTTGAGTCCTGAG	244
Tcfap2a wt rev1	GAGGTTGAAGTGGGTCAAGC	

Conditions:

Step	Temperature (°C)	Time	
1	95	2 minutes	
2	95	30 seconds	Repeat steps 2-4 30 times
3	58	30 seconds	
4	72	30 seconds	
5	72	10 minutes	
6	4	10 minutes	

Tcfap2a-null

Primer name	Primer Sequence	Product size (bp)
neo 3' KO	AACGCACGGGTGTTGGGTCGTTTGTTCG	1200
Kyko3	GGAGGGGGAGTCTTACCCAAACCTTGG	

Conditions:

Step	Temperature (°C)	Time	
1	95	2 minutes	
2	95	30 seconds	Repeat steps 2-4 36 times
3	66	52 seconds	
4	72	1 minute	
5	72	15 minutes	
6	4	10 minutes	

Tcfap2a flox

Primer name	Primer Sequence	Product size (bp)
Alflox4	CCCAAAGTGCCTGGGCTGAATTGAC	wild type – 490 floxed – 560
Alfscsq	GAATCTAGCTTGGAGGCTTATGTC	

Conditions:

Step	Temperature (°C)	Time	
1	95	2 minutes	
2	95	30 seconds	Repeat steps 2-4 34 times
3	58	30 seconds	
4	72	1 minute	
5	72	10 minutes	
6	4	10 minutes	

Tcfap2a del

Primer name	Primer Sequence	Product size (bp)
Alflox4	CCCAAAGTGCCTGGGCTGAATTGAC	wild type – 490 floxed – 560 deleted – 185
Alfscsq	GAATCTAGCTTGGAGGCTTATGTC	
Alflp	CCTGCCTTGGAACCATGACCCTCAG	

Conditions:

Step	Temperature (°C)	Time	
1	95	2 minutes	
2	95	30 seconds	Repeat steps 2-4 30 times
3	58	30 seconds	
4	72	1 minute	
5	72	10 minutes	
6	4	10 minutes	

Primer concentrations: All primers used at 0.5 µM. Water adjusted accordingly.

Cre lines

Wnt1cre

Primer name	Primer Sequence	Product size (bp)
Wnt1Cre-1 fw	ACAGCAACCACAGTCGTCAG	174
Wnt1Cre-1 rev	TCCCTGAACATGTCCATCAG	

Conditions:

Step	Temperature (°C)	Time	
1	95	2 minutes	
2	95	30 seconds	Repeat steps 2-4 30 times
3	56	30 seconds	
4	72	1 minute	
5	72	10 minutes	
6	4	10 minutes	

Nkx2.5cre

Primer name	Primer Sequence	Product size (bp)
Nkx2-5Cre-3 fw	ATACTCCCTGCCACCCCTAC	215
Nkx2-5Cre-3 rev	ACATGTCCATCAGGTTCTTGC	

Conditions:

Step	Temperature (°C)	Time	
1	95	2 minutes	
2	95	30 seconds	Repeat steps 2-4 35 times
3	65	35 seconds	
4	72	35 seconds	
5	72	15 minutes	
6	4	10 minutes	

Foxg1cre

Primer name	Primer Sequence	Product size (bp)
Foxg1Cre-2 fw	GCTTTTGCTACATGCCTTGC	250
Foxg1Cre-2 rev	TCTTGCGAACCTCATCACTC	

Conditions:

Step	Temperature (°C)	Time	
1	95	2 minutes	
2	95	30 seconds	Repeat steps 2-4 30 times
3	58	30 seconds	
4	72	1 minute	
5	72	10 minutes	
6	4	10 minutes	

Reporter constructs

R26R^{LacZ} and R262^{EYFP}

Primer name	Primer Sequence	Product size (bp)
r1 eyfp common	AAAGTCGCTCTGAGTTGTTAT	wild type – 500 mutant -250
r2 mut	GCGAAGAGTTTGTCCTCAACC	
r3 wt	GGAGCGGGAGAAATGGATATG	

Conditions:

Step	Temperature (°C)	Time	
1	95	2 minutes	
2	95	30 seconds	Repeat steps 2-4 30 times
3	59	30 seconds	
4	72	1 minute	
5	72	5 minutes	
6	4	10 minutes	

Primer concentrations per reaction: 1 µM r1, 0.5 µM r2, 0.5 µM r3. Water adjusted accordingly.

Dlx5

Primer name	Primer Sequence	Product size (bp)
S1X-A	GCATAACCAGTGAAACAGCATTGCTG	280
S1X-B	GGACATGTTCAGGGATCGCCAGGCG	

Conditions:

Step	Temperature (°C)	Time	
1	95	2 minutes	
2	95	30 seconds	Repeat steps 2-4 30 times
3	55	30 seconds	
4	72	30 seconds	
5	72	10 minutes	
6	4	10 minutes	

Appendix B. Genetic backgrounds of embryos examined.

	Genetic background (%)		
Litter no.	**Male**	**Female**	**Offspring**
Tcfap2a$^{f/-}$Wnt1cre			
Litter 74	95.0125	93.15	94.08
Litter 108	95.0125	93.15	94.08
Litter 109	95.0125	93.15	94.08
Litter 112	95.8689	93.15	94.509
Litter 119	95.8689	93.15	94.509
Tcfap2a$^{f/-}$;Wnt1cre			
Litter 272	47.846	97.078	72.46
Litter 273	47.846	97.078	72.46
Litter 274	47.846	97.078	72.46
Litter 283	47.846	97.078	72.46
Tcfap2a$^{f/-}$;Wnt1cre;Foxg1cre			
Litter 214	94.3156	97.078	95.6968
Litter 220	94.3156	97.078	95.6968
Litter 224	94.3156	97.078	95.6968
Litter 230	94.3156	97.078	95.6968
Tcfap2a$^{f/-}$;Wnt1cre;Nkx2.5cre			
Litter 239	97.078	97.668	97.373
Litter 284	96.916	97.078	96.997
Litter 294	96.916	97.078	96.997
Litter 296	96.916	97.078	96.997
Litter 303	96.916	97.078	96.997
Tcfap2a$^{f/f}$;PGKcre			
Litter 335	97.391	97.078	97.2235
Litter 337	97.391	97.078	97.2235
Litter 346	97.391	97.078	97.2235
Litter 348	97.391	97.078	97.2235
Tcfap2a$^{f/-}$;PGKcre			
Litter 374	97.408	97.078	97.219
Litter 375	97.408	97.078	97.219
Litter 376	97.408	97.078	97.219
Tcfap2a$^{f/f}$Sox2cre			
Litter 564	98.286	97.078	97.682
Litter 572	98.286	97.078	97.682
Litter 578	98.286	97.078	97.682

	Genetic background (%)		
Litter no.	**Male**	**Female**	**Offspring**
Tcfap2a$^{\Delta/\Delta}$			
Litter 587	98.286	98.286	98.286
Litter 606	98.286	98.286	98.286
Litter 610	98.286	98.286	98.286
Litter 611	98.286	98.286	98.286
Tcfap2a$^{-/-}$ (MRI, e15.5)			
Litter 41	93.45	93.45	93.45
Litter 42	93.45	93.45	93.45
Litter 45	93.45	96.725	95.088
Litter 48	93.45	93.45	93.45
Tcfap2a$^{-/-}$ (PECAM-1 staining)			
Litter 410	97.112	97.112	97.112
Litter 421	97.112	97.112	97.112
Litter 551	97.584	97.584	97.584
Litter 393	97.112	97.112	97.112
Litter 422	97.112	97.112	97.112
Litter 436	98.056	98.056	98.056
Litter 579	97.584	97.584	97.584
Litter 586	97.584	97.584	97.584
Litter 378	97.112	97.112	97.112
Litter 451	97.481	98.056	97.769
Litter 474	97.297	97.584	97.441
Litter 481	97.297	97.584	97.441
Tcfap2a$^{-/-}$ (Immunofluorescence)			
Litter 515	97.953	97.584	97.769
Litter 524	97.953	97.584	97.769
Litter 532	97.953	97.584	97.769
Litter 538	97.953	97.584	97.769
Litter 474	97.297	97.584	97.441
Litter 486	98.741	97.584	97.663
Tcfap2a$^{+/-}$;Dlx5$^{+/-}$			
Litter 597	100	97.584	98.792
Litter 609	100	98.678	99.339
Litter 617	100	97.584	98.792
Litter 620	100	97.584	98.792
Litter 627	100	97.584	98.792

References

Abel, T. and Maniatis, T. (1989) 'Gene regulation. Action of leucine zippers', *Nature*, 341(6237), pp. 24-5.

Abu-Issa, R., Smyth, G., Smoak, I., Yamamura, K. and Meyers, E.N. (2002) 'Fgf8 is required for pharyngeal arch and cardiovascular development in the mouse', *Development*, 129(19), pp. 4613-25.

Acampora, D., Merlo, G.R., Paleari, L., Zerega, B., Postiglione, M.P., Mantero, S., Bober, E., Barbieri, O., Simeone, A. and Levi, G. (1999) 'Craniofacial, vestibular and bone defects in mice lacking the Distal-less-related gene Dlx5', *Development*, 126(17), pp. 3795-809.

Acloque, H., Adams, M.S., Fishwick, K., Bronner-Fraser, M. and Nieto, M.A. (2009) 'Epithelial-mesenchymal transitions: the importance of changing cell state in development and disease', *J Clin Invest*, 119(6), pp. 1438-49.

Anderson-Berry, A., O'Brien, E.A., Bleyl, S.B., Lawson, A., Gundersen, N., Ryssman, D., Sweeley, J., Dahl, M.J., Drake, C.J., Schoenwolf, G.C. and Albertine, K.H. (2005) 'Vasculogenesis drives pulmonary vascular growth in the developing chick embryo', *Dev Dyn*, 233(1), pp. 145-53.

Anderson, M.J., Pham, V.N., Vogel, A.M., Weinstein, B.M. and Roman, B.L. (2008) 'Loss of unc45a precipitates arteriovenous shunting in the aortic arches', *Dev Biol*, 318(2), pp. 258-67.

Arnold, J.S., Werling, U., Braunstein, E.M., Liao, J., Nowotschin, S., Edelmann, W., Hebert, J.M. and Morrow, B.E. (2006) 'Inactivation of Tbx1 in the pharyngeal endoderm results in 22q11DS malformations', *Development*, 133(5), pp. 977-87.

Baldini, A. (2006) 'The 22q11.2 deletion syndrome: a gene dosage perspective', *ScientificWorldJournal*, 6, pp. 1881-7.

Bamforth, S.D., Braganca, J., Eloranta, J.J., Murdoch, J.N., Marques, F.I., Kranc, K.R., Farza, H., Henderson, D.J., Hurst, H.C. and Bhattacharya, S. (2001) 'Cardiac malformations, adrenal agenesis, neural crest defects and exencephaly in mice lacking Cited2, a new Tfap2 co-activator', *Nat Genet*, 29(4), pp. 469-74.

Bamforth, S.D., Braganca, J., Farthing, C.R., Schneider, J.E., Broadbent, C., Michell, A.C., Clarke, K., Neubauer, S., Norris, D., Brown, N.A., Anderson, R.H. and Bhattacharya, S. (2004) 'Cited2 controls left-right patterning and heart development through a Nodal-Pitx2c pathway', *Nat Genet*, 36(11), pp. 1189-96.

Bamforth, S.D., Chaudhry, B., Bennett, M., Wilson, R., Mohun, T.J., Van Mierop, L.H., Henderson, D.J. and Anderson, R.H. (2012a) 'Clarification of the identity of the mammalian fifth pharyngeal arch artery', *Clin Anat*.

Bamforth, S.D., Schneider, J.E. and Bhattacharya, S. (2012b) 'High-throughput analysis of mouse embryos by magnetic resonance imaging', *Cold Spring Harb Protoc*, 2012(1), pp. 93-101.

Barr, R.J., Santa Cruz, D.J. and Pearl, R.M. (1989) 'Dermal thymus. A light microscopic and immunohistochemical study', *Arch Dermatol*, 125(12), pp. 1681-4.

Barrallo-Gimeno, A., Holzschuh, J., Driever, W. and Knapik, E.W. (2004) 'Neural crest survival and differentiation in zebrafish depends on mont blanc/tfap2a gene function', *Development*, 131(7), pp. 1463-77.

Bartram, U., Molin, D.G., Wisse, L.J., Mohamad, A., Sanford, L.P., Doetschman, T., Speer, C.P., Poelmann, R.E. and Gittenberger-de Groot, A.C. (2001) 'Double-outlet right ventricle and overriding tricuspid valve reflect disturbances of looping, myocardialization, endocardial cushion differentiation, and apoptosis in TGF-beta(2)-knockout mice', *Circulation*, 103(22), pp. 2745-52.

Bauer, R., Imhof, A., Pscherer, A., Kopp, H., Moser, M., Seegers, S., Kerscher, M., Tainsky, M.A., Hofstaedter, F. and Buettner, R. (1994) 'The genomic structure of the human AP-2 transcription factor', *Nucleic Acids Res*, 22(8), pp. 1413-20.

Bennaceur, S., Buisson, T., Bertolus, C. and Couly, G. (1998) 'Branchio-oculo-facial syndrome with cleft lip and bilateral dermal thymus', *Cleft Palate Craniofac J*, 35(5), pp. 454-9.

Bergwerff, M., DeRuiter, M.C., Hall, S., Poelmann, R.E. and Gittenberger-de Groot, A.C. (1999) 'Unique vascular morphology of the fourth aortic arches: possible implications for pathogenesis of type-B aortic arch interruption and anomalous right subclavian artery', *Cardiovasc Res*, 44(1), pp. 185-96.

Bergwerff, M., Verberne, M.E., DeRuiter, M.C., Poelmann, R.E. and Gittenberger-de Groot, A.C. (1998) 'Neural crest cell contribution to the developing circulatory system: implications for vascular morphology?', *Circ Res*, 82(2), pp. 221-31.

Besson, W.T., 3rd, Kirby, M.L., Van Mierop, L.H. and Teabeaut, J.R., 2nd (1986) 'Effects of the size of lesions of the cardiac neural crest at various embryonic ages on incidence and type of cardiac defects', *Circulation*, 73(2), pp. 360-4.

Beverdam, A., Merlo, G.R., Paleari, L., Mantero, S., Genova, F., Barbieri, O., Janvier, P. and Levi, G. (2002) 'Jaw transformation with gain of symmetry after Dlx5/Dlx6 inactivation: mirror of the past?', *Genesis*, 34(4), pp. 221-7.

Boehm, T. (2008) 'Thymus development and function', *Curr Opin Immunol*, 20(2), pp. 178-84.

Bosher, J.M., Williams, T. and Hurst, H.C. (1995) 'The developmentally regulated transcription factor AP-2 is involved in c-erbB-2 overexpression in human mammary carcinoma', *Proc Natl Acad Sci U S A*, 92(3), pp. 744-7.

Braganca, J., Eloranta, J.J., Bamforth, S.D., Ibbitt, J.C., Hurst, H.C. and Bhattacharya, S. (2003) 'Physical and functional interactions among AP-2 transcription factors, p300/CREB-binding protein, and CITED2', *J Biol Chem*, 278(18), pp. 16021-9.

Breckenridge, R.A., Anderson, R.H. and Elliott, P.M. (2007) 'Isolated left ventricular non-compaction: the case for abnormal myocardial development', *Cardiol Young*, 17(2), pp. 124-9.

Brewer, S., Feng, W., Huang, J., Sullivan, S. and Williams, T. (2004) 'Wnt1-Cre-mediated deletion of AP-2alpha causes multiple neural crest-related defects', *Dev Biol*, 267(1), pp. 135-52.

Brewer, S., Jiang, X., Donaldson, S., Williams, T. and Sucov, H.M. (2002) 'Requirement for AP-2alpha in cardiac outflow tract morphogenesis', *Mech Dev*, 110(1-2), pp. 139-49.

Brewer, S. and Williams, T. (2004) 'Loss of AP-2alpha impacts multiple aspects of ventral body wall development and closure', *Dev Biol*, 267(2), pp. 399-417.

Brown, C.B., Feiner, L., Lu, M.M., Li, J., Ma, X., Webber, A.L., Jia, L., Raper, J.A. and Epstein, J.A. (2001) 'PlexinA2 and semaphorin signaling during cardiac neural crest development', *Development*, 128(16), pp. 3071-80.

Bruneau, B.G. (2008) 'The developmental genetics of congenital heart disease', *Nature*, 451(7181), pp. 943-8.

Buettner, R., Kannan, P., Imhof, A., Bauer, R., Yim, S.O., Glockshuber, R., Van Dyke, M.W. and Tainsky, M.A. (1993) 'An alternatively spliced mRNA from the AP-2 gene encodes a negative regulator of transcriptional activation by AP-2', *Mol Cell Biol*, 13(7), pp. 4174-85.

Bush, J.O. and Jiang, R. (2012) 'Palatogenesis: morphogenetic and molecular mechanisms of secondary palate development', *Development*, 139(2), pp. 231-43.

Byrd, N.A. and Meyers, E.N. (2005) 'Loss of Gbx2 results in neural crest cell patterning and pharyngeal arch artery defects in the mouse embryo', *Dev Biol*, 284(1), pp. 233-45.

Cai, C.L., Liang, X., Shi, Y., Chu, P.H., Pfaff, S.L., Chen, J. and Evans, S. (2003) 'Isl1 identifies a cardiac progenitor population that proliferates prior to differentiation and contributes a majority of cells to the heart', *Dev Cell*, 5(6), pp. 877-89.

Cai, D.H., Vollberg, T.M., Sr., Hahn-Dantona, E., Quigley, J.P. and Brauer, P.R. (2000) 'MMP-2 expression during early avian cardiac and neural crest morphogenesis', *Anat Rec*, 259(2), pp. 168-79.

Calmont, A., Ivins, S., Van Bueren, K.L., Papangeli, I., Kyriakopoulou, V., Andrews, W.D., Martin, J.F., Moon, A.M., Illingworth, E.A., Basson, M.A. and Scambler, P.J. (2009) 'Tbx1 controls cardiac neural crest cell migration during arch artery development by regulating Gbx2 expression in the pharyngeal ectoderm', *Development*, 136(18), pp. 3173-83.

Camenisch, T.D., Schroeder, J.A., Bradley, J., Klewer, S.E. and McDonald, J.A. (2002) 'Heart-valve mesenchyme formation is dependent on hyaluronan-augmented activation of ErbB2-ErbB3 receptors', *Nat Med*, 8(8), pp. 850-5.

Chazaud, C., Oulad-Abdelghani, M., Bouillet, P., Decimo, D., Chambon, P. and Dolle, P. (1996) 'AP-2.2, a novel gene related to AP-2, is expressed in the forebrain, limbs and face during mouse embryogenesis', *Mech Dev*, 54(1), pp. 83-94.

Chen, H., Shi, S., Acosta, L., Li, W., Lu, J., Bao, S., Chen, Z., Yang, Z., Schneider, M.D., Chien, K.R., Conway, S.J., Yoder, M.C., Haneline, L.S., Franco, D. and Shou, W. (2004) 'BMP10 is essential for maintaining cardiac growth during murine cardiogenesis', *Development*, 131(9), pp. 2219-31.

Clouthier, D.E., Hosoda, K., Richardson, J.A., Williams, S.C., Yanagisawa, H., Kuwaki, T., Kumada, M., Hammer, R.E. and Yanagisawa, M. (1998) 'Cranial and cardiac neural crest defects in endothelin-A receptor-deficient mice', *Development*, 125(5), pp. 813-24.

Crackower, M.A., Scherer, S.W., Rommens, J.M., Hui, C.C., Poorkaj, P., Soder, S., Cobben, J.M., Hudgins, L., Evans, J.P. and Tsui, L.C. (1996) 'Characterization of the split hand/split foot malformation locus SHFM1 at 7q21.3-q22.1 and analysis of a candidate gene for its expression during limb development', *Hum Mol Genet*, 5(5), pp. 571-9.

Danielian, P.S., Muccino, D., Rowitch, D.H., Michael, S.K. and McMahon, A.P. (1998) 'Modification of gene activity in mouse embryos in utero by a tamoxifen-inducible form of Cre recombinase', *Curr Biol*, 8(24), pp. 1323-6.

de Croze, N., Maczkowiak, F. and Monsoro-Burq, A.H. (2011) 'Reiterative AP2a activity controls sequential steps in the neural crest gene regulatory network', *Proc Natl Acad Sci U S A*, 108(1), pp. 155-60.

Depew, M.J., Liu, J.K., Long, J.E., Presley, R., Meneses, J.J., Pedersen, R.A. and Rubenstein, J.L. (1999) 'Dlx5 regulates regional development of the branchial arches and sensory capsules', *Development*, 126(17), pp. 3831-46.

Drut, R. and Galliani, C. (2003) 'Thymic tissue in the skin: a clue to the diagnosis of the branchio-oculo-facial syndrome: report of two cases', *Int J Surg Pathol*, 11(1), pp. 25-8.

Duijf, P.H., van Bokhoven, H. and Brunner, H.G. (2003) 'Pathogenesis of split-hand/split-foot malformation', *Hum Mol Genet*, 12 Spec No 1, pp. R51-60.

Echelard, Y., Vassileva, G. and McMahon, A.P. (1994) 'Cis-acting regulatory sequences governing Wnt-1 expression in the developing mouse CNS', *Development*, 120(8), pp. 2213-24.

Eckert, D., Buhl, S., Weber, S., Jager, R. and Schorle, H. (2005) 'The AP-2 family of transcription factors', *Genome Biol*, 6(13), p. 246.

Elliott, A.M. and Evans, J.A. (2008) 'The association of split hand foot malformation (SHFM) and congenital heart defects', *Birth Defects Res A Clin Mol Teratol*, 82(6), pp. 425-34.

Engleka, K.A., Manderfield, L.J., Brust, R.D., Li, L., Cohen, A., Dymecki, S.M. and Epstein, J.A. (2012) 'Islet1 derivatives in the heart are of both neural crest and second heart field origin', *Circ Res*, 110(7), pp. 922-6.

Erami, C., Charaf-Eddine, A., Aggarwal, A., Rivard, A.L., Giles, H.W. and Nowicki, M.J. (2013) 'Dysphagia lusoria in an infant', *J Pediatr*, 162(6), pp. 1289-90.

Feiner, L., Webber, A.L., Brown, C.B., Lu, M.M., Jia, L., Feinstein, P., Mombaerts, P., Epstein, J.A. and Raper, J.A. (2001) 'Targeted disruption of semaphorin 3C leads to persistent truncus arteriosus and aortic arch interruption', *Development*, 128(16), pp. 3061-70.

Frisch, S.M. and Morisaki, J.H. (1990) 'Positive and negative transcriptional elements of the human type IV collagenase gene', *Mol Cell Biol*, 10(12), pp. 6524-32.

Gaubatz, S., Imhof, A., Dosch, R., Werner, O., Mitchell, P., Buettner, R. and Eilers, M. (1995) 'Transcriptional activation by Myc is under negative control by the transcription factor AP-2', *EMBO J*, 14(7), pp. 1508-19.

Genevieve, D., Sanlaville, D., Faivre, L., Kottler, M.L., Jambou, M., Gosset, P., Boustani-Samara, D., Pinto, G., Ozilou, C., Abeguile, G., Munnich, A., Romana, S., Raoul, O., Cormier-Daire, V. and Vekemans, M. (2005) 'Paternal deletion of the GNAS imprinted locus (including Gnasxl) in two girls presenting with severe pre- and post-natal growth retardation and intractable feeding difficulties', *Eur J Hum Genet*, 13(9), pp. 1033-9.

Gestri, G., Osborne, R.J., Wyatt, A.W., Gerrelli, D., Gribble, S., Stewart, H., Fryer, A., Bunyan, D.J., Prescott, K., Collin, J.R., Fitzgerald, T., Robinson, D., Carter, N.P., Wilson, S.W. and Ragge, N.K. (2009) 'Reduced TFAP2A function causes variable optic fissure closure and retinal defects and sensitizes eye development to mutations in other morphogenetic regulators', *Hum Genet*, 126(6), pp. 791-803.

Gille, J., Swerlick, R.A. and Caughman, S.W. (1997) 'Transforming growth factor-alpha-induced transcriptional activation of the vascular permeability factor (VPF/VEGF) gene requires AP-2-dependent DNA binding and transactivation', *EMBO J*, 16(4), pp. 750-9.

Graham, A. and Smith, A. (2001) 'Patterning the pharyngeal arches', *Bioessays*, 23(1), pp. 54-61.

Grevellec, A. and Tucker, A.S. (2010) 'The pharyngeal pouches and clefts: Development, evolution, structure and derivatives', *Semin Cell Dev Biol*, 21(3), pp. 325-32.

Hammer, S., Toenjes, M., Lange, M., Fischer, J.J., Dunkel, I., Mebus, S., Grimm, C.H., Hetzer, R., Berger, F. and Sperling, S. (2008) 'Characterization of TBX20 in human hearts and its regulation by TFAP2', *J Cell Biochem*, 104(3), pp. 1022-33.

Hayashi, S., Lewis, P., Pevny, L. and McMahon, A.P. (2002) 'Efficient gene modulation in mouse epiblast using a Sox2Cre transgenic mouse strain', *Gene Expr Patterns*, 2(1-2), pp. 93-7.

Hayashi, S., Tenzen, T. and McMahon, A.P. (2003) 'Maternal inheritance of Cre activity in a Sox2Cre deleter strain', *Genesis*, 37(2), pp. 51-3.

Hebert, J.M. and McConnell, S.K. (2000) 'Targeting of cre to the Foxg1 (BF-1) locus mediates loxP recombination in the telencephalon and other developing head structures', *Dev Biol*, 222(2), pp. 296-306.

Helms, J.A., Cordero, D. and Tapadia, M.D. (2005) 'New insights into craniofacial morphogenesis', *Development*, 132(5), pp. 851-61.

High, F.A. and Epstein, J.A. (2008) 'The multifaceted role of Notch in cardiac development and disease', *Nat Rev Genet*, 9(1), pp. 49-61.

Hilger-Eversheim, K., Moser, M., Schorle, H. and Buettner, R. (2000) 'Regulatory roles of AP-2 transcription factors in vertebrate development, apoptosis and cell-cycle control', *Gene*, 260(1-2), pp. 1-12.

Hiraumi, H., Tabuchi, K. and Kitajiri, S. (2001) 'Dermal thymus: case report and review of the literature', *Am J Otolaryngol*, 22(4), pp. 294-6.

Hiroshi, F., Satoru, S., Eisuke, U., Kunihiro, K. and Yuhei, Y. (2006) 'Bilateral dermal thymus of neck in branchio-oculo-facial syndrome', *J Plast Reconstr Aesthet Surg*, 59(12), pp. 1385-7.

Hiruma, T., Nakajima, Y. and Nakamura, H. (2002) 'Development of pharyngeal arch arteries in early mouse embryo', *J Anat*, 201(1), pp. 15-29.

Hoffman, J.I. (1995) 'Incidence of congenital heart disease: I. Postnatal incidence', *Pediatr Cardiol*, 16(3), pp. 103-13.

Hoffman, J.I., Kaplan, S. and Liberthson, R.R. (2004) 'Prevalence of congenital heart disease', *Am Heart J*, 147(3), pp. 425-39.

Hoffman, T.L., Javier, A.L., Campeau, S.A., Knight, R.D. and Schilling, T.F. (2007) 'Tfap2 transcription factors in zebrafish neural crest development and ectodermal evolution', *J Exp Zool B Mol Dev Evol*, 308(5), pp. 679-91.

Huang, S., Jean, D., Luca, M., Tainsky, M.A. and Bar-Eli, M. (1998) 'Loss of AP-2 results in downregulation of c-KIT and enhancement of melanoma tumorigenicity and metastasis', *EMBO J*, 17(15), pp. 4358-69.

Hutson, M.R. and Kirby, M.L. (2003) 'Neural crest and cardiovascular development: a 20-year perspective', *Birth Defects Res C Embryo Today*, 69(1), pp. 2-13.

Hutson, M.R. and Kirby, M.L. (2007) 'Model systems for the study of heart development and disease. Cardiac neural crest and conotruncal malformations', *Semin Cell Dev Biol*, 18(1), pp. 101-10.

Ivey, K., Tyson, B., Ukidwe, P., McFadden, D.G., Levi, G., Olson, E.N., Srivastava, D. and Wilkie, T.M. (2003) 'Galphaq and Galpha11 proteins mediate endothelin-1 signaling in neural crest-derived pharyngeal arch mesenchyme', *Dev Biol*, 255(2), pp. 230-7.

Jeong, J., Li, X., McEvilly, R.J., Rosenfeld, M.G., Lufkin, T. and Rubenstein, J.L. (2008) 'Dlx genes pattern mammalian jaw primordium by regulating both lower jaw-specific and upper jaw-specific genetic programs', *Development*, 135(17), pp. 2905-16.

Jiang, X., Rowitch, D.H., Soriano, P., McMahon, A.P. and Sucov, H.M. (2000) 'Fate of the mammalian cardiac neural crest', *Development*, 127(8), pp. 1607-16.

Joensuu, H. and Dimitrijevic, S. (2001) 'Tyrosine kinase inhibitor imatinib (STI571) as an anticancer agent for solid tumours', *Ann Med*, 33(7), pp. 451-5.

Jones, N. (1990) 'Transcriptional regulation by dimerization: two sides to an incestuous relationship', *Cell*, 61(1), pp. 9-11.

Kannan, P., Buettner, R., Chiao, P.J., Yim, S.O., Sarkiss, M. and Tainsky, M.A. (1994) 'N-ras oncogene causes AP-2 transcriptional self-interference, which leads to transformation', *Genes Dev*, 8(11), pp. 1258-69.

Kannan, P., Yu, Y., Wankhade, S. and Tainsky, M.A. (1999) 'PolyADP-ribose polymerase is a coactivator for AP-2-mediated transcriptional activation', *Nucleic Acids Res*, 27(3), pp. 866-74.

Kirby, M.L. (1987) 'Cardiac morphogenesis--recent research advances', *Pediatr Res*, 21(3), pp. 219-24.

Kirby, M.L. (1993) 'Cellular and molecular contributions of the cardiac neural crest to cardiovascular development', *Trends Cardiovasc Med*, 3(1), pp. 18-23.

Kirby, M.L., Turnage, K.L., 3rd and Hays, B.M. (1985) 'Characterization of conotruncal malformations following ablation of "cardiac" neural crest', *Anat Rec*, 213(1), pp. 87-93.

Kirby, M.L. and Waldo, K.L. (1990) 'Role of neural crest in congenital heart disease', *Circulation*, 82(2), pp. 332-40.

Kitamura, K., Miura, H., Miyagawa-Tomita, S., Yanazawa, M., Katoh-Fukui, Y., Suzuki, R., Ohuchi, H., Suehiro, A., Motegi, Y., Nakahara, Y., Kondo, S. and Yokoyama, M. (1999) 'Mouse Pitx2 deficiency leads to anomalies of the ventral body wall, heart, extra- and periocular mesoderm and right pulmonary isomerism', *Development*, 126(24), pp. 5749-58.

Knight, R.D., Javidan, Y., Nelson, S., Zhang, T. and Schilling, T. (2004) 'Skeletal and pigment cell defects in the lockjaw mutant reveal multiple roles for zebrafish tfap2a in neural crest development', *Dev Dyn*, 229(1), pp. 87-98.

Knight, R.D., Javidan, Y., Zhang, T., Nelson, S. and Schilling, T.F. (2005) 'AP2-dependent signals from the ectoderm regulate craniofacial development in the zebrafish embryo', *Development*, 132(13), pp. 3127-38.

Knight, R.D., Nair, S., Nelson, S.S., Afshar, A., Javidan, Y., Geisler, R., Rauch, G.J. and Schilling, T.F. (2003) 'lockjaw encodes a zebrafish tfap2a required for early neural crest development', *Development*, 130(23), pp. 5755-68.

Kohlbecker, A., Lee, A.E. and Schorle, H. (2002) 'Exencephaly in a subset of animals heterozygous for AP-2alpha mutation', *Teratology*, 65(5), pp. 213-8.

Komiyama, M., Ito, K. and Shimada, Y. (1987) 'Origin and development of the epicardium in the mouse embryo', Anat Embryol 176(2), pp. 183-9.

Kouzarides, T. (2000) 'Acetylation: a regulatory modification to rival phosphorylation?', *EMBO J*, 19(6), pp. 1176-9.

Kurihara, Y., Kurihara, H., Oda, H., Maemura, K., Nagai, R., Ishikawa, T. and Yazaki, Y. (1995) 'Aortic arch malformations and ventricular septal defect in mice deficient in endothelin-1', *J Clin Invest*, 96(1), pp. 293-300.

Kutsche, L.M. and Van Mierop, L.H. (1984) 'Cervical origin of the right subclavian artery in aortic arch interruption: pathogenesis and significance', *Am J Cardiol*, 53(7), pp. 892-5.

Lakso, M., Sauer, B., Mosinger, B., Jr., Lee, E.J., Manning, R.W., Yu, S.H., Mulder, K.L. and Westphal, H. (1992) 'Targeted oncogene activation by site-specific recombination in transgenic mice', *Proc Natl Acad Sci U S A*, 89(14), pp. 6232-6.

Lallemand, Y., Luria, V., Haffner-Krausz, R. and Lonai, P. (1998) 'Maternally expressed PGK-Cre transgene as a tool for early and uniform activation of the Cre site-specific recombinase', *Transgenic Res*, 7(2), pp. 105-12.

LeBlanc, S.K., Yu, S. and Barnett, C.P. (2013) '6p.24 microdeletion involving TFAP2A without classic features of branchio-oculo-facial syndrome', *Am J Med Genet A*, 161(4), pp. 901-4.

Lee, K.F., Simon, H., Chen, H., Bates, B., Hung, M.C. and Hauser, C. (1995) 'Requirement for neuregulin receptor erbB2 in neural and cardiac development', *Nature*, 378(6555), pp. 394-8.

Leung, D.W., Cachianes, G., Kuang, W.J., Goeddel, D.V. and Ferrara, N. (1989) 'Vascular endothelial growth factor is a secreted angiogenic mitogen', *Science*, 246(4935), pp. 1306-9.

Li, H., Sheridan, R. and Williams, T. (2013) 'Analysis of TFAP2A mutations in Branchio-Oculo-Facial Syndrome indicates functional complexity within the AP-2alpha DNA-binding domain', *Hum Mol Genet*.

Li, P., Pashmforoush, M. and Sucov, H.M. (2012) 'Mesodermal retinoic acid signaling regulates endothelial cell coalescence in caudal pharyngeal arch artery vasculogenesis', *Dev Biol*, 361(1), pp. 116-24.

Li, W. and Cornell, R.A. (2007) 'Redundant activities of Tfap2a and Tfap2c are required for neural crest induction and development of other non-neural ectoderm derivatives in zebrafish embryos', *Dev Biol*, 304(1), pp. 338-54.

Lin, A.E., Yuzuriha, S., McLean, S. and Mulliken, J.B. (2009) 'Lesser forms of cleft lip associated with the branchio-oculo-facial syndrome', *J Craniofac Surg*, 20 Suppl 1, pp. 608-11.

Lindsay, E.A. (2001) 'Chromosomal microdeletions: dissecting del22q11 syndrome', *Nat Rev Genet*, 2(11), pp. 858-68.

Lindsay, E.A. and Baldini, A. (2001) 'Recovery from arterial growth delay reduces penetrance of cardiovascular defects in mice deleted for the DiGeorge syndrome region', *Hum Mol Genet*, 10(9), pp. 997-1002.

Lindsay, E.A., Botta, A., Jurecic, V., Carattini-Rivera, S., Cheah, Y.C., Rosenblatt, H.M., Bradley, A. and Baldini, A. (1999) 'Congenital heart disease in mice deficient for the DiGeorge syndrome region', *Nature*, 401(6751), pp. 379-83.

Lindsay, E.A., Vitelli, F., Su, H., Morishima, M., Huynh, T., Pramparo, T., Jurecic, V., Ogunrinu, G., Sutherland, H.F., Scambler, P.J., Bradley, A. and Baldini, A. (2001) 'Tbx1 haploinsufficieny in the DiGeorge syndrome region causes aortic arch defects in mice', *Nature*, 410(6824), pp. 97-101.

Luo, T., Lee, Y.H., Saint-Jeannet, J.P. and Sargent, T.D. (2003) 'Induction of neural crest in Xenopus by transcription factor AP2alpha', *Proc Natl Acad Sci U S A*, 100(2), pp. 532-7.

Luo, T., Matsuo-Takasaki, M., Thomas, M.L., Weeks, D.L. and Sargent, T.D. (2002) 'Transcription factor AP-2 is an essential and direct regulator of epidermal development in Xenopus', *Dev Biol*, 245(1), pp. 136-44.

Macatee, T.L., Hammond, B.P., Arenkiel, B.R., Francis, L., Frank, D.U. and Moon, A.M. (2003) 'Ablation of specific expression domains reveals discrete functions of ectoderm- and endoderm-derived FGF8 during cardiovascular and pharyngeal development', *Development*, 130(25), pp. 6361-74.

MacDonald, S.T., Bamforth, S.D., Chen, C.M., Farthing, C.R., Franklyn, A., Broadbent, C., Schneider, J.E., Saga, Y., Lewandoski, M. and Bhattacharya, S. (2008) 'Epiblastic Cited2 deficiency results in cardiac phenotypic heterogeneity and provides a mechanism for haploinsufficiency', *Cardiovasc Res*, 79(3), pp. 448-57.

Manley, N.R. and Blackburn, C.C. (2003) 'A developmental look at thymus organogenesis: where do the non-hematopoietic cells in the thymus come from?', *Curr Opin Immunol*, 15(2), pp. 225-32.

McBurney, M.W., Staines, W.A., Boekelheide, K., Parry, D., Jardine, K. and Pickavance, L. (1994) 'Murine PGK-1 promoter drives widespread but not uniform expression in transgenic mice', *Dev Dyn*, 200(4), pp. 278-93.

Merlo, G.R., Paleari, L., Mantero, S., Genova, F., Beverdam, A., Palmisano, G.L., Barbieri, O. and Levi, G. (2002) 'Mouse model of split hand/foot malformation type I', *Genesis*, 33(2), pp. 97-101.

Merlo, G.R., Zerega, B., Paleari, L., Trombino, S., Mantero, S. and Levi, G. (2000) 'Multiple functions of Dlx genes', *Int J Dev Biol*, 44(6), pp. 619-26.

Milunsky, J.M., Maher, T.A., Zhao, G., Roberts, A.E., Stalker, H.J., Zori, R.T., Burch, M.N., Clemens, M., Mulliken, J.B., Smith, R. and Lin, A.E. (2008) 'TFAP2A mutations result in branchio-oculo-facial syndrome', *Am J Hum Genet*, 82(5), pp. 1171-7.

Milunsky, J.M., Maher, T.M., Zhao, G., Wang, Z., Mulliken, J.B., Chitayat, D., Clemens, M., Stalker, H.J., Bauer, M., Burch, M., Chenier, S., Cunningham, M.L., Drack, A.V., Janssens, S., Karlea, A., Klatt, R., Kini, U., Klein, O., Lachmeijer, A.M., Megarbane, A., Mendelsohn, N.J., Meschino, W.S., Mortier, G.R., Parkash, S., Ray, C.R., Roberts, A., Reardon, W., Schnur, R.E., Smith, R., Splitt, M., Tezcan, K., Whiteford, M.L., Wong, D.A., Zori, R. and Lin, A.E. (2011) 'Genotype-phenotype analysis of the branchio-oculo-facial syndrome', *Am J Med Genet A*, 155A(1), pp. 22-32.

Mitchell, P.J., Timmons, P.M., Hebert, J.M., Rigby, P.W. and Tjian, R. (1991) 'Transcription factor AP-2 is expressed in neural crest cell lineages during mouse embryogenesis', *Genes Dev*, 5(1), pp. 105-19.

Mitchell, P.J., Wang, C. and Tjian, R. (1987) 'Positive and negative regulation of transcription in vitro: enhancer-binding protein AP-2 is inhibited by SV40 T antigen', *Cell*, 50(6), pp. 847-61.

Mitchell, S.C., Korones, S.B. and Berendes, H.W. (1971) 'Congenital heart disease in 56,109 births. Incidence and natural history', *Circulation*, 43(3), pp. 323-32.

Mjaatvedt, C.H., Nakaoka, T., Moreno-Rodriguez, R., Norris, R.A., Kern, M.J., Eisenberg, C.A., Turner, D. and Markwald, R.R. (2001) 'The outflow tract of the heart is recruited from a novel heart-forming field', *Dev Biol*, 238(1), pp. 97-109.

Molin, D.G., DeRuiter, M.C., Wisse, L.J., Azhar, M., Doetschman, T., Poelmann, R.E. and Gittenberger-de Groot, A.C. (2002) 'Altered apoptosis pattern during pharyngeal arch artery remodelling is associated with aortic arch malformations in Tgfbeta2 knock-out mice', *Cardiovasc Res*, 56(2), pp. 312-22.

Molin, D.G., Roest, P.A., Nordstrand, H., Wisse, L.J., Poelmann, R.E., Eriksson, U.J. and Gittenberger-De Groot, A.C. (2004) 'Disturbed morphogenesis of cardiac outflow tract and increased rate of aortic arch anomalies in the offspring of diabetic rats', *Birth Defects Res A Clin Mol Teratol*, 70(12), pp. 927-38.

Moser, M., Dahmen, S., Kluge, R., Grone, H., Dahmen, J., Kunz, D., Schorle, H. and Buettner, R. (2003) 'Terminal renal failure in mice lacking transcription factor AP-2 beta', *Lab Invest*, 83(4), pp. 571-8.

Moser, M., Imhof, A., Pscherer, A., Bauer, R., Amselgruber, W., Sinowatz, F., Hofstadter, F., Schule, R. and Buettner, R. (1995) 'Cloning and characterization of a second AP-2 transcription factor: AP-2 beta', *Development*, 121(9), pp. 2779-88.

Moser, M., Pscherer, A., Roth, C., Becker, J., Mucher, G., Zerres, K., Dixkens, C., Weis, J., Guay-Woodford, L., Buettner, R. and Fassler, R. (1997a) 'Enhanced apoptotic cell death of renal epithelial cells in mice lacking transcription factor AP-2beta', *Genes Dev*, 11(15), pp. 1938-48.

Moser, M., Ruschoff, J. and Buettner, R. (1997b) 'Comparative analysis of AP-2 alpha and AP-2 beta gene expression during murine embryogenesis', *Dev Dyn*, 208(1), pp. 115-24.

Moses, K.A., DeMayo, F., Braun, R.M., Reecy, J.L. and Schwartz, R.J. (2001) 'Embryonic expression of an Nkx2-5/Cre gene using ROSA26 reporter mice', *Genesis*, 31(4), pp. 176-80.

Murray, B., Wagle, R., Amat-Alarcon, N., Wilkens, A., Stephens, P., Zackai, E.H., Goldmuntz, E., Calkins, H., Deardorff, M.A. and Judge, D.P. (2013) 'A family with a complex clinical presentation characterized by arrhythmogenic right ventricular

dysplasia/cardiomyopathy and features of branchio-oculo-facial syndrome', *Am J Med Genet A*, 161A(2), pp. 371-6.

Neuhauss, S.C., Solnica-Krezel, L., Schier, A.F., Zwartkruis, F., Stemple, D.L., Malicki, J., Abdelilah, S., Stainier, D.Y. and Driever, W. (1996) 'Mutations affecting craniofacial development in zebrafish', *Development*, 123, pp. 357-67.

Nishibatake, M., Kirby, M.L. and Van Mierop, L.H. (1987) 'Pathogenesis of persistent truncus arteriosus and dextroposed aorta in the chick embryo after neural crest ablation', *Circulation*, 75(1), pp. 255-64.

O'Brien, E.K., d'Alencon, C., Bonde, G., Li, W., Schoenebeck, J., Allende, M.L., Gelb, B.D., Yelon, D., Eisen, J.S. and Cornell, R.A. (2004) 'Transcription factor Ap-2alpha is necessary for development of embryonic melanophores, autonomic neurons and pharyngeal skeleton in zebrafish', *Dev Biol*, 265(1), pp. 246-61.

Offermanns, S., Zhao, L.P., Gohla, A., Sarosi, I., Simon, M.I. and Wilkie, T.M. (1998) 'Embryonic cardiomyocyte hypoplasia and craniofacial defects in G alpha q/G alpha 11-mutant mice', *EMBO J*, 17(15), pp. 4304-12.

Ohuchi, H., Yoshioka, H., Tanaka, A., Kawakami, Y., Nohno, T. and Noji, S. (1994) 'Involvement of androgen-induced growth factor (FGF-8) gene in mouse embryogenesis and morphogenesis', *Biochem Biophys Res Commun*, 204(2), pp. 882-8.

Oike, Y., Takakura, N., Hata, A., Kaname, T., Akizuki, M., Yamaguchi, Y., Yasue, H., Araki, K., Yamamura, K. and Suda, T. (1999) 'Mice homozygous for a truncated form of CREB-binding protein exhibit defects in hematopoiesis and vasculo-angiogenesis', *Blood*, 93(9), pp. 2771-9.

Okubo, T., Kawamura, A., Takahashi, J., Yagi, H., Morishima, M., Matsuoka, R. and Takada, S. (2011) 'Ripply3, a Tbx1 repressor, is required for development of the pharyngeal apparatus and its derivatives in mice', *Development*, 138(2), pp. 339-48.

Olaopa, M., Zhou, H.M., Snider, P., Wang, J., Schwartz, R.J., Moon, A.M. and Conway, S.J. (2011) 'Pax3 is essential for normal cardiac neural crest morphogenesis but is not required during migration nor outflow tract septation', *Dev Biol*, 356(2), pp. 308-22.

Orban, P.C., Chui, D. and Marth, J.D. (1992) 'Tissue- and site-specific DNA recombination in transgenic mice', *Proc Natl Acad Sci U S A*, 89(15), pp. 6861-5.

Oulad-Abdelghani, M., Bouillet, P., Chazaud, C., Dolle, P. and Chambon, P. (1996) 'AP-2.2: a novel AP-2-related transcription factor induced by retinoic acid during differentiation of P19 embryonal carcinoma cells', *Exp Cell Res*, 225(2), pp. 338-47.

Park, B.K., Sperber, S.M., Choudhury, A., Ghanem, N., Hatch, G.T., Sharpe, P.T., Thomas, B.L. and Ekker, M. (2004) 'Intergenic enhancers with distinct activities regulate Dlx gene expression in the mesenchyme of the branchial arches', *Dev Biol*, 268(2), pp. 532-45.

Peirson, S.N., Butler, J.N. and Foster, R.G. (2003) 'Experimental validation of novel and conventional approaches to quantitative real-time PCR data analysis', *Nucleic Acids Res*, 31(14), p. e73.

Pfisterer, P., Ehlermann, J., Hegen, M. and Schorle, H. (2002) 'A subtractive gene expression screen suggests a role of transcription factor AP-2 alpha in control of proliferation and differentiation', *J Biol Chem*, 277(8), pp. 6637-44.

Phillips, M.T., Kirby, M.L. and Forbes, G. (1987) 'Analysis of cranial neural crest distribution in the developing heart using quail-chick chimeras', *Circ Res*, 60(1), pp. 27-30.

Porras, D. and Brown, C.B. (2008) 'Temporal-spatial ablation of neural crest in the mouse results in cardiovascular defects', *Dev Dyn*, 237(1), pp. 153-62.

Randall, V., McCue, K., Roberts, C., Kyriakopoulou, V., Beddow, S., Barrett, A.N., Vitelli, F., Prescott, K., Shaw-Smith, C., Devriendt, K., Bosman, E., Steffes, G., Steel, K.P., Simrick, S., Basson, M.A., Illingworth, E. and Scambler, P.J. (2009) 'Great vessel

development requires biallelic expression of Chd7 and Tbx1 in pharyngeal ectoderm in mice', *J Clin Invest*, 119(11), pp. 3301-10.

Rauch, R., Rauch, A., Koch, A., Kumpf, M., Dufke, A., Singer, H. and Hofbeck, M. (2002) 'Cervical origin of the subclavian artery as a specific marker for monosomy 22q11', *Am J Cardiol*, 89(4), pp. 481-4.

Reiber, J., Sznajer, Y., Posteguillo, E.G., Muller, D., Lyonnet, S., Baumann, C. and Just, W. (2010) 'Additional clinical and molecular analyses of TFAP2A in patients with the Branchio-Oculo-Facial syndrome: Previously reported patient', *Am J Med Genet A*, 152A(8), p. 2143.

Rizzo, R., Micali, G., Calvieri, S., Sorge, G. and Mazzone, D. (1995) 'Branchio-oculo-facial syndrome and dermal thymus: case report and review of the literature', *Pediatr Dermatol*, 12(1), pp. 24-7.

Roberts, C., Ivins, S., Cook, A.C., Baldini, A. and Scambler, P.J. (2006) 'Cyp26 genes a1, b1 and c1 are down-regulated in Tbx1 null mice and inhibition of Cyp26 enzyme function produces a phenocopy of DiGeorge Syndrome in the chick', *Hum Mol Genet*, 15(23), pp. 3394-410.

Ryan, A.K., Blumberg, B., Rodriguez-Esteban, C., Yonei-Tamura, S., Tamura, K., Tsukui, T., de la Pena, J., Sabbagh, W., Greenwald, J., Choe, S., Norris, D.P., Robertson, E.J., Evans, R.M., Rosenfeld, M.G. and Izpisua Belmonte, J.C. (1998) 'Pitx2 determines left-right asymmetry of internal organs in vertebrates', *Nature*, 394(6693), pp. 545-51.

Sajan, S.A., Rubenstein, J.L., Warchol, M.E. and Lovett, M. (2011) 'Identification of direct downstream targets of Dlx5 during early inner ear development', *Hum Mol Genet*, 20(7), pp. 1262-73.

Sato, A., Scholl, A.M., Kuhn, E.B., Stadt, H.A., Decker, J.R., Pegram, K., Hutson, M.R. and Kirby, M.L. (2011) 'FGF8 signaling is chemotactic for cardiac neural crest cells', *Dev Biol*, 354(1), pp. 18-30.

Satoda, M., Zhao, F., Diaz, G.A., Burn, J., Goodship, J., Davidson, H.R., Pierpont, M.E. and Gelb, B.D. (2000) 'Mutations in TFAP2B cause Char syndrome, a familial form of patent ductus arteriosus', *Nat Genet*, 25(1), pp. 42-6.

Scambler, P.J. (2010) '22q11 deletion syndrome: a role for TBX1 in pharyngeal and cardiovascular development', *Pediatr Cardiol*, 31(3), pp. 378-90.

Schilling, T.F., Piotrowski, T., Grandel, H., Brand, M., Heisenberg, C.P., Jiang, Y.J., Beuchle, D., Hammerschmidt, M., Kane, D.A., Mullins, M.C., van Eeden, F.J., Kelsh, R.N., Furutani-Seiki, M., Granato, M., Haffter, P., Odenthal, J., Warga, R.M., Trowe, T. and Nusslein-Volhard, C. (1996) 'Jaw and branchial arch mutants in zebrafish I: branchial arches', *Development*, 123, pp. 329-44.

Schmittgen, T.D. and Livak, K.J. (2008) 'Analyzing real-time PCR data by the comparative C(T) method', *Nat Protoc*, 3(6), pp. 1101-8.

Schorle, H., Meier, P., Buchert, M., Jaenisch, R. and Mitchell, P.J. (1996) 'Transcription factor AP-2 essential for cranial closure and craniofacial development', *Nature*, 381(6579), pp. 235-8.

Shapiro, S.D. (1998) 'Matrix metalloproteinase degradation of extracellular matrix: biological consequences', *Curr Opin Cell Biol*, 10(5), pp. 602-8.

Singh, N., Trivedi, C.M., Lu, M., Mullican, S.E., Lazar, M.A. and Epstein, J.A. (2011) 'Histone deacetylase 3 regulates smooth muscle differentiation in neural crest cells and development of the cardiac outflow tract', *Circ Res*, 109(11), pp. 1240-9.

Siu, S.C. and Silversides, C.K. (2010) 'Bicuspid aortic valve disease', *J Am Coll Cardiol*, 55(25), pp. 2789-800.

Snider, P., Olaopa, M., Firulli, A.B. and Conway, S.J. (2007) 'Cardiovascular development and the colonizing cardiac neural crest lineage', *ScientificWorldJournal*, 7, pp. 1090-113.

Soriano, P. (1999) 'Generalized lacZ expression with the ROSA26 Cre reporter strain', *Nat Genet*, 21(1), pp. 70-1.

Sperling, S., Grimm, C.H., Dunkel, I., Mebus, S., Sperling, H.P., Ebner, A., Galli, R., Lehrach, H., Fusch, C., Berger, F. and Hammer, S. (2005) 'Identification and functional analysis of CITED2 mutations in patients with congenital heart defects', *Hum Mutat*, 26(6), pp. 575-82.

Srinivas, S., Watanabe, T., Lin, C.S., William, C.M., Tanabe, Y., Jessell, T.M. and Costantini, F. (2001) 'Cre reporter strains produced by targeted insertion of EYFP and ECFP into the ROSA26 locus', *BMC Dev Biol*, 1, p. 4.

Srivastava, D. and Olson, E.N. (2000) 'A genetic blueprint for cardiac development', *Nature*, 407(6801), pp. 221-6.

Srivastava, D., Thomas, T., Lin, Q., Kirby, M.L., Brown, D. and Olson, E.N. (1997) 'Regulation of cardiac mesodermal and neural crest development by the bHLH transcription factor, dHAND', *Nat Genet*, 16(2), pp. 154-60.

Stalmans, I., Lambrechts, D., De Smet, F., Jansen, S., Wang, J., Maity, S., Kneer, P., von der Ohe, M., Swillen, A., Maes, C., Gewillig, M., Molin, D.G., Hellings, P., Boetel, T., Haardt, M., Compernolle, V., Dewerchin, M., Plaisance, S., Vlietinck, R., Emanuel, B., Gittenberger-de Groot, A.C., Scambler, P., Morrow, B., Driscol, D.A., Moons, L., Esguerra, C.V., Carmeliet, G., Behn-Krappa, A., Devriendt, K., Collen, D., Conway, S.J. and Carmeliet, P. (2003) 'VEGF: a modifier of the del22q11 (DiGeorge) syndrome?', *Nat Med*, 9(2), pp. 173-82.

Stuckmann, I., Evans, S. and Lassar, A.B. (2003) 'Erythropoietin and retinoic acid, secreted from the epicardium, are required for cardiac myocyte proliferation', *Dev Biol*, 255(2), pp. 334-49.

Taddei, I., Morishima, M., Huynh, T. and Lindsay, E.A. (2001) 'Genetic factors are major determinants of phenotypic variability in a mouse model of the DiGeorge/del22q11 syndromes', *Proc Natl Acad Sci U S A*, 98(20), pp. 11428-31.

Tadros, T.M., Klein, M.D. and Shapira, O.M. (2009) 'Ascending aortic dilatation associated with bicuspid aortic valve: pathophysiology, molecular biology, and clinical implications', *Circulation*, 119(6), pp. 880-90.

Taniguchi, H., He, M., Wu, P., Kim, S., Paik, R., Sugino, K., Kvitsiani, D., Fu, Y., Lu, J., Lin, Y., Miyoshi, G., Shima, Y., Fishell, G., Nelson, S.B. and Huang, Z.J. (2011) 'A resource of Cre driver lines for genetic targeting of GABAergic neurons in cerebral cortex', *Neuron*, 71(6), pp. 995-1013.

Threadgill, D.W., Dlugosz, A.A., Hansen, L.A., Tennenbaum, T., Lichti, U., Yee, D., LaMantia, C., Mourton, T., Herrup, K., Harris, R.C. and et al. (1995) 'Targeted disruption of mouse EGF receptor: effect of genetic background on mutant phenotype', *Science*, 269(5221), pp. 230-4.

Topouzis, S. and Majesky, M.W. (1996) 'Smooth muscle lineage diversity in the chick embryo. Two types of aortic smooth muscle cell differ in growth and receptor-mediated transcriptional responses to transforming growth factor-beta', *Dev Biol*, 178(2), pp. 430-45.

Toyofuku, T., Yoshida, J., Sugimoto, T., Yamamoto, M., Makino, N., Takamatsu, H., Takegahara, N., Suto, F., Hori, M., Fujisawa, H., Kumanogoh, A. and Kikutani, H. (2008) 'Repulsive and attractive semaphorins cooperate to direct the navigation of cardiac neural crest cells', *Dev Biol*, 321(1), pp. 251-62.

Tuli, R., Seghatoleslami, M.R., Tuli, S., Howard, M.S., Danielson, K.G. and Tuan, R.S. (2002) 'p38 MAP kinase regulation of AP-2 binding in TGF-beta1-stimulated chondrogenesis of human trabecular bone-derived cells', *Ann N Y Acad Sci*, 961, pp. 172-7.

Tuteja, N. (2009) 'Signaling through G protein coupled receptors', *Plant Signal Behav*, 4(10), pp. 942-7.

Vincent, S.D. and Robertson, E.J. (2003) 'Highly efficient transgene-independent recombination directed by a maternally derived SOX2CRE transgene', *Genesis*, 37(2), pp. 54-6.

Vitelli, F., Taddei, I., Morishima, M., Meyers, E.N., Lindsay, E.A. and Baldini, A. (2002) 'A genetic link between Tbx1 and fibroblast growth factor signaling', *Development*, 129(19), pp. 4605-11.

von Gise, A. and Pu, W.T. (2012) 'Endocardial and epicardial epithelial to mesenchymal transitions in heart development and disease', *Circ Res*, 110(12), pp. 1628-45.

Waldo, K., Miyagawa-Tomita, S., Kumiski, D. and Kirby, M.L. (1998) 'Cardiac neural crest cells provide new insight into septation of the cardiac outflow tract: aortic sac to ventricular septal closure', *Dev Biol*, 196(2), pp. 129-44.

Waldo, K.L., Kumiski, D. and Kirby, M.L. (1996) 'Cardiac neural crest is essential for the persistence rather than the formation of an arch artery', *Dev Dyn*, 205(3), pp. 281-92.

Wankhade, S., Yu, Y., Weinberg, J., Tainsky, M.A. and Kannan, P. (2000) 'Characterization of the activation domains of AP-2 family transcription factors', *J Biol Chem*, 275(38), pp. 29701-8.

Werling, U. and Schorle, H. (2002) 'Transcription factor gene AP-2 gamma essential for early murine development', *Mol Cell Biol*, 22(9), pp. 3149-56.

Williams, T. and Tjian, R. (1991a) 'Analysis of the DNA-binding and activation properties of the human transcription factor AP-2', *Genes Dev*, 5(4), pp. 670-82.

Williams, T. and Tjian, R. (1991b) 'Characterization of a dimerization motif in AP-2 and its function in heterologous DNA-binding proteins', *Science*, 251(4997), pp. 1067-71.

Xu, H., Cerrato, F. and Baldini, A. (2005) 'Timed mutation and cell-fate mapping reveal reiterated roles of Tbx1 during embryogenesis, and a crucial function during segmentation of the pharyngeal system via regulation of endoderm expansion', *Development*, 132(19), pp. 4387-95.

Xu, H., Morishima, M., Wylie, J.N., Schwartz, R.J., Bruneau, B.G., Lindsay, E.A. and Baldini, A. (2004) 'Tbx1 has a dual role in the morphogenesis of the cardiac outflow tract', *Development*, 131(13), pp. 3217-27.

Yamaguchi, T.P., Dumont, D.J., Conlon, R.A., Breitman, M.L. and Rossant, J. (1993) 'flk-1, an flt-related receptor tyrosine kinase is an early marker for endothelial cell precursors', *Development*, 118(2), pp. 489-98.

Yanagisawa, H., Hammer, R.E., Richardson, J.A., Williams, S.C., Clouthier, D.E. and Yanagisawa, M. (1998a) 'Role of Endothelin-1/Endothelin-A receptor-mediated signaling pathway in the aortic arch patterning in mice', *J Clin Invest*, 102(1), pp. 22-33.

Yanagisawa, H., Yanagisawa, M., Kapur, R.P., Richardson, J.A., Williams, S.C., Clouthier, D.E., de Wit, D., Emoto, N. and Hammer, R.E. (1998b) 'Dual genetic pathways of endothelin-mediated intercellular signaling revealed by targeted disruption of endothelin converting enzyme-1 gene', *Development*, 125(5), pp. 825-36.

Yao, T.P., Oh, S.P., Fuchs, M., Zhou, N.D., Ch'ng, L.E., Newsome, D., Bronson, R.T., Li, E., Livingston, D.M. and Eckner, R. (1998) 'Gene dosage-dependent embryonic development and proliferation defects in mice lacking the transcriptional integrator p300', *Cell*, 93(3), pp. 361-72.

Yashiro, K., Shiratori, H. and Hamada, H. (2007) 'Haemodynamics determined by a genetic programme govern asymmetric development of the aortic arch', *Nature*, 450(7167), pp. 285-8.

Yelbuz, T.M., Waldo, K.L., Kumiski, D.H., Stadt, H.A., Wolfe, R.R., Leatherbury, L. and Kirby, M.L. (2002) 'Shortened outflow tract leads to altered cardiac looping after neural crest ablation', *Circulation*, 106(4), pp. 504-10.

Zeng, Y.X., Somasundaram, K. and el-Deiry, W.S. (1997) 'AP2 inhibits cancer cell growth and activates p21WAF1/CIP1 expression', *Nat Genet*, 15(1), pp. 78-82.

Zhang, J., Hagopian-Donaldson, S., Serbedzija, G., Elsemore, J., Plehn-Dujowich, D., McMahon, A.P., Flavell, R.A. and Williams, T. (1996) 'Neural tube, skeletal and body wall defects in mice lacking transcription factor AP-2', *Nature*, 381(6579), pp. 238-41.

Zhang, Z., Cerrato, F., Xu, H., Vitelli, F., Morishima, M., Vincentz, J., Furuta, Y., Ma, L., Martin, J.F., Baldini, A. and Lindsay, E. (2005) 'Tbx1 expression in pharyngeal epithelia is necessary for pharyngeal arch artery development', *Development*, 132(23), pp. 5307-15.

Zhang, Z., Huynh, T. and Baldini, A. (2006) 'Mesodermal expression of Tbx1 is necessary and sufficient for pharyngeal arch and cardiac outflow tract development', *Development*, 133(18), pp. 3587-95.

Zhao, F., Bosserhoff, A.K., Buettner, R. and Moser, M. (2011) 'A heart-hand syndrome gene: Tfap2b plays a critical role in the development and remodeling of mouse ductus arteriosus and limb patterning', *PLoS One*, 6(7), p. e22908.